Age-related changes of glutathione homeostasis in *Caenorhabditis elegans*

A Thesis submitted as fulfilment

of the requirement for the degree of

DOCTOR OF PHILOSOPHY

By

Gavin Douglas Ferguson

School of Biotechnology and Biomolecular Sciences

University of New South Wales

2019

THE UNIVERSITY OF NEW SOUTH WALES

THESIS/DISSERTATION SHEET

Surname/Family Name	:	**Ferguson**
Given Name/s	:	**Gavin Douglas**
Abbreviation for degree as give in the University calendar	:	**PhD**
Faculty	:	**Science**
School	:	**Biotechnology and Biomolecular Science**
Thesis Title	:	**Age-related changes of glutathione homeostasis in *Caenorhabditis elegans***

Abstract 350 words maximum:

The *de novo* glutathione (GSH) synthesis pathway is highly conserved throughout all aerobic eukaryotic organisms. Intracellular *de novo* GSH synthesis involves two ATP-dependent enzyme-catalysed reactions; the rate-limiting and first reaction is mediated by glutamate cysteine ligase (GCL), which condenses glutamate and cysteine, to form gamma-glutamylcysteine (γ-GC). The second reaction involves the addition of glycine to γ-GC by glutathione synthetase (GS) to form GSH.

During ageing, a progressive decline in cysteine availability or the expression and activity of the GCL enzyme has been implicated to contribute to a corresponding decline in cellular GSH levels. In mammals, the GCL enzyme is a heterodimeric holoenzyme composed of the catalytic (GCLC) and modifier (GCLM) subunits. Though GCLC contains all the substrate binding sites required for γ-GC production, its interaction with GCLM modulates its catalytic efficiency. The relative abundance of each subunit determines holoenzyme formation, with the GCLM subunit almost always being limiting. Tissues that are more vulnerable to oxidative stress, such as the brain, have been demonstrated in various rodent studies to have relatively lower levels of the GCLM subunit.

The nematode, *Caenorhabditis elegans*, presents a useful alternative ageing model to investigate the changes in glutathione homeostasis due to its relatively short lifespan, and its expression of both the GCLC subunit (*gcs-1* gene) and the recently identified GCLM orthologue (*E01A2.1* gene). In this study, *C. elegans* were used to show that ageing leads to a pro-oxidising shift of the GSH/GSSG ratio with declines in GSH and γ-GC levels beginning from early adulthood. The regulatory role of the GCLM orthologue was also shown to maintain GSH levels in a manner similar to that of mammals, demonstrating *C. elegans* as an appropriate model to investigate the regulatory function of the GCLM subunit.

Increasing the availability of the thiol precursor substrates, cysteine and γ-GC, were investigated to determine if the decline in GSH synthesis is a result of limited cysteine availability or the decline in the enzymatic production of γ-GC. Experiments comparing the efficacy of the cysteine prodrug, *N*-acetylcysteine (NAC), with exogenous γ-GC treatment were conducted to establish a bioavailability profile of both GSH precursors and to elucidate any phenotypic differences associated with improving longevity in GSH-compromised worms.

FOR OFFICE USE ONLY

Date of completion of requirements for Award:

ORIGINALITY STATEMENT

‘I hereby declare that this submission is my own work and to the best of my knowledge it contains no materials previously published or written by another person, or substantial proportions of material which have been accepted for the award of any other degree or diploma at UNSW or any other educational institution, except where due acknowledgement is made in the thesis. Any contribution made to the research by others, with whom I have worked at UNSW or elsewhere, is explicitly acknowledged in the thesis. I also declare that the intellectual content of this thesis is the product of my own work, except to the extent that assistance from others in the project's design and conception or in style, presentation and linguistic expression is acknowledged.’

Signed …….....

Date 20/02/2019 …….....

INCLUSION OF PUBLICATIONS STATEMENT

UNSW is supportive of candidates publishing their research results during their candidature as detailed in the UNSW Thesis Examination Procedure.

Publications can be used in their thesis in lieu of a Chapter if:

- The student contributed greater than 50% of the content in the publication and is the "primary author", ie. the student was responsible primarily for the planning, execution and preparation of the work for publication
- The student has approval to include the publication in their thesis in lieu of a Chapter from their supervisor and Postgraduate Coordinator.
- The publication is not subject to any obligations or contractual agreements with a third party that would constrain its inclusion in the thesis

Please indicate whether this thesis contains published material or not.

☐ *This thesis contains no publications, either published or submitted for publication (if this box is checked, you may delete all the material on page 2)*

☒ *Some of the work described in this thesis has been published and it has been documented in the relevant Chapters with acknowledgement (if this box is checked, you may delete all the material on page 2)*

☐ *This thesis has publications (either published or submitted for publication) incorporated into it in lieu of a chapter and the details are presented below*

CANDIDATE'S DECLARATION

I declare that:

- I have complied with the Thesis Examination Procedure
- where I have used a publication in lieu of a Chapter, the listed publication(s) below meet(s) the requirements to be included in the thesis.

Name	**Signature**	**Date (dd/mm/yy)**
Gavin Douglas Ferguson		20/02/19

Table of contents

List of Figures

Publications from this thesis

Ferguson, G. Bridge, W. (2016) Glutamate cysteine ligase and the age-related decline in cellular glutathione: the therapeutic potential of γ-glutamylcysteine. *Archives of Biochemistry and Biophysics*, doi: 10.1016/j.abb.2016.01.017.

Manuscripts in preparation

***Ferguson, G.** Bridge, W. The glutathione system and the related thiol network in *Caenorhabditis elegans.*

***Ferguson, G**. Pickford, R. Bridge, W. Quantification of cysteine, γ-glutamylcysteine, GSH and GSSG in aged *Caenorhabditis elegans* using LC-MS/MS.

Presentations

Ferguson, G. Pickford, R. & Bridge, W. Profiling the thiol levels of the *de novo* glutathione synthesis pathway over the lifespan of *Caenorhabditis elegans*. The 24th Annual Meeting of the Society for Free Radical Research (Australasia), Gold Coast, Australia, December 5-7, 2016. (Poster presentation).

Ferguson, G. & Bridge, W. *Caenorhabditis elegans* as a model to investigate age-related changes in glutathione homeostasis. The 2nd Australian Biology of Ageing Conference, Rhodes, Australia, April 27-28, 2017. (Poster presentation).

Ferguson, G. & Bridge, W. The role of the glutamate cysteine ligase modifier subunit in regulating glutathione homeostasis in aged *Caenorhabditis elegans*. The inaugural Australian *C. elegans* meeting, Brisbane, Australia, October 23-25, 2017. (Poster presentation).

Ferguson, G. Pickford, R. & Bridge, W. LC-MS/MS quantification of thiol-containing metabolites within the *de novo* glutathione synthesis pathway over the lifespan of *Caenorhabditis elegans*. The 22nd International Mass Spectrometry Conference (IMSC) 2018, Florence, Italy, August 26-31, 2018. (Poster presentation).

Awards and Prizes

Australian Postgraduate Award (APA) Scholarship (Aug 2014- Feb 2018)

Adrian Lee Travel Scholarship (2017)

BABS Top-Up Scholarship (2016)

BABS Travel Scholarship (2016)

Grants from this work

Expansion of LC-MS/MS methods enabling reliable measurement of labile, low-molecular weight thiols in tissue samples. Pickford, R., **Ferguson, G.**, Bridge, W. The Mark Wainwright Analytical Centre Research Grants 2018 ($2,000).

Abbreviations

ARE	antioxidant response element
Cas9	CRISPR-associated protein 9 endonuclease
CHAPS	3-[(3-Cholamidopropyl)dimethylammonio]-1-propanesulfonate
CGC	*Caenorhabditis* Genetics Center
CI	chemotaxis index
CRISPR	clustered regularly interspaced short palindromic repeats
Cryo-EM	cryogenic electron microscopy
CysGly	cysteinylglycine
DNA	deoxyribonucleic acid
dsRNA	double-stranded RNA
DAABD-Cl	7-chloro-*N*-[2-(dimethylamino)ethyl]-2,1,3-benzoxadiazole-4-sulfonamide
DTNB	5,5-dithiobis(2-nitrobenzoic acid)
E01A2.1	*Caenorhabditis elegans* glutamate cysteine ligase modifier subunit gene orthologue
FUdR	5-fluorodeoxyuridine
GCEE	gamma-glutamylcysteine ethyl ester
GCL	glutamate cysteine ligase
GCLC	glutamate cysteine ligase (catalytic subunit)
GCLM	glutamate cysteine ligase (modifier subunit)
γ-GC	gamma-glutamylcysteine
gcs-1	*Caenorhabditis elegans* glutamate cysteine ligase catalytic subunit gene orthologue
γ-GT	gamma-glutamyl transpeptidase
GPx	glutathione peroxidase
GR	glutathione reductase
Grx	glutaredoxin
GS	glutathione synthetase
GSH	glutathione reduced
GSSG	glutathione disulfide
GST	glutathione-*S*-transferase
GS-x	glutathione-*S*-conjugate

h	hour(s)
H_2O_2	hydrogen peroxide
HCys	homocysteine
HPLC-MS/MS	high-performance liquid chromatography-tandem mass spectrometry
IGF-1	insulin-like growth factor-1
IPTG	isopropyl β-D-1-thiogalactopyranoside
K_i	inhibition constant
LMV	large multilamellar vesicles
LUV	large unilamellar vesicles
MAPK	mitogen-activated protein kinase
MLV	multilaminar vesicles
MVV	multivesicular vesicles
mRNA	messenger RNA
NAC	*N*-acetylcysteine
$NADP^+$	nicotinamide adenine dinucleotide phosphate
NADPH	reduced nicotinamide adenine dinucleotide phosphate
NEM	*N*-ethylmaleimide
NGM	nematode growth medium
$\cdot O_2^-$	superoxide
PCR	polymerase chain reaction
Prx	peroxiredoxin
qPCR	quantitative polymerase chain reaction
PI3H	phosphatidylinositol 3-kinase
ROS	reactive oxygen species
RNA*i*	RNA interference
RNS	reactive nitrogen species
sgRNA	single guide RNA
SD	standard deviation
SEM	standard error of the mean
SRM	selected reaction monitoring
SUV	small unilamellar vesicles
Trx	thioredoxin
TrxR	thioredoxin reductase
WT	wild-type

Acknowledgements

The receipt of an Australian Postgraduate Award is gratefully acknowledged for 3.5 years of this project. I would like to thank Wallace for the opportunity to complete my PhD in your lab. I am grateful for you providing me with the freedom to pursue my ideas, allowing me to experience absolute ownership of something that I believe other PhD projects would not have permitted.

I would like to thank my panel, Professor Ian Dawes and Associate Professor Kyle Hoehn, for their insight and advice throughout the performance reviews. I would like to express my gratitude to the Laboratory for Ageing Research for access to facilities and reagents. Thank you to the people from BABS and SoMS for their help throughout the project including, Tereza Grigoriadis, Jeff Welch, Lindsay Wu, Myung-Jin Kang, Nic Bentley, and Allison Arndt. A special thank you to Hannah Nicholas and Tessa Sherry from The University of Sydney for their assistance with the CRISPR/Cas9 experimental work presented herein. Thank you to all the members of the Zuryn lab at the Clem Jones Centre for Ageing Dementia Research (CJCADR), a part of the Queensland Brain Institute (QBI), for hosting me as a part of a collaborative effort. I gratefully acknowledge the support of the Adrian Lee Travel Award, granted through the School of BABS, for making the collaborative work at the CJCADR possible.

Mass spectrometric results were obtained at the Bioanalytical Mass Spectrometry Facility (BMSF) within the Mark Wainwright Analytical Centre of UNSW. A big thanks to Russell Pickford for your patience with any questions that I have had over the last couple of years. I would like to acknowledge the researchers at several other core facilities within the Mark Wainwright Analytical Centre that assisted with the work presented herein, including Rhiannon Kuchel from the Electron Microscope Unit (EMU), Emma Johansson

Beves from the Biological Resources Imaging Laboratory (BRIL), and Peter Geelan-Small and Brigid Betz-Stablein from Stats Central.

Finally, to all my friends and family who have supported me throughout the last 4 years. I am especially appreciative for a strong network of family that have always been there for me. None of this would have been achieved if it wasn't for you.

Abstract

The intracellular *de novo* glutathione (GSH) synthesis pathway is highly conserved throughout all aerobic eukaryotic organisms and involves two ATP-dependent enzyme-catalysed reactions. The rate-limiting and first reaction is mediated by glutamate cysteine ligase (GCL), which condenses glutamate and cysteine, to form γ-glutamylcysteine (γ-GC). Glutathione synthetase (GS) then catalyses the addition of glycine to form GSH. During mammalian ageing, a progressive decline in cysteine availability or the expression and activity of the GCL enzyme has been implicated to contribute to a corresponding decline in cellular GSH levels. GCL is a heterodimer composed of the catalytic (GCLC) and modifier (GCLM) subunits. Though GCLC contains all the substrate binding sites, its interaction with GCLM modulates the GCL holoenzyme's substrate affinity.

The short lifespan of *Caenorhabditis elegans* and its expression of GCLC (*gcs-1*) and GCLM (*E01A2.1)* orthologues makes it a suitable model to investigate age-associated changes in glutathione homeostasis. Using a novel LC-MS/MS thiol analysis method, a progressive pro-oxidising shift of the GSH/GSSG ratio with declines in both GSH and γ-GC levels was observed beginning from early adulthood, with no significant change in cysteine levels over the first 10 days of adulthood. This metabolomic approach provided evidence to support the hypothesis that the majority of the net loss of GSH levels in ageing worms is due to lowered GCL activity.

Using reverse genetics (RNA*i*), silencing of the *gclm* gene in worms was shown to correspond with a decline in GSH and an increase in cysteine levels. To understand the temporal requirements of the *gclm* gene for ageing, RNA*i* was conditionally induced in wild-type worms either immediately after hatching (through larval development) or

beginning at the start of adulthood. Silencing of *gclm* during larval development, increased the incidence of vulval rupture and thrashing movement during ageing. Considering the vulval rupture phenotype, the increase in thrashing rates of *gclm* knockdown worms were perhaps indicative of a compensatory stress-response. Pharyngeal pumping rates were lowered in *gclm* knockdown worms irrespective of the timing of RNA*i* induction.

Liposome-encapsulated γ-GC was fed to wild-type worms and *gcs-1* mutants to explore its therapeutic potential against chronic GSH depletion. Lifespan was significantly increased in the wild-types as was the brood size of the *gcs-1* mutants suggesting γ-GC is orally bioavailable and can bypass the rate-limiting GCL enzyme to directly act as a substrate for GS.

CHAPTER ONE

Introduction

1 Chapter One

1.1 Ageing

Ageing is the most significant risk factor for a wide range of diseases including cancer, neurodegeneration and cardiovascular diseases. Interventions directed towards treating the underlying ageing process as a preventive measure, rather than targeting the onset of individual chronic diseases, will require a shift in the current paradigm of how ageing is viewed in terms of disease (1). With global population growth expected to reach close to 10 billion by 2050 (2), coupled with the projected rise in the proportion of people over the age of 65, the higher demand for health services will lead to increased socio-economic strain. Efforts to delay morbidity and condense the fraction of life spent in poor health (3), also known as increasing healthspan, is a practical approach to address these issues of future generations. Interventions that increase the current healthspan trajectories will significantly lower the economic burden, healthcare challenges and societal impacts to meet the demands of an ever-increasing ageing population.

Biological ageing is the process by which a gradual decline of physiological integrity causes impaired function and increased vulnerability of the organism to morbidity and mortality (4). The hallmarks of ageing represent intrinsic biological processes conserved across diverse species, with several being exclusive to mammalian ageing (4). These include: genomic instability, telomere attrition, epigenetic alterations, loss of proteostasis, dysregulated nutrient sensing, mitochondrial dysfunction, cellular senescence, stem cell exhaustion, and altered intercellular communication (4). Understanding the interconnectedness between these individual factors and their relative contributions to physiological decline is one of the main objectives within the field of ageing research.

1.1.1 Ageing theories, oxidative stress and antioxidant systems

There is a diverse range of physiological changes associated with ageing. Several hypotheses attempt to clarify this complex biological process to facilitate our understanding of these changes that occur (5, 6). One of the more widely held theories, the *free radical theory of ageing*, first proposed in 1956 by Denham Harman, suggests that the causal mechanism of ageing is due to free radicals, formed endogenously from respiratory metabolism, having damaging interactions with cellular macromolecules (7). These free radicals include reactive oxygen species (ROS), which are partially reduced metabolites of molecular oxygen, that are mainly generated as by-products of oxidative phosphorylation (8). ROS were initially considered to be strictly toxic molecules and detrimental to cellular processes. Antioxidant defences are organised by a complex and integrated network of enzymes and small molecules that serve to protect against the damaging effects of ROS and other free radicals. Oxidative stress is defined as an imbalance involving excess production of ROS and/or limited availability of antioxidant systems to protect against potential cellular damage (9). Numerous studies have demonstrated that oxidative damage correlates with an increase in age (10). Oxygen-centred radicals, including superoxide ($\cdot O_2^-$) and the hydroxyl radical ($\cdot OH$), involve one-electron transfer, whereas oxygen-centred non-radicals, such as hydrogen peroxide (H_2O_2), are involved in two-electron transfer (11). The process of oxidative stress is thought to predominantly involve non-radical (>99%) reactions rather than the commonly perceived free radical reactions (<1%) (12, 13). In general, Harman's original free radical theory has since been adapted to include the role of all forms of ROS, reactive nitrogen species (RNS), and other free radicals that may contribute to oxidative stress (14).

Interestingly in more recent discoveries, ROS have been shown to play dual functions within aerobic cells, serving as either beneficial signalling molecules in normal cellular processes, or as detrimental oxidising agents that can damage cellular macromolecules, such as proteins, lipids or nucleic acids (15-17). While there is frequently a correlation between oxidative damage and lifespan, studies across species appear to contradict the free radical theory by reporting cases in which oxidative damage and lifespan are uncoupled (18, 19). Interestingly, increasing exposure to oxidants can also increase lifespan (20). These findings provide further evidence for the key roles of various ROS in the signalling process.

The most intuitive approach to delay the progression of ageing and mitigate the accumulation of oxidative damage by replenishing cellular antioxidant defences has been inconsistent in various organisms (21). For example, it has been suggested that the recommended dietary intake of Vitamin C is perhaps too low to protect from oxidative stress based on human clinical data (22). Others have shown that excess administration of endogenous antioxidants, including Vitamin C and E, may lead to pro-oxidative effects under certain conditions (23, 24). Conversely, the hormesis hypothesis describes the phenomenon by which a mild stress, such as an increase in ROS production, can induce a protective response against subsequent stresses where the protection afforded exceeds the initial damage caused by the insult (25). The relationship between antioxidant defences and ROS and their effect on ageing is indeed complex. Accordingly, research investigating the ageing process needs to consider the dual roles of ROS and free radicals as oxidative stressors/signalling molecules and their contributions to the fluctuations in cellular redox potential (26-28).

1.1.2 Influence of the redox environment with ageing

The *redox theory of ageing* postulated by Jones in 2015, integrates several key concepts related to the free radical theory that explains the physiological process resulting from disruption of the redox network, in addition to the cellular damage resulting from an imbalance of pro-oxidants and antioxidants (29). The redox environment is the overall spatiotemporal balance of oxidation-reduction systems within the integrated compartments of the cell, tissues and the organism as a whole (30). Redox systems are regulated under dynamic, non-equilibrium conditions, which become progressively oxidised in the ageing process (31, 32).

The redox theory of ageing describes the role of electron transfer to provide energy currencies to support metabolism and coordinate the overall organisation of living organisms, including cell structure and function (29, 33, 34). The cellular redox state is determined by the activity of relative ratios of cellular and extracellular redox couples. The two major systems, the pyridine nucleotide ($NADH/NAD^+$, $NADPH/NADP^+$) and thiol systems differ considerably in organisation but both co-ordinate the cellular redox environment (30). The thiol system includes the low molecular-weight thiol/disulfide couples such as glutathione (GSH/GSSG) and cysteine/cystine, and the oxidised/reduced states of redox enzymes that have cysteine residues at their active-sites such as thioredoxins, glutaredoxins (32), and peroxiredoxins (35, 36). All these play major roles in the maintenance of the cellular redox environment. The electron carriers NADH and NADPH support metabolic requirements and maintain the redox status of the cell. The $NADH/NAD^+$ redox couple assists in ATP synthesis, while the $NADPH/NADP^+$ system supports the maintenance of the thiol system which includes recycling of GSH from GSSG (37). The oxidation-reduction state of a given redox couple, can be calculated by

the Nernst equation. The redox state of the $NADH/NAD^+$ and $NADPH/NADP^+$ couples operate at equilibrium, whereas the GSH/GSSG couple operates at low flux rather than near-equilibrium. When calculating the redox status, only an estimation of the ratio of the oxidised and reduced forms of the NAD and NADP couples are necessary, while absolute concentrations of GSH and GSSG are both required for calculations using the Nernst equation (31).

Glutathione (GSH) is a ubiquitous intracellular thiol tripeptide (γ-L-glutamyl-L-cysteinyl-glycine), synthesised in the cytosol of all eukaryotic cells (38). GSH is often referred to as the major antioxidant of the cell, though the functions of GSH extend beyond its antioxidant properties to many other essential cellular processes, including detoxification of xenobiotic compounds, modulation of cell proliferation, transport and storage of cysteine and maintenance of redox status (38-40). GSH plays a central role in the thiol-based redox network (Figure 1-1). Current evidence suggests that the cellular redox environment is governed by the enzymatically-controlled reactions that facilitate the turnover of GSH rather than by the thermodynamic control of the GSH/GSSG couple (41). This challenge of the accepted view that the GSH/GSSG couple acts as the major redox buffer in the cytosol is supported by *in vivo* studies that utilise the application of genetically encoded redox sensors in *Caenorhabditis elegans* to understand the spatial patterning of cellular redox potentials (42). The authors concluded that the GSH/GSSG couple amplifies small changes in its oxidation state to large changes in redox potential by the oxidation of cysteine residues embedded in proteins, rather than having a direct buffering effect on the cellular redox potential.

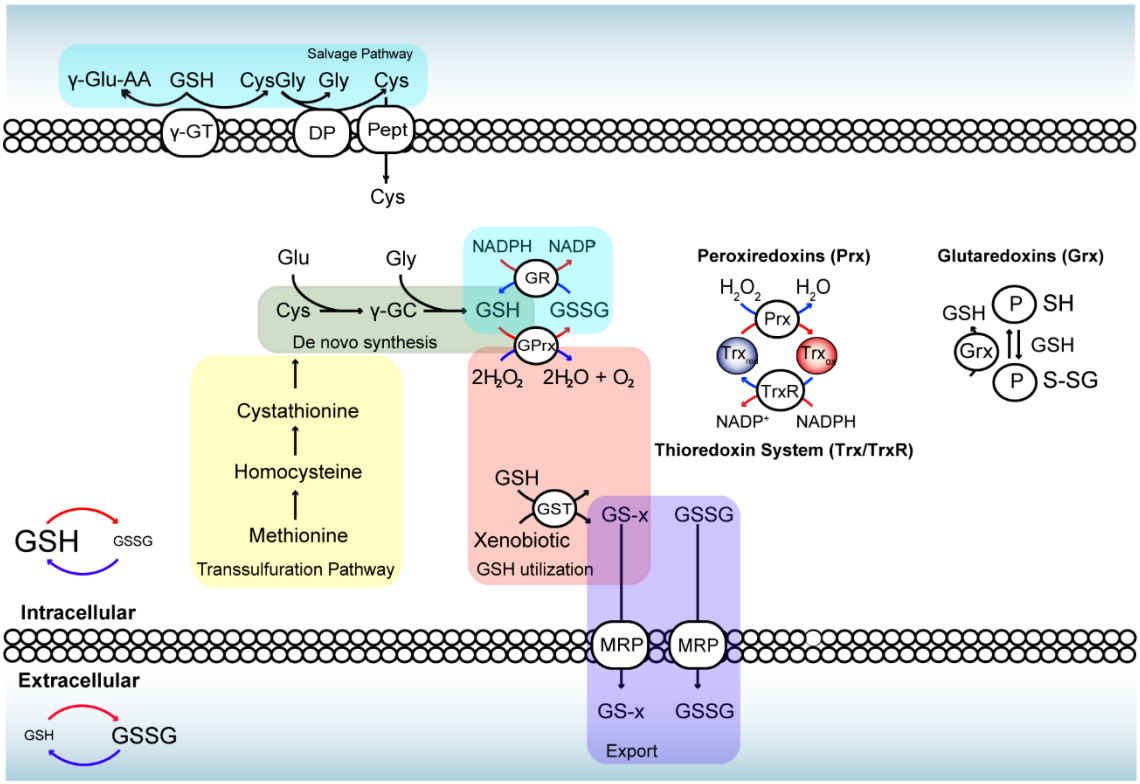

Figure 1-1. Thiol-based redox network in eukaryotes

Glutathione (GSH) is synthesised in the cytosol via the de novo *pathway (green box). The GSH salvage pathway (light blue boxes) occurs intracellularly via the reduction of GSSG by glutathione reductase (GR), and extracellularly through γ-glutamyl transpeptidase (γ-GT) mediated degradation of exogenous GSH. The γ-GT activity generates cysteinylglycine (CysGly) and a gamma-glutamyl amino acid (γ-Glu-AA). CysGly is hydrolysed by dipeptidases (DP) and the Cys is taken up by peptide transporters (Pept) to become available for* de novo *GSH synthesis. The transsulfuration pathway provides an alternate source of cysteine via methionine. GSH is utilised by several major GSH-dependent enzymes; glutathione peroxidases (GPx) to reduce hydroperoxides; glutathione S-transferases (GST) to solubilise xenobiotics by the formation of GSH conjugates (GS-x). These GSH-conjugates, and GSSG, can then be exported from the cell via multidrug resistance proteins (MRP). Glutaredoxins (Grx) are primarily responsible for the de-glutathionylation of cysteine residues (PS-SG) present on proteins. The NADPH-dependent thioredoxin system (Trx/TrxR) functions by reducing peroxiredoxins (Prx) which are usually bound together as oxidised dimeric forms owing to their peroxidase activity.*

1.2 Thiol-based redox signalling

Thiol-based redox signalling occurs as part of normal cellular processes in response to elevated free radical and ROS production, which can affect many essential cellular processes including; phosphorylation pathways, gene transcription, cytoskeletal organisation and ion channel activity (43-45). Protein thiols undergo post-translational oxidative modifications including, *S*-glutathionlyation, *S*-nitrosylation and metal binding at specific cysteine residues that can affect redox signalling (41, 46, 47). The abundance of cysteine residues in proteins increases with organism complexity, ranging from ~0.50% in archaea to ~2.25% in mammals (48), and is postulated to reflect the evolution of cysteine's signalling and control functions (49, 50).

The distinction between redox signalling-thiols and redox-sensing thiols has recently been discussed by Jones (51). Redox-signalling thiols are involved in specific signalling processes in which a redox element initiates an activation or inhibition signal and comprise a relatively small number of total cysteine residues (within the cysteine proteome) compared to redox-sensing thiols (52). Redox-sensing thiols on the other hand, mediate global protein thiol-dependent control by altering the rates or conditions in which a signalling pathway can function without fundamentally altering the signalling mechanism (Figure 1-2) (33, 51, 52). Current methods are limited for a systems biology approach to understand redox-sensing thiols and thus they remain poorly defined. This technical difficulty is largely due to the reactivity of thiols differing by several orders of magnitude (52).

Disruption of the cell's ability to effectively facilitate the redox environment due to aberrations in the optimal function of both redox-signalling and redox-sensing thiols may possibly have a causative role in the ageing process that explains, at least in part, the

nuances of the redox theory of ageing (13, 29, 32, 53). There remains much to be elucidated about the functional roles of the respective residues of the cysteine proteome in redox signalling and how these are affected during ageing.

The human cysteine proteome contains an estimated 214,000 unique residues, comprising approximately 2% of the total proteome (12). The majority of cysteine residues support redox-signalling, largely by non-radical two-electron transfer, that coordinate and integrate functional networks in the redox circuitry system (12). A recent review has also discussed the possible role that free radicals have in signal transmission of thiol-based signalling (43). In the thiol network, hydrogen peroxide (H_2O_2) has a notable role as a second messenger in transmitting the signal regardless of which oxidant initiates the signal (43, 54). The extent of the involvement of H_2O_2 as a second messenger is not yet fully understood, especially in the context of ageing.

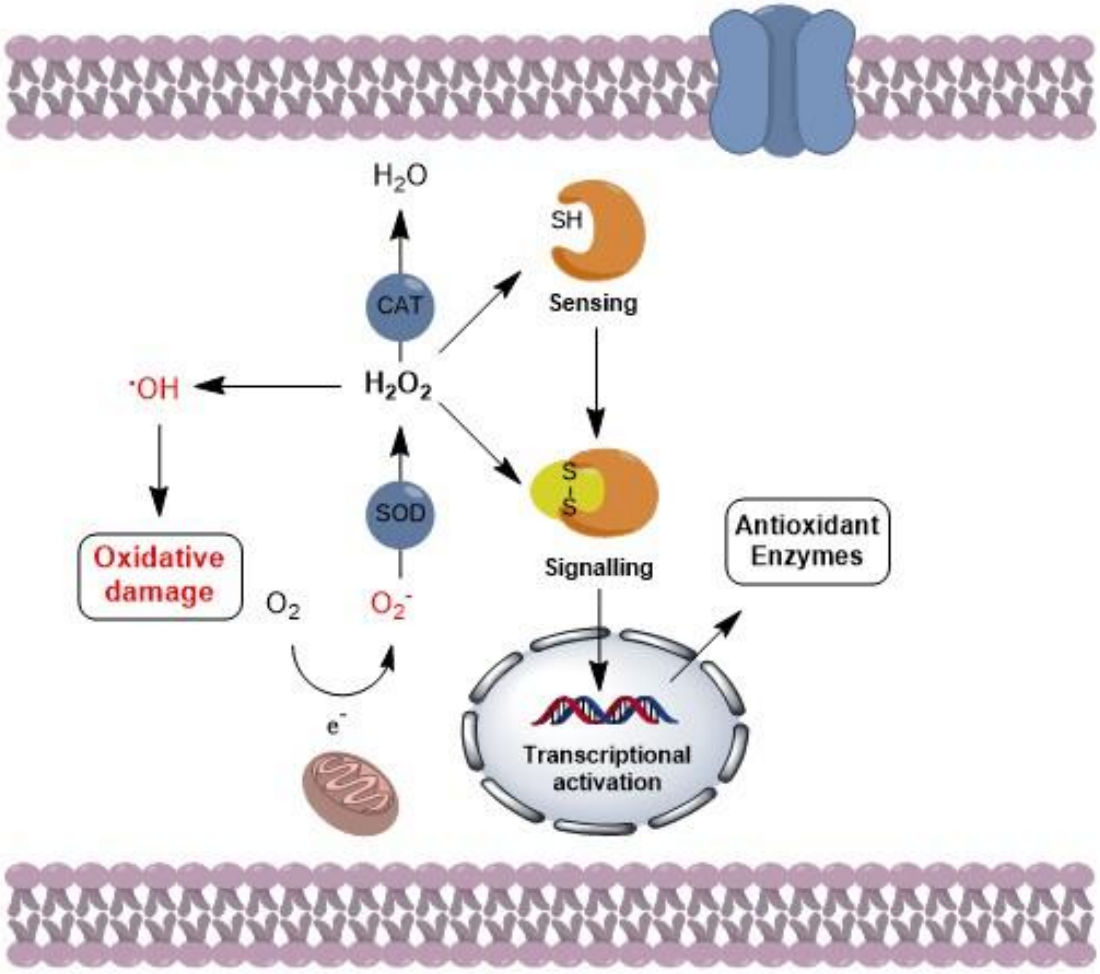

Figure 1-2. Redox sensing and redox signalling thiols

Redox signalling thiols are thought to comprise a small subset in cell signalling, while a larger number of redox sensing thiols coordinate cell functions in response to redox changes. The concept of redox-sensing is that modification of these sensing thiols provides means to alter protein activity which can govern the global signal activities without fundamentally altering the signalling mechanism per se. *The distinction that can be made between the two is that redox-signalling thiols are directly involved in a signalling pathway, and redox-sensing thiols function in regulation and coordination of cell signalling but are not obligatory to the mechanism.*

1.2.1 Reversible and irreversible oxidative modifications

The reversible oxidation of protein thiols can act as 'redox switches' that control a range of functions of the protein, including regulation of protein activity, stabilisation of protein structure, formation of protein activation complexes, and control of protein distribution (51, 55). The reactivity of the thiol group of cysteine residues plays a role in determining the catalytic and structural roles of a protein. The interdependence of the structural and chemical characteristics of the cysteine residue such as, the oxidation state of the sulfur atom, the bond lengths and angles of the cysteine residue, the structural location of the residue within a protein, and its properties as an acid/base or as a nucleophile/electrophile all influence the reactivity of the thiol (49). The redox states of the sulfur atom in cysteine residues can exist as a thiol, a thiyl radical, a disulfide, or as a sulfenic-, sulfinic-, or sulfonic acid (Figure 1-3).

Protein thiols that form intra- or intermolecular disulfide bonds can be classified as catalytic or structural disulfides based on their half-life. Short-lived disulfides are usually involved in catalytic redox cycles and once formed can be rapidly broken. Structural disulfides, formed under partially oxidising conditions in the endoplasmic reticulum, typically stabilise a protein in a defined tertiary or quaternary structure until the protein is degraded. Allosteric disulfide bonds are a different type of disulfide bond that can control protein function by the formation or breaking of a disulfide bond at an allosteric site of the protein, resulting in a conformational and/or functional change at another distinct site of the protein (56).

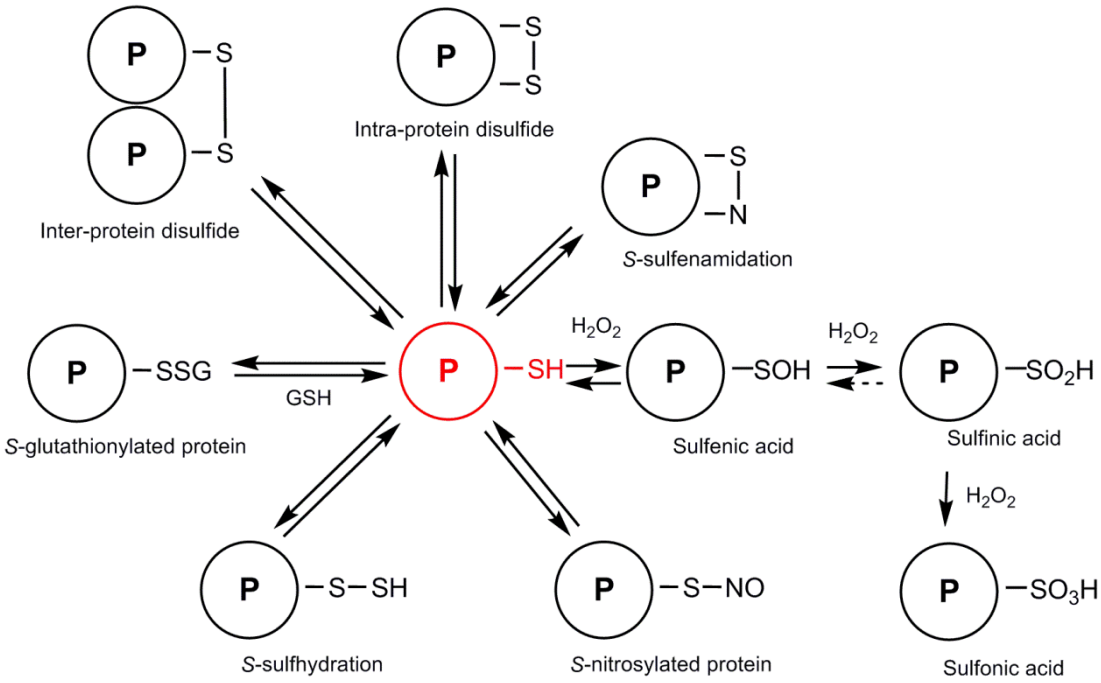

Figure 1-3. Summary of protein thiol modifications

Protein thiols can undergo a variety of oxidative modifications, including reversible and irreversible redox states that have roles in the thiol-mediated signalling network. It is proposed that oxidative modifications do not occur at random, but are selective and dependant on factors such as, the oxidant that is in excess in the system, the antioxidant system compromised, and the structural proximity of the thiols. Protein S-glutathionylation is proposed to help sustain the thiol-mediated signalling pathway in ageing to protect against damaging irreversible modifications. Prolonged exposure to oxidants can result in irreversible modifications such as S-sulfinic acid or S-sulfonic acid, which are formed by an excess of the second messenger, H_2O_2.

1.3 Glutathionylation: A possible role in the ageing process?

Many intracellular redox responses involved in signalling and protein function are regulated by protein *S*-glutathionylation, which forms disulfide bonds between GSH and the cysteine residues of proteins. In an early review by Klatt and Lamas (57), the potential roles for *S*-glutathionation in stress signalling pathways and in the adaptive cellular response to oxidative and nitrosative stress were initially discussed. Since then, the mechanistic role of protein *S*-glutathionylation has gained prominence with many proteins now known to be modulated by this post-translational modification (58, 59). Protein *S*-glutathionylation can either activate or inhibit the activity of a range of proteins, including enzymes, mitochondrial and cytoskeletal proteins, signalling molecules, transcription factors, heat shock proteins (HSPs), and ion channels. The resulting modifications serve as dynamic regulatory events in the control of the cellular redox environment (60-62). In the case of enzymes, where the target cysteine is located at the active site, *S*-glutathionylation can result in inhibition of the enzyme activity (63). Some proteins can be *S*-glutathionylated at more than one cysteine residue, allowing for their activities to be modulated in a site selective manner (61). *S*-Glutathionylation also prevents the irreversible oxidation of cysteine residues and thereby conserve the functions of the redox signalling pathways (64). Other low-molecular weight thiols, such as cysteine, homocysteine and cysteinylglycine can also form protein-mixed disulfides which can prevent irreversible oxidation. *S*-Glutathionylation is recognised as the predominant intracellular mechanism of reversible cysteine modification due to the relatively high cellular concentrations of GSH compared to other thiols (61). Proposed mechanisms by which thiol moieties of proteins can form glutathione mixed-disulfides

(*S*-glutathionylation) include, thiol-disulfide exchange, and through other intermediates such as sulfenic acid, sulfenylamide, thiyl radical, thiosulfinate and *S*-nitrosylation (65).

1.3.1 Glutaredoxins: catalysts of reversible de-glutathionylation reactions

The reversal of protein *S*-glutathionylation (de-glutathionylation) involves the removal of the GSH moiety from the cysteine residue of the protein and is most notably catalysed by the family of small enzymes known as glutaredoxins (GRx) (61). Protein *S*-glutathionylation is recognised as an efficient regulator of redox signal transduction largely due to the reversibility of the reaction (60). Though it is now recognised that *S*-glutathionylation is involved in redox signalling, the dynamics of the enzymatic control by the redox network that lead to *S*-glutathionylated proteins remain unclear (58). The glutaredoxin enzymes have been commonly accepted as the main catalysts of reversible protein de-glutathionylation, which is analogous to the post-translational modifications of phosphatases in dephosphorylation reactions (61). The activities of the two key human glutaredoxin isoforms, Grx1 (predominantly cytosolic) and Grx2 (mitochondrial) are vital to the reversible signalling response of protein *S*-glutathionylation in several tissue types by mediating the de-glutathionylation reaction (66, 67). Additional alternate pathways leading to protein de-glutathionylation have also been proposed, however these remain poorly characterised (58).

1.3.2 Implications of *S*-glutathionylation in ageing and disease

Changes in protein *S*-glutathionylation influence many cellular regulatory events intrinsically linked with the ageing process (68). While the impairment of protein *S*-glutathionylation has not been extensively studied in the context of age-related GSH depletion, a recent review has outlined several major neurogenerative diseases that are

linked with changes in protein *S*-glutathionylation (69). It is imperative to understand how altered GSH metabolism leads to changes in thiol-mediated signalling, and to elucidate the mechanisms by which the age-associated changes in GSH control the degree and specificity of protein *S*-glutathionylation targets. This will assist to determine how central this post-translational modification is in the context of cellular redox signalling. Currently, there are no studies that have investigated the global changes in cellular protein *S*-glutathionylation in human ageing. However, the concentrations of several low-molecular weight thiols (including cysteine, cysteinylglycine, homocysteine and GSH) and the concomitant levels of *S*-thionylated proteins (i.e. the sum of all forms of *S*-thionylation) to total protein thiol residues have been measured in the plasma of ageing humans (70, 71). In two landmark studies testing plasma levels of *S*-thionylated proteins of healthy individuals (20-93 years), *S*-cysteinylated and *S*-homocysteinylated proteins were shown to increase significantly in aged individuals compared to no significant difference in *S*-glutathionylation modification of proteins between the age groups (70, 71). Cysteine is the most abundant plasma thiol, with concentrations two orders of magnitude higher than GSH in humans. Accordingly, the authors concluded that cysteine is the main low-molecular weight thiol involved in protecting plasma proteins by *S*-thionylation, whereas intracellular proteins are predominantly *S*-glutathionylated due to the high intracellular GSH levels (70). This suggests that intracellular protein *S*-glutathionylation possibly increases in a similar manner to that of the extracellular *S*-cysteinylation levels, which may lead to discoveries for the fate of the decline in free thiol GSH levels with ageing.

1.4 Glutathione

1.4.1 Synthesis

Cellular GSH is maintained by the *de novo* synthesis and the salvage pathways (72). *De novo* synthesis of GSH occurs in the cytosol and involves two consecutive ATP-dependent reactions (Figure 1-4). The first is catalysed by glutamate cysteine ligase (GCL) to produce γ-glutamylcysteine (γ-GC) (73). The second, catalysed by glutathione synthase (GS), condenses γ-GC with glycine to produce GSH. The activity of the GCL enzyme is regulated by non-allosteric feedback inhibition exerted by GSH (74). Unlike GCL, no feedback control mechanisms have been observed that affect the specific activity of the GS enzyme (38). During neutralisation of ROS and free radicals, GSH donates an electron, with two of the resulting GSH molecules becoming oxidised through the formation of a disulfide bond to form glutathione disulfide (GSSG). The GSSG may then be excreted from the cell or recycled back into two molecules of GSH by the activity of the NADPH-dependent glutathione reductase (GR) enzyme to maintain GSH levels at >98% of the total cellular glutathione pool (75, 76).

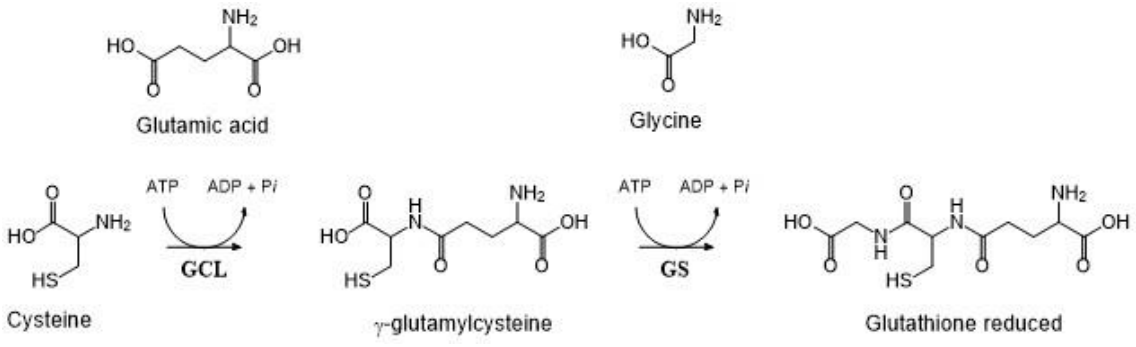

Figure 1-4. The *de novo* GSH synthesis pathway

For the extracellular salvage pathway, the membrane-bound γ-glutamyl transpeptidase (γ-GT), transfers GSH's γ-glutamyl moiety to a free amino acid, commonly cystine, releasing cysteinylglycine in the process. The cysteinylglycine is then further broken down by dipeptidases located on the outer surface of the cell membrane to generate cysteine and glycine which are then taken up by the cell (38). GSH is both the major antioxidant of the cell and the main regulator of thiol redox status via the GSH/GSSG redox couple. A consistent underlying index of ageing is a decline in the cellular levels of GSH and/or a pro-oxidising shift in the GSH/GSSG redox couple. The role of the GSH/GSSG redox couple ratio in maintaining redox status and its decline with ageing has been previously reviewed (32). The ratio is the primary determinant of the redox status of the cell due to the GSH pool being approximately three to four orders of magnitude higher in abundance than other major redox couples, such as the pyridine nucleotide and related thiol couples (32, 77).

1.4.2 Age-related loss in GCL regulation

Glutamate cysteine ligase (GCL), also known as γ-glutamylcysteine synthetase (GCS), is a heterodimeric holoenzyme comprising a catalytic (GCLC) and modifier (GCLM) subunit. Across several divergent species, including human, mouse and *Drosophila melanogaster* both subunits are encoded on separate chromosomes (78, 79). The specific activity of GCL is a major determinant of the rate of GSH synthesis and homeostasis. Changes in GCL activity can result from regulation at multiple levels affecting both catalytic and modifier subunits together or each individually (Figure 1-5). Studies examining the regulation of synthesis of each of the two subunits have identified that they are independently regulated and display cell-specific differences in both constitutive and inducible expression, presumably due to the difference in loci of each subunit gene (80).

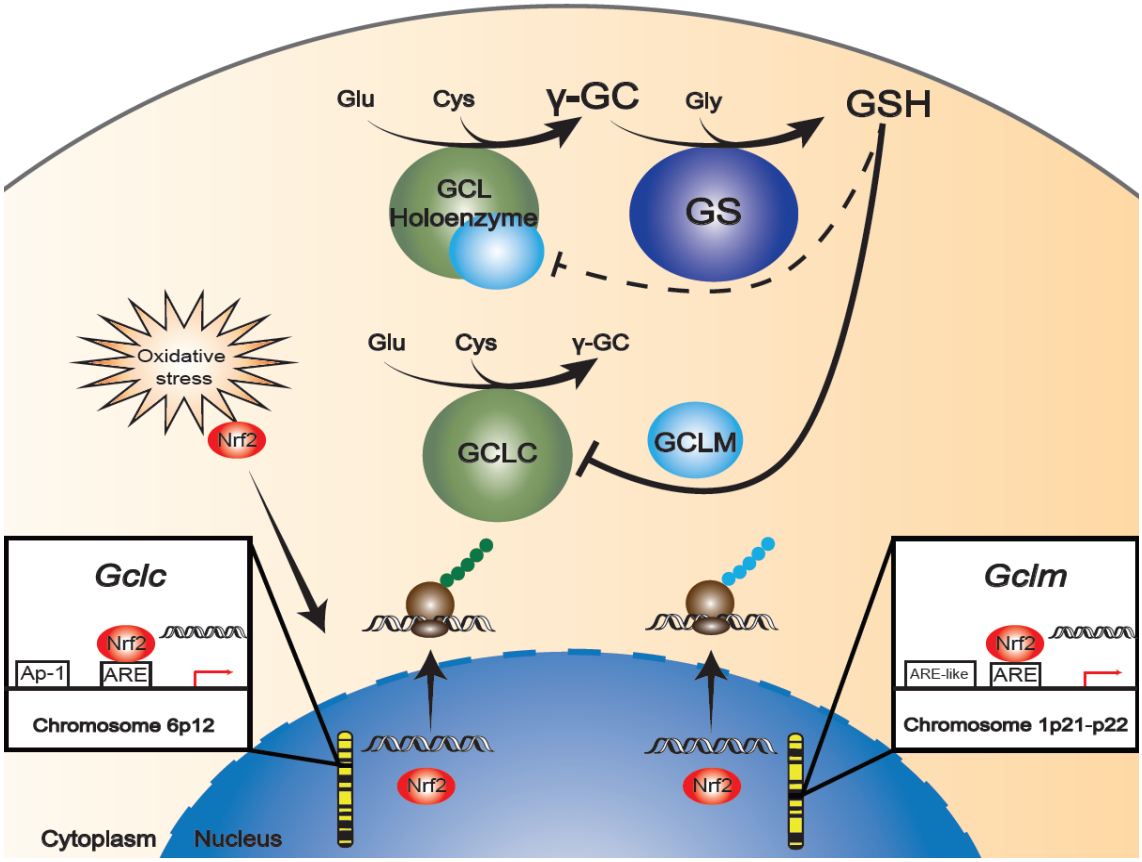

Figure 1-5. Cellular regulation of human glutamate cysteine ligase (GCL)

The GCL enzyme is regulated at multiple levels. The Gclc *gene is located on chromosome 6p12 and* Gclm *on chromosome 1p21-p22. Transcription of each subunit can be individually induced with the mRNA of each subunit able to be post-transcriptionally controlled by different signalling pathways. Holoenzyme formation is determined largely by the availability of the limiting GCLM protein subunit. Upon holoenzyme formation, the production of γ-GC (indicated by larger lettering) increases due to the decrease in K_m for glutamate and ATP, while the K_i for GSH increases. The decrease in the inhibitory effect of GSH on GCL is represented by dashed-lines of GCL holoenzyme inhibition compared to full lines for the GCLC subunit alone. The Nrf2 transcription factor remains localised in the cytosol in the absence of oxidative stress. When the cell is subjected to oxidative stress, Nrf2 translocates to the nucleus where it can induce both the* Gclc *and* Gclm *genes by binding to their respective antioxidant response elements (AREs).*[1]

[1] This figure was published in Ferguson, G & Bridge, W. (2016) Glutamate cysteine ligase and the age-related decline in cellular glutathione: the therapeutic potential of γ-glutamylcysteine. *Archives of Biochemistry and Biophysics*. 593, 12-23.

The GCLC active site facilitates the formation of the peptidic amide between cysteine's amino group and glutamate's γ-carboxyl group (81). Although the GCLC subunit contains all the substrate and cofactor sites required to catalyse the production of γ-GC, its interaction with GCLM both increases the K_i for inhibition by GSH and enhances the enzyme activity by lowering the K_m for glutamate and ATP, without lowering it for cysteine (82). The inhibition constant (K_i) is defined as the concentration of inhibitor required to lower the maximum reaction rate (V_{max}) to half of the uninhibited rate observed in the presence of a low substrate concentration. The lower the K_i, the lower the concentration of inhibitor required to decrease the rate of γ-GC formation. The lowering of K_m for glutamate and ATP indicates that the enzyme has a higher binding affinity for the substrates upon holoenzyme formation. Though it had been initially assumed that the GCLM subunit did not alter the catalytic properties of the GCLC subunit (83), it has since become more apparent that the modifier subunit plays a critical regulatory role in the overall activity of the holoenzyme across phylogenetically divergent species (79, 82, 84-87). Work that investigated the age-related changes of kinetic activity of GCL in the housefly (*Musca domestica*) has supported the hypothesis that *de novo* GSH homeostasis declines with age in the organism primarily due to a decline in GCL activity (88). Longevity studies in *D. melanogaster* have observed a 50% increase in lifespan in flies that had the GCLC subunit overexpressed in neuronal cells, with an increase up to 24% observed when the GCLM was expressed systemically in the organism (89-91).

The majority of *in vivo* research investigating the age-related decline in GCL activity has been conducted in rodents. Work published in 2000 reported for the first time, an age-related decrease of the mRNA and protein levels of GCLC and GCLM in the livers, kidneys and lungs of aged rats (24 months) compared to young rats (3 months) (92).

Numerous studies have since reported the age-related decline of GSH to be correlated with a decline in the expression and activity of the GCLC and/or GCLM subunit levels. A decline in the activity of the nuclear factor erythroid 2-related factor 2 (Nrf2 transcription factor) has been reported to be involved in the transcriptional mechanisms that contribute to the decline in GCL expression in the livers of aged rats (93). It was observed that ageing results in a 50% loss in total and nuclear Nrf2 levels, accompanied by a reduced binding capacity of Nrf2 to the antioxidant response element (ARE) (93). The impairment of the Nrf2 transcriptional activation activity currently remains the only molecular mechanism elucidated that explains, at least in part, the age-related decline of GCL in mammals. Defining these unknown mechanisms of the age-related decline in GCL regulation may inform our understanding of the aetiology of many age-related diseases and assist in formulating appropriate therapeutic strategies.

There appears to be tissue-specific differences with the basal regulation of both GCL subunits. The GCLC:GCLM ratios in mice have been reported to range from approximately 2:1 in heart and spleen tissue to 7:1 in neuronal tissue (85). These lower relative levels of neuronal GCLM may explain the role of the modifier subunit in age-related diseases and describe the susceptibility of neuronal tissue to oxidative stress in age-related disorders. The degree of disproportionate regulation for the two subunits can influence the activity of GCL under various cellular stresses (94). Studies conducted in the ageing rat brain for example, indicate that changes leading to a decrease in GCLM expression are a major cause of the decline in GSH levels in the cerebellum, cerebral cortex, and hippocampus (95).

1.4.3 The therapeutic potential of γ-GC to increase cellular GSH

Due to its potential to bypass the rate-limiting step of the *de novo* GSH synthesis pathway, we have proposed that the most immediate precursor to GSH, γ-GC, be explored as a therapeutic strategy to elevate GSH levels with ageing (96). In 1983, Anderson and Meister were the first to report on the ability of γ-GC to augment cellular GSH levels, demonstrating GSH increases in the kidneys of mice following intraperitoneal γ-GC administration (97). Further studies have shown that treatment of various cell types with γ-GC and its esterified form, gamma-glutamylcysteine ethyl ester (GCEE), can protect against oxidative damage by increasing the intracellular levels of GSH (98-105). Evidence suggests that γ-GC exhibits antioxidant properties independent of GSH due to the sulfhydryl group of the cysteine residue which is conserved in both γ-GC and GSH. It has been known for several decades that γ-GC can also serve as a substrate for several isoforms of rat liver glutathione *S*-transferases (GSTs), indicating that the immediate GSH precursor can potentially have a role in GSH-dependent reactions (106). Initial evidence indicating that γ-GC exhibits antioxidant protection was in yeast models lacking the *gsh2* gene which codes for GSH synthetase (GS), this resulted in γ-GC accumulation and compensatory protection under conditions of oxidative stress (107). Studies in humans with an inherited GS deficiency, have demonstrated that endogenous γ-GC accumulation affords protection against oxidative stress in fibroblast cells, providing further evidence of the antioxidant capacity of γ-GC (108). More recent studies have demonstrated the ability of γ-GC to maintain redox control, both *in vitro* and *in vivo* cell models, by acting as a glutathione peroxidase-1 (GPx1) cofactor during detoxification of mitochondrial H_2O_2 (109).

Intracellular γ-GC concentrations are exceedingly low in the presence of GS (110). Therefore, any exogenously administered γ-GC taken up actively or passively via putative dipeptide transporters on the cell membrane should effectively bypass any dysfunction of the GCL enzyme (111). It could be expected that all γ-GC taken up by cells would be converted to GSH by the uninhibited and constitutively expressed GS, providing that glycine and ATP do not become limiting. The degree to how much cellular GSH levels could be increased by γ-GC administration would be determined by the rate of γ-GC uptake and the rate of GSH consumption. A recent human clinical study in healthy individuals has demonstrated that orally administered γ-GC can significantly increase lymphocyte GSH levels suggesting it has systemic bioavailability (112).

Administration with γ-GC offers potential advantages over other substrate-based approaches, such as treatment with cysteine or GSH. Cysteine supplementation feeds directly into the rate limiting GCL enzyme, which is unfavourable if the activity of the GCL enzyme declines with age. While the high intracellular concentration of GSH making passive cellular uptake thermodynamically unfavourable, along with the presence of the membrane-bound γ-GT enzyme, and absence of GSH transporters in the majority of cell types, makes administration of exogenous GSH an ineffective strategy for increasing cellular GSH levels above homeostasis (96).

1.5 *Caenorhabditis elegans* as a model organism for human ageing

Caenorhabditis elegans has become a prominent model to study various aspects of ageing and longevity due the advantages of genetic analysis, a well characterised larval lifecycle, and a relatively short median lifespan of approximately 2-3 weeks (Figure 1-6). After embryonic development and egg hatching, the life cycle of the worm includes a series of four larval stages (L1-L4). During these stages, an alternative, intermediary stage (known as dauer) after L2 can occur resulting in the worm entering a state of arrested development. Dauer arrest is usually in response to environmental stresses such as overcrowding or starvation. Following larval development, there are four phenotypically distinct stages of the adult lifespan (113). Stage I is the period of self-fertile reproduction. Stage II is defined as a post-reproductive period and is characterised by fast body movement. Stage III commences with reduced motor activity and proceeds to the end of the pharyngeal pumping. Stage IV begins at the period of minimal motor activity to the end of the lifespan (113).

The initial work in *C. elegans* that led to its adoption as a popular model for ageing began with studies investigating mutations in genes of the insulin-like growth factor (IGF-1) signalling pathway. A mutation in the *age-1* gene, which encodes for the phosphatidylinositol-3-OH kinase (PI3K) orthologue in the worm, was observed to increase the mean lifespan by 40% and the maximal lifespan by 60% (114). Later investigations revealed that knocking down the *daf-2* gene, which encodes for the IGF-1 receptor (upstream of *age-1*), results in the decline in signalling of the pathway, doubling the lifespan of the worm compared to the wild-type (115). Many other significant findings have since been made regarding the influence of signalling pathways and molecular mechanisms on longevity in *C. elegans* (116).

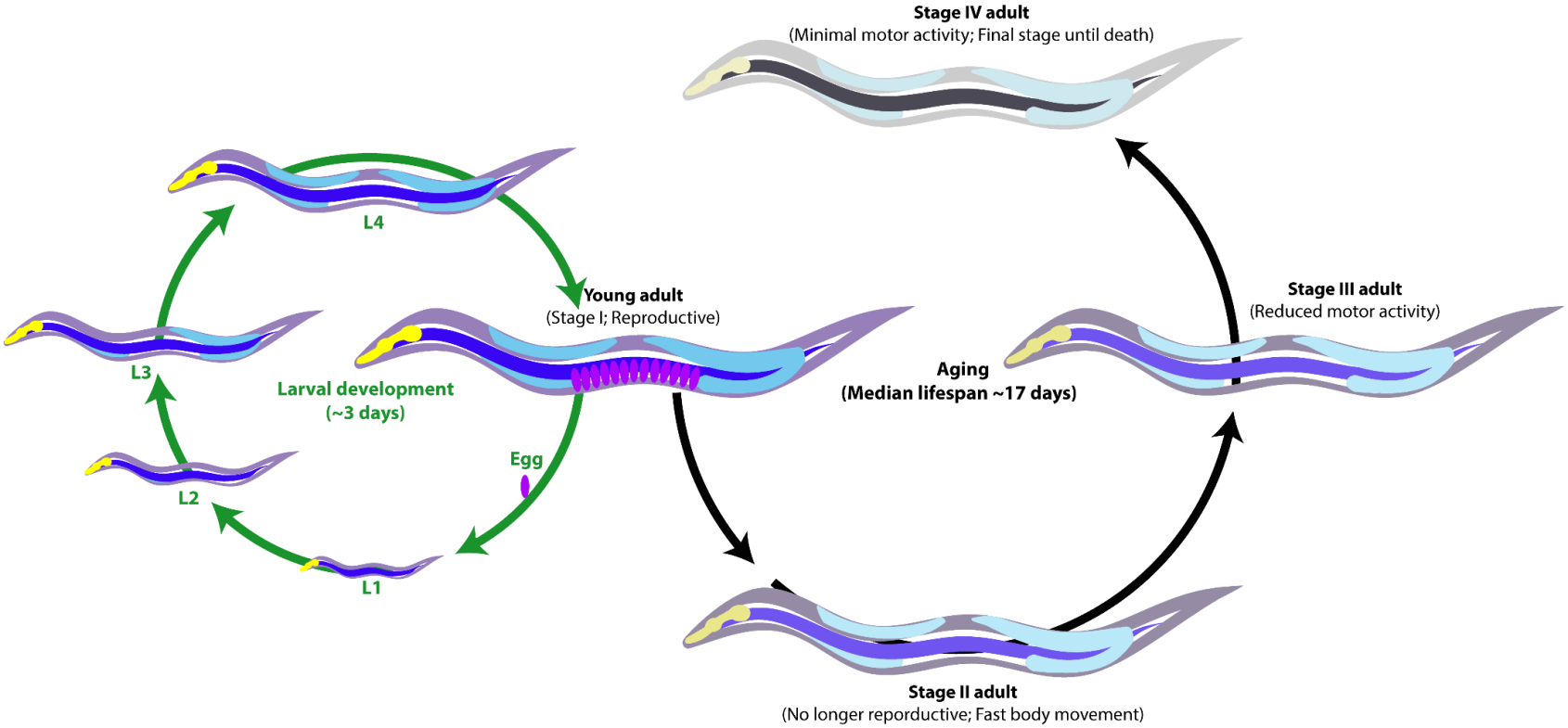

Figure 1-6. Life cycle and age-related changes of wild-type *Caenorhabditis elegans*

The majority of C. elegans *are hermaphrodites with only a small proportion of male (<0.1%) produced each generation. Under controlled laboratory conditions, the common food source used throughout most studies is* Escherichia coli *OP50. To reach the gravid adulthood, the larvae must pass through four distinct larval stages (L1-L4).*

Once DAF-2 becomes activated, it initiates a signalling kinase cascade (Figure 1-7), resulting in the phosphorylation and consequently cytoplasmic retention of DAF-16 (117). Downstream of the DAF-2 receptor are a series of highly conserved proteins, including the AGE-1 and the FOXO family transcription factor DAF-16 (118). In the *daf-2* mutants, the reduced signalling in this pathway leads to the translocation of DAF-16 to the nucleus where it is constitutively active and able to induce the expression of a variety of stress-related genes that control heat shock proteins (HSPs), pathogen resistance, metabolism, transcriptional repression, protein degradation and antioxidant defence (119, 120). The involvement of DAF-16 in determining the lifespan of the worm is illustrated in *daf-16* mutants which are severely short-lived, show increased sensitivity towards paraquat-induced oxidative stress, and exhibit higher protein carbonylation levels (121, 122). Mutations in the *C. elegans* insulin-signalling pathway have indicated that an increase in oxidative stress protection may contribute, at least in part, to the lifespan extension. However, the roles of the DAF-16-regulated genes associated with this increase remain unclear, as does the mechanisms by which antioxidant systems function in the insulin-like signalling pathway. Besides being used as a model for investigating signalling pathways, *C. elegans* have also been used to investigate other processes that affect ageing in humans, such as oxidative stress and redox homeostasis (19, 123-129). Interestingly, the percentage of cysteine in the proteome of *C. elegans* is 1.97%, which is near the levels of mammals (2.25%) when compared to the simpler single-celled archaea (0.50%) (48). This similarity in cysteine abundance between mammals and nematodes makes *C. elegans* a promising model to understand thiol-mediated signalling during ageing.

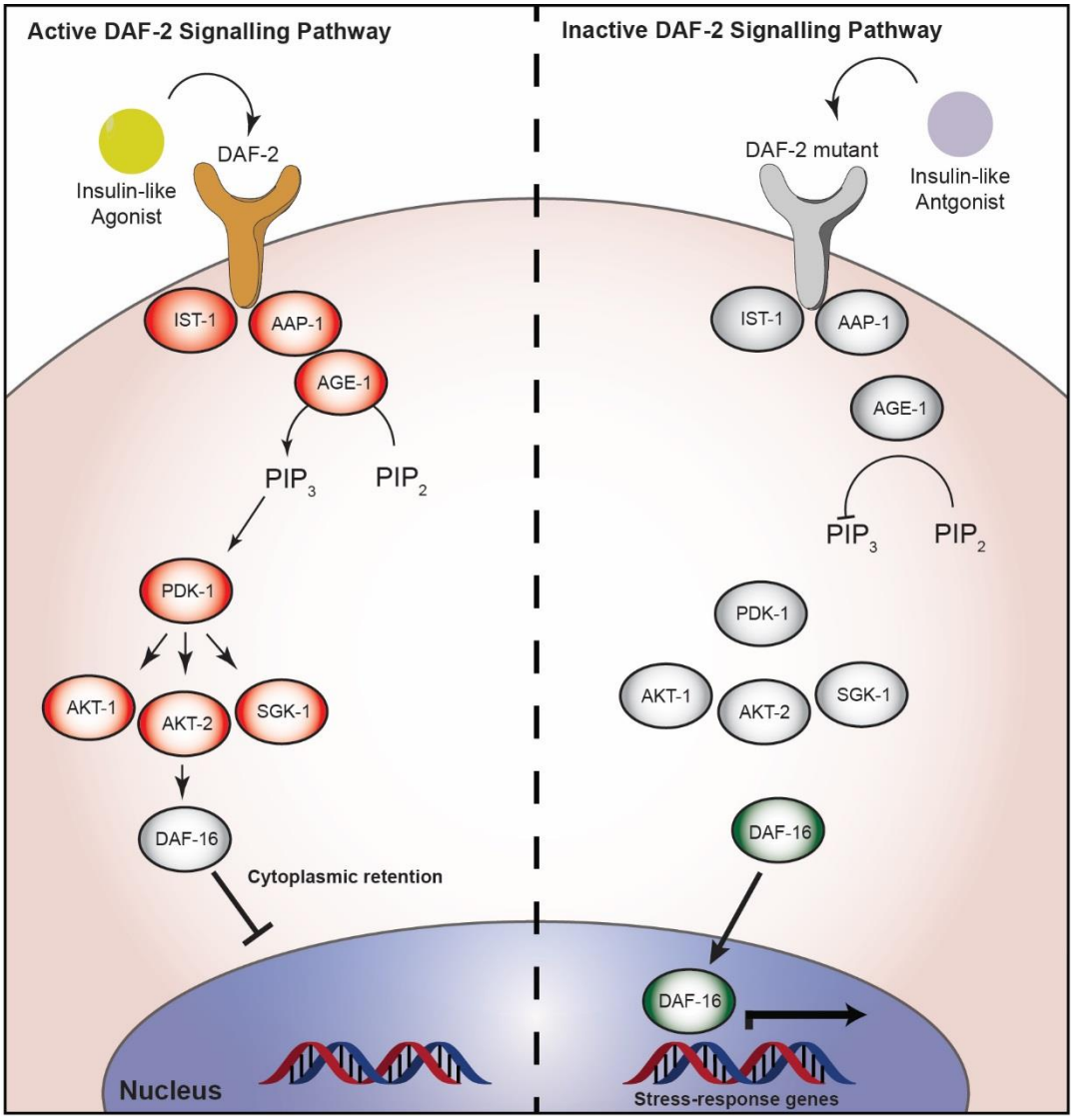

Figure 1-7. The canonical insulin/insulin-like signalling pathway in *C. elegans*

Left panel: *Proteins involved in cytoplasmic retention of DAF-16 are shown in red. Briefly, an extracellular insulin-like agonist binds to and activates the DAF-2 receptor. The AGE-1 adaptor protein (AAP-1) and the putative insulin receptor substrate homolog (IST-1) potentiates the insulin-like signalling. This activates the phosphatidylinositol-3 OH kinase (AGE-1) that catalyses the conversion of phosphatidylinositol bisphosphate (PIP_2) into phosphatidylinositol trisphosphate (PIP_3). By binding to PIP_3, the phosphoinositide-dependent kinase (PDK-1) can phosphorylate and activate the AKT-1/2, SGK-1 complex. These active kinase complexes lead to the phosphorylation of the DAF-16 transcription factor restricting it to the cytoplasm (130).* ***Right panel:*** *Suppression of DAF-2 signalling in* daf-2 *loss-of-function mutants or in the presence of an antagonist ligand, results in DAF-16 not becoming phosphorylated. It can then be translocated to the nucleus where it regulates the transcription of several stress response genes.*

1.5.1 The *de novo* and salvage glutathione synthesis pathway genes of *C. elegans*

The identification of the GSH cycle thiol intermediates in *C. elegans* indicated that it has a GSH metabolic network similar to that present in mammals (131), where *de novo* GSH synthesis occurs in the cytosol and involves the same two consecutive ATP-dependent reactions. In whole worm homogenates, the GSH concentrations have been reported to range between ~10-40 nmol/mg protein (132-134), with the GSH:GSSG ratio of young adult wild-types being approximately 70:1 (132, 135). In *C. elegans*, the *gcs-1* gene encodes for the ortholog of the human GCLC (catalytic) subunit. Based on the predicted amino acid sequence homology, the *C. elegans* GCS-1 has a 54% identity to the human GCLC ortholog (26). The expression of *gcs-1* is regulated by the SKN-1 transcription factor in both constitutive and stress-induced conditions in various tissue types of *C. elegans* (136, 137). The SKN-1 transcription factor is a functionally conserved homologue of Nrf2 that controls the up- or down-regulation of approximately 300 genes under non-stressed conditions (138, 139). The p38 mitogen-activated protein kinase (p38 MAPK) pathway in *C. elegans* has been shown to upregulate *gcs-1* expression in the intestine via the PMK-1-mediated phosphorylation of and subsequent accumulation of SKN-1 to the intestinal nuclei in response to oxidative stress (140).

However, intestinal *gcs-1* expression in *C. elegans* has also been demonstrated in RNA interference (RNA*i*) studies to be induced by pathways that are exclusive or independent to either p38 MAPK or SKN-1 (141). Inhibition of SKN-1 occurs through phosphorylation by the activity of glycogen synthase kinase-3 (GSK-3), which has been shown to inhibit *gcs-1* transcription (142). The WD40 protein, WDR-23, is a direct repressor of SKN-1 (143). WD40 proteins are ~40 amino acid repeats that preferentially end with a tryptophan and aspartic acid (WD) motif which facilitate protein-protein

interactions (144). One study has shown that *wdr-23(tm1817)* mutants produce over 4-fold higher levels of GSH compared to age-matched wild-type worms (145). RNA*i* knockdown of *skn-1* in the *wdr-23* mutant worms completely suppressed the increase in GSH levels observed in the *wdr-23* mutants, indicating that the high levels observed in the *wdr-23(tm1817)* mutants is SKN-1-dependent (145).

An investigation of the protein-protein interactions of *C. elegans* using yeast two-hybrid (Y2H) screens, initially showed that the E01A2.1 protein interacts directly with the GCS-1 protein (146). Though these studies reported these findings in the supplementary information, later studies identified the *E01A2.1*[2] gene in *C. elegans* to encode the regulatory homologue of the GCLM subunit (139, 147). RNA*i* knockdown of the *E01A2.1* gene in wild-type worms has been shown to have no effect on lifespan under 1.5 mM paraquat challenge, whereas it decreased the lifespan of the long-lived *daf-2*(*e1370*) mutant (148). Microarray analysis of the genes involved in GSH synthesis, including the salvage synthesis pathway, did not show any changes in the abundance of mRNA levels in the long-lived *daf-2* strains (*daf-2* and *daf2;pept-1*) when compared to the wild-type that could explain the high GSH levels. The authors postulated that regulation of GSH levels in the long-living worms occur mainly at the post-transcriptional level (148).

[2] In the following sections of this thesis, the *C. elegans* gene "*E01A2.1*" and its product will now be referred to as *gclm* and GCLM, respectively.

The current information available on the *C. elegans gclm* gene indicates that its involvement in stress-response is similar to those mechanisms conserved in mammalian cells. An RNA*i* screen of a library of 11,511 full-length cDNA clones had shown that a total of 37 *C. elegans* genes, one of which included *gclm*, induced *gcs-1* (catalytic subunit) expression in the intestine via SKN-1 activation (141). Under conditions of arsenite-induced stress, the *gclm* gene has been shown to be upregulated by the SKN-1 transcription factor (139, 149). With the discovery of the *E01A2.1* gene encoding for the *C. elegans* homologue of the mammalian GCLM subunit, there remains few reports using the ageing *C. elegans* as a model to investigate the regulatory role of the GCLM subunit in the *de novo* GSH synthesis pathway.

In the second step of the *de novo* GSH synthesis pathway, glutathione synthetase is encoded by the *gss-1* gene in *C. elegans*, which shares 39% identity with the human isoform (26). RNA*i* knockdown of *gss-1* has no effect on the lifespan of wild-type or the *daf-2* mutants under non-stressed conditions (148). Other studies have shown that knockdown of the *gss-1* gene increases the intensity of a *gcs-1* fluorescent reporter strain indicating that a decrease in GSH synthesis upregulates the expression of the rate-limiting GCS-1 enzyme (150). The *gss-1* gene has been shown to be upregulated by SKN-1 following arsenite (139), and benzo-α-pyrene exposure (151), with several predicted SKN-1 binding sites present in the *gss-1* gene promoter region (136). The degree of conservation of GSH synthesis with mammals, including the transcriptional control by the Nrf2 ortholog, SKN-1, make *C. elegans* a viable alternative model to investigate various aspects of glutathione homeostasis (Figure 1-8).

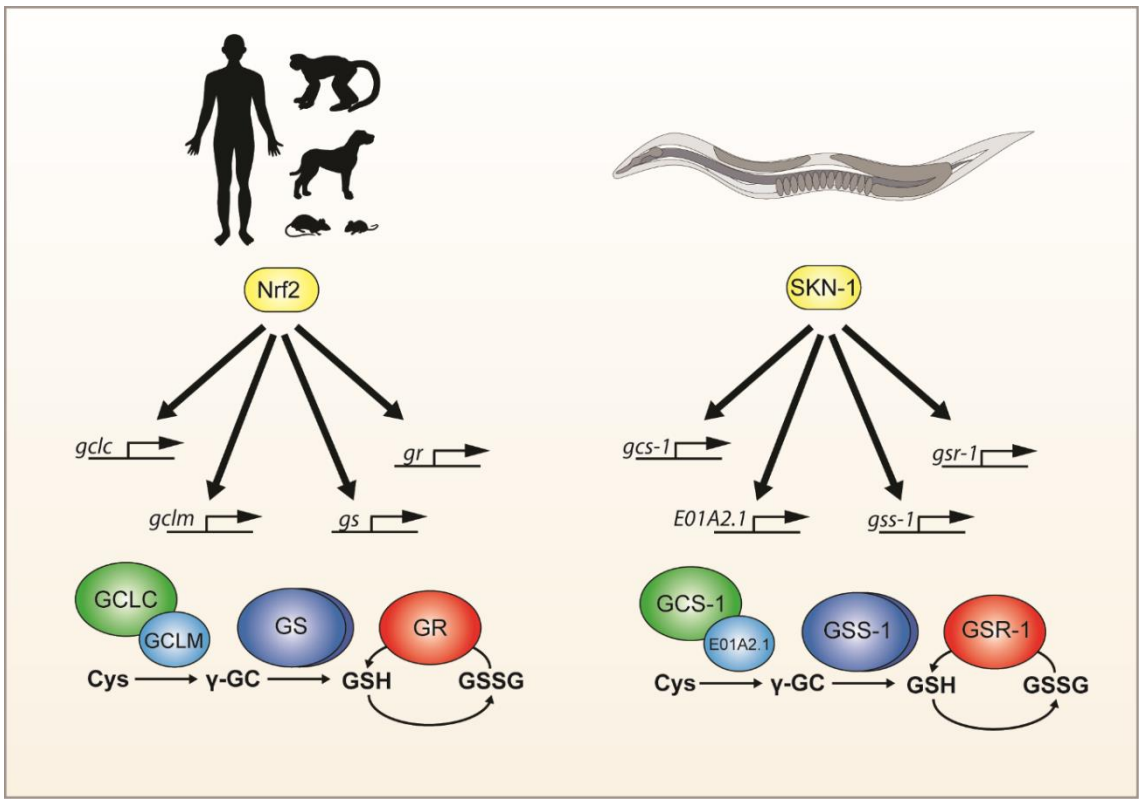

Figure 1-8. Homology of GSH synthesis between mammals and *C. elegans*

Protein-encoding genes of the de novo *(*gcs-1, E01A2.1 *and* gss-1*) and recycling pathway (*gsr-1*) are conserved in* C. elegans. *These genes are transcriptionally upregulated by the SKN-1 (Nrf2 ortholog) under constitutive and stress-induced conditions. In mammals, the de novo synthesis pathway is comprised of the glutamate cysteine ligase catalytic (GCLC) and modifier subunits (GCLM), and glutathione synthetase (GS); with glutathione reductase (GR) involved in recycling intracellular GSSG to GSH. In worms, the respective orthologs are designated as glutamate cysteine synthetase heavy (GCS-1) and light (E01A2.1) subunits, glutathione synthetase (GSS-1) and glutathione reductase (GSR-1). The metabolites of the pathway are conserved for the mammalian and nematode systems.*

In *C. elegans*, the *gsr-1* gene encodes for the glutathione reductase protein (GSR-1), which produces two isoforms (GSR-1a and GSR-1b) that are positioned at the same locus (152). The GSR-1b isoform has been shown to be present in the cytoplasm (152). The GSR-1a isoform possesses an additional 14 amino acid *N*-terminal extension which is predicted to include a mitochondrial targeting sequence (MTS) (152). Using recombinant protein expression, it was shown that the enzymatic activity of loss-of-function GSR-1b mutants were unable to reduce GSSG to GSH, whilst the recombinant wild-type GSR-1b catalysed the reduction of GSSG in a dose-dependent manner (152). Isoform-specific rescue of the embryonic lethal phenotype of *gsr-1(tm3574)* mutants, indicated that lethality is prevented by expressing the GSR-1b cytoplasmic form and not the GSR-1a mitochondrial form, demonstrating that GSR-1b is essential for embryonic development (152). GSR-1 has also been shown to be vital in the stress response against several oxidants including juglone, cumene hydroperoxide, diamide, tert-butyl hydroperoxide and paraquat (129, 132, 148). Knockdown of the *gsr-1* gene in the wild-type worm using RNA*i* reduced the lifespan under non-stressed conditions (132). However these results have not been reproduced with other researchers observing no difference in lifespan when the *gsr-1* gene was knocked down (145).

The initial detection of cysteinylglycine in *C. elegans* suggested the presence of the γ-GT ectoenzyme (131), and indeed subsequent work has reported at least six γ-GT genes present in the worm (132). A small RNA*i* screen testing for stress tolerance against juglone and arsenite in worms showed no significant differences in survival for the RNA*i* knockdown of each γ-GT isoform (132). In eukaryotes, GSH can be exported from the cell as glutathione-*S*-conjugated and disulfide forms, mainly via multidrug resistance proteins (MRPs) (153). In *C. elegans*, it is still unclear how GSH or its conjugates are

transported out of the cell or between tissue types. However, drug resistance against the broad-spectrum anti-parasitic nematode agent, ivermectin, has shown that MRPs require GSH synthesis for drug efflux in *C. elegans* (154).

1.5.2 Glutathione peroxidases

The glutathione peroxidase (GPx) family catalyses the reduction of H_2O_2 and a variety of organic hydroperoxides to water or to the corresponding alcohol (155). They are categorised into two subfamilies; the selenium subfamily containing a selenocysteine (SeCys) in the catalytic triad of amino acids (Trp-Glu-SeCys) and the non-selenium subfamily containing a cysteine (Trp-Glu-Cys) (156). Sequence analysis of the eight *C. elegans* GPx genes (*gpx-1* to *gpx-8*) revealed that none contain a selenocysteine (125). Selenium-containing GPx generally prefer GSH or other monothiols as a substrate, whereas the majority of non-mammalian/non-selenium containing GPx enzymes are reported to use redoxin-type proteins as a reducing substrate (157, 158). It has been suggested that *C. elegans* GPx homologues may use a peroxiredoxin-like mechanism with thioredoxin as their reducing substrate (26). Though the majority of *C. elegans* GPx isoforms contain the Trp-Glu-Cys catalytic triad, the predicted amino acid sequence of GPX-4 lacks the Trp residue, and GPX-8 lacks both the Trp and Cys (125). The authors concluded that the absence of cysteine at the catalytic site indicates that the GPX-8 protein is likely not acting as a glutathione peroxidase (125).

Across several studies, the GPx activity in worms has been shown to range between 7-600 U/mg protein (159-161). Copper exposure ($CuSO_4$) in wild-types led to approximately 10-fold increases the overall GPx enzyme activity in a dose-dependent manner, with the mRNA expression levels of all GPx isoforms, except *gpx-5*, also

significantly increasing in a dose-dependent manner (161). Glutathione peroxidase activity in worms has been shown to decline when treated with chemical stressors including paraquat (160) and the neurotoxin 6-hydroxydopamine (6-ODHA) (162). The expression patterns of *gpx-5* follow a pattern of circadian-rhythm, with mRNA levels reported to be higher at night compared to day time under 12 h light-dark cycles (163). A single strain generated with deletions for the four phospholipid hydroperoxide GPx isoforms (*gpx-1, gpx-2, gpx-6* and *gpx-7*) showed no differences in the median lifespan when compared to the wild-types (125). Each of the four phospholipid hydroperoxides were reported to be expressed primarily in the intestine (125). In an RNA*i* screening study of 162 genes that are exclusively expressed in the intestine of the worm, the *gpx-1* gene was the only RNA*i*-targeted gene shown to increase expression and activity of PEPT-1 (164). PEPT-1 is a transporter, located on the apical membrane of the enterocyte, responsible for the uptake of di- and tripeptides in *C. elegans* (165). This suggests that lower *gpx-1* transcript levels may stimulate uptake of dietary glutathione and its precursors.

Selenocysteine-containing GPxs have been the subject of many mammalian model studies, yet the physiological roles of the non-selenium GPxs remain largely unclear. The absence of selenocysteine at the active site of any of the *C. elegans* GPx isoforms suggests that the major mechanistic peroxidase activity of this enzyme family differs to that in mammals.

1.5.3 Glutathione-*S*-transferases (GST)

Glutathione *S*-transferases (GSTs) are a functionally diverse family of enzymes that utilise GSH in detoxifying conjugation and reduction reactions (166). Based on their sequence similarity and substrate specificities, evolutionary divergent forms of GSTs are subdivided into at least ten subfamilies; alpha, delta, epsilon, kappa, mu, pi, sigma, theta, zeta, and omega (167). GSTs represent a major class of enzymes that are involved in phase II detoxification in *C. elegans* (168). The *C. elegans* genome contains 56 validated and putative GST genes (169), with several proposed to be nematode specific (170, 171). Though most *C. elegans* GST isoforms are categorised within the sigma subfamily, other subfamilies that are present include the pi, kappa, zeta, omega and alpha. Changes in differential expression patterns of specific GSTs in response to certain compounds suggest substrate-specific roles of GSTs in xenobiotic detoxification (151, 172-174). The correlation between GST activity and longevity has been described among divergent species, including *C. elegans* and *D. melanogaster* (175). In the long-lived *daf-2* mutants, the upregulation of several GST genes has been shown to be exclusive to the expression profile of these worms when compared to dauer worms, which are both controlled by the insulin/insulin-like growth factor-1 signalling pathway (176). Due to the large number of isoforms, and the high degree of sequence identity in this superfamily, a proteomics approach has been utilised to monitor any off-target gene silencing, or potential compensatory upregulation of other members within the GST superfamily (177). The RNA*i* targeting of *gst-1*, *gst-5* and *gst-7* resulted in concomitant declines in their respective protein levels, with differences observed in 1 out of the 11 other proteins measured, comprising of the sigma and pi subfamilies (177). Proteomic studies have indicated that *C. elegans* GST isoforms have a multitude of functions, and are involved in signalling pathways via direct protein-protein interactions with various kinases,

phosphatases, G proteins, transcriptional regulators, and ubiquitination proteins, under H_2O_2-stressed and non-stressed conditions (171, 178-180).

Sigma and Pi GST subfamilies

The most rigorously investigated GST gene in *C. elegans* is *gst-4*, which shares sequence similarity with the human sigma subfamily. An early study demonstrated that *gst-4* expression increases in response to paraquat challenge (181). With the advent of GFP reporter strains of *gst-4* (*gst-4*::GFP), many studies have investigated the effect that certain compounds have on the expression of *gst-4* (Table 1-1). Most compounds elicit an increase in the intensity of the *gst-4*::GFP reporter in a stress-dependent manner. In contrast, other compounds such as folic acid are reported to increase the expression of *gst-4*, resulting in an increase in stress resistance. Transcriptional activation of the *gst-4* gene is often used as an indication of SKN-1 activity; with several inducers of *gst-4* including H_2O_2 and sodium azide being shown to be *skn-1* dependent (182). SKN-1 has also been shown to control the induction of several other GST genes (136, 139, 183). Induction of *gst-4* has also recently been shown to be upregulated independent of SKN-1, by the EOR-1 transcription factor that mediates the effects of the epidermal growth factor (EGF) pathway involved in regulating cell growth and differentiation (184). The authors concluded that the discovery that *gst-4* transcriptional regulation is not exclusively controlled by the SKN-1 transcription factor should serve as a cautionary note for work that utilises the *gst-4*::*gfp* reporter as a measurement of SKN-1 activity (184).

Though WDR-23 protein is a direct repressor of SKN-1 induction, under conditions of oxidative stress, SKN-1 can bypass the inhibitory effects of WDR-23 to increase expression of target genes, such as *gst-4* and *gst-30* (143). WDR-23 is the strongest

known suppressor of *gst-4* and has been reported to possibly function with the CUL4/DDB1 ubiquitin ligase to repress SKN-1 activity by proteasomal degradation (143). Another WD40 family member, WDR-46, located in the nucleolus and involved in 18S ribosomal ribonucleic acid (rRNA) processing, has also been shown to be a negative regulator of SKN-1-mediated expression of several GST genes (185). Unlike the WDR-23 protein, WDR-46, has been suggested to indirectly interact with SKN-1 (185).

Table 1-1. Compounds shown to affect *gst-4* expression in *C. elegans*

Compound	*gst-4* response	References
acrylamide	↑	(186, 187)
aspirin	↑	(174)
fluoxetine*	Repressed	(188)
folic acid	↑	(189)
3β-hydroxy-urs-12-en-28-oic acid	↑	(173)
juglone	↑	(190-193)
lithium compounds (LiCl, L_2CO_3)	Suppressed	(194)
microplastic particles	↑	(195)
mianserin*	↑	(188)
mirtazapine	↑	(188)
3-nitropropionic acid	↑	(196)
paraquat	↑	(181)
quinolinic acid	↑	(196)
tributyltin	↑	(197)

*Co-treatment with fluoxetine repressed the mianserin-induced increase of the *gst*-4::GFP reporter, though had negligible effect on reporter activity when treated with fluoxetine alone.

The *gst-1* gene, which is similar to the pi class of human GST, has been shown to protect against dopaminergic neuron degeneration in *C. elegans*, which may have implications for understanding the progression of Parkinson's Disease (198). Another pi class gene, *gst-10*, catalyses the conjugation of GSH to the lipid peroxidation product, 4-hydroxyneoneal (4-HNE) (199-201). An RNA*i* screening study of 26 of the 44 then known *C. elegans* GST genes showed that knockdown of five (*gst-5*, *gst-6*, *gst-8*, *gst-10*, and *gst-24*) sensitised the nematode to electrophilic stress elicited by exposure to 4-HNE (199, 200). In worms carrying a mutation for mitochondrial complex I-deficiency (*gas-1* mutants), the pharyngeal-specific expression levels of *gst-14* were shown to be higher than wild-type worms (169). RNA*i* knockdown of the *gst-14* gene in the *gas-1* mutants increased lifespan and the incidence of 4-HNE-modified mitochondrial proteins, without any improvement in the function of complex I (169). This increase in the incidence of 4-HNE-modified mitochondrial proteins was implicated to be involved in the signalling events that led to the observed increases in lifespan (169).

Kappa GST subfamily

Unlike most vertebrates, which encode only one GST kappa gene, *C. elegans* encodes for two; *gstk-1* and *gstk-2* (202, 203). GSTK-1 is expressed in the intestine, body wall muscles and epidermis and contains a C-terminal peroxisomal-targeting sequence which directs its localisation to the peroxisome (202). The GSTK-2 is localised in the mitochondria with expression patterns shown in the pharynx, muscles and epidermis (202). RNA*i* knockdown of both *gstk-1* and *gstk-2* genes showed no difference in several measures of worm health compared to controls including, reproduction, development, locomotion and lifespan (202). Simultaneous double RNA*i* knockdown of both genes resulted in a significant decline in oxygen consumption and monounsaturated fatty acid

cis-vaccenic acid (18:1ω7) content, suggesting that both genes are involved in respiration and lipid metabolism (202).

Omega GST subfamily

Several isoforms of the GST omega subfamily are encoded in the *C. elegans* genome, including *gsto-1*, *gsto-2*, *gsto-3*, *gst-44* and C02D5.4 (169). Overexpression and RNA*i* studies have shown *gsto-1* to be implicated with increased stress resistance and to be exclusively expressed in the intestine (204). *Gsto-1* is upregulated under transient hypoxic conditions leading to an extension of lifespan mediated by the GATA-type erythroid-like-2 transcription factor (ELT-2), which is downstream of the mechanistic Target of Rapamycin (mTOR) signalling pathway; a longevity pathway associated with dietary restriction (205).

The GST superfamily carry out a diverse range of functions in *C. elegans*. While there remains much to be elucidated about the substrate-specificities, expression patterns and the relative levels of the many GST isoforms in *C. elegans*, research into the dynamic roles of this enzyme superfamily in detoxification and signalling will further our understanding on how the redox environment is mediated by enzymatically-controlled GSH-dependent redox processes.

1.5.4 Glutaredoxins

Glutaredoxins are small heat-stable proteins, ranging between 9-15 kDa (206), that are regarded as the main catalysts of reversible protein de-glutathionylation (61). Depending on the number of cysteine residues in the active site of the enzyme, glutaredoxins are classified as either monothiol (1-Cys) or dithiol (2-Cys) forms (207). The five annotated glutaredoxin genes are, *glrx-3, glrx-5, glrx-10, glrx-21, glrx-22* (132) with the putative

glutaredoxins genes F10D7.3, ZC334.7 and F26F4.9 also reported to exist (26). Analysis of the glutaredoxin sequences indicates that the GLRX-3 and GLRX-5 are monothiol forms, while the other annotated forms, GLRX-10, GLRX-21 and GLRX-22 and putative isoforms (F10D7.3, ZC334.7 and F26F4.9) are dithiols (26).

In a *C. elegans* model of Parkinson's Disease which expresses two pathogenic mutations in the human leucine-rich repeat kinase 2 (LRRK2) gene, loss of the *glrx-10* gene has been shown to lead to an increase in the degeneration of dopaminergic neurons (208-210). For the loss of *glrx-10* function mutants, expression of the active form of the *glrx-10* homologue partially afforded protection in dopaminergic neurons. Two separate studies have shown that loss-of-function of *glrx-21* results in selenium-induced reduction of movement (211), and egg-laying capacity (212). Both studies suggested that GLRX-21 is required for the partial protection afforded by GSH during selenium-induced impairment.

1.5.5 Thioredoxin systems

The thioredoxin system is comprised of thioredoxins (Trx) and NADPH-dependent thioredoxin reductases (TrxR) (213). Thioredoxins are small (~12 kDa) ubiquitous oxidoreductases that contain a highly specific thiol-disulfide active site to co-ordinate the regulation of the cellular redox environment largely by the supply of reducing equivalents for peroxiredoxins (214). Oxidised thioredoxins (Trx_{ox}) are reduced (Trx_{red}) by thioredoxin reductases (TrxR), utilising NADPH as a cofactor (32). In *C. elegans*, the thioredoxin system is composed of five thioredoxin genes (*trx-1* to *trx-5*) and two thioredoxin reductase genes, *trxr-1* and *trxr-2* (215). Expression patterns of the *trx-1* gene have been observed in ASJ neurons (126, 216), ASI neurons and the posterior intestine (126). TRX-1 has been implicated to potentially have a redox-independent

mechanistic role in dauer formation via the down-regulation of the insulin-like DAF-28 signalling neuropeptide in ASJ neurons (217).

Discovery of an ASJ motif, a functional *cis*-regulatory promoter region, has been reported to regulate the ASJ-specific gene expression of *trx-1* by binding SPTF-1, an ortholog to the *Sp* family zinc-finger transcription factor (218). Mutant worms that lack the *trx-1* gene are more vulnerable to paraquat-induced oxidative stress (126) and have decreased lifespans (126, 216). TRX-1 has been shown to regulate lifespan extension in genetic (*eat-2* mutants) and nutrient-based models of dietary restriction possibly via its upregulation in ASJ neurons (219). Interestingly, *trx-1* was later shown to regulate SKN-1 nuclear localisation in a cell non-autonomous manner, with loss of *trx-1* from ASJ neurons promoting the nuclear localisation of intestinal SKN-1 (220). This regulation of SKN-1 was exclusively controlled by TRX-1 and not by TRX-2 or TRX-3 (220).

The *trx-2* and *trxr-2* genes comprise the mitochondrial thioredoxin system and are upregulated upon induction of the mitochondrial unfolded protein response (UPR^{mt}) (221, 222). Characterisation of the intestine-specific TRX-3 have shown that the *trx-3*(*tm2820*) mutant has no significant difference in reproductive capacity, longevity, and resistance to stress (including 37°C heat-treatment, juglone and paraquat exposure) compared to the wild-type, though they exhibit a slight reduction in size and a shorter timing of their defecation cycle (223). However, overexpression of TRX-3 protected against pathogen infection, which suggested that TRX-3 may have a role in the worm's innate immune response (223). The thioredoxin reductase (TrxR) gene, *trxr-1*, was shown to significantly afford partial protection from degeneration of dopaminergic neurons against the neurotoxin 6-hydroxydopamine (6-OHDA) (215). Both the *trxr-1* and *gsr-1* (glutathione reductase) genes work in conjunction during *C. elegans* larval development by the

reduction of disulfide bonds to achieve precise removal of the cuticle from the surface of epidermal cells (224).

Protein structure studies have determined the *C. elegans* TRXR-1 (~74 kDa) to be 667 amino acids and the TRXR-2 (~55 kDa) to be 503 amino acids (225). TRXR-1 is located in the cytosol and is highly expressed in the pharynx, vulva and intestine, whilst TRXR-2 is expressed in the mitochondria of the pharyngeal and body wall muscles (226). TRXR-1 has been shown to have no effect on the survival of *C. elegans* in response to acute (2 h) exposure to 2 mM H_2O_2 (224). Interestingly, the TRXR-1 thioredoxin reductase is the only selenoprotein that has been detected in the worm (224, 227). Having only one selenoprotein, TRXR-1, has made *C. elegans* a valuable *in vivo* model to investigate dose-dependent beneficial and toxicological properties of selenium-based compounds (135, 228-230). Expression of *trxr-1* is upregulated in wild-type worms exposed to lethal doses (560 μM), but not low doses (10 μM), of the organic selenium compound, 4-phenylselanyl-7-chloroquinoline (PSQ) (135). The *trxr-1* mutants were much more sensitive to the toxic effects of PSQ when compared to wild-type worms (135). Deletion mutant strains for *trxr-1*(*tm3462*) and *trxr-2*(*ok2267*) and double mutants of the two were found to have no significant role in modulating the toxicity of the median lethal concentration (LC_{50}) of several inorganic selenium compounds when compared to wild-type worms (230). Studies using the nematode could potentially facilitate our understanding of the safety profiles of organic and inorganic selenium compounds, and possibly elucidate differences in therapeutic efficacy.

1.5.6 Peroxiredoxins

Peroxiredoxins (Prx) are a class of thiol peroxidases that scavenge organic and inorganic peroxides. They are highly abundant proteins involved in the conversion of the majority of cellular H_2O_2 to water (231, 232). *C. elegans* contain three known peroxiredoxins, *prdx-2*, *prdx-3,* and *prdx-6* (128). Both *prdx-2* and *prdx-3* genes are typical 2-Cys peroxiredoxins, with *prdx-6* encoding for a 1-Cys peroxiredoxin. Expression patterns of *prdx-2* have been reported in the I4 (pharyngeal) and I2 (sensory) interneurons (233), intestine, epithelial cells, muscle (pharyngeal, vulval and body wall), and various neurons in the head and tail (234). In *C. elegans*, PRDX-2 constitutes ~0.5% of the total protein abundance (124).

In *prdx-2*(*gk169*) mutants, loss of peroxiredoxin activity leads to an increase in *de novo* GSH synthesis compared to wild-types, with an ~2-fold increase in *gcs-1* mRNA and GSH levels (235), possibly indicating a compensatory response by the *de novo* GSH synthesis network. Loss-of-function *prdx-2*(*gk169*) mutants show a shorter lifespan compared to wild-types at 15°C (124, 235) and 20°C (235), with no difference observed at 25°C (124), indicating a dynamic temperature-dependent response for the PRDX-2 enzyme. In support of this, transient changes in housing temperature during development have been shown to increase lifespan through a PRDX-2-dependent stress response (236). Moreover, survival rates of *prdx-2*(*gk169*) mutants exposed to 10 h heat-shock treatments at 35°C show a marked decline when compared to wild-types (237). Interestingly, loss of PRDX-2 increased stress resistance against 5 mM arsenite exposure, while overexpression of PRDX-2 also showed a slight increase (235). The increased arsenite resistance was initially attributed to be due to an increase in SKN-1 and DAF-16 activity (235). A recent study has reported that PRDX-2 is required for insulin secretion (in the

form of the DAF-28 neuropeptide), leading to higher activity of the DAF-2 insulin signalling pathway and inhibition of the nuclear localisation of SKN-1 and DAF-16 (238). This later study provides an explanation for the paradoxical observation seen in the loss-of-function *prdx-2*(*gk169*) mutants that exhibit increases in arsenite stress resistance, yet temperature-dependent declines in lifespan (238).

Over-oxidation of PRDX-2 has been contested to have a negligible effect on worm physiology, with the suggestion that *C. elegans* perhaps relies on degradation and subsequent clearance of over-oxidised PRDX-2; with *de novo* synthesis of PRDX-2 potentially playing a role in the physiological response (239). In higher eukaryotes, sulfiredoxins reduce over-oxidised peroxiredoxins to restore peroxidase activity, however, these enzymes are not present in *C. elegans* (239). The cyclic oxidation state of PRX-2 possibly represents a circadian-rhythm mechanism in the worm (240) which has also been shown to be conserved in other eukaryotic models (241). In a study investigating the lifespan-extension properties of metformin, the antihyperglycemic drug used in the treatment of type II diabetes, it was shown that hormetic effects leading to increases in lifespan were mediated by PRDX-2 (242). Exposure of worms to H_2O_2 over the range of 0.01-1 μM reported a beneficial increase in the sensory response of the ASH neurons via the PRDX-2-mediated p38/PMK-1 signalling cascade (243). The lesser studied *prdx-3* gene is predicted to be located in the mitochondria (27, 244). Though RNA*i*-targeted *prdx-3* knockdown worms had no difference in lifespan or protein oxidation, they exhibited increased mitochondrial uncoupling, with lower ATP levels, motility, and brood size, indicating that while *prdx-3* expression is not required for lifespan, it may be important for healthspan (244).

1.5.7 Application of *C. elegans* to understand age-related changes in GSH homeostasis

Advances in the field of redox biology has contributed to the understanding of the complexity of the thiol-based system in mediating signal transduction in the redox network (126, 245, 246). Undoubtedly, the glutathione redox couple plays a major role in this network. The reaction mechanisms of glutathione-dependent enzymes and other thiol-based enzymes involved in the redox network have a fundamental role in the function of GSH as a redox regulator (41, 76). Phylogenetic analysis of the protein-encoding genes related to the major redox systems have shown that *C. elegans* redox systems possess a considerable amount of similarity with human isoforms (26). The impact of age-related changes on thiol-based redox-regulating genes has been discussed in a recent review (128). This significant level of evolutionary conservation with higher eukaryotes suggests that *C. elegans* should be a suitable multicellular model to explore the age-related mechanisms in the redox thiol-related system with the advantage of resolving tissue and subcellular differences (Figure 1-9).

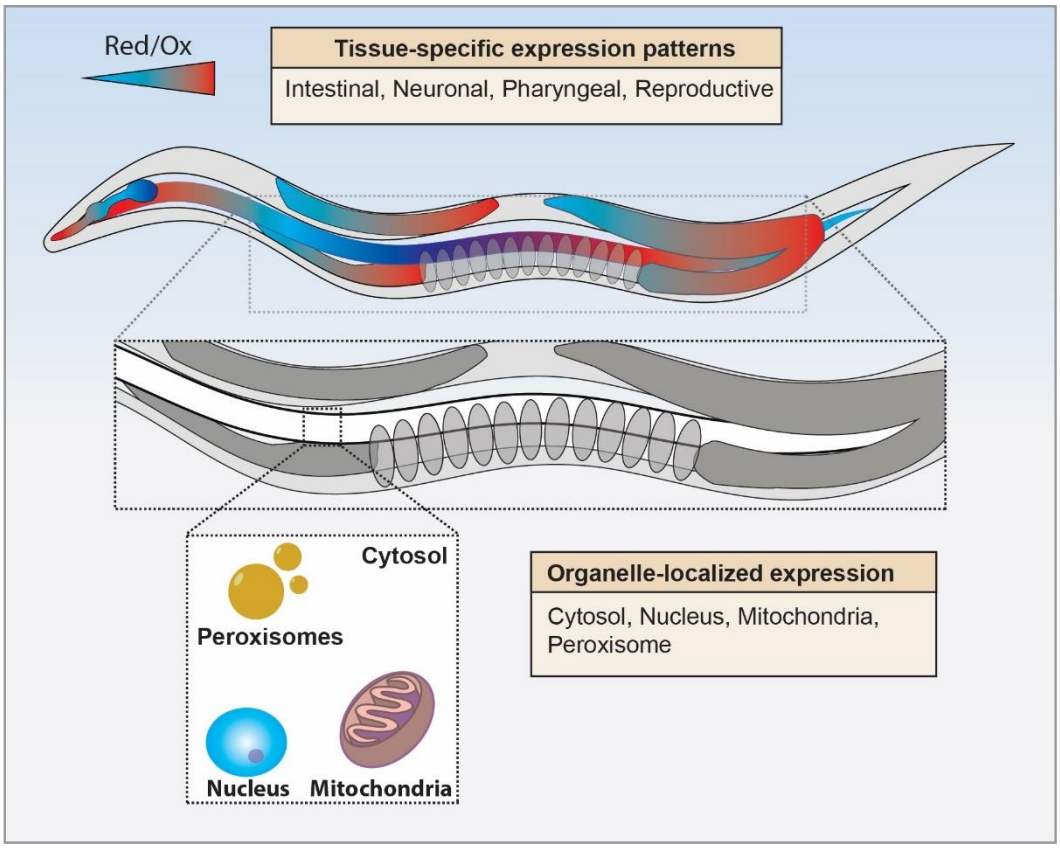

Figure 1-9. Expression patterns and subcellular localisation of thiol-related systems in *C. elegans*

The tissue- and subcellular-specific differences in redox potential and expression patterns of thiol-related redox genes in the worm. Generation of GFP reporter strains, allows the investigation of tissue and organelle specific gene expression patterns. The redox environment is heterogeneous throughout the various tissue types, which is illustrated by the gradients of the intestine, pharynx and reproductive organs. Within the same tissue types and subcellular compartments (e.g. mitochondria), localised gene expression of the thiol-related system can control the redox environment of respective compartments.

1.6 Thesis Aims and Chapter Outlines

In this work, we propose that the nematode *Caenorhabditis elegans* be explored as an *in vivo* model to investigate changes in GSH homeostasis during ageing. Conventionally, rodent models have been used to study changes in the *de novo* GSH synthesis pathway in pathophysiological conditions that affect ageing. *C. elegans* has become a well-established model for ageing studies applying genetic techniques and pharmacologic interventions that all aim to explore various mechanisms that influence lifespan. Since its genome sequence was published in 1998 (247), *C. elegans* has been extensively utilised as a genetic model to understand various biological processes at a multicellular level. One major limitation of using *C. elegans* as a biochemical model for human ageing includes their size, which makes investigation difficult without the use of the DNA synthesis inhibitor, 5-fluorodeoxyuridine (FUdR), to obtain large-enough numbers in age-matched populations (248). *C. elegans,* however, has several advantages over rodent models such as a short lifespan (~3 weeks as opposed to ~2 years in rodents), negligible husbandry costs, and larger obtainable sample numbers. This thesis aims to use *C. elegans* as a model organism to investigate age-associated decline in *de novo* GSH. To enable this study, the project will address the analytical challenges of accurately measuring the GSH/GSSG molar ratio in biological samples (249).

To accurately quantify bioactive redox molecules GSH/GSSG in biological samples, a novel high-performance liquid chromatography-tandem mass spectrometry (LC-MS/MS) analytical method was developed and extensively validated (Chapter 2). The establishment of this powerful analytical tool enabled experiments to be designed to gain a deeper understanding into the protective role of GSH in the ageing nematode.

The hypothesis that the predicted modifier subunit of the *C. elegans* GCL has a role in regulating glutathione homeostasis during ageing was investigated in Chapter 3. The *in vivo* regulatory role that the GCLM subunit has on GSH synthesis was explored by using RNA interference (RNA*i*) to initially determine the regulatory effect in worms. Observations of several phenotypic markers intrinsic to worm ageing were also made under optimal and stressed environmental conditions. No study to date has investigated how the rate-limiting step in *C. elegans* causes the decline of the *de novo* GSH synthesis. To facilitate such work, the relatively unexplored GCLM orthologue of *C. elegans* is functionally characterised for the first time.

Chapter 4 explored the therapeutic potential of the most immediate GSH precursor, γ-GC, to determine its bioavailability profile and to investigate if γ-GC afford protection in GSH compromised worms against oxidative stress. The bioavailability of γ-GC was assessed by using several delivery methods including: liquid medium, liposome-encapsulation and heat-treatment of the *E. coli*, all with the intent to determine the most efficient administration route. This chapter presents data of the first ageing model that investigates the administration with the immediate precursor, γ-GC, to increase GSH levels.

CHAPTER TWO

A novel LC-MS/MS method to investigate the age-related dysregulation of GSH homeostasis in *Caenorhabditis elegans*

2 Chapter Two

2.1 Introduction

Despite the interest in measuring the reduced to oxidised ratio of the glutathione redox couple (GSH:GSSG) in biological samples, there remains a lack of standardisation of both measurement and pre-analytical sample preparation (249, 250). The most common methodologies for quantification of thiol/disulfide ratios are based on the Tietze GSH recycling technique (251), which employs 5,5'-dithiobis(2-nitrobenzoic acid) (DTNB) and glutathione reductase (GR) for the cyclical production of GSH in the presence of NADPH (252). DTNB reacts with GSH to form the mixed disulfide GS-TNB and the chromophore 5-thio-2-nitrobenzoic acid (TNB), the absorbance of which at 412 nm is proportional to the abundance (252). The GS-TNB is then recycled back to GSH by GR and NADPH (252).

Accurate measurements of GSSG are difficult to obtain using the Tietze methodology (herein referred to the GSH-recycling method). Indirect estimations of GSSG are usually made by reducing the disulfide bonds and subsequent spectrophotometric determination of the free thiol groups (GSH) generated from the GSSG present in the sample. However, autooxidation of GSH due to poor sample preparation can produce inaccuracies in the GSH/GSSG ratio estimations (249). Furthermore, a comparison of several commercially available glutathione assay kits (based on the GSH-recycling method) indicated that considerable autooxidation of GSH occurs in each of the kits, leading to artefactual variations in the estimation of GSH/GSSG ratios of the same samples (249). This illustrates the need for more accurate and reliable methods for GSH/GGSG measurement.

2.1.1 Principles of mass spectrometry

Mass spectrometry involves the application of magnetic and electric fields to guide charged particles (ions) in a mass-dependent manner to selectively measure chemical species. Mass spectrometers typically are comprised of three major components: an ion source, a mass analyser and a detector. Charges are placed on molecules in a process called ionisation. Early ionisation techniques suffered from the inherent problem of biomolecule fragmentation occurring due to high levels of energy impacting the molecule during ionisation. In 1989, the development of electrospray ionisation (ESI) greatly advanced analytical chemistry by enabling the ionisation of large biomolecules from solution without fragmentation occurring (253). This 'soft' ionisation method earned John Fenn a share of the Nobel Prize in Chemistry in 2002 and has since remained an indispensable analytical tool in biochemical applications**.**

The process of ESI involves dispersal of a liquid sample into highly charged droplets which are then decomposed due to solvent evaporation (desolvation), producing smaller and more highly charged droplets (254). This process continues until charged molecular ions are formed (255), which are then transferred to the mass analyser. Ions are then selected by application of magnetic and/or electric fields to guide the charged particles based on their mass-to-charge ratio (m/z) and are subsequently directed to the detector. Briefly, detectors rely on the use of an electron multiplier to amplify the signal generated from the ion selected by the mass analyser. This involves a sequence of dynodes that amplify the initial signal. Each dynode will amplify the electrons generated from the preceding one, until the current output from the last dynode is converted to a voltage signal and translated into the signal intensity corresponding to the target analyte.

Advances in the use of high performance liquid chromatography (HPLC) coupled with tandem mass spectrometry (herein referred to as LC-MS/MS) later allowed for superior sensitivity and structural resolution of complex biological mixtures (256). Tandem mass spectrometry increases the selectivity of target analytes by multiple stages of mass selection; typically involving fragmentation of the molecule in between each mass selection stage. Selected reaction monitoring (SRM) is a technique used in LC-MS/MS in which a precursor ion possessing a specific *m*/*z* is selected in the first stage of a tandem mass spectrometer. This precursor ion is then fragmented in a collision cell filled with an inert gas and the product ion is selected in the second mass analyser for detection, enabling greater selectivity and sensitivity compared to LC-MS alone (Figure 2-1).

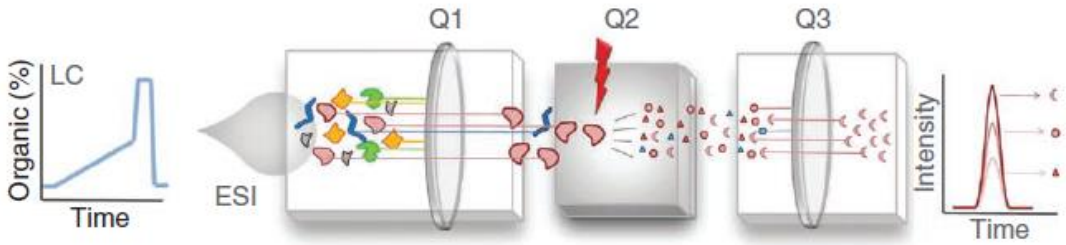

Figure 2-1. LC-MS/MS using selected reaction monitoring

*Selected reaction monitoring (SRM) is a technique used in LC-MS/MS in which an ion possessing a specific mass-to-charge (*m/z*) ratio, known as the precursor ion, is selected by the first mass filter (Q1) of a triple quadrupole mass spectrometer. The precursor ion is fragmented (Q2) to form product ions. One resulting product ion is selected by the second mass filter (Q3) and subsequently detected. Figure reproduced from (257).*[3]

[3] Reprinted by permission from Copyright Clearance Centre: Springer Nature, (*Nature Methods*), Selected reaction monitoring–based proteomics: workflows, potential, pitfalls and future directions, Paola Picotti and Ruedi Aebersold (2012). Licence number: 4411231244005.

In this chapter, we introduce a novel LC-MS/MS method using SRM that has the selectivity and sensitivity to simultaneously quantify the levels of cysteine, γ-GC, GSH and GSSG in a single biological sample. The use of HPLC-based methods to quantify thiol/disulfide couples potentially offers a more reliable GSH/GSSG measurement than the recycling-based methods. Several recent studies have described utilising LC–MS/MS to simultaneously measure GSH and GSSG in biological samples (258-260). Compared to other methods of measuring the GSH/GSSG couple, LC–MS/MS confers greater sensitivity and specificity (259), and unlike classical spectrophotometry techniques, obviates the need to perform separate or multistep recycling assays to determine the GSSG levels.

The impetus for developing a sensitive LC-MS/MS-based method was due to the challenge of obtaining age-matched cohorts without the use of the DNA synthesis inhibitor, 5-fluorodeoxyuridine (FUdR). Commonly used in many *C. elegans* ageing studies, FUdR blocks the synthesis of thymidine, preventing DNA replication (261). Addition of FUdR to the nematode growth medium (NGM) causes sterility in the parental worms with the overall purpose to reduce the work load involved in the daily separation of parental worms from their progeny during the reproductive period. Several studies, however, have shown that FUdR can directly increase the worm's lifespan under various conditions (261, 262). More pertinent to the work presented herein, it has also been shown that the metabolic effects elicited by FUdR in the long-lived *daf-2* mutant and wild-type worms were unable to be compensated for even with the use of appropriate controls (263).

We report here a novel protocol which allows quantification of GSH and GSSG in the same assay, together with several other low-molecular weight thiols involved in glutathione synthesis. This protocol utilised the relatively unexplored thiol-derivatising

agent 7-chloro-N-[2-(dimethylamino)ethyl]-2,1,3-benzoxadiazole-4-sulfonamide (DAABD-Cl) to prevent autooxidation and increase the detection sensitivity for the low-molecular weight thiols. Initial use of DAABD-Cl in proteomic studies of *C. elegans*, led to improvements in assay sensitivity by over 100-fold compared to underivatised cysteine residues (264). The sensitivity of the method presented herein enabled measurement of derivatised cysteine, γ-GC, GSH and in addition, native GSSG levels to be assayed in low worm numbers (<500 per sample) which permitted FUdR to be excluded from procuring aged-matched cohorts. Previous reports of applications of the plate-based GSH recycling method in *C. elegans* have described the requirement of 20,000 L4/adults per sample for quantification of GSH alone (265), which proportionally limits the scalability of the experimental strategy. Such a method would have resulted in the unavoidable use of FUdR.

By measuring the thiol GSH precursors, cysteine and γ-GC, in addition to GSH and GSSG, further interpretation of GSH homeostasis can be made in regards to the *de novo* synthesis pathway, which is typically overlooked in studies investigating glutathione metabolism (266). This enabled us to test the hypothesis that changes in GSH homeostasis during the lifespan of *C. elegans* results from either cysteine limitation or the progressive change in γ-GC levels as a marker for dysregulated glutamate cysteine ligase (GCL) activity. Observations of progressively lower homeostatic GSH and γ-GC levels during ageing in the absence of cysteine limitation would be supportive of lower GCL activity playing a key role in GSH decline, provided there is no increase in GSSG levels resulting from age-dependent deficiencies in the GSH recycling enzyme, glutathione reductase (GR). Investigations using the *C. elegans* model could potentially provide insight into how the GSH decline occurs during human ageing (Figure 2-2).

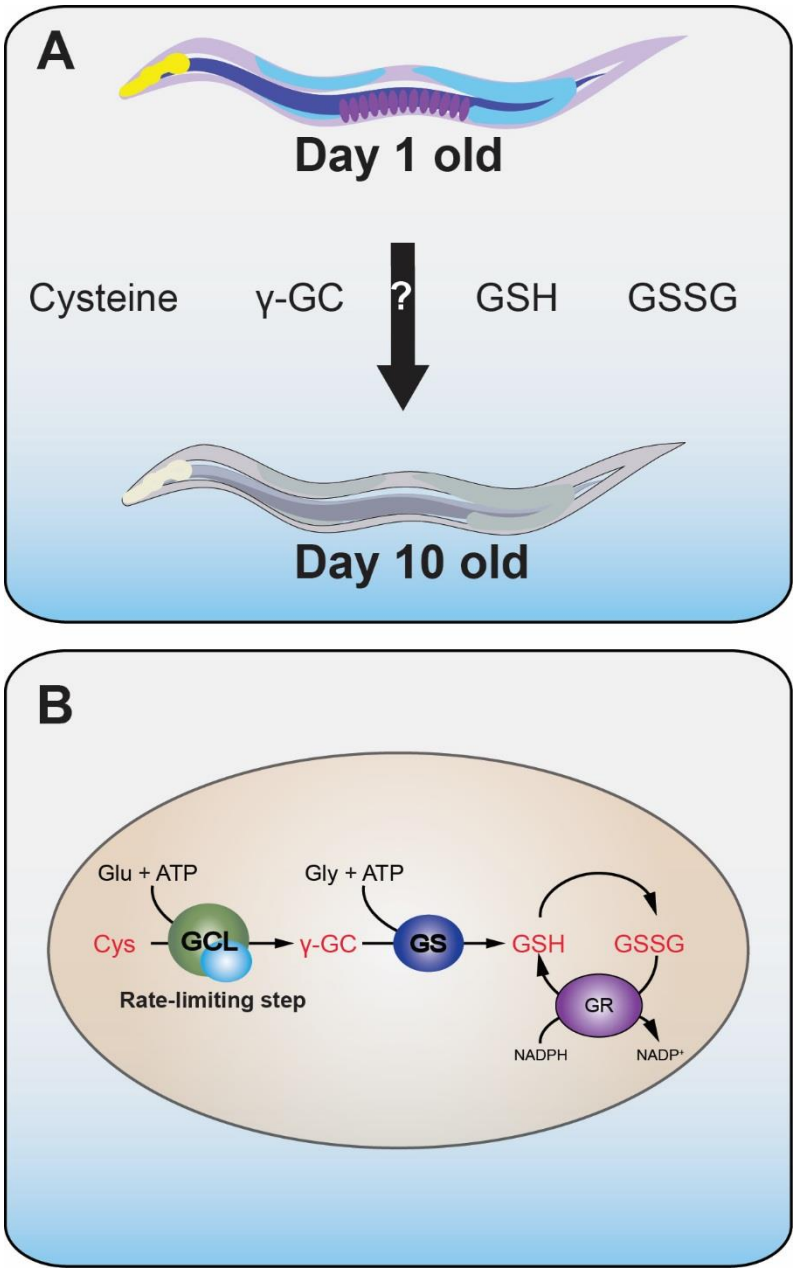

Figure 2-2. The age-related changes in glutathione homeostasis using *C. elegans*

(A) Using C. elegans *as an ageing model, changes in the levels of the key sulfur-containing metabolites involved in glutathione homeostasis may provide important information to understand the GSH decline during human ageing (B) All the metabolites monitored (shown in red) using LC-MS/MS, are either a substrate or a product of one of the enzymatic reactions in the glutathione synthesis pathway. Profiling of each of these metabolites in aged* C. elegans *will serve as an activity proxy for each of the enzymatic steps of the pathway.*

2.2 Materials and Methods

2.2.1 Chemicals and reagents

All chemicals were purchased through Sigma-Aldrich (Australia) unless otherwise stated. 7-chloro-*N*-[2-(dimethylamino)ethyl]-2,1,3-benzoxadiazole-4-sulfonamide (DAABD-Cl) was purchased through Chem-Supply Pty Ltd (Australia). The γ-GC used in this study was provided by Biospecialties International (Australia). Stable isotope labelled-GSH (glycine $^{13}C_2$, ^{15}N) was purchased through Novachem Pty Ltd (Australia). Solvents and consumables required for mass spectrometry work were provided by the Bioanalytical Mass Spectrometry Facility within the Mark Wainwright Analytical Centre, University of New South Wales.

2.2.2 Preparation of GSH, γ-GC, cysteine and GSSG standards

The thiol and GSSG stocks were freshly prepared on the day of each analytical run. Nine-point calibration curves (including the blank) for the thiol derivatives (cysteine, γ-GC and GSH) were measured over the concentration range between 0.25-125 pmol/20 µl. The concentration range for the GSSG calibration curves was between 0.01- 5 pmol/20 µl. Standards were prepared in the same derivatisation buffer as the biological samples. The labelled GSH internal standard (GSH-ISTD) was spiked in the pooled thiol standards and the biological samples at a concentration of 12.5 pmol/20 µl.

The labelled ($^{13}C_4{}^{15}N_2$)-GSSG stock solution was prepared by oxidising the commercially available ($^{13}C_2{}^{15}N$)-GSH using H_2O_2 by adapting a previously reported method (267). The original method used equimolar amounts of H_2O_2 to oxidise the labelled GSH to labelled GSSG. In this work, commercially available glutathione peroxidase (GPx) from

bovine erythrocytes (Sigma, cat# G6137) was used to enzymatically reduce the H_2O_2, forming oxidised ($^{13}C_4{}^{15}N_2$)-GSSG. Briefly, lyophilised GPx was reconstituted in 10 mM sodium phosphate (pH 7.0) containing 1 mM dithiothreitol (DTT) according to a previous method (268). Labelled ($^{13}C_4{}^{15}N_2$)-GSSG stock was prepared in 500 µl total volume reaction mix, containing 1 mM ($^{13}C_2{}^{15}N$)-GSH, 20 mM H_2O_2 and 5 U GPx in 10 mM sodium phosphate buffer. The reaction was carried out at room temperature for 30 min, followed by heating at 60°C to remove any residual H_2O_2. Separation of GPx from ($^{13}C_4{}^{15}N_2$)-GSSG was achieved using an Amicon Ultra-15 Centrifugal Filter Unit (30,000 MWCO) spun at 12,000 *g* for 15 min at 4°C.

2.2.3 Sample Preparation

Age-matched worms were individually transferred on a daily basis to separate them from their progeny. Approximately 500 worms were collected for each sample and separated from the *Escherichia coli* OP50 lawns by sucrose flotation (269). The worms were suspended in 100 µl M9 buffer in 1.5 ml Eppendorf tubes using Sorenson™ low binding standard tips to minimise worm adherence and stored at -80°C prior to being analysed for their thiol content. Thiol levels in *C. elegans* were normalised to protein content measured using a Bicinchoninic acid (BCA) protein assay kit (Pierce).

2.2.4 Thiol derivatisation reaction

Lysis of the worm samples were performed immediately prior to the mass spectrometry analytical run and involved the addition of an equal volume (100 µl) of derivatisation reaction mixture to the frozen samples to achieve a final volume containing: 10 mM CHAPS (3-[(3-Cholamidopropyl) dimethylammonio]-1-propanesulfonate) hydrate, 2 mM Na_2EDTA, 7 mM DAABD-Cl (dissolved in acetonitrile) in 1 mM borate buffer

(1 mM boric acid solution + 0.25 mM sodium tetraborate [pH 9.0], personal communication with Emeritus Professor Kazuhiro Imai, Musashino University, Tokyo). The worms were then homogenised with a motorised micropestle with 3× freeze/thaw cycles in liquid nitrogen followed by immediate incubation on a heating block for 10 min at 40°C. The thiol derivatisation reaction was quenched after 10 min by the addition of 4.5 µl trifluoroacetic acid (TFA). The soluble fraction was then collected after centrifugation at 22,000 *g* for 15 min at 4°C. To avoid reduction of disulfides in the sample, including GSSG and cystine (disulfide form of cysteine), the reducing agent tris(2-carboxyethyl)phosphine (TCEP), was excluded from the reaction mix that was outlined in the original method (131).

2.2.5 BCA Protein Assay

Frozen worm homogenates were thawed immediately prior to assaying. The BCA working solution was prepared by mixing the BCA reagent A with the 4% $CuSO_4$ solution (B) at a ratio of 50:1 (v/v). The assay was performed in a clear 96-well plate in triplicates, with a final volume of 225 µl per well (25 µl sample and 200 µl BCA working solution). Bovine serum albumin (BSA) was used as the standard (0-2000 µg/mL protein) and prepared in reaction buffer according to the manufacturers' instructions (Pierce).

2.2.6 Chromatography

Mixtures of the low-molecular weight thiols were separated using a Thermo Scientific Accela UHPLC System, with an Agilent Poroshell 120, 2.1 mm × 150 mm SB-C18 (2.7 µm pore size) column over a 10 min gradient at 0.4 ml/min. Samples were queued in an autosampler and maintained at 10°C for the duration of the run. The injection volume for all samples was 20 µl. The column was heated at 40°C using a Hot Pocket column

heater (Thermo Scientific). Eluent A was 0.1% formic acid in water and Eluent B was 100% acetonitrile with 0.1% formic acid. A programmed gradient was used for separation of GSSG and the derivatised thiols. Initial solvent conditions consisted of 100% Eluent A from 0-2 min. This was followed by a linear gradient from 2-6 min to 100% Eluent B followed by isocratic delivery of 100% Eluent B between 6-6.9 min, and a shift from 0-100% of Eluent A between 6.9-7 min, followed by a final re-equilibration at 100% Eluent A from 7-10 min.

2.2.7 Tandem mass spectrometry

Tandem mass spectrometry (MS/MS) was performed using a ThermoFisher Scientific TSQ Quantum Access triple quadrupole mass spectrometer, with a heated electrospray ionisation (HESI) source that operated in positive ion mode. Optimal selected reaction monitoring (SRM) transitions, their collision energies, collision gas pressure and S-lens voltages were obtained from infusion of standards using Quantum Tune software. The most intense transition was used as a quantifying ion and the second most intense transition was also acquired for use as a qualifying ion. The SRM transitions and collision energies used for the collision-induced dissociation (CID) of the analyte fragments are shown in Table 2-1. The gas pressure was kept constant at 2.0 mTorr throughout each run. Dwell times of 100 ms for each transition were programmed, with a cycle time of 1.2 seconds (sum of all analyte transitions).

Standard curves were measured at the start and end of each run, with the biological samples being scheduled in the middle. Cysteine, γ-GC, GSH and GSSG levels in the *C. elegans* extracts were determined using calibration curves. The pooled thiol curves and biological samples were spiked with 12.5 pmol/20 µl GSH-ISTD. The standards were ordered in ascending concentrations to minimise any possible carry-over effects from one

sample to the next. Injection of methanol as a wash step between standards and samples obviated the risk of any cross-contamination. Data acquisition and sample peak area integration was performed using Xcalibur software (ThermoFisher Scientific). Manual corrections of the automated integration of detected peaks was performed as required using the Qual Browser application.

2.2.8 Statistics

A summary of the method validation results is presented in Table 2-3. Analysis of the changes in metabolite levels in aged *C. elegans* were performed using regression analysis to calculate the correlation coefficient (R^2) in the GraphPad Prism software (version 7.02). For non-linear regression modelling the p-values were calculated using Microsoft Excel.

2.3 Results

2.3.1 Method development

A HPLC method coupled with fluorescent detection has previously demonstrated that the fluorogenic properties of the thiol-specific derivatisation compound, 7-chloro-N-[2-(dimethylamino)ethyl]-2,1,3-benzoxadiazole-4-sulfonamide (DAABD-Cl) can be utilised for low-molecular weight thiol detection in *C. elegans* (131). The method was adapted for HPLC-tandem mass spectrometry (LC-MS/MS) to allow for the simultaneous quantification of cysteine, γ-GC, GSH and GSSG.

Briefly, the products of DAABD-Cl-derivatised thiol conjugates and the free GSSG disulfide were observed in positive ion mode as protonated molecules $[M+H]^+$. Chromatographic conditions were optimised for rapid simultaneous quantification of cysteine, γ-GC and GSH when pooled in equimolar amounts. Further optimisation of the protocol required the exclusion of the reducing agent TCEP from the reaction mix to permit measurement of native GSSG. The SRM transitions of each analyte were initially determined using infusion of standards under optimised run conditions (Table 2-1).

Instrument performance for each analyte was initially tested by establishing the linear dynamic range over which ion signal was proportional to analyte concentration. Ten-fold serial dilutions of 1 mM analyte stocks were measured, and the range was determined by the lowest concentration limit that maintained curve linearity. Instrument performance was assessed by running standard curves in duplicates to determine any within-run variation in analyte signal. Reproducibility was assessed in worm samples to confirm the simultaneous detection of each analyte in the biological matrix.

Table 2-1. Quantifying and qualifying ion transitions *m/z*, collision energies and column elution times for thiol and disulfide analytes

Compound	Transition (*m/z*)	Collision energy	Average elution time (min)
DAABD-Cys (Quantifier)†	391→303	30 eV	5.1
DAABD-Cys (Qualifier)*	391→192	30 eV	5.1
DAABD-γ-GC (Quantifier)†	519→303	30 eV	5.4
DAABD-γ-GC (Qualifier)*	519→391	30 eV	5.4
DAABD-GSH (Quantifier)†	576→447	24 eV	5.4
DAABD-GSH (Qualifier)*	576→303	29 eV	5.4
DAABD-GSH (SIL) (Quantifier)†	579→450	24 eV	5.4
DAABD-GSH (SIL) (Qualifier)*	579→303	29 eV	5.4
GSSG (Quantifier)†	613→231	30 eV	3.7
GSSG (Qualifier)*	613→355	30 eV	3.7
GSSG (SIL) (Quantifier)†	619→231	30 eV	3.7
GSSG (SIL) (Qualifier)*	619→361	30 eV	3.7

†Quantifying ions: the most intense signal from the SRM transitions. *Qualifying ions: the second most intense signal from the SRM transitions.

2.3.2 Optimisation of chromatographic conditions and analyte quantification

Compared to conventional spectrophotometric and HPLC-based methods for low-molecular weight thiol quantification, LC-MS/MS enables the separation and quantification of closely related but structurally distinct thiol species based on mass. Detection selectivity of each thiol was evaluated by looking for interference between the thiols. For any thiol to interfere with the detection of another, the two would have to elute at a near identical retention time and both would also have the same SRM transitions (270). Cysteine is potentially more prone to interference than γ-GC and GSH as it is a constituent component of both. Though, γ-GC generated a signal in the cysteine SRM channel, due to differences in elution time (cysteine, 4.61 min; γ-GC, 4.77 min) their peaks could be individually resolved (Figure 2-3).

The C_{18} column provided an acceptable peak-shape for GSSG without modification of the run conditions. The observed quantifying transition of GSSG (*m/z* 613→231) was identical to that reported by a previous study that used a similar solvent gradient with a C_{18} column (271). Other studies have reported the observed qualifying transition of GSSG (*m/z* 613→355) in their analysis (259, 272-274).

Calibration curves of the pooled derivatised thiols typically provided a linear response from 0.25-125 pmol/20 µl (R^2>0.998). GSSG maintained linearity between 0.1-5 pmol/20 µl. All standard curves covered biologically relevant concentrations in the sample mixtures (Figure 2-4).

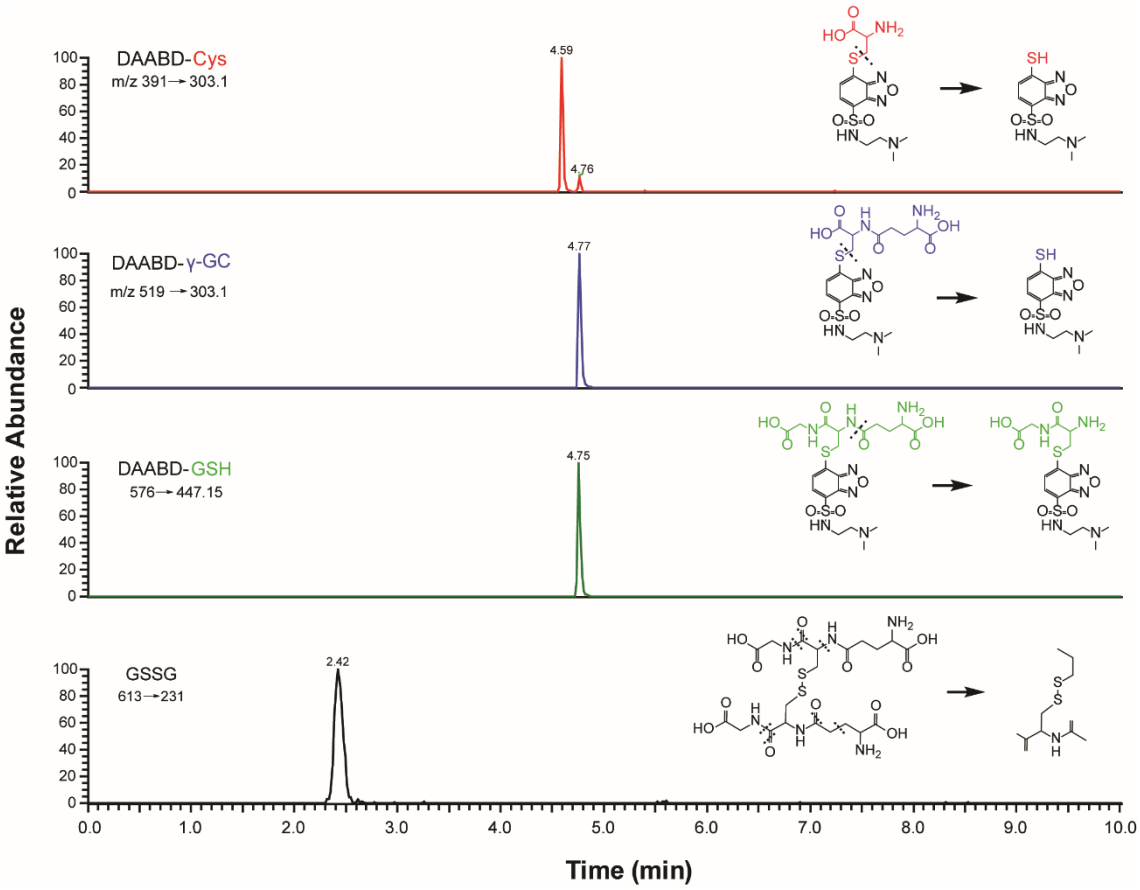

Figure 2-3. Chromatograms of the derivatised thiols and GSSG

The chromatograms show the peak shapes of DAABD-derivatised cysteine (red), γ-GC (blue), and GSH (green). Peak shapes and the retention times for the quantifying transitions of each thiol were simultaneously generated from a single sample. The second small peak for cysteine at 4.76 min (red), corresponds to the transition of γ-GC which is separated in the analysis. The predicted collision induced dissociation (CID) transition patterns monitored for the quantifying ions DAABD-cysteine, DAABD-γ-GC, DAABD-GSH, and native GSSG form are represented. Dashed lines of the molecular structures indicate the bond cleavage sites that undergo fragmentation. Structures drawn using ChemDraw Professional software (version 16.0).

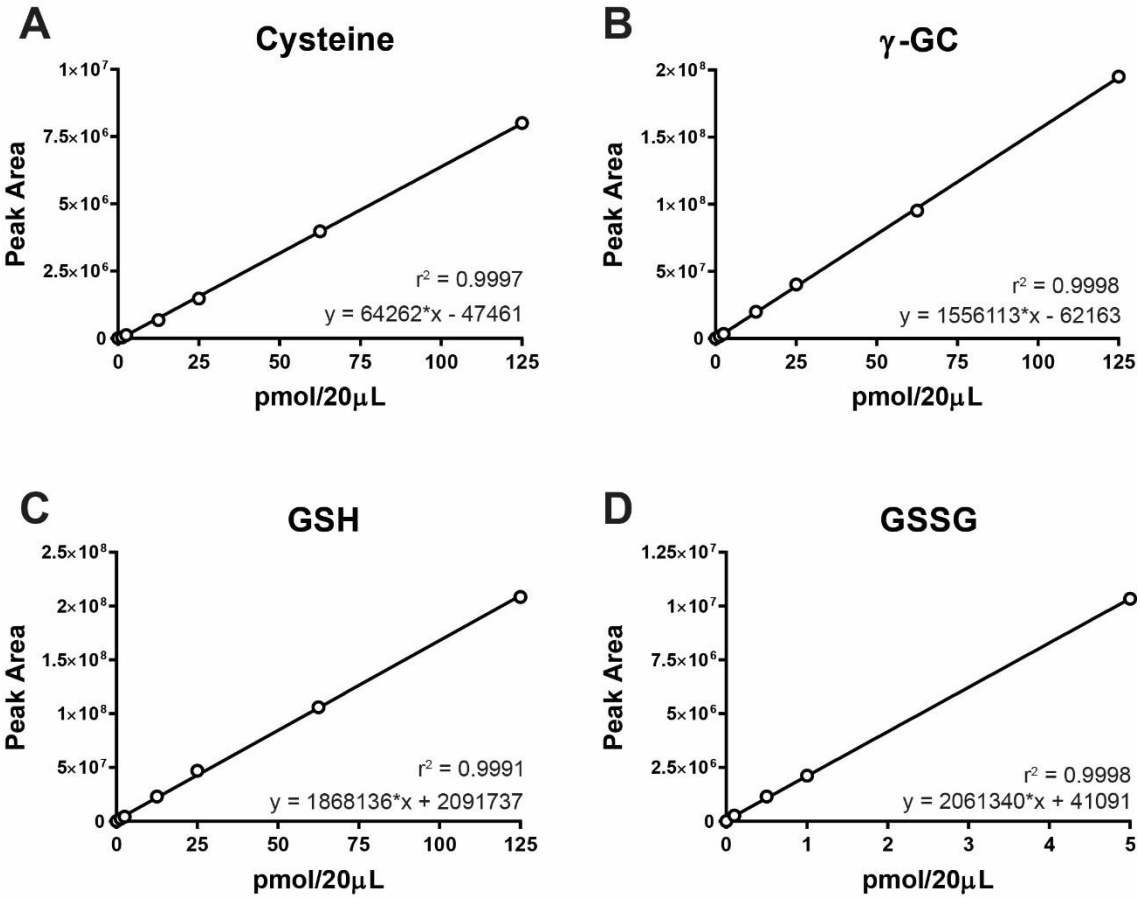

Figure 2-4. Standard curves for thiols and GSSG

Equimolar amounts of (A) cysteine, (B) γ-GC, and (C) GSH were pooled and assayed over the range of 0.025 - 125 pmol/20 µl. The standard solutions were prepared in borate buffer, immediately prior to derivatisation with DAABD-Cl. Concentrations of (D) GSSG between 0.1 - 5 pmol/20 µl maintained linearity (R^2>0.99).

2.3.3 Measuring the potential occurrence of GSH autoxidation

Due to the high relative levels of cellular GSH to GSSG, even a small fraction of autooxidation occurring could significantly increase GSSG levels (249). For example, at the theoretical cellular ratio of ~100:1 (GSH:GSSG), occurrence of 2% autoxidation of GSH would decrease the molar ratio estimates to ~50:1. The rate of reaction between the thiol and the derivatising agent is a critical consideration to avoid autooxidation of the thiols (249, 275). The complete derivatisation reaction rate of DAABD-Cl (<5 min) (264) has been demonstrated to proceed faster than commonly used reagents such as monobromobimane and iodoacetic acid (between 15-40 min) which have estimated high GSSG values in previous reports, suggesting the possibility of autooxidation being a confounding artefact of the methodology (275). One potential caveat of the LC-MS/MS method presented herein is that autooxidation of the thiol groups may occur when using a pH 9 reaction buffer, due to formation of the thiolate anion. To test the occurrence of GSH autoxidation, the percentage of GSSG present in the GSH standard was measured using separate GSH and GSSG standards in the same analytical run. Across several inter-day replicates, the amounts of GSSG present (<1%) in the GSH standards indicated negligible amounts of autoxidation (Table 2-2).

Table 2-2. GSSG present in GSH standards

GSH (pmol/20 µl)	GSSG (pmol/20 µl)	GSSG (%)	Inter-day replicates
125	0.62±0.04	0.49±0.02	4
62.5	0.41±0.12	0.65±0.09	4
25	0.14±0.07	0.58±0.13	4
12.5	0.10±0.04	0.81±0.25	2
≤ 2.5	n.d.	n.d.	N/A

n.d.= not detected

2.3.4 GSH internal standard (GSH-ISTD)

Due to GSH being the key analyte in this study, an internal stable isotope-labelled GSH was included to correct for any measurement error. At the highest concentration of GSH (125 pmol/20 µl), naturally occurring carbon-13 (C^{13}) isotopes appeared to cause interference of the ($^{13}C_2{}^{15}N$)-GSH internal standard. This obstructed the linearity of the calibration curve of the measured peak area ratios observed between GSH and the GSH-ISTD (GSH/GSH-ISTD). To avoid this interference, the initial quantifying ion was changed from *m/z* 579→450 to include the transition of *m/z* 579→303 (Figure 2-4). This improved curve linearity and increased the GSH/GSH-ISTD signal ratio, at the expense of a negligible loss in sensitivity. The ratio between signal intensity of GSH and the internal standard from the standard curve was used to correct for the quantification of GSH in the biological matrix.

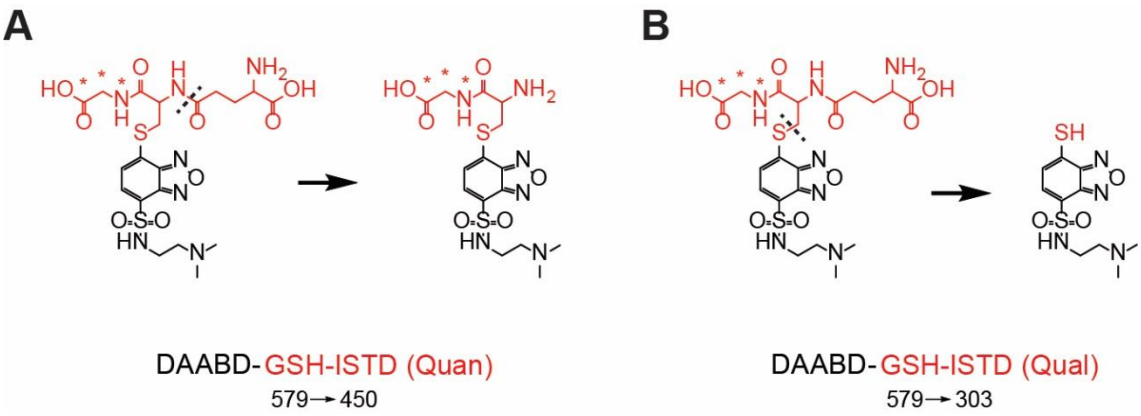

Figure 2-5. Proposed structures of the quantifying and qualifying ions of GSH-ISTD

A) The quantifying ion transition of ($^{13}C_2{}^{15}N$)-GSH produced the most intense signal. B) The qualifying ion transition of ($^{13}C_2{}^{15}N$)-GSH produced the most second intense signal and was selected for use in this study to improve standard curve linearity.

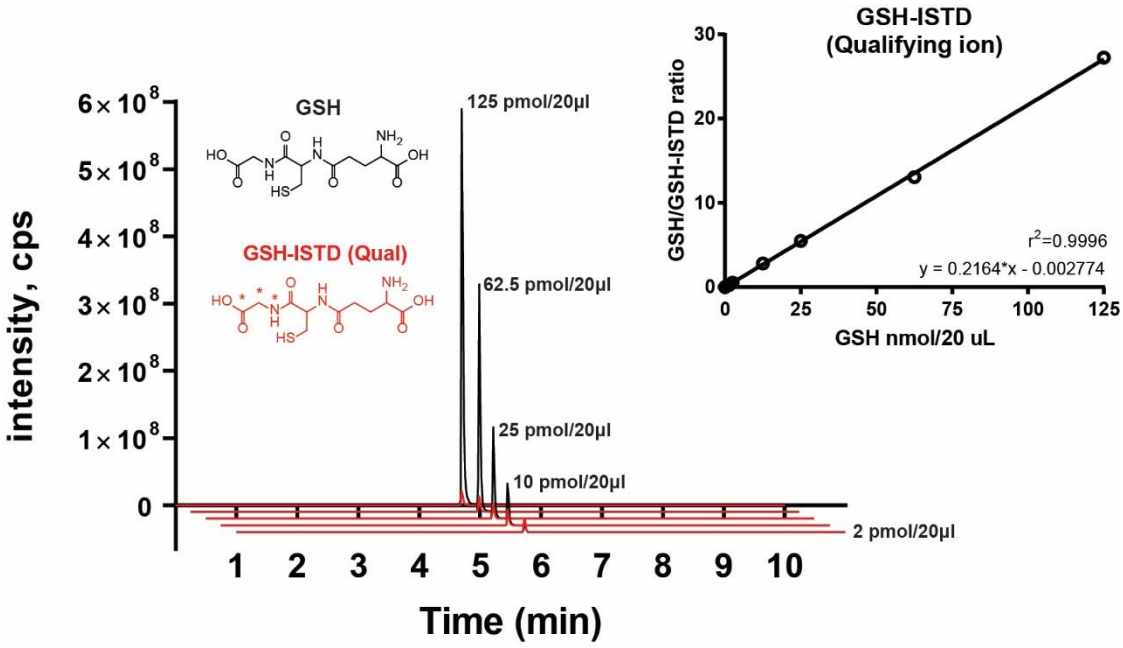

Figure 2-6. Linearity of GSH standard with spiked with ($^{13}C_2{}^{15}N$)-GSH internal standard

*A representative SRM chromatogram of GSH standards (black peaks) spiked with ($^{13}C_2{}^{15}N$)-GSH (red peaks). The intensity of signal counts per second (cps) of GSH-ISTD is shown for the qualifying ion (*m/z *579→303)* ***Inset:*** *Linearity of measurement of the total area ratio of the relative signals (GSH/GSH-ISTD).*

2.3.5 Tandem mass spectrometry performance and method validation

Partial validation of the method and the tandem mass spectrometry performance of each analyte was evaluated (Table 2-3).

Accuracy of the method was determined by measuring known amounts compared to the theoretical value deduced from the calibration curves. The inter-day accuracy (n=3) was assessed by inclusion of quality control (QC) samples of known concentrations that compared to the mid-range values on the standard curve. Accuracy values are expressed the percent deviation of the determined experimental concentration from the proposed theoretical concentration.

The precision of an analytical method describes the closeness of individual measures of an analyte when the procedure is applied repeatedly to multiple aliquots of a single homogenous volume of biological matrix. Intra-day precision (n=4) was assessed by comparing duplicate values of the biological matrices.

Sensitivity was assessed by measuring the lower limits of detection (LLOD) and lower limits of quantification (LLOQ) for each analyte. The LLOD was defined as the analyte concentration that generated a signal-to-noise ratio at least three times greater than the signal from the blank sample (S/N>3). The LLOQ was defined as the concentration with a signal-to-noise ratio at least ten times greater than the blank (S/N>10) that was reproducible throughout every run, with the percent of the coefficient of variance (%CV) within 20%.

Each analyte showed acceptable levels of stability (within 15%) in run conditions (6-8 h, 10°C). However, in one run the cysteine standard curve did show poor within-run stability (77%; data not shown). This was later attributed to the change in pH of the borate buffer after one-month storage at room temperature. To address the risk cysteine instability, the borate buffer was used within two weeks of preparation. Standards were also prepared fresh on the day of each run.

Table 2-3. Partial method validation summary

Assessment	**Cysteine**	**γ-GC**	**GSH**	**GSSG**
Accuracy (% bias)	-8%	+5%	+1%	n. a
Precision	93%	97%	98%	n. a
Sensitivity				
LLOD (pmol/20µl)	0.25	0.025	0.025	0.01
LLOQ (pmol/20µl)	2.5	0.25	0.025	0.1
Stability				
Processed sample stability	93%	95%	97%	92%

n. a = not assessed

2.3.6 Glutathione homeostasis declines with age in *C. elegans*

To explore the nature of the age-related changes in glutathione homeostasis, GSH and its precursors cysteine and γ-GC, as well as GSSG were monitored over the first 10 days of worm adulthood. Each sample (n=23-34) comprised between 250 to 500 worms, with the majority of samples (n=20-30) taken from day 1 to day 5 old adults. Though a slight decline in cysteine levels with age was observed (Figure 2-7A), linear regression analysis revealed no significant difference (p=0.074; r^2=0.0963). Both γ-GC (p<0.01) and GSH (p<0.0001) significantly declined exponentially (non-linear) at similar proportional rates over the first 10 days (Figures 2-7B & C). This suggested that GCL dysregulation may be occurring during ageing given the progressive decline in γ-GC production in the absence of cysteine limitation.

The decline in GSH was unlikely related to any dysfunction in the reducing capacity of glutathione reductase (GR). At the theoretical GSH:GSSG ratio of 100:1, if the glutathione couple was in equilibrium, a 50% decline in GSH should correspond to a 25-fold increase in the molar GSSG concentration, based on the equation for the half-cell reduction potential (276) of the glutathione redox couple:

$$2GSH - 2e^- - 2H^+ \leftrightarrows GSSG$$

As there was no significant change in GSSG levels, the decline in GSH cannot be explained by a limitation in the recycling of GSSG by GR (Figure 2-7D). The GSH/GSSG molar ratio did follow a pattern of decline with increasing age (Figure 2-8), indicating a pro-oxidising shift in the glutathione redox state occurs due to dysfunction in the *de novo* GSH synthesis pathway rather than dysfunction of GR.

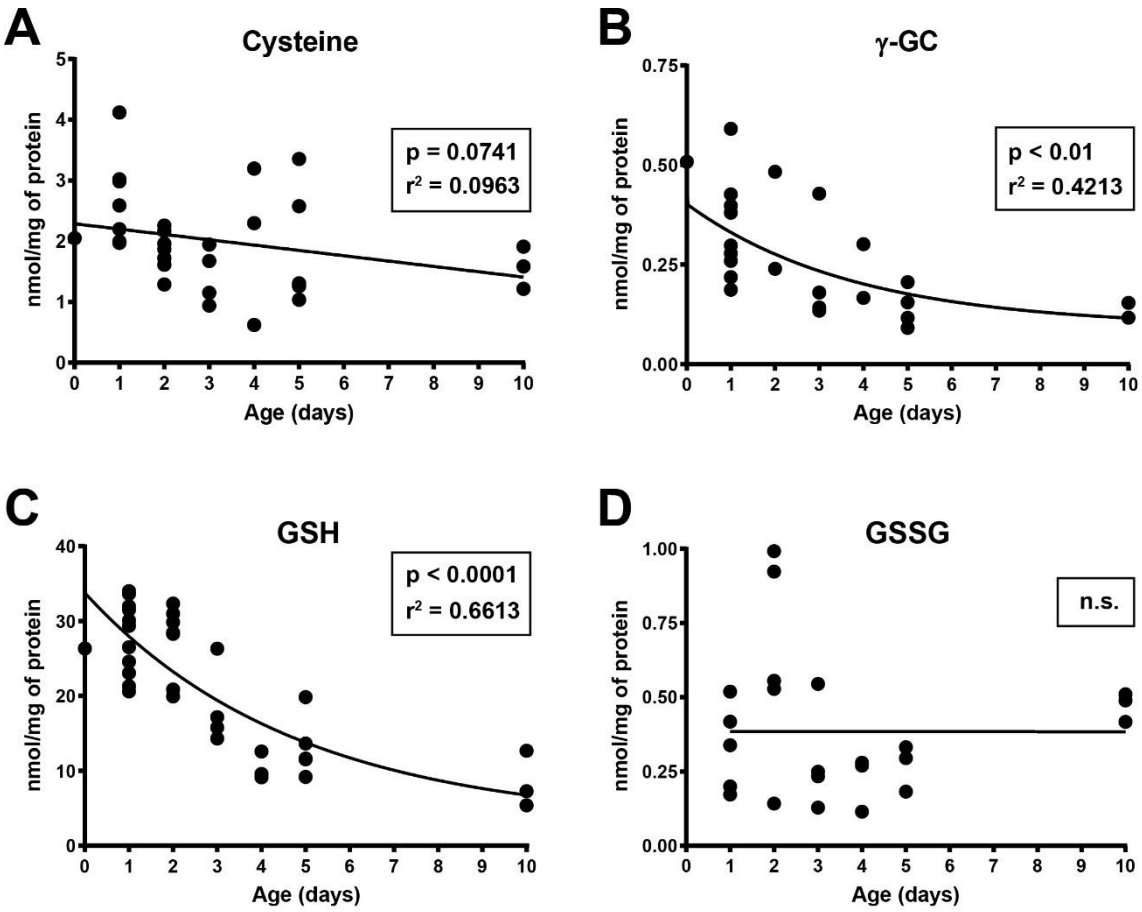

Figure 2-7. Levels of the metabolites of glutathione homeostasis in ageing *C. elegans*

Age-matched cohorts (approx. 500 worms) of wild-type C. elegans *were grown at 20°C and collected between 0-10 days of adulthood. Regression analysis was used to determine any age-dependent trends in thiol levels (n=23-34).*

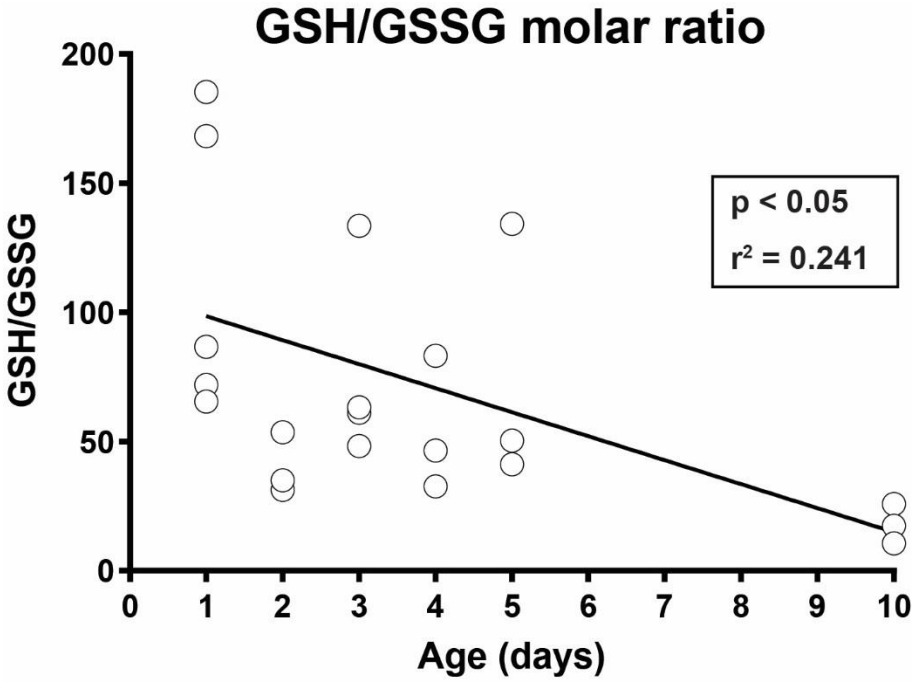

Figure 2-8. GSH/GSSG molar ratios of ageing *C. elegans*

The molar ratio of GSH/GSSG declined over the first 10 days of adulthood. The mean of the GSH/GSSG molar ratios declined from approximately 115:1 at day 1 to 25:1 at day 10.

2.3.7 Cysteine is limiting in GSH synthesis beginning at day 1 of adulthood

Day 1 old adults were treated with increasing concentrations (0-10 mM) of the cysteine prodrug, *N*-acetylcysteine (NAC) in liquid medium for 2 h (Figure 2-9). Dose-dependent increase in cysteine and γ-GC levels were observed, though only the 5 mM NAC doses were considered significant for increasing γ-GC levels ($p<0.05$). An observed increase in mean GSH levels was also observed for the 5 mM NAC treated group, yet this increase was considered not significant. No change was observed for any of the thiol levels in the 10 mM NAC-treatment group, suggesting that the higher concentration was causing aberrations of dose-dependency in the system resulting in an observed inverted U-shape dose-response.

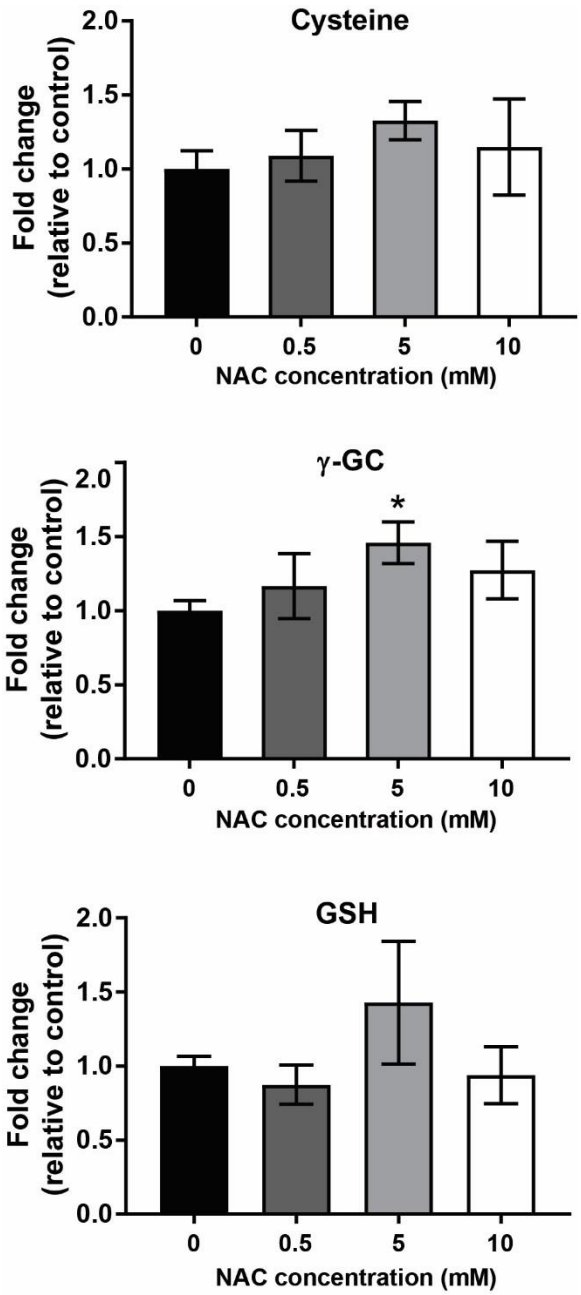

Figure 2-9. Thiol levels in day 1 adult nematodes treated with NAC

*Synchronised day 1 old wild-type adults were incubated for 2 h at 20°C in M9 buffer containing NAC (0-10 mM). At 5 mM NAC, the γ-GC content of the worms had significantly increased (*p<0.05). Though a similar increase in the cysteine and GSH levels were observed they were not determined to be significant. A one-way ANOVA test was performed using Dunnett's multiple comparisons test as a follow up for comparisons of each treatment and their controls. Data presented as mean ±SD* (*n=3*).

2.4 Discussion

The decline in glutathione homeostasis has long been considered a key factor in human ageing (277, 278). In various higher organisms, this decline is typically considered to result from dysregulation of the gamma-glutamyl cycle, which can lead to decreases in the GSH synthetic capacity or a pro-oxidising shift in the GSH/GSSG ratio. Studies that have explored the *in vivo* changes in human GSH levels have tended to focus on monitoring either plasma, erythrocytic or lymphocytic GSH content as endpoint measurements. Investigating GSH in human lymphocytes is arguably more representative of cellular GSH regulation as they, unlike mature erythrocytes, contain a nucleus, and hence the ability to maintain cellular GSH homeostasis via the upregulation of GSH synthesis enzymes. Post-mortem measurement of GSH levels in several sections of the adult ageing human brain (23-99 years) have suggested that levels may not decline (279). The authors did, however note that the rapid post-mortem breakdown of GSH levels may have influenced results. This is supported by others that have shown that post-mortem changes in GSH decline to 88% after 30 min and to as low as 50% after 24 h (280). The application of ^{1}H magnetic resonance spectroscopy (MRS) in human clinical studies may offer a non-invasive alternative to measure brain GSH concentrations *in vivo* (281).

The results presented in this chapter demonstrate that the age-related GSH changes in *C. elegans* follow a similar pattern of decline to that observed in aged human lymphocytes (282). The lymphocytic GSH content of 60-80 year olds (12.3 nmol/mg protein) was shown to be ~57% the content of 20-40 year olds (21.5 nmol/mg protein) (282). Here we show that *C. elegans* is a powerful model to investigate the human age-equivalent changes in glutathione homeostasis.

2.4.1 A novel LC-MS/MS method resolves glutathione homeostasis changes during *C. elegans* ageing

The use of benzofurazans have been discussed, though rarely reported, as an alternative derivatising agent to commonly used alkylating agents, such as *N*-ethylmaleimide (NEM), for the measurement of low-molecular weight thiols in biological systems (249, 283). The use of NEM for HPLC-based methods has limitations, including the potential for non-thiol peptide binding (284) and the formation of diastereomers of NEM-thiol adducts which can lead to two chromatographic peaks for each analyte (285, 286). The benzofurazan, DAABD-Cl, was initially purposed for the identification of cysteine-containing proteins using LC-MS/MS (264). Its fluorogenic properties made it amenable for the detection of several proteins and other low-molecular weight thiols, including homocysteine and cysteinylglycine in *C. elegans* extracts using HPLC coupled with fluorescence detection (131, 264). Increased sensitivity enabled the detection of thiol derivatives at the femtomole level (264), which qualified DAABD-Cl a suitable alternative derivatising agent to explore in this work.

A major concern in *C. elegans* ageing work is the lack of consensus between studies on what concentration of 5-fluorodeoxyuridine (FUdR) should be included in the nematode growth medium (NGM) to inhibit progeny production. Concentrations ranging between 40-500 μM FUdR are typically used (287), which may have an effect on the worm's physiology and introduce experimental artefacts. It has been suggested recently that the findings of lifespan studies that have employed FUdR may need to be reinterpreted (261). The experimental approach for this, and the work detailed in subsequent chapters, was to exclude FUdR to avoid possible artefacts. Accordingly, provision of the high sensitivity LC-MS/MS method allowed the measurement of each of the analytes in a relatively low

number of worms (<500). Though this approach was exorbitantly more time consuming than the inclusion of FUdR in the NGM, the results presented herein will not require the scrutiny of reinterpretation due to possible FUdR related artifactual bias. Ultimately, the development of more sensitive analytical methods will allow FUdR to be excluded from experiments that investigate important mechanistic metabolic questions and limit its use as a tool for screening only.

2.4.2 Potential caveats relating to the LC-MS/MS method

It is critical to consider the acid dissociation constant (K_a) of a thiol when preparing the pH buffered conditions of the derivatisation reaction. The intrinsic pK_a for the thiol-thiolate equilibrium in an aqueous solution is reported to be approximately 8.6 for cysteine (288), 9.9 for γ-GC and 8.9 for GSH (289). Previous studies have also expressed similar concerns when using a borate buffer at pH 9 where the complete derivatisation between iodoacetic acid and thiols occurs rapidly within 5 min (290, 291). Most pre-analytical sample preparation methods include protein precipitation by acidification as a precautionary step to avoid the deprotonation of the thiol group forming the more reactive thiolate (S^-) anion. Derivatisation reaction conditions between organic thiols and benzofurazans is favoured between pH 8.5–9 (292). The DAABD-Cl derivatisation takes less than 5 min at pH 9 (264) and 20 min at pH 8 (293).

It has been discussed that errors can occur when making the assumption that acidification is essential during sample preparation for GSH analysis as this has been reported to result in oxidation of sulfhydryl groups, possibly as a consequence of the release of ROS from the biological matrices (249). During the method development, pre-treatment of the worm samples with DAABD-Cl reaction mixture before sample homogenisation was implemented to ensure immediate derivatisation and to avoid any thiol autooxidation.

Previous HPLC studies have demonstrated that pre-treatment with the alkylating agent *N*-ethylmaleimide (NEM) can minimise autooxidation when added prior to sample acidification (286). Minor occurrences of artefactual oxidation of GSH can lead to a considerable relative increase in GSSG and inherent misreporting of the GSH/GSSG ratio. Even recent innovations to image GSH in live cells in real-time (294) have caveats to the methodology (295, 296). The fundamental challenges of measuring cellular redox couples pertain to the analytical practices causing unavoidable perturbations in the redox system (291).

2.4.3 Glutathione homeostasis declines with age in *C. elegans*

To develop appropriate therapeutic strategies, it is essential to understand how GSH is declining with age. Here we have shown that *C. elegans* can be used as a model to determine dysfunctions in the GSH *de novo* synthesis pathway that can explain this decline. Young adult wild-type worms (day 0) have previously been reported to contain 40 nmol GSH/mg protein with a GSH/GSSG ratio of 70:1 (132), which agrees with findings in day 1 adult wild-types presented in this chapter (27.8 nmol GSH/mg protein, 115:1). Our findings of a GSH decline are in agreement with others that have shown similar trends with nematode ageing (127, 145). The development of the LC-MS/MS single assay method for the detection and quantitation of thiols and GSSG, has overcome the technical limitations of current commercially available glutathione assay kits, which has prevented investigations of age-associated changes in the GSH/GSSG ratio and the related thiol metabolites in *C. elegans* (145).

Glutamate, cysteine, and glycine are amino acids that intersect with major metabolic pathways including, nitrogen-, sulfur-, and one-carbon metabolism. Although cysteine is

generally considered the limiting substrate for GSH synthesis, there is the possibility that glutamate, glycine or ATP partitioning to other pathways (266) could also impact on GSH levels during ageing, and should be investigated in future work. Compared to other free amino acids, measurement of cysteine is considered difficult in biological samples without an alkylating agent, such as iodoacetic acid (297), which presumably has led to cysteine levels often being omitted from metabolic studies.

2.4.4 Cysteine availability is limiting in GSH synthesis from day 1 adulthood

Cysteine levels did not show a significant age-dependent trend that could fully explain the observed decline in GSH. If cysteine levels do not decline as rapidly as GSH in *C. elegans*, then perhaps it is limiting at every stage of adulthood. Accordingly, the method we present herein was used to determine whether cysteine, in the form of *N*-acetylcysteine (NAC) supplementation, can increase GSH levels (Figure 2-9). Physiological benefits of NAC have been reported in several worm studies (298, 299), yet none have monitored changes in GSH levels post-treatment. The availability of cysteine needs to be sufficient to support the substrate requirements for the high turnover rate of GSH. Though the data from aged worms suggests that cysteine levels may not decline with increasing age, day 1 old worms treated with NAC showed corresponding dose-dependent (0-5 mM NAC) increases in cysteine and γ-GC, indicating that while cysteine levels may not significantly decline with age, they may in fact be limiting from young adulthood.

2.4.5 Age-related changes in the GSH/GSSG ratio

The GSH/GSSG ratio is an indicator of a cell's oxidative status and the efficiency of the *de novo* and salvage GSH synthesis pathways. Measuring the GSH/GSSG redox couple over the life of the worm could offer insight into disturbances in the network that cannot

be gained by measuring GSH alone. For example, if NADPH levels, which are determined by the pentose phosphate pathway (PPP), become limiting for the recycling of GSSG to GSH by glutathione reductase (GR), it will be apparent by increases in GSSG and a decline in the GSH/GSSG ratio.

The generation of transgenic worms strains encoded with a redox sensitive ratiometric green fluorescent protein (GFP) probe capable of measuring the relative abundance of GSH and GSSG have been recently reported (300). However, autofluorescence in the green emission wavelength was shown to increase with ageing leading to compounding interference obscuring the readings and limiting the use of the strain (300). It has been advised by the same researchers that when designing redox probes to consider generating fluorescent tags with the emission spectrums in the red region where autofluorescence is absent (301). A study using a variant of the redox sensitive ratiometric GSH:GSSG reporter strain, which investigated tissue-specific differences in young worms, concluded that the glutathione redox balance varies even among individuals of isogenic populations, likely due to variation in GSSG levels (42). This concurs with the considerable variation of GSSG levels that we have observed in aged matched wild-type populations (Figure 2-7D).

A decline in the activity of the glutathione reductase (GR) enzyme could also be occurring, though it is not clear based on our observations. One possible, but perhaps unlikely, explanation could be that the worm excretes excess cellular GSSG at a certain concentration threshold via multidrug resistance proteins (MRP) when the enzymatic action of GR is unable to maintain the age-related increases in GSSG levels. Though this is not obvious from the results, it should not be disregarded in the interpretations. The ability to measure the thiol and disulfide content of the worm's waste products from the

excretory system would provide useful information if any changes in the redox milieu were attributable to such a mechanism.

Another possibility of the decline in free thiol GSH could be that it is forming protein-mixed disulfides by *S*-glutathionylation. Increases in protein *S*-glutathionylation could be a mechanism to protect cysteine residues in response to an increased load of hydrogen peroxide. This hypothesis is consistent with work in worms that have shown that hydrogen peroxide levels increase with age (300). The net loss of GSH is possibly a result of dysregulation occurring at multiple levels with age. Modelling the decline in GSH in *C. elegans* will assist future efforts to understand the multifaceted levels of this dysregulation (Figure 2-10).

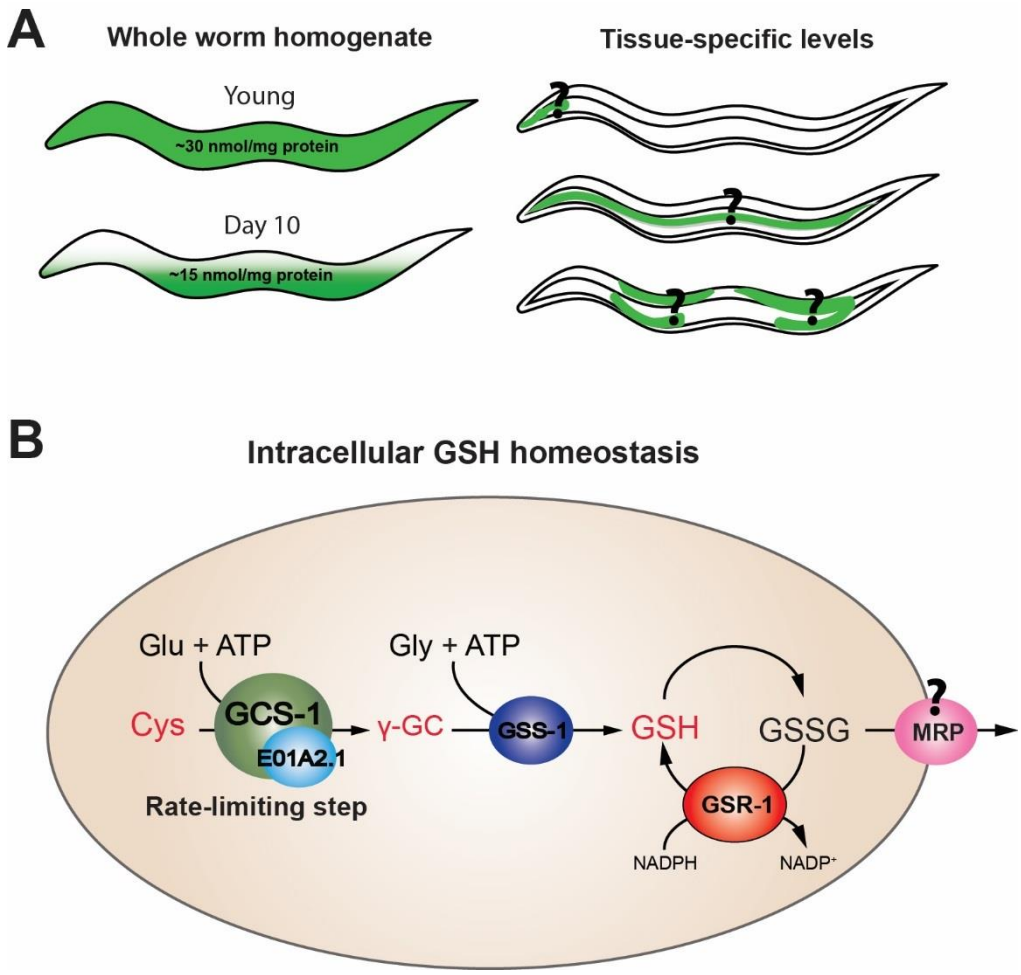

Figure 2-10. Modelling the decline of glutathione homeostasis in aged worms

(A) Whole worm lysates are sufficient to demonstrate a decline in GSH levels with ageing but lack the resolution to determine any tissue-specific changes. (B) Though a net loss of free GSH may be due to substrate limitation in the ATP-dependent reactions of the worm GCL holoenzyme orthologue (GCS-1/E01A2.1) or glutathione synthetase orthologue (GSS-1), a concomitant decline in γ-GC levels suggests a decrease in activity of the rate-limiting enzyme, which may be due to dysfunctional interactions between GCS-1 and the E01A2.1 modifier subunit. No changes in the GSSG levels were observed with ageing. Multidrug resistant proteins (MRP) may be involved in excreting cellular GSSG, yet the involvement of MRP in maintaining glutathione homeostasis remains poorly defined in worms.

2.4.6 Sub-cellular concentrations of the glutathione redox couple

The majority of glutathione redox research that is based on the chemical analysis of whole-cell extracts to deduce oxidation-reduction potential (E_h) of the cell has recently been challenged (302). Given that cellular GSH concentrations are heterogeneously distributed throughout the cytosol and sub-cellular compartments (303), whole cell extract data used to estimate cellular electrochemical potential may be misleading if using the Nernst equation (276). Use of the information obtained in the work described in this chapter to calculate the E_{GSH} redox potential using the Nernst equation would be uninformative on the nature of the cytosolic glutathione pool (302). The advent of genetically-encoded fluorescent probes to measure GSH/GSSG in yeast has broadened our understanding that GSSG is not restricted to the cytosol, but can be sequestered in the vacuoles (302) and that the cytosolic GSH:GSSG ratio is several orders of magnitude higher (10,000:1) than previously thought (304).

One of the limitations of measuring GSH and GSSG levels in whole-worm extracts is the unavoidable loss of tissue and subcellular compartment specific information (Figure 2-10A). Moreover, if measuring whole worm cellular concentrations (mM levels), worm volumes would have to be determined at each age as worm size increases with age (305). Investigations that use analytical chemistry to directly measure redox compounds should use caution when drawing conclusions on the redox environment based on the assumption that redox couples are homogeneous throughout the cell. Results from this chapter show that the molar ratio of GSH/GSSG in whole worm extracts declines with age. Though this index cannot be used to accurately deduce the redox potential, based on the Nernst equation, it does serve as an informative measure to detect disturbances in the redox network (276).

Based on what is now known about subcellular levels of the glutathione redox couple in yeast, GSH/GSSG ratios in *C. elegans* likely play a dynamic role influencing the redox environment of subcellular compartments, including the mitochondria and the endoplasmic reticulum. Moreover, little is known about the extracellular levels of GSH and GSSG and it may be difficult to conclude much about the extracellular redox environment due to the worm's lack of a circulatory system, whereas in humans, extracellular levels are largely based on plasma content.

2.5 Conclusions and chapter summary

Maintenance of glutathione homeostasis is required to regulate redox signalling and for a healthy cellular physiology to protect against excessive ROS production. In this chapter, we present work demonstrating that *C. elegans* can be an effective model organism to observe changes in GSH levels during ageing. The inherent difficulties with the methodologies for measuring glutathione homeostasis have proved perennially problematic in the performance of studies aimed at determining the relationship of GSH and various aspects of cellular health. Reliable reporting of the *in vivo* GSH/GSSG ratio in biological samples is challenging largely due to, autooxidation of GSH's highly reactive sulfhydryl group, the possibility of enzymatic reduction of disulfides (including protein-mixed disulfides), and the low abundance of GSSG relative to GSH (306). Similarly, when measuring protein *S*-glutathionylation, both GSH and GSSG can interfere with protein-mixed disulfide (PSSG) estimation, causing significant errors due to unbound GSH concentrations being several orders of magnitude greater than PSSG levels (307).

The additional challenge of maintaining age-matched populations without the use of the DNA synthesis inhibitor, FUdR, led to our development of a sensitive LC-MS/MS technique for the detection and quantification of all the thiol metabolites involved in the *de novo* GSH synthesis pathway. The advent of this method, which requires only a small number (<500) of worms per assay enabled our investigations into how modulating GSH levels can affect the redox status of the worm. The determination of several key metabolites in a single assay provides data that can be interpreted as a proxy for substrate availability and enzyme activity, which allows the detection of any significant changes during ageing. Due to the corresponding decline of γ-GC and GSH with increasing age,

the focus of the next chapter was the role that GCL plays in the regulation of GSH synthesis in worms.

Chapter 3 explores the regulatory role of the *gclm* gene (*E01A2.1*), which is predicted to be the protein-encoding gene for the modifier subunit (GCLM) orthologue of the mammalian GCL enzyme. The two aims of Chapter 3 were to, first, determine if the GCLM subunit does in fact regulate GSH levels and, second, to observe the consequences of its gene silencing on healthspan and lifespan.

CHAPTER THREE

Functional characterisation of the predicted *gclm* gene in *Caenorhabditis elegans*

3 Chapter Three

3.1 Introduction

Though numerous studies have used rodent and *Drosophila* models to investigate the role of the GCLM subunit in ageing and oxidative stress (86, 87, 89, 92), there are no in-depth reports that characterise the predicted function of the *C. elegans gclm* orthologue (Figure 3-1). The majority of the work that has investigated GSH synthesis in *C. elegans* has focused primarily on the *gcs-1* gene which encodes for the catalytic subunit. Work published in 2004, studied the protein-protein interactions of *C. elegans* using yeast two-hybrid (Y2H) screens and showed that the GCLM protein (E01A2.1) interacts directly with the GCS-1 (GCLC orthologue) protein (146). The only known function of the GCLM subunit in mammals is to form the holoenzyme complex with the GCLC subunit as a seemingly ancillary role in the regulation of *de novo* GSH synthesis. The GCLC subunit contains all the substrate and cofactor binding sites to synthesise γ-GC, though evidence suggests that due to the non-allosteric feedback inhibition exerted by GSH on the activity of GCL, physiological concentrations (~5 mM) remain unattainable if the GCLC is unbound to GCLM (308). In most cell types, physiological GSH levels exceed the inhibition constant (K_i) for GCLC (309), suggesting that a significant proportion of the GCL exists as the heterodimer holoenzyme where GSH concentrations exceed ~1 mM. This is supported by observations in *Gclm*(-/-) null mice where GSH levels are ~10-20% of that of wild-types (310, 311). By targeting the function of *Gclm* rather than *gcs-1* in *C. elegans*, GSH synthesis can be compromised without completely inhibiting its synthesis, which has previously been shown to be embryonically lethal in *Gclc*(-/-) null mice (86, 312).

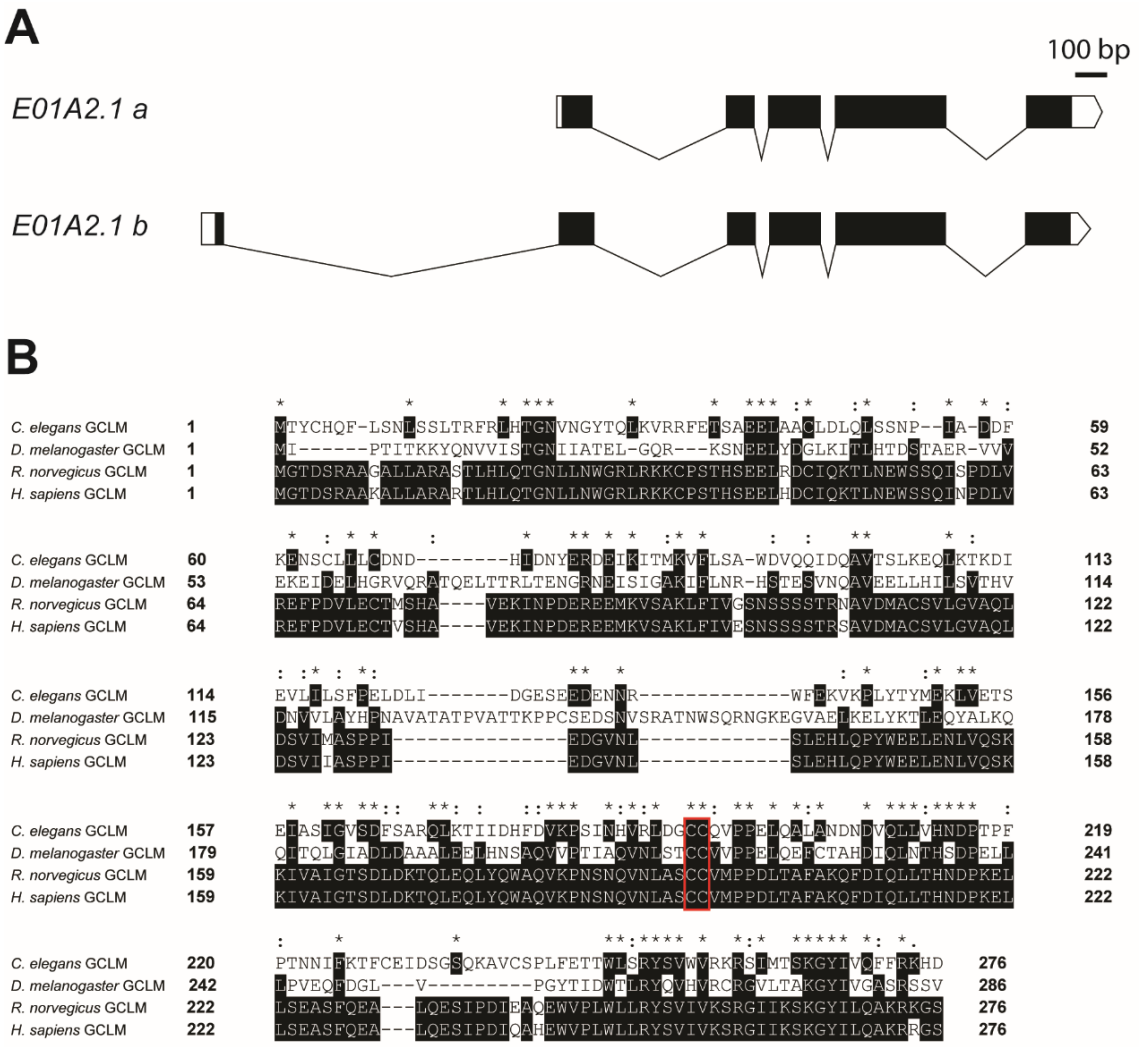

Figure 3-1. Schematic of the *gclm* genomic locus and predicted amino acid sequence of *C. elegans* GCLM aligned with *D. melanogaster*, rat and human homologues

A) The E01A2.1 locus is proposed to encode two different isoforms; E01A2.1a and E01A2.1b. B) Multiple sequence alignments of C. elegans *isoform a (E01A2.1a), comprising 276 amino acids, suggests it is more closely related to* D. melanogaster, *rat and human than isoform b (E01A2.1 b), which has an additional predicted 14 amino acid N-terminal extension (not shown in alignment). Amino acid sequence alignments were generated using the online T-Coffee program (313) with subsequent manual curations. The black squares indicate the sequence identity between* C. elegans *and the mammalian species, with the asterisks (*), indicating the identity between* C. elegans *and human. Semicolons indicate the residues that are conserved across all species except* C. elegans. *The two conserved cysteine residues (Cys-192, Cys-193) outlined in red have been shown to have a role in the GCLC and GCLM subunit interaction in the higher organisms.*

Differences in chromosomal location of the genes that encode for the respective mammalian GCL holoenzyme subunits is also conserved in *C. elegans*. The *E01A2.1* gene is located on chromosome I and the *gcs-1* gene on chromosome II (http://www.wormbase.org).

Analysis of the predicted amino acid sequences of the *gcs-1* and *gclm* subunit genes in *C. elegans*, indicated that GCLC (*gcs-1*) shares 53.3% and GCLM subunit shares 31% identity with their human orthologues (314). This level of conservation qualifies *C. elegans* as a suitable *in vivo* model to investigate the relatively unexplored *gclm* gene and to study how GSH synthesis is regulated.

3.2 Materials and Methods

3.2.1 Chemicals and reagents

The *E. coli* HT115(DE3) RNA*i* strain that expresses double-stranded RNA (dsRNA) corresponding to the *E01A2.1* (*gclm*) gene was generated from the original library constructed by the lab of Julie Ahringer (315) and was supplied by Source BioScience. The vector control consisted of the empty pL4440 vector transformed into the HT115(DE3) strain. The HT115 strain is deficient in RNAseIII, an enzyme that normally degrades the majority of dsRNA in the bacterial cells (316). The HT115 strain contains the T7 RNA polymerase gene under the control of *lac* operon regulatory elements. T7 RNA polymerase expression in HT115 bacterial cultures was induced with 1 mM isopropyl β-D-1-thiogalactopyranoside (IPTG). The pL4440 plasmid contains two convergent T7 promoter regions in opposite orientation flanking the gene-specific cDNA (317). The induction of T7 RNA polymerase results in RNA being transcribed in both directions of the T7 promoter regions to form dsRNA. Following uptake by the worm, the dsRNA initiates RNA*i* against the corresponding target gene of the worm (318).

3.2.2 Nematode propagation and strains

The N2 Bristol strain (wild-type) was provided by the *Caenorhabditis* Genetics Center (CGC), which is funded by the NIH National Center for Research Resources (NCRR). *C. elegans* were maintained in Petri dishes on nematode growth medium (NGM) and fed with *Escherichia coli* OP50 strain according to standard practices (319).

3.2.3 RNA interference

RNA*i* was induced by feeding worms with *E. coli* HT115 strains that produce dsRNA, specific for the *gclm* (*E01A2.1*) mRNA, following a method previously described (320). The bacterial RNA*i* strain was grown overnight on Luria-Bertani (LB) agar containing 15 µg/ml tetracycline and 50 µg/ml ampicillin. Single colonies were inoculated into 5 ml LB broth containing 50 µg/ml ampicillin and cultured at 37°C in a shaking incubator for between 12-18 h according to previous methods (321). The bacterial cultures, containing the dsRNA for the *E01A2.1* gene, were seeded onto RNA*i* worm plates (NGM agar containing 25 µg/ml carbenicillin and IPTG at 1 mM concentrations) and were incubated overnight at 37°C to allow bacterial growth and to begin induction of the dsRNA. Gravid worms were then transferred to new RNA*i* plates for 6-8 h at 20°C to lay eggs. Once the adults were removed, a synchronised population of worms was maintained. Worms were grown on RNA*i* plates until they reached the age of interest for analysis. To control the consistency of bacterial density from the start of each 24 h period, the worms were transferred daily to fresh plates containing dsRNA bacteria.

3.2.4 Lifespan analysis

Synchronisation of *C. elegans* was achieved using the egg laying method (322). Briefly, L4 larvae, characterised by the presence of a white patch approximately halfway along the ventral side (323), were picked and plated on NGM containing *E. coli* OP50 and incubated overnight at 20ºC until they developed into reproductive adult hermaphrodite worms. Age-matched, gravid worms were then transferred onto individual RNA*i* plates containing *E. coli* HT115 strains and were kept at 20ºC for 3 h to continue to lay eggs. The worms were then removed, and the eggs incubated for ~72 h until they reached day 0 of adulthood. Groups of 20 synchronised adult (day 0) worms were transferred to fresh

35 mm RNA*i* plates for a total of 60 worms per treatment group. Survival numbers were recorded daily with death as the endpoint. Worms that either escaped the plate, or were injured during handling, displayed internal hatching (commonly known as "bagging"), or bursting were censored (324). To separate adult worms from their progeny, adults were moved to new RNA*i* plates each day until the end of the lifespan experiment**.** To maintain consistent optical density of bacterial lawns, each 35 mm RNA*i* plate was seeded with 100 µl × *E. coli* HT115 cells at a density of 100 mg/ml.

3.2.5 Thrashing assay

Thrashing behaviour was assessed by observing individual nematodes placed in 200 µl M9 buffer per well of a 96-flat bottom well tissue culture-treated plate. Worms that were aged at 20°C were assessed at days 1, 5 and 9 for the average number of spontaneous body bends (thrashes) per min. Each animal was gently placed in an individual well of M9 buffer and acclimated for 1 min at room temperature. Measurements were blinded for treatment groups and performed in two or three individual experimental repeats on between 4-18 randomly selected worms per time point.

3.2.6 Egg laying assay

The egg laying assay used in this study was modified according to a previous method (325). Investigations of the effect of *gclm* RNA*i* was performed in 35 mm RNA*i* plates and seeded with 100 µl *E. coli* HT115 strain (100 mg/ml) targeting the *E01A2.1* gene or the containing the pL4440 vector only. To maintain a constant *E. coli* cell density and hence induction of RNA interference, worm plates were seeded the day before and incubated at room temperature overnight to induce the RNA*i* strains. One L4 worm was added per 35 mm plate ~64 h after synchronisation prior to reaching reproductive

maturity; this was considered day 0. At the end of each 24 h period, the worms were transferred from the hatching plate to new laying plates. The hatching plates were kept at 20°C for 72 h and the progeny of each worm was scored until egg-laying ceased.

3.2.7 Pharyngeal pumping

Pharyngeal pumping was measured by counting the number of contractions of the posterior bulb of the pharynx per min using a Nikon SMZ800N Stereomicroscope (326). Measurements were blinded for treatment groups and performed in two or three individual experimental repeats on between 4-24 randomly selected worms per time point treatment.

3.2.8 Hydrogen peroxide stress-test

Recovery of worms after short-term exposure (1 h) to 5 mM H_2O_2 was assessed according to a previous method (184). Synchronised worms were removed from plates and washed three times in M9 medium to remove the bacteria. Approximately one hundred worms per group were incubated for 1 h at 20°C in individual wells of a 24-well tissue culture-treated plate containing 1 ml H_2O_2 solution. After treatment, the H_2O_2 solution was aspirated and worms washed three times before being collected using Sorenson™ low-binding tips and transferred to *E. coli* OP50-seeded NGM plates. Survival scoring over the recovery period was blinded for all treatment groups.

3.2.9 Generation of GFP reporter strains for the *gclm* promoter

Transcriptional GFP reporters were generated using a PCR-fusion based approach (327). Fragments of the promotor region of the *gclm* gene were fused to the nucleotide sequence of GFP, whereby 22-26 bp overlapping extensions were used to fuse the two PCR products together. Individual PCR products were first amplified separately and used as

templates for the subsequent fusion PCR reaction at ~0.1–1 ng per 50 µl reaction mix. The promoter region that contained the entire 5.6 kb for *E01A2.1a* upstream of the start codon was PCR amplified from genomic worm DNA (Figure 3-2). DNA amplification procedures were performed using Phusion high-fidelity DNA polymerase (Cat. #M0530, New England Biolabs) except for the 5.6 kb promotor region of the *E01A2.1a* variant, which was amplified using PrimeSTAR GXL DNA polymerase (Cat. # R050A, Takara Bio). The promoter fragment was fused to the GFP nucleotide sequence from the pPD95.67 vector (a gift from Andrew Fire, Addgene plasmid #1490) which included the *unc-54* 3′ untranslated region (UTR). The fused PCR products were purified using the Qiaquick PCR purification kit, with the final elution step performed using ultrapure water. Injection mixes contained the purified PCR-fusion product (~10 ng/µl) and *Odr-1p*::*DsRed* (50 ng/µl) as a co-injection marker to be injected in the gonads of young adult hermaphrodite nematodes to generate extrachromosomal arrays (328). A Scheme for the PCR fusion workflow is shown in Figure 3-2.

3.2.10 Microinjection, Screening and Fluorescence Microscopy

N2 wild-type worms were selected at L4 and placed on fresh NGM plates and allowed to grow overnight to gravid adults before microinjection. Each injected P_0 worm was placed on an individual 35 mm NGM plate seeded with *E. coli* OP50 and allowed to produce progeny between 2-3 days. Worms were screened using a fluorescence dissecting microscope. The F_1 worms that had taken up the co-injection marker were picked and placed on individual 35 mm plates. Transcriptional GFP reporter strains were isolated by transferring F2 generation worms that had maintained the co-injection marker, to new plates. Worms carrying the extrachromosomal array were mounted on 2% agarose pads and immobilised using 25 mM sodium azide. A cover slip was then placed on the worms

immediately before imaging by differential interference contrast (DIC) fluorescence microscopy.

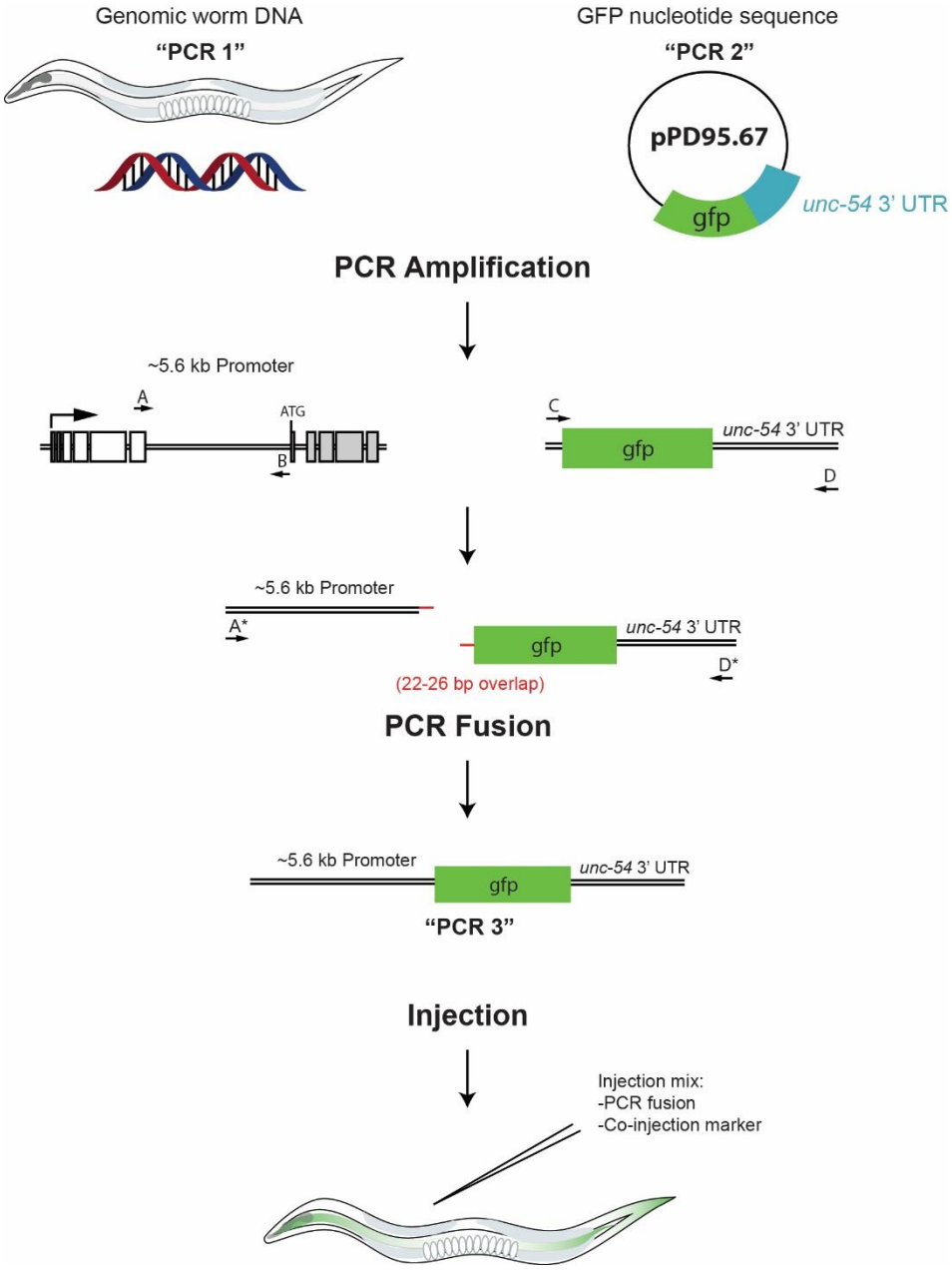

Figure 3-2. Scheme of PCR fusion approach for the generation of transcriptional GFP reporter strains

Generation of the promoter-GFP fusion required two-PCR products. The first was the promoter, which was amplified from genomic C. elegans *DNA (Primers A and B) and the other was the gfp nucleotide sequence cloned in the pPD95.67 vector (Primers C and D). The primers B and C were designed with a complementary overlap to assist the PCR fusion reaction. PCR 3 used the nested primers (A* and D*), by which the two fragments were fused together with the 22-26 bp overlap of the two fragments. For primer sequences used in the fusion reactions see Appendix (A-1).*

3.2.11 Strategy for generating *gclm* mutants using the CRISPR/Cas9 system

Targeted Cas9-mediated cleavage of the *C. elegans gclm* locus was attempted to produce heritable insertion or deletion (indel) mutations by error-prone repair (Figure 3-3A). Screening for indel mutations was conducted using PCR genotyping performed according to a previously described method (329). Briefly, two outside primers amplify a region across (~500 bp) the targeted site (Figure 3-3B). A second primer (the flank primer) sits on the target site with the 3′ end of the primer binding immediately before the PAM site (Figure 3-3B top), which is approximately 200-300 bp downstream of the F1 primer. Binding of the flank primer should produce 2 amplicons in wild-type worms: the 500 bp attributed to the two outside primers, and the 200-300 bp amplicon of the flank and one of the outside primers. Alternatively, the PCR can be conducted with the flank primer as a reverse primer, where the 3′ end binds 4 bases upstream of the PAM site.

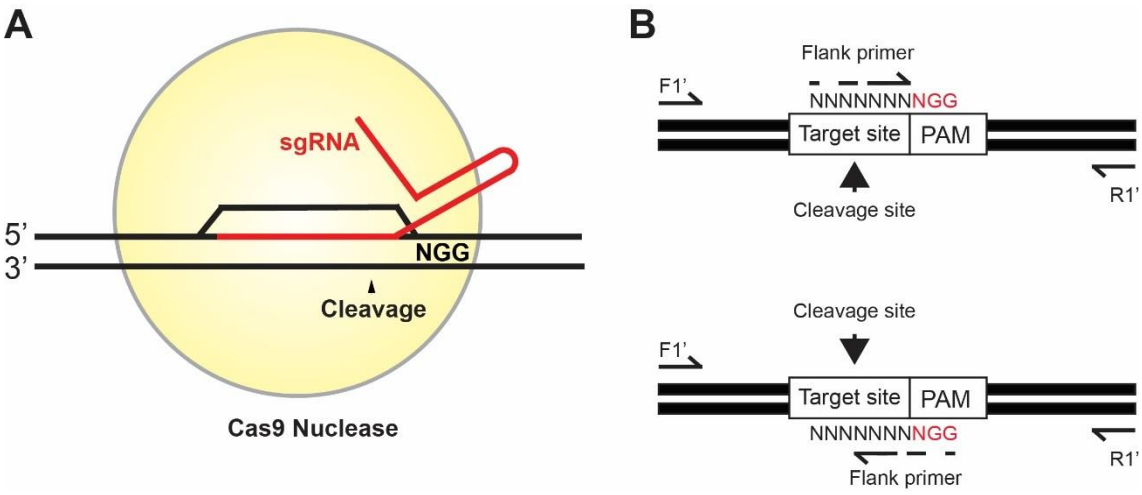

Figure 3-3. CRISPR/Cas9 target and genotyping strategies

(A) The sgRNA (red) is a synthetic oligonucleotide containing both the CRISPR-targeting RNA (crRNA) and trans-activating RNA (tracrRNA) sequences, complexed with the Streptococcus pyogenes *Cas9 protein (yellow). The double-stranded break is said to occur ~3-4 bases within the PAM. (B) Two external primers (F1′ and R1′) span the cleavage site (~500 bp). The cleavage site is flanked by an additional primer, which should result in an additional band in the same PCR reaction in worms that have not been modified around the cleavage site. Two flank primer design options are shown.*

The protocol for generating CRISPR/Cas9-induced mutations was followed according to the previously described method (330). The target sites were identified using the openly available CRISPR guide RNA selection tool (331). The single-guide RNA (sgRNA) primers complementary to the coding sequences in the *E01A2.1* gene were designed according to a previously described method (330). Briefly, the sgRNAs were cloned into the *pU6*::*klp-12* vector (a gift from John Calarco, Addgene plasmid #46170) and transformed into Alpha-Select Silver Efficiency Competent Cells according to the manufacturer's instructions (Bioline). For sgRNA specific primers, including the universal reverse primer, see Appendix (A-2). Clones were validated by sequencing and the plasmids were midiprepped before injection into the worms. Plasmid DNA was eluted in the final midiprep step using MilliQ water rather than the elution buffer provided in the ZymoPURE commercial kit (Zymo Research). Elution with MilliQ increases the chance of transgenics and lowers the toxicity of the injection mix (330). Injection mixes contained the Cas9 expression plasmid (*Peft-3*::*Cas9 SV40 NLS*::*tbb-2* 3′ UTR), the *pU6*::*klp-12* sgRNA vector, and the two co-injection markers: 2.5 ng/µl pCFJ90 (*Pmyo-2*::*mCherry*::*unc-54* 3′ UTR) and 5 ng/µl pCFJ104 (*Pmyo-3*::*mCherry*), which were used to visualise the red-pharynx and red body wall muscles, respectively. A Scheme for the CRISPR/Cas9 screening and genotyping workflow is shown in Figure 3-4.

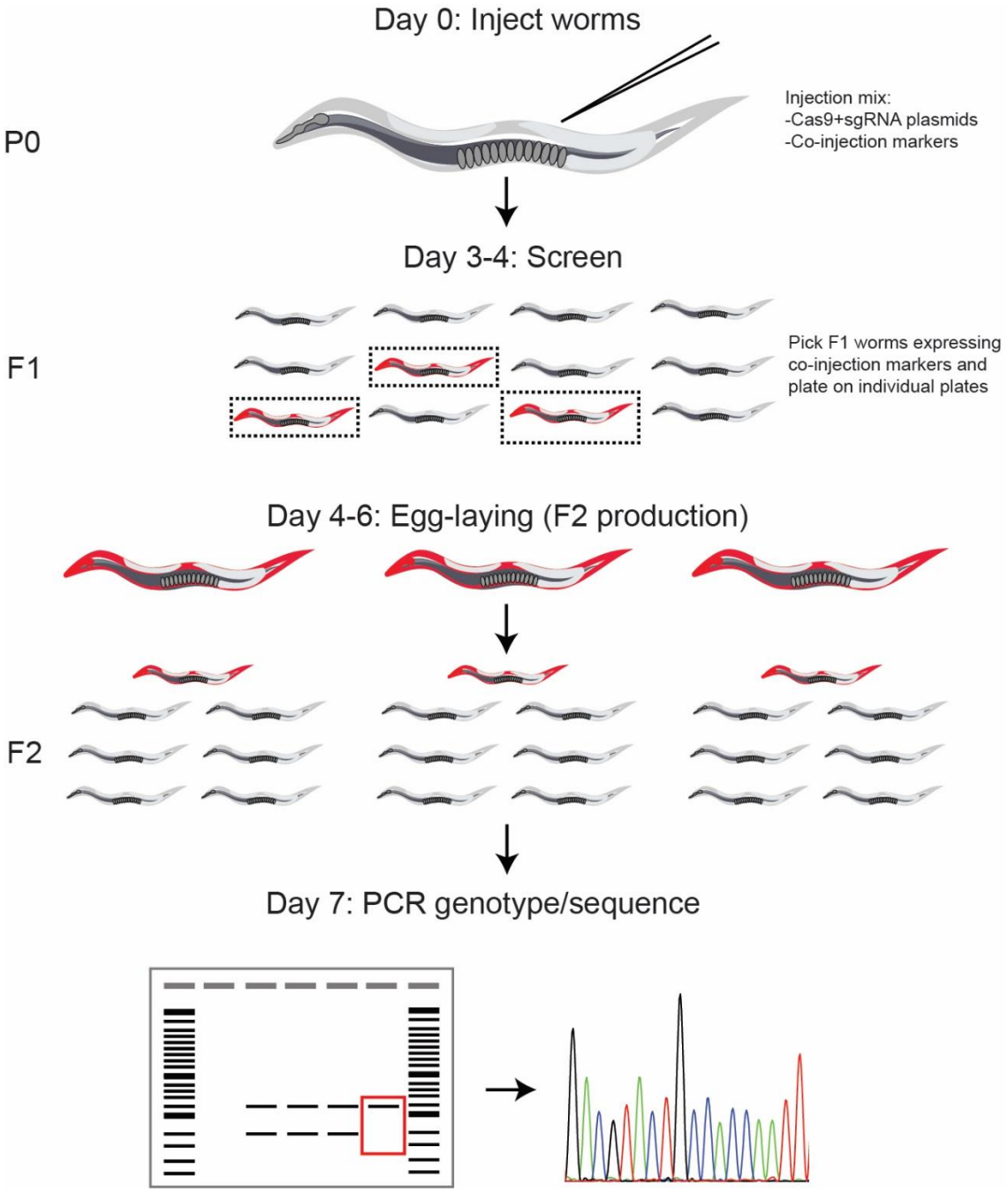

Figure 3-4. CRISPR/Cas9 strategy for the generation of mutant *gclm* worms

For each injection round approximately 20 young adult wild-type worms (P0) were injected with the CRISPR-Cas9 injection mix, which included the co-injection markers. Each worm was plated on an individual plate and allowed to lay eggs for up to 3 days. F_1 progeny that had the co-injection marker expressed in either the pharynx or body wall were transferred to individual plates and allowed to lay eggs for 3 days to generate F2 progeny. The initial F_1 worms from each plate were then PCR genotyped and screen candidates were sequenced to determine if an indel was present.

3.2.12 Genotyping using single worm PCR

PCR was used to genotype potential mutants that had taken up the co-injection marker. Genomic DNA was released in 10 µl of worm lysis buffer containing 50 mM KCl, 10mM Tris (pH 8.3), 2.5mM $MgCl_2$, 0.45% NP-40, 0.45% Tween-20, 0.01% gelatin and 0.1 mg/ml proteinase K. Each worm was added to individual tubes of 8-strip 0.2 ml PCR tubes and quickly centrifuged (2000×*g*) to ensure the worms were positioned in the bottom of the tubes. This was then followed by freezing at -80°C for at least 15 min to allow cuticle rupture. After which, the PCR tubes were placed in a thermocycler and heated to 65°C for 90 min followed by heating at 95°C for 15 min to inactivate the proteinase K. All DNA amplification procedures were performed using Mango*Taq*™ DNA polymerase (Bioline). Cycle conditions were 94°C for 2 min, followed by 30 cycles of (94°C for 15 s, 56°C for 15 s and 72°C for 30 s) and an additional 5 min at 72°C.

Table 3.2 Primers used for genotyping using PCR

Guide	Primer name	Sequence (5′-3′)
#1	11 F1	CTCCCGACGAGTGATGTAAT
	12 R1	TCTTTCGTCCCGCTCAAG
	17 Flank 1	CTCAGAAATTGGTGGCAGT
#2	13 F2	ATCAAGCAATTCTGTGTGTGG
	14 R2	ATTGGCCTATCTGGACGC
	7 Flank 2	ACCCGATTTCGTCTTCACAC

3.2.13 Agarose gel electrophoresis

For the separation of DNA fragments, PCR products were run on a 1.5% agarose gel (DNA grade) in 1× TAE buffer. Ethidium bromide was added to the molten agarose at a concentration of 0.5 μg/ml before pouring in the gel casts. Electrophoresis was performed at 80-90 mV over 25-30 min.

3.2.14 Statistics

Statistical analyses for data sets requiring unpaired t-tests and lifespan curves using log-rank tests (Mantel-Cox) were performed using the GraphPad Prism software (version 7.02). The log-rank test, which gives equal weight to deaths at all time points, is commonly used for *C. elegans* lifespan data (332). Analysis for unequal sample sizes/replication number that required ANOVA (with a Tukey post hoc test), were performed in the using the 'R' program.

3.3 Results

3.3.1 GSH homeostasis is regulated by the *gclm* gene in *C. elegans*

Impairment in GSH synthetic capacity by RNA*i* knockdown of the *gclm* subunit was confirmed by LC-MS/MS analysis of thiol levels. At day 1 of adulthood, an approximate 35% decline in GSH content ($p<0.05$) was observed in *gclm* knockdown worms compared to the empty vector control (Figure 3-5). This is within the range that has been recently reported when the glutamate cysteine ligase catalytic subunit, *gcs-1*, was knocked down after 3 days (~35%) and 5 days (~50%) (133).

Levels of cysteine ($p<0.05$) were higher in the *gclm* RNA*i* worms. This could have occurred either by an increase in cysteine production via an intrinsic compensatory mechanism such as the transsulfuration pathway, or most likely from cysteine being accumulated due to it not being efficiently converted to γ-GC when the *gclm* gene becomes silenced. These results taken together indicate that the *gclm* subunit is a suitable target to knockdown and investigate the effects of compromised GSH synthesis in *C. elegans*.

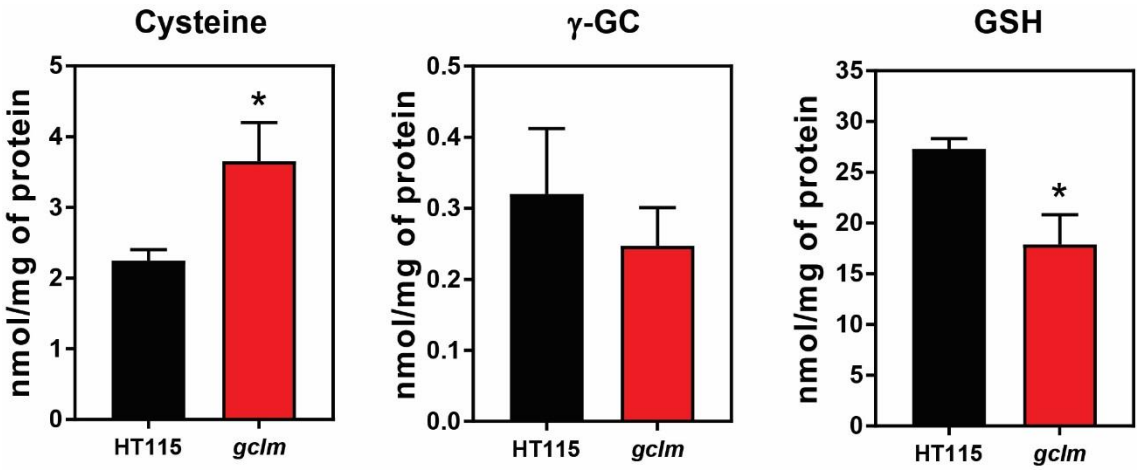

Figure 3-5. Effect of *gclm* RNA*i* on thiol levels in day 1 adults

Wild-type worms were synchronised and maintained on RNAi plates seeded with the E. coli *strains containing the dsRNA complementary to the gclm gene or empty vector (HT115). Cysteine, γ-GC and GSH content was measured in day 1 old adults. Unpaired t-tests were performed. Significance was determined for cysteine (*p<0.05) and GSH (*p<0.05). Data presented as ±SEM (n = 3-4).*

3.3.2 Knockdown of the *gclm* gene at the egg stage increases vulval rupture

Given that most *C. elegans* lifespan experiments use 20°C for the housing temperature, it was hypothesised that impairment of GSH synthesis by RNA*i* of the *gclm* gene may lead to dynamic temperature-dependent differences in stress resistance that may affect lifespan. Initial RNA*i* lifespan experiments were conducted at 15°C, 20°C and 25°C. Worms with the *gclm* gene knocked down immediately after hatching were prone to vulval rupture as fertile adults. At the highest temperature tested (25°C), only 17% of *gclm* knockdown worms were censored due to vulval rupture (Figure 3-7A), which was significantly lower than the 62% observed at both 15°C and 20°C (Figures 3-6A/B). No temperature-dependent effect on lifespan was observed for worms that had the *gclm* gene knocked down beginning from hatching (Figures 3-6A/B). The analysis of the survival curves at 15°C and 20°C were underpowered due to the high number of total censored subjects. Increasing sample size may alleviate this problem, however the introduction of the rupture phenotype would likely continue to confound results. To limit the number of censored worms when grown at 15°C and 20°C, the lifespan method was revised to delay inducing *gclm* RNA*i* until the worms reached adulthood. Interestingly, when the *gclm* gene was knocked down at the beginning of adulthood at 25°C the frequency of the vulval rupture phenotype was low at 1.7% of the total cohort (Figure 3-7B). Accordingly, *gclm*-targeted knockdown beginning at synchronisation (hatching) or at day 0 of adulthood, was used to explore the differences in *gclm* silencing at different life cycle stages.

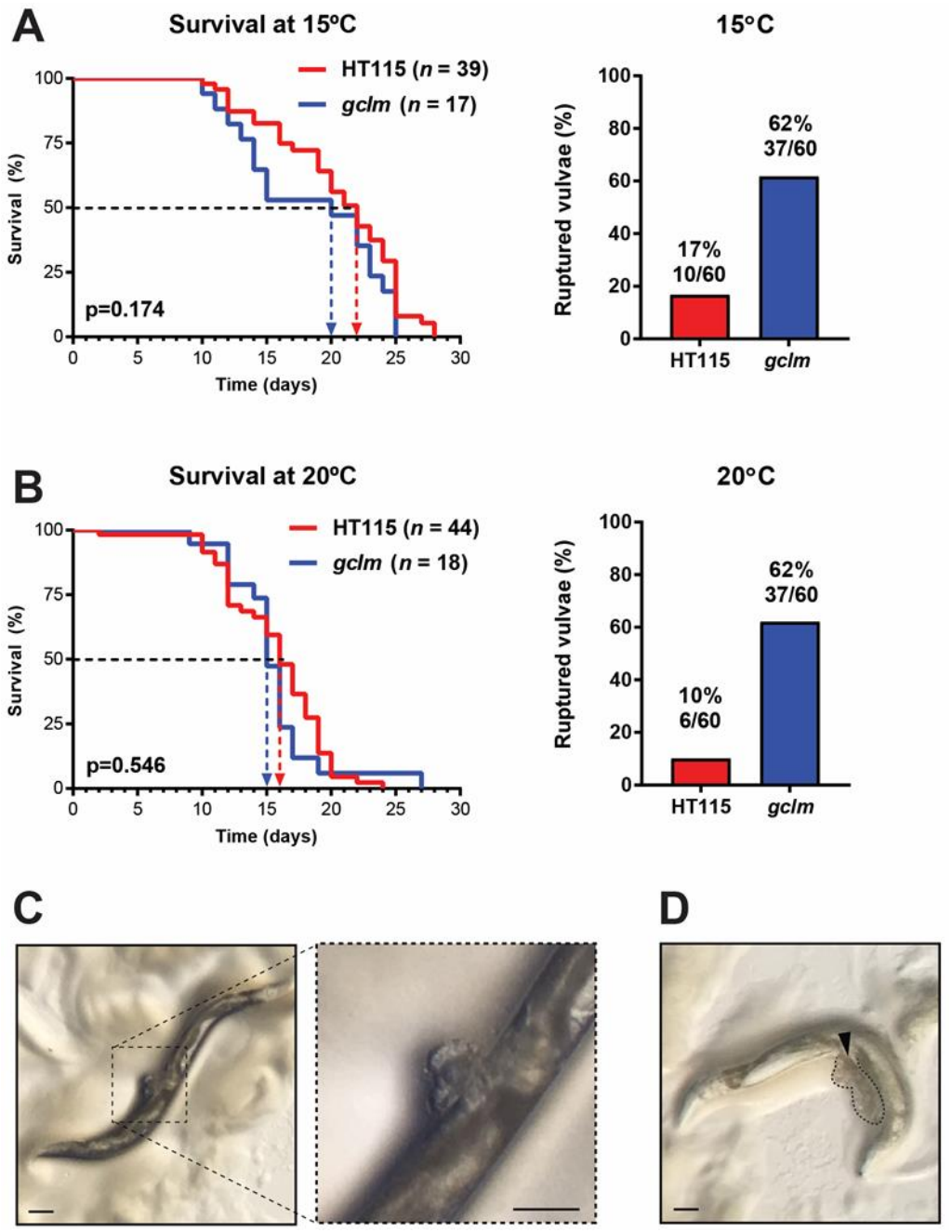

Figure 3-6. Temperature dependent survival and vulval rupture frequency following RNA*i*-targeted *gclm* knockdown beginning immediately after hatching

Wild-type worms were grown from the egg stage on RNAi plates containing either the gclm *knockdown or the HT115* E. coli *strains and incubated at 20°C for 64-72 h until the worms reached adulthood. After this period, the worms were separately incubated at either (A) 15°C or (B) 20°C and survival recorded. Kaplan-Meier survival curves were statistically analysed using a log-rank (Mantel-Cox) test. No statistical differences in lifespan were observed. The incidence of the vulval rupture phenotype was consistent in each of the temperatures tested. C) Early onset of mild rupture of the vulvae. D) Later stages of the more severe rupture phenotype are indicated with arrowhead and black dotted outline. Scale bars, 50 μm.*

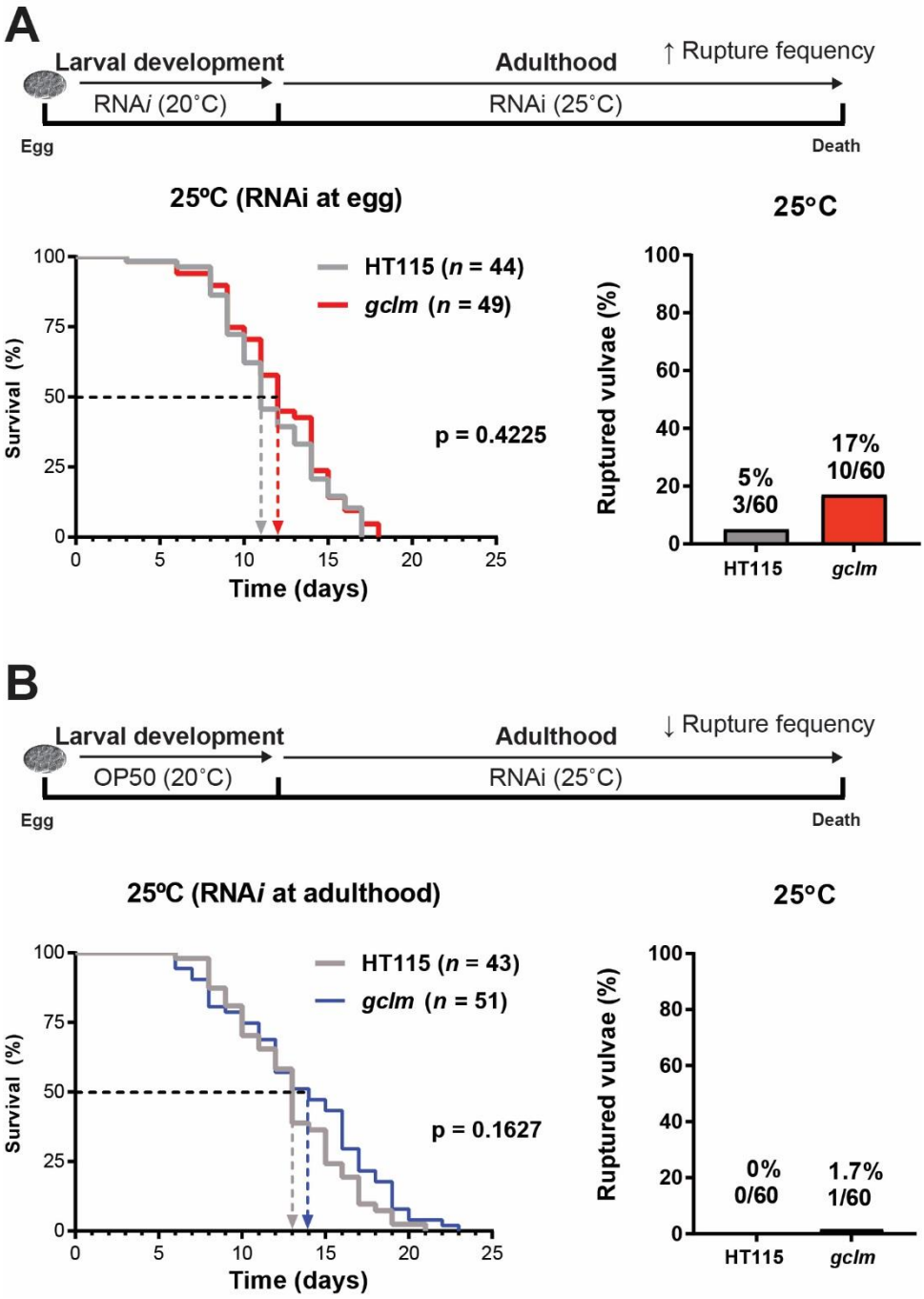

Figure 3-7. Survival and vulval rupture frequency following RNA*i*-targeted *gclm* knockdown beginning at hatching and day 0 adulthood

(A) RNAi was targeted in wild-type worms from the egg stage. Larvae were grown on RNAi plates containing either the gclm *knockdown or the HT115 strains and incubated at 20°C for 64-72 h until the worms reached adulthood. After this period, the worms were incubated at 25°C and survival recorded daily. (B) RNAi was targeted in wild-type worms beginning at adulthood. Larvae were grown on plates containing* E. coli *OP50 and incubated at 20°C for 64-72 h until the worms reached adulthood. After this period, the worms were incubated at 25°C and survival recorded daily on RNAi plates containing either* gclm *knockdown or the HT115 strains. Survival curves were statistically analysed using a log-rank (Mantel-Cox) test. No statistical differences were observed between treatments.*

3.3.3 Knockdown of *gclm* beginning at adulthood shows no difference in brood size or daily progeny production

A decrease in GSH synthetic capacity resulting from knockdown of the *gclm* gene beginning at adulthood was associated with a slight decline (7.6%) in the total progeny production, but was not considered significant (Figure 3-8A). The daily rate of viable progeny production did not differ between the *gclm* knockdown and the empty vector control (Figure 3-8B). Though no difference was observed in the egg-laying capacity of the worms when knocked down at adulthood, it is important to monitor worm fertility in lifespan studies. Delays in fecundity have been associated with increases in lifespan (287) and could potentially introduce artefacts into the interpretation of lifespan effects attributed to oxidative stress resistance.

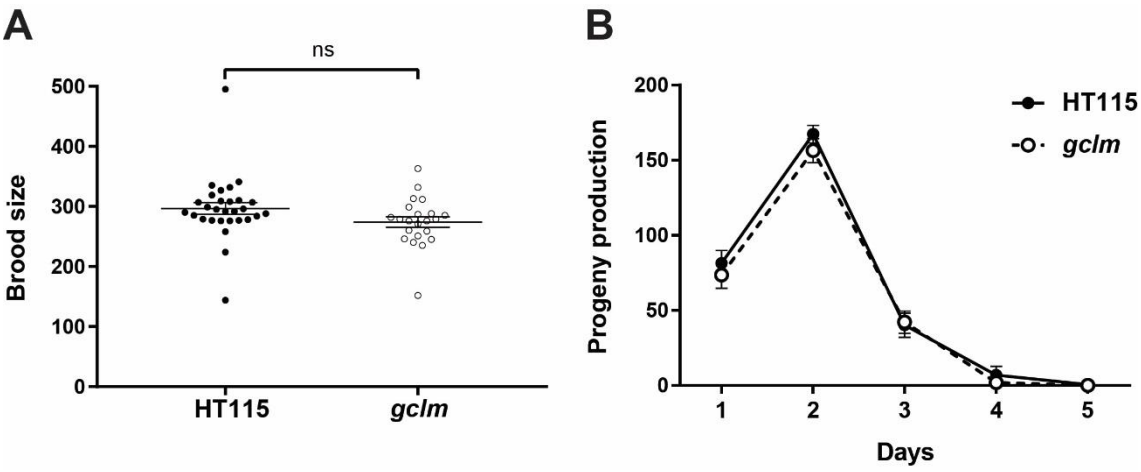

Figure 3-8. Brood size and daily progeny production in *gclm* knockdown worms

Wild-type worms were grown from the egg stage on NGM containing OP50. Before reproductive maturity was reached, worms were moved to RNAi plates targeting either the gclm *knockdown or the HT115 strain. Progeny production was followed from the beginning of adulthood until the self-fertile reproduction cycle ceased. Data presented as mean ±SEM of three independent experiments. (n.s. = not significant).*

3.3.4 Motility and pharyngeal pumping performance of *gclm* RNA*i* worms

Motility (thrashing) and the feeding activity of the pharyngeal contractions (pumping) were used as measures to determine if RNA*i* of the *gclm* gene has any effect on the physical phenotypes related to worm ageing. Fast body movement span and fast pharyngeal pumping span are two measures that have been shown to predict lifespan amongst several mutant strains (113). For example, the longer-lived *daf-2* and *age-1* mutants of the insulin/IGF-1 signalling (IIS) pathway have longer fast pharyngeal pumping and movement spans compared to wild-type worms, whereas the *daf-16* mutants downstream of the IIS pathway, which encode the FOXO transcription factor, have considerably shorter pharyngeal pumping, movement and lifespans than the longer-living (*daf-2* and *age-1*) and wild-type strains (113).

To understand the temporal impact of the *gclm* gene during ageing, RNA*i* was conditionally induced in wild-type worms either immediately after hatching or beginning at the start of adulthood. This allowed for the thrashing and pharyngeal pumping performance to be examined in adult worms where *gclm* expression was either silenced or uninhibited throughout larval development. Significant declines in the pharyngeal pumping rates were observed in day 9 old adult worms regardless when the *gclm* gene was silenced (Figures 3-9A & B). Unexpectedly, worms with the *gclm* gene silenced throughout development appeared to have increased thrashing in days 5 to 9 when compared to the vector control (Figure 3-9C). However, when *gclm* was silenced at adulthood a decline in thrashing was observed at day 9 (Figure 3-9D). The observed increase in thrashing behaviour when *gclm* was silenced throughout development could potentially be indicative of a compensatory stress-response in the worm.

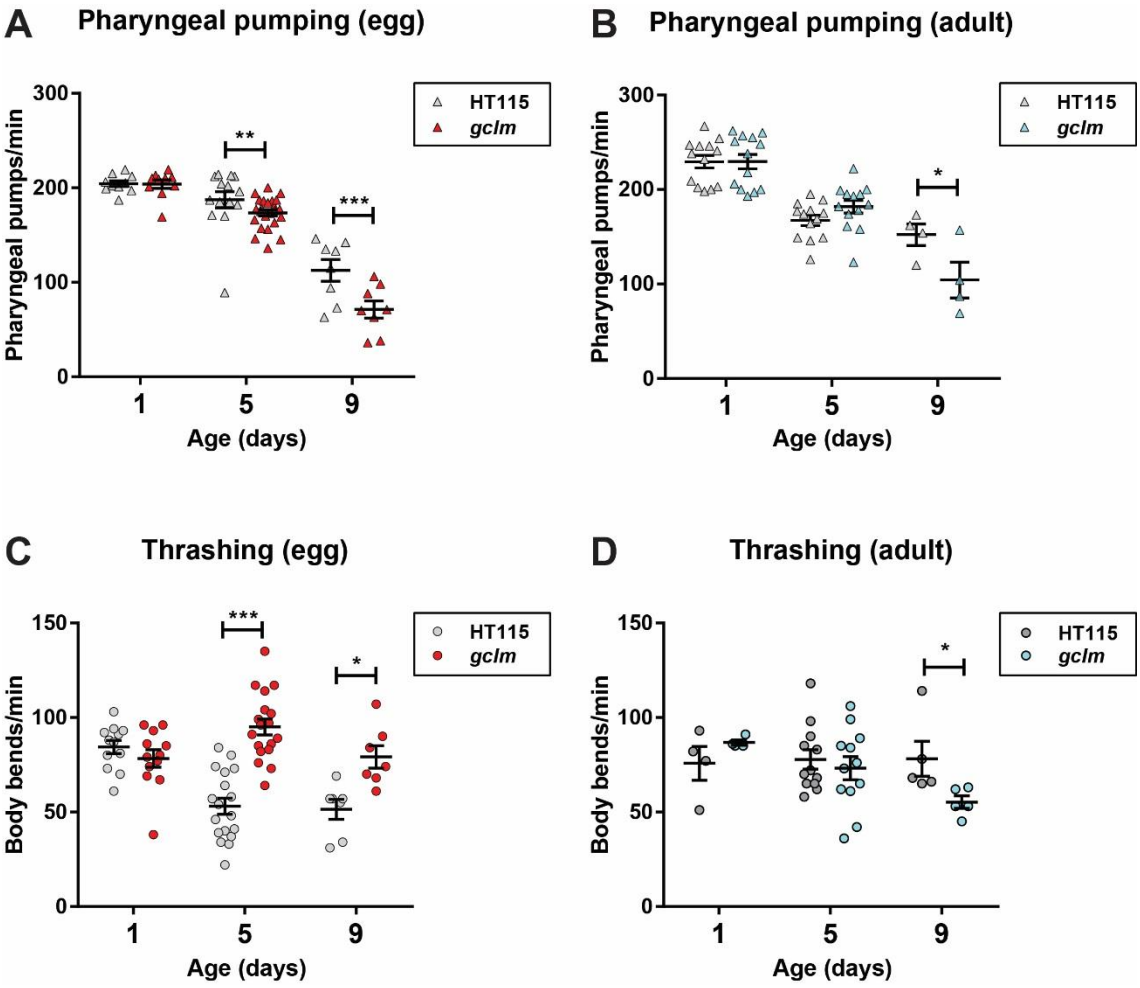

Figure 3-9. Pharyngeal pumping and thrashing performance in ageing *gclm* knockdown worms

Pharyngeal pumping and thrashing rates were assessed in worms where RNAi was conditionally induced for the gclm *gene, either beginning from hatching (egg) or adulthood (adult). The empty vector RNAi strain (HT115) was used as the control. Worms that were RNAi treated beginning from adulthood (B & D), were maintained through the larval stages on NGM plates seeded with OP50. Declines in pumping were observed regardless of temporal control of RNAi treatment (A & B). Increases in thrashing were observed at days 5 and 9 when* gclm *was knocked down beginning at (egg) synchronisation (C). Thrashing declined in the* gclm *silenced worms (adult) at day 9 (D). Data presented as mean ±SEM and were analysed by two-way ANOVA with a Tukey post-hoc test to determine differences between days, *p<0.05, **<0.01, ***p<0.001.*

3.3.5 Hydrogen peroxide stress test in *gclm* knockdown worms

To investigate if the increase in thrashing rates of *gclm* knockdown worms (beginning from egg-stage) were indicative of a stress-response, a hydrogen peroxide stress-test was conducted to determine if *gclm* conferred any protective role against an acute challenge under these conditions.

Day-3 old worms were selected as the increase in thrashing phenotype was beginning to be present in day-4 old worms (data not shown). These worms that had the *gclm* gene knocked down beginning from synchronisation were exposed to H_2O_2 for 1 h in liquid medium and transferred to seeded NGM plates, with survival scored after the subsequent 6 h recovery period (Figure 3-10A). Although a general trend of decreased survival was observed in *gclm* knockdown worms exposed to 5 mM H_2O_2, these differences were not statistically significant (Figure 3-10B).

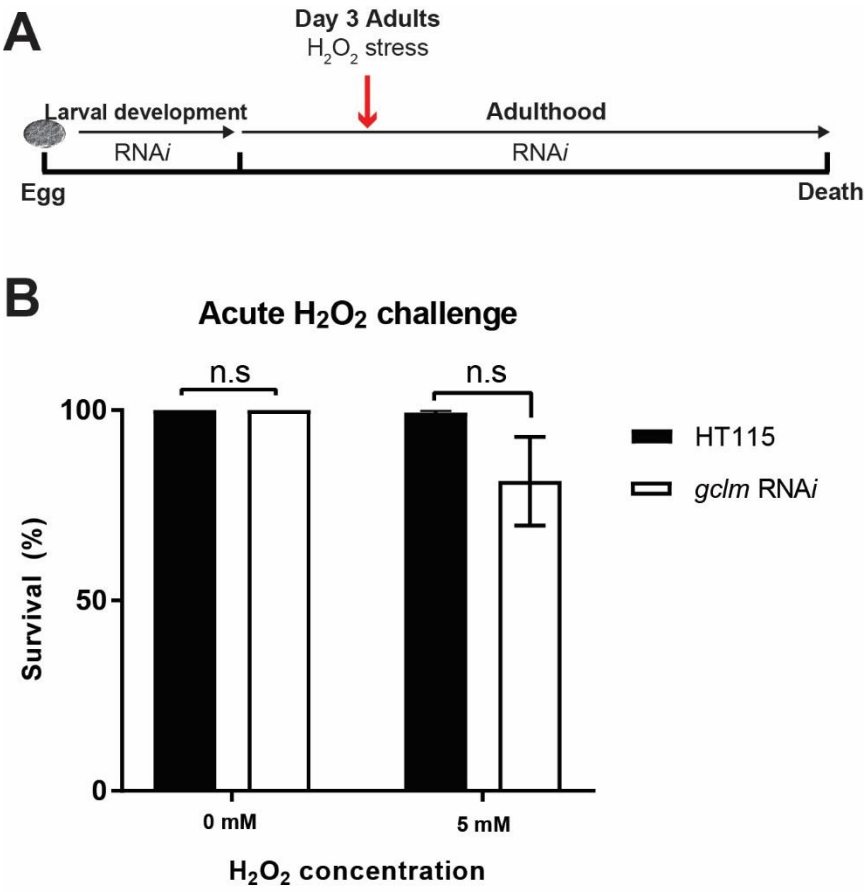

Figure 3-10. H_2O_2 stress test in *gclm* knockdown worms

A) Worms were synchronised on RNAi plates seeded with gclm *or the empty vector (HT115) RNAi strains. Day 3 adults were washed from the plates with M9 buffer and treated with either 0 or 5 mM H_2O_2 for 1 h at 20°C. B) After the treatment, worms were washed and scored for survival 6 h post-treatment on NGM plates seeded with OP50 (recovery). Each condition consisted of 3 individual experimental repeats, with between 50-100 worms per experimental repeat. Unpaired t-tests were performed (n.s. = not significant).*

3.3.6 Expression patterns of the p*E01A2.1*::*gfp* transcriptional reporter

To study the expression patterns of the *gclm* gene in worms, a reporter strain was generated by fusing the entire 5.6 kb promoter region of the *E01A2.1a* transcript isoform with the nucleotide sequence coding for GFP (327). Representative images of the expression of the *E01A2.1a* promoter region show fluorescence in the hindgut (Figure 3-11B), the anterior intestine and possibly one neuron, that was distinguishable from the red fluorescence of the *odr-1::DsRed* co-injection marker (Figure 3-11C). The *odr-1* promoter drives expression in the AWB and AWC sensory neurons. Initial reports of the *odr-1::DsRed* co-injection marker have shown that it can express patterns of moscism in these neurons (333). Our results suggest that the *odr-1::DsRed* is being expressed in one of the AWC neurons and that the GFP expression observed could not be the result of autofluorescence in *odr-1::DsRed* (Figure 3-11C).

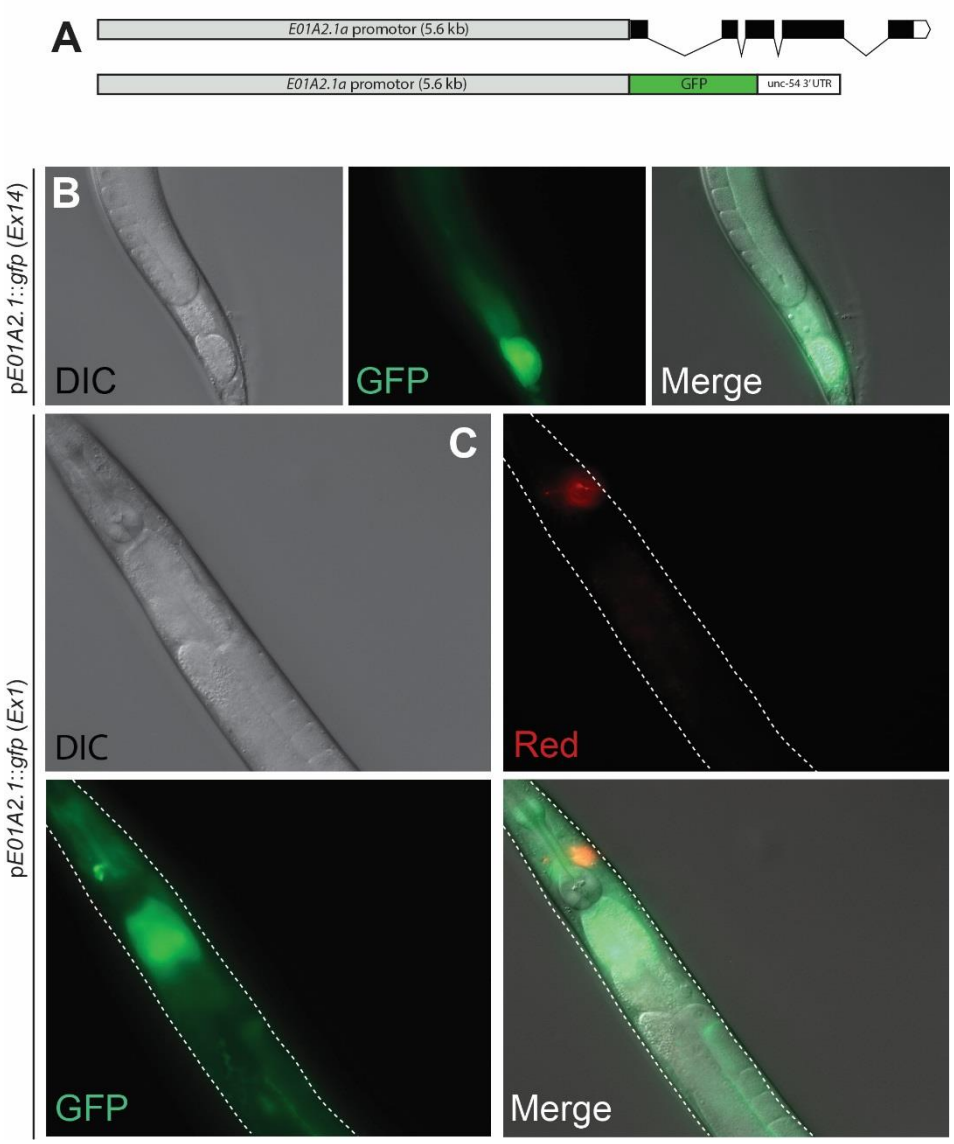

Figure 3-11. Transcriptional expression patterns of the *gclm* promotor

(A) The transcriptional gclm *reporter had the entire 5.6 kb promoter region of the E01A2.1a variant fused with GFP. (B) The GFP expression patterns located near the posterior intestine of the worm around the region of the hindgut. (C) Expression patterns appear to be present possibly in one neuron located near the posterior bulb of the pharynx, and cells of the anterior intestine.*

3.3.7 Strategy for the generation of *gclm* mutants

Attempts to utilise the CRISPR/Cas9 genome editing technology to generate a viable *gclm* mutant were unsuccessful. Single guide RNAs (sgRNA) were constructed to target candidate sites of the first exon of E01A2.1a variant (Figure 3-12). PCR genotyping was used to screen and assess the efficiency of the sgRNAs and to determine if Cas9-mediated cleavage occurred. The two guides that were investigated (Guide #1 and Guide #2) differed in their predicted efficiency to target the protospacer-adjacent motif (PAM) site. Guide #1 was chosen due to its terminal di-guanine motif (GG) that immediately preceded the PAM sequence. This allows the Cas9 to target a GGNGG sequence which has been reported to increase the guide efficiency in *C. elegans* compared to targeting only the NGG sequence (334). Guide #2 (Shown in Figure 3-12) was included as it had the lowest predicted possibility of off-targeted sequence recognition according to the CRISPR sgRNA selection tool (331).

Figure 3-12. CRISPR target exon site(s)

Schematic of the target site for Guide #2. The Cas9 recognition site consists of 20 nucleotides complementary to the guide RNA. This sequence targets directly 5′ of the *PAM (NGG). The crRNA sequence is underlined in bold with the PAM in red.*

Worms that expressed the co-injection markers (P*myo-2*::*mCherry* or P*myo*-3::*mCherry*) were genotyped for the presence of mutations in the *E01A2.1* allele. Several rounds of injection of Guide #1 produced worms that exhibited developmental deficiency phenotypes. This included worms with decreased brood sizes and developmental delays, that in some instances did not progress beyond the larval stages. This may have been due to components of the injection mix being toxic to the worms, which has previously been reported (335). Attempts were made to genotype F_1 worms that expressed the co-injection marker but had suffered from larval lethality. However, this was unsuccessful due to the fragility of larval carcasses.

Injection mix toxicity has been previously observed, with several reports suggesting that the concentration of the components, including the sgRNA, should be minimised. No considerable difference was observed in the development phenotype when injecting the sgRNA at 100 ng/µl concentrations compared to 250 ng/µl. As for the co-injection markers, the concentrations that were used for this work, were within the tolerated concentrations that have been used previously (330). It was inconclusive from the genotyping experiments if the lethal developmental phenotype observed in several F_1 larvae was due to the possible mutations that occurred from the guide successfully targeting the *gclm* gene or due to the co-injection components having a toxic effect on the worms.

3.4 Discussion

Despite numerous studies conducted in mammalian models, in-depth investigations of the role of *gclm* in *C. elegans* is currently lacking. Mammalian studies implicating that physiological concentrations of GSH are controlled by GCLM, show that the feedback inhibition concentration (K_i) of GSH increases five-fold to levels corresponding to physiological concentrations (~5 mM) upon holoenzyme formation, when compared to the monomeric GCLC alone (1 mM) (309). This observed 5-fold change in GSH levels is similar to several tissue types of *Gclm*(-/-) mice compared to wild-type littermates (86). Moreover, the seemingly ancillary role of the GCLM, makes it a feasible subunit for null knockout studies to investigate the GSH synthetic capacity in worms which cannot be achieved in *gcs-1* null worms which suffer from larval lethality (42).

Methods that investigate the role of GSH in biological systems tend to do so by either depleting GSH using a thiol-depleting agent, or by direct inhibition of GCL using L-buthionine sulfoximine (BSO), which is a γ-glutamyl amino acid analogue that competes at the enzyme's active site. BSO can potentially also competitively inhibit the cellular transport of γ-glutamyl amino acids, which can affect the GSH salvage pathway (336). We did not use BSO due to the possibility of increased extracellular γ-glutamyl amino acid uptake in GSH-compromised worms being important for this study. This concern has also been expressed in rodent models that explore GSH homeostasis (110). RNA*i* has become widely used in functional genomics studies to generate knockdown phenotypes in *C. elegans* and is most commonly induced in the worm by feeding bacteria that express the desired dsRNA (317).

An advantage of using the worm for ageing studies is the ability to conduct a battery of behavioural experiments. Due to the nature of ageing studies being labour-intensive and

time-dependent, work in this chapter endeavoured to utilise robust and reproducible measures that would be able to test the role of GCLM in the ageing worm. The most reproducible phenotyping experiments were pharyngeal pumping, thrashing, and brood size experiments (113). Phenotyping experiments have been implicated as important pathological markers when studying age-related disease models using *C. elegans*, including Parkinson's Disease (337).

3.4.1 Is *gclm* more critical for worm development rather than adult ageing?

Gclm knockdown commencing immediately after hatching rendered young adult worms prone to vulval rupture during the reproductive egg-laying period which was not observed when knocking down at adulthood. Interestingly, this phenotype was consistent with a recent study from Urban *et al.* that had investigated the RNA*i* knockdown of the *gcs-1* gene encoding for the GCL catalytic subunit orthologue (133). Urban *et al.* showed that knocking down the *gcs-1* gene resulted in a similar degree of vulval rupture when inducing RNA*i* immediately after egg-laying; with the rupture phenotype also absent when knocking down at adulthood (133). Our results showed that knocking down *gclm* beginning from adulthood had no difference in the lifespan of worms at 25°C. In the study from Urban *et al.*, no effect was observed when *gcs-1* was knocked down beginning at egg-stage, but increased lifespan was observed when knocked down beginning at adulthood (133). This observation may have been afforded by the compensatory increase (~2-fold) in expression levels of several genes of the thioredoxin system (*trx-1*, *trxr-1*, *trxr-2*) and glutathione *S*-transferase gene, *gst-4* (133). Results presented in this chapter and from the study by Urban *et al.* indicate that GSH plays a crucial role in *C. elegans* development which may be dispensable under certain circumstances in the in adult ageing, such as in the absence of exposure to oxidative insults.

During *C. elegans* development, exposure to various environmental stresses, perhaps with an inability to mount an adaptive response, may cause irreversible stress-related effects later in post-mitotic (adult) ageing. Early oxidative insults caused by hydrogen peroxide during larval development have been shown to play a role in the ageing adult nematode (338). This indicates that the ability to mount an adaptive response towards certain stresses is not established in the developing nematode and therefore can prove detrimental to later stages in life, rather than if the worm was subjected to a similar level of stress later in adulthood, the effect may not have been amplified. In the case presented in this chapter, oxidative stress defences that utilise GSH may have a more detrimental effect on post-mitotic ageing when affected during development, rather than during post-mitotic (adult) ageing.

3.4.2 Motility differences in *gclm* knockdown worms

Motility was tested in liquid as opposed to solid medium as it offers two key advantages including, being able to keep the viscosity constant between experiments, and locomotion in liquid medium requiring more energy than movement on solid agar (339). When *gclm* was knocked down at the beginning of the egg-stage, worms exhibit a significant increase in thrashing which is not observed when knocked down at the beginning of adulthood (Figure 3-9C/D). This increase in thrashing behaviour remained a strong phenotype even in the oldest worms tested (day 9). Considering that the thrashing assay was the only phenotypic measurement where the *gclm* knockdown worms outperformed the control, yet did not correlate with lifespan extension, suggests that this phenotype may be indicative of a stress-response rather than a correlative marker of longevity.

3.4.3 GSH protection against environmental factors

Due to H_2O_2 being an important secondary messenger molecule in thiol mediated signalling (340), treatment with H_2O_2 was used to investigate GSH's role in stress response. To determine if silencing of the *gclm* gene levels affected the worm's stress response, survival was monitored after an acute 1 h H_2O_2 treatment in day 3 old adults. Initial H_2O_2 insults had added the oxidant to the *E. coli* OP50 lawn immediately prior to bacterial seeding and scored survival 24 h post-treatment. However, the tendency of the worms to move off the plate as an avoidance behaviour, along with the short-term stability of H_2O_2, required a brief treatment in liquid M9 buffer followed by scoring of survival on solid NGM in the presence of *E. coli* feed. The H_2O_2 stress assay that was used to test the stress response in *gclm* knockdown worms was designed so that the worms were subjected to a 1 h stress in M9 medium and transferred to seeded NGM plates with scoring of surviving worms 6 h post-treatment. An observed decrease in the mean survival rates of *gclm* knockdown worms exposed to 5 mM H_2O_2 was not considered significant (Figure 3-10B).

The ability of antioxidant systems to mount a compensatory response under normal conditions has been illustrated in mutant worms that lack all five superoxide dismutase (SOD) genes (*sod-12345*), where no difference in median lifespan was observed when compared to wild-type worms (341). However, treatment under several conditions of stress including, heat and paraquat exposure, resulted in decreased lifespan of the *sod-12345* worms compared to wild-type (341). It is important to determine if genetic and environmental factors not only affect lifespan, but also healthspan. These two factors are however, not necessarily linked. The healthspan of worms under several environmental and genetic conditions have been shown to be uncoupled with longer-lived

worms prolonging the period of frailty as a result of the lifespan extension (342). Though it is apparent that oxidative stress increases with age in *C. elegans*, it remains uncertain that oxidative damage is indeed the cause of ageing in the organism (19).

3.4.4 Possible temperature-dependent differences effect on thiol system

When testing the effect of *gclm* knockdown at different temperatures (15°C, 20°C and 25°C), no significant difference was observed at any of the temperatures tested (Figures 3-6A/B and 3-7A/B). In this chapter, all worms had been incubated for 3 days during the larval life cycle at 20°C to ensure that synchronisation was achieved at day 0 of adulthood. Interestingly, it has recently been shown that dynamic changes in temperature exposure during *C. elegans* development, results in alterations of the cellular redox environment that can increase lifespan (236). Worms exposed to 25°C during development followed by a shift to 15°C in adulthood exhibited an increase in lifespan compared to worms kept at 15°C from the beginning of development. The authors suggested that peroxiredoxin-2 (*prx-2*) may have played a role in the extended longevity with expression levels increasing approximately 10-fold in L3 worms exposed to the dynamic temperature shift (236).

3.4.5 Promoter of the *gclm* gene requires the *cis*-regulatory region of the *E01A2.1a* variant to drive expression of GFP

The transcriptional reporter strains generated in this work were designed to investigate the expression patterns of the *E01A2.1a* transcript variant. Typically, promoter fragments of a few kilobases immediately upstream of the start codon contain a significant portion of the *cis*-regulatory information necessary to provide a tentative expression pattern of the endogenous gene under study (343). We have shown that when the entire promoter

region of the *E01A2.1a* variant is fused with GFP, the expression patterns are present in several tissue types of the worm. Though transcriptional reporters can provide valuable information about upstream regulatory elements, these may not accurately represent the expression patterns due to the absence of the endogenous 3′ UTR. A number of examples for which crucial *cis*-regulatory sequences have been found include, within introns (344), or even the 3′ UTR (345, 346).

In a 2016 report, neuron-specific RNA sequencing data showed that the *E01A2.1* transcript is expressed in neurons throughout various stages of the worm lifecycle (347). Using neuronal promotors tagged with GFP, fluorescence activated cell sorting (FACS) was used to separate neuronal cells from worm homogenates to subsequently sequence the transcriptomes of the neurons in all the main stages of the worm's lifecycle, including embryos, larvae and adults. The expression of *E01A2.1* is present at each stage tested, which was not characteristic of all the gene transcripts that were measured (347). Here we have provided evidence in support of previous RNAseq data to show that the *E01A2.1* gene is possibly neuronally expressed (347). Future work should validate this hypothesis by determining which neuron corresponds with the apparent expression patterns of the *gclm* transcriptional reporter. To resolve cell-specific localisation, the generation of a translational reporter, coupled with performing confocal microscopy, will provide a more reliable representation of the *gclm* expression patterns.

3.4.6 Design and practical considerations for generating CRISPR *gclm* mutant strains

The most recent publication from the *C. elegans* Deletion Mutant Consortium reports that 6764 genes with associated molecular lesions of either deletions or null mutations are available (348). Currently no *gclm* mutants are available from the two major *C. elegans*

strain repositories: the *Caenorhabditis* Genetics Center (CGC) and the National BioResource Project (NBRP). Accordingly, generation of *gclm* mutants using CRISPR/Cas9 was attempted in this project to confirm the role of GCLM with loss-of-function experiments. The CRISPR/Cas9 genome editing tool has provided a method for heritable modifications of the *C. elegans* genome (349). Practical considerations have recently been described including, guide RNA design, the delivery and expression of Cas9 and guide RNA in to germline cells, and screening methods to identify successful editing events (350). Guide design is a crucial element of the success of CRISPR/Cas9 editing with guide specificity important for minimising off-target mutations. Guide efficiency is difficult to predict, however previous efforts have been made to quantify sgRNA efficiency as being the fraction of F_1 worms that were identified with deletions from the brood that had expressed the co-injection marker (349, 351, 352).

Delivery of Cas9 and guide RNA can be introduced into germline cells by several methods including, using an expression plasmid, as mRNA, or as purified Cas9 protein complexed with sgRNA (349, 353, 354). Cas9 is fused to an SV40 nuclear localisation signal (NLS) to direct its localisation in to the nucleus. To repair a double-strand break (DSB), *C. elegans* incorporates error-prone repair via an end-joining pathway mediated by DNA polymerase θ (355). Error-prone repair can result in insertions or deletions (indels) at the DSB site, which can shift the reading frame and produce a premature stop codon (350). This is becoming the preferred method to produce loss-of-function alleles in *C. elegans* (335, 350) which was attempted in this work. It has been discussed that the injection of 20 worms should generally produce multiple mutant alleles (356).

Current CRISPR screening strategies include, visible phenotypes, positive selectable markers and PCR (350). In this work, a PCR strategy was employed to detect indels by

amplifying the region surrounding the target site, and running the PCR amplicons on agarose gels to detect size differences (329). The main disadvantage of PCR screening was the laborious process required to analyse large numbers of F_1 progeny compared to other methods of screening (350).

Considering the *gclm* RNA*i* results from this Chapter, it could be possible that a heritable mutation causing larval developmental complications is occurring, but we have not been able to confirm this by DNA sequencing. The most comprehensive way to test this would be to target as many sites on the *gclm* exons as possible until a viable loss-of-function strain is generated. If all the possible guides are attempted and cannot generate viable mutants, and the guide efficiencies are confirmed through sequencing, then it may provide evidence to support the theory that *gclm* is crucial in *C. elegans* development.

3.5 Conclusions and chapter summary

The aim of this chapter was to investigate the role of the *gclm* gene in ageing by initially using RNA*i*-targeted knockdown to observe the resulting phenotypes. Work presented herein confirms that the *gclm* subunit regulates the endogenous levels of GSH in the worm. This has proven the suitability of *C. elegans* as a model to investigate *gclm* and provides the basis for future work that plans to further understand its regulatory role *in vivo*. One conclusion that can be drawn from this work, is the importance of GSH on the development of the worm. When the *gclm* gene is silenced immediately after embryogenesis, a strong vulval rupture phenotype is observed. Accordingly, the RNA*i* treatment method was adapted so that the *gclm* gene was conditionally silenced beginning from adulthood. Future work should investigate the importance of *de novo* GSH synthesis in the lifecycle of the larval development of *C. elegans* to elucidate the mechanisms of this rupture phenotype.

Though it is beyond the scope of this work, an interesting direction could investigate the potential pleiotropic effects of the *gclm* gene in addition to its involvement in GSH synthesis. A body of evidence suggests that *gclm* may have a role in lipid homeostasis. An early RNA*i* screening study, demonstrated that the targeted knockdown of the *E01A2.1* gene from the L1 stage resulted in reduced fat content in wild-type worms (357). In agreement with this early work, the *gclm* gene has been recently implicated to have a role in lipid metabolism in *C. elegans* embryos (358). A screen of 316 genes found that 22 candidates possessed altered lipid droplet phenotype in *C. elegans* embryos. The most robust droplet phenotypes were observed in *asm-3* (acid sphingomyelinase 3), *hosl-1* (hormone sensitive lipase) and the *gclm* (*E01A2.1*) gene. The strong phenotype of alteration in lipid droplets of the RNA*i*-targeted knockdown of the *gclm* gene, was

observed using a *rrf-3*(*pk1426*) mutant strain that is hypersensitive to RNA*i* (358). Explanations of the differences in *gclm* knockdown worms may be either due to the role of GSH in lipid organisation or a potentially putative role of the *C. elegans gclm* gene in lipid homeostasis.

The *C. elegans* protein-protein interactome study that initially reported the interaction of the *C. elegans* GCLM with GCLC (*gcs-1* gene), also reported the interaction between GCLM and the F25H9.6 gene product (146). In *C. elegans*, the F25H9.6 gene is an ortholog of human phosphopantothenoylcysteine decarboxylase (*Ppcdc*), which is involved in coenzyme A (CoA) synthesis. Though the interaction between GCLM and PPCDC is yet to be confirmed beyond the high-throughput Y2H study, this proposed putative role of GCLM in *C. elegans* may have implications for the addition of cysteine (thiol group) in the metabolic pathway for CoA biosynthesis from pantothenate (vitamin B5). However, the addition of the cysteine moiety to 4'-phosphopantothenate occurs one step before the PDCDC-catalysed reaction (Figure 3-13). Though speculative at this stage, the potential putative role of GCLM in the synthesis of the CoA via the addition of the thiol group is an interesting prospect for future work.

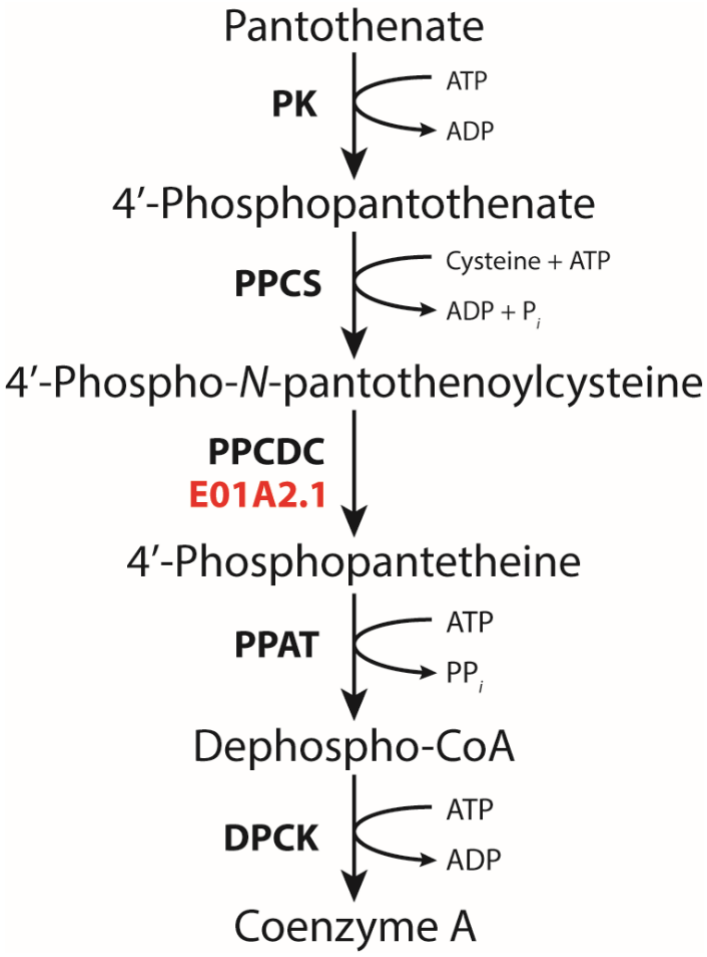

Figure 3-13. The pathway of coenzyme A synthesis and the hypothetical involvement of *gclm* in *C. elegans*

The first reaction in Coenzyme A synthesis is catalysed by pantothenate kinase (PK) which is encoded by pnk-1 and pnk-4 in C. elegans*. Cysteine is then added to 4'-phosphopantothenate by the enzyme phosphopantothenoylcysteine synthetase (PPCS) to form 4'-phospho-N-pantothenoylcysteine, which is decarboxylated to 4'-phosphopantetheine by phosphopantothenoylcysteine decarboxylase (PPCDC), followed by conversion to coenzyme A by CoA synthase (the bifunctional PPAT/DPCK protein found in most eukaryotes). Evidence has suggested that* E01A2.1 (gclm) *possibly interacts with PPCDC in* C. elegans.

CHAPTER FOUR

Supplementation with γ-GC as a strategy for replenishing chronic depletion of GSH

4 Chapter Four

4.1 Introduction

The original free radical theory of ageing (7) prompted Denham Harman's research to investigate if consumption of dietary antioxidants could be an effective strategy to slow the ageing process, with some promising results, notably with the inclusion of sulfur-containing compounds in the diet, including cysteine and cysteamine (359). Subsequent extensive experimentation of antioxidant systems and therapies has provided inconsistent data, and at times has failed to support the theory (21, 360, 361). Conversely, the administration of pro-oxidants has also been proposed as an approach to increase longevity in various models (362). Experimentation that tests the therapeutic potential of antioxidant compounds based solely on their reported ability to neutralise ROS and free radicals without considering the mechanistic basis for the compound's action, ultimately provides little support to understand the complexity of the redox environment. Antioxidant therapies may not provide any benefit unless the compound is bioavailable and a deficiency is occurring. Treatments with pro-oxidants based on the hormesis hypothesis may lead to more damaging effects if the organism is unable to deal with the increase in oxidative load. When considering antioxidant efficacy, one should assess the perturbations of the system and demonstrate how they are ameliorated by the investigated treatments.

Work described in the previous chapters concluded that the age-related decline in GSH levels is likely due to dysfunctions occurring in the *de novo* synthesis pathway. The two major substrate-based strategies to increase GSH levels include administration with the cysteine prodrug, *N*-acetylcysteine (NAC) and with GSH itself. Treatment with exogenous GSH is the most intuitive approach to replenish levels of the tripeptide.

However, GSH suffers from poor bioavailability in mammals and the breakdown of extracellular GSH by the action of membrane bound γ-GT prohibits the uptake of intact GSH to directly raise cellular concentrations above homeostatic levels. *N*-acetylcysteine (NAC) is a low-toxicity source of cysteine that becomes deacetylated and subsequently utilised by GCL for synthesis of the GSH precursor, γ-GC. Treatment with exogenous γ-GC offers the potential to cross the cellular membrane by putative mechanisms, where it would effectively bypass the rate-limiting GCL enzyme, to be converted by glutathione synthetase (GS) to GSH (Figure 4.1A). In a recent clinical study, oral administration of γ-GC has been shown to increase GSH levels in the lymphocytes in healthy humans, demonstrating its systemic bioavailability (112). We have proposed that γ-GC has the potential to treat conditions associated with the age-related dysfunction of GSH synthesis (96). Despite this theoretical basis, no studies to date have investigated the therapeutic potential of γ-GC to replenish chronically depleted GSH using an ageing model.

In this chapter, the focus was to establish an effective delivery vehicle for orally dosing *C. elegans* with exogenous γ-GC. To investigate the bioavailability of γ-GC in worms, a liposome encapsulation method (363) was adapted to simulate oral administration of γ-GC and potentially increase its bioavailability (Figure 4-1C). Using the *gcs-1*(*ok436*) mutant strain (VC337), which has ~70% the GSH levels of the wild-type (137), γ-GC was evaluated for its capacity to increase GSH levels (Figure 4-1B). If exogenous γ-GC can enter systemic distribution in the worm, it should effectively bypass the rate-limiting GCL enzymatic step (GCS-1 in worms) to directly act as a substrate for glutathione synthetase (GSS-1) and increase GSH above homeostatic levels (Figure 4-1A). This chapter describes for the first time, the use of *C. elegans* as an ageing model to investigate the therapeutic potential of γ-GC in chronic GSH depletion.

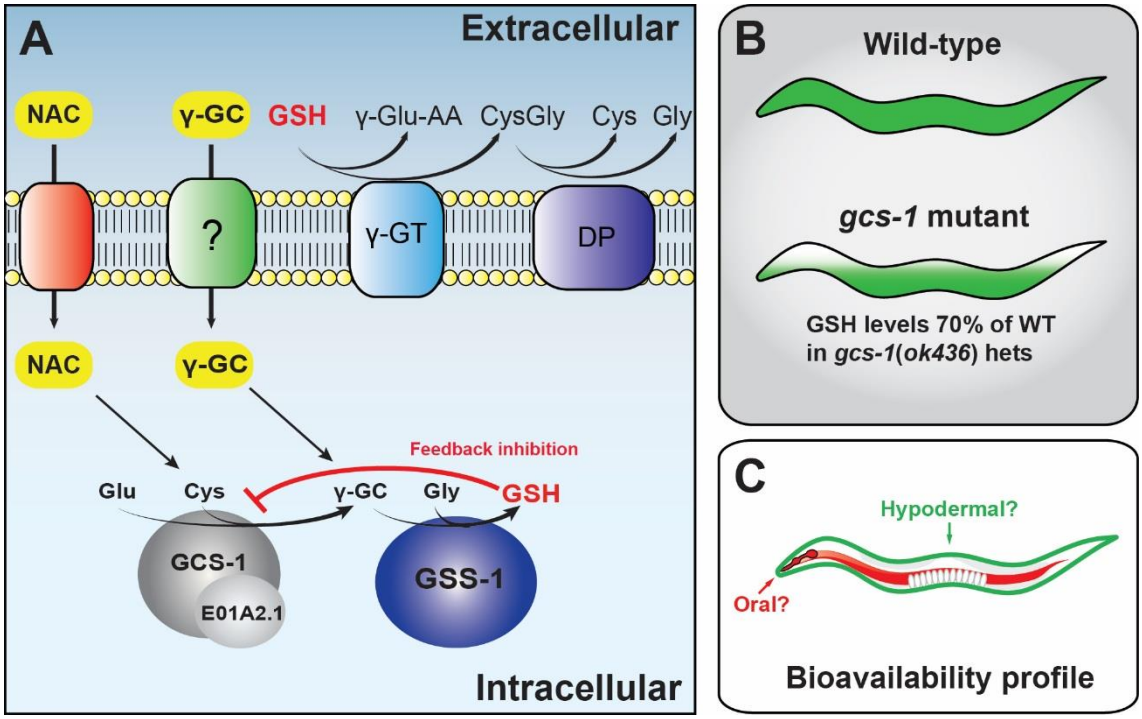

Figure 4-1. Proposed substrate-treatment models for investigating γ-GC

The upper limit of cellular GSH concentrations are controlled by feedback inhibition on the GCL enzyme (GCS-1 in C. elegans*) exerted by GSH. In mammals, glutathione synthetase (GSS-1 in* C. elegans*) is not known to be controlled by any feedback inhibition. (A) Cellular uptake of γ-GC is proposed to bypass GCS-1 and increase GSH levels above homeostasis. Both NAC and hydrolysed exogenous GSH are cysteine sources for GCL and cannot theoretically increase GSH levels above homeostasis. (B) If the bioavailability profile of NAC and γ-GC is comparable in worms, γ-GC treatment theoretically would bypass the GCS-1 and lead to increases in GSH levels in both* gcs-1(ok436) *mutants and wild-types. (C) Establishing a bioavailability profile for compound absorption through the hypodermis or via oral administration was of interest to this study.*

4.2 Materials and Methods

4.2.1 Chemicals and equipment

The thiol compounds *N*-acetylcysteine (NAC) and GSH were supplied by Sigma Aldrich (Australia). The γ-GC used in this study was provided by Biospecialties International (Mayfield, Australia) as a monosodium salt (364). Liposome kits (L4395) for the preparation of cationic (positively charged) liposomes were supplied by Sigma Aldrich. The Avanti Mini-extruder apparatus for the preparation of liposomes was supplied by Avanti Polar Lipids, Inc.

4.2.2 Nematode propagation and strains

The N2 Bristol strain (wild-type) was provided by the *Caenorhabditis* Genetics Center (CGC), which is funded by the NIH National Center for Research Resources (NCRR). The *gcs-1*(*ok436*) mutant strain (VC337) from the CGC was used as a model for compromised GSH synthesis. The VC337, [*gcs-1(ok436)/mIn1[mIs14 dpy-10(e128)*] II, strain is a variant N2 Bristol (wild-type) strain that possesses an 837 bp chromosomal deletion (*ok436*) of the *gcs-1* locus (Figure 4-2A). This *gcs-1*(*ok436*) null allele causes larval lethality, whereby homozygotes arrest at approximately the L2 larval stage. This strain is balanced with a variant of the *mIn1*[*dpy-10*(*e128*) *mIs14*] balancer strain which carries an integrated pharyngeal GFP element [*myo-2*::*gfp*; *pes-10*::*gfp*]. One copy of *mIs14* can be distinguished from two by GFP signal brightness (365). Homozygotes for the balancer exhibit the dumpy phenotype, with heterozygotes possessing one copy of the *gcs-1(ok436)* mutation. Heterozygotes exhibit no dumpy phenotype and have a weaker pharyngeal GFP signal compared to dumpy worms (Figure 4-2B).

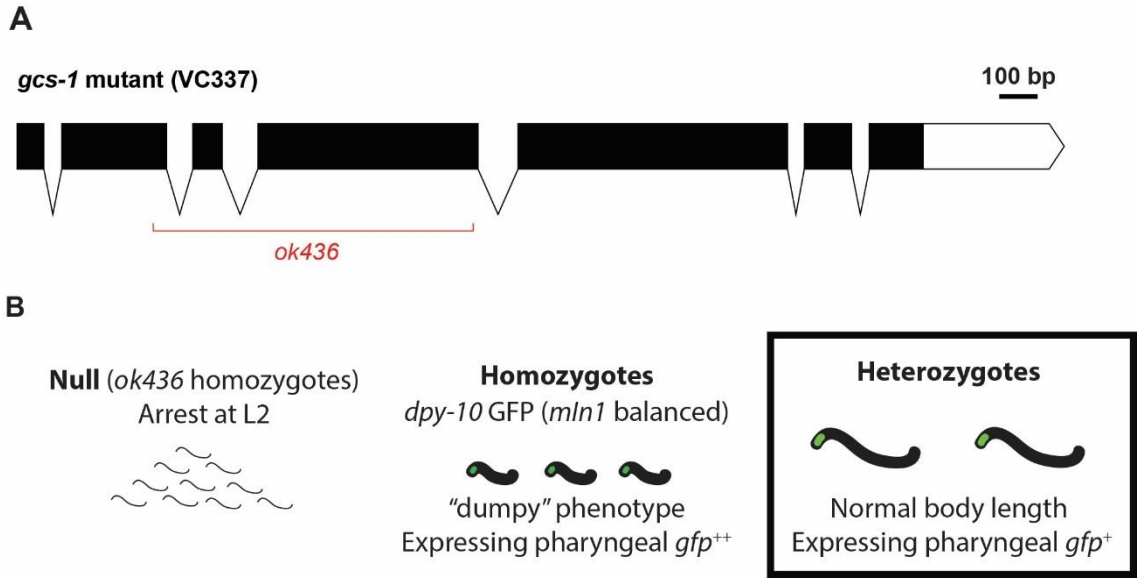

Figure 4-2. The *gcs-1*(*ok436*) mutant strain

(A) The gcs-1*(*ok436*) mutant strain (VC337) possesses a deletion that spans across exon 2 to exon 4. (B) Null mutants arrest at L2. To maintain heterozygotes, the strain is balanced with a semi-dominant pharyngeal GFP and dumpy-10 selection marker. Homozygotes contain copies of the gcs-1 gene that possess the dumpy phenotype and two copies of the pharyngeal GFP (which expresses brighter than the heterozygotes). The heterozygotes carry one copy of the GFP and express 'normal' body size phenotype (i.e. not dumpy).*

4.2.3 Thiol liposome-encapsulation method

The liposomes were prepared by adding 1 ml of the desired thiol concentration dissolved in sterile PBS to the lyophilised liposome powder. Each 1 ml vial preparation contained: 63 µmol L-α-phosphatidylcholine, 18 µmol stearylamine and 9 µmol cholesterol (7:2:1 molar ratio). This suspension was vortexed for 5 min at room temperature followed by 5× freeze/thaw cycles at -80°C for increased encapsulation efficiency of the hydrophilic compounds. The liposome suspensions were then drawn up using one of the two gas-tight syringes included with the Avanti Mini-Extruder apparatus (Avanti Polar Lipids, Inc.). The Mini-Extruder was assembled according to the manufacturer's instructions and the liposome suspensions were filtered through the extruder at 65°C using a Nucleopore

track-etched polycarbonate membrane (pore size 1.0 µm) (363). Aliquots of the liposome suspensions were briefly vortexed with the *E. coli* OP50 suspension to achieve the desired final liposome concentration (*v*/*v*) before being seeded on NGM plates. To ensure liposome/*E.coli* concentrations were consistent at the beginning of each 24 h period, the worms were transferred each day to new plates containing fresh (prepared the previous day) liposome/*E. coli* lawns.

4.2.4 Characterisation of liposomes

The physical heterogeneity of liposome shapes and sizes were examined using Cryo-electron microscopy (Cryo-EM) according to previous methods (366). High resolution images were generated using a FEI Tecnai G2 20 TEM electron microscope. Liposome stocks were prepared and frozen at -80°C under nitrogen to prevent lipid peroxidation. For image acquisition, stocks were thawed, vortexed and diluted in PBS within 1 h of preparation for the Cryo-electron microscopy. To determine nanoparticle size distributions throughout solutions, liposomes sizes were measured via their light scattering properties with a Malvern Zetasizer Nano ZS and nanoparticle tracking analysis using the NanoSight NS300 (Malvern Instruments).

4.2.5 Thrashing, egg-laying, pharyngeal pumping and H_2O_2 stress-tests

Thrashing, egg-laying and pharyngeal pumping assays were performed according to methods outlined in Chapter 3 (Thrashing, 3.2.5; egg-laying, 3.2.6; pharyngeal pumping, 3.2.7). The LC_{50} dose curve for H_2O_2 (1 h treatment) in *gcs-1*(*ok436*) worms was determined graphically by the 50% plateau level of worm survival (6 h post treatment).

4.2.6 A method to screen compounds that extend lifespan

A screening method was conducted using liposome-encapsulated thiols to allow for a range of concentrations to be tested with minimal work load (Figure 4-3). Each treatment was conducted in a blinded manner to avoid any operator bias (367). Initially, a liposome tolerance test was performed to determine any toxicity of the liposome vehicle that would affect the lifespan over the range of 0.5% to 10% (*Step 1*). Next, each liposome-encapsulated thiol was tested over the range of 0.1% to 1% (*Step 2*). Twenty worms were housed per well of a 6-well plate with 100 µM FUdR added to the nematode growth medium (NGM). The addition of FUdR reduced the work load to avoid daily transfer of the worms by inhibiting egg hatching. For wild-type worms, survival was recorded at day 5, 10, 15 and every second day thereafter until death.

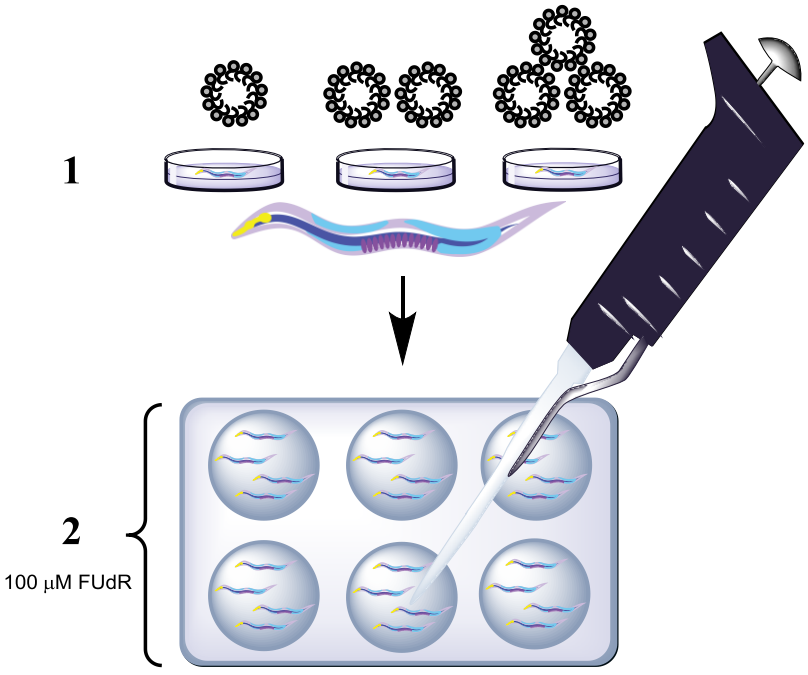

Figure 4-3. Work flow of the liposome-encapsulated compound screening method

Step 1. Liposomes over the range of 0.5-10% concentrations were added to *E. coli* OP50. *Step 2*. Liposome-encapsulated γ-GC and the PBS vehicle control were tested in 6-well plates. Reproduction was inhibited by the addition of 100 µM FUdR into the NGM which allowed survival to be scored over regular intervals without the need for daily transfer of worms.

4.2.7 Statistics

Statistical analysis for Kaplan-Meier survival curves for lifespan studies were analysed in GraphPad Prism using a log-rank (Mantel-Cox) test. Statistical analysis including, one-way AVOVA (Dunnett's multiple comparisons) test and two-way ANOVA tests (with Bonferroni multiple comparisons) were performed using GraphPad Prism (version 7.02).

4.3 Results

4.3.1 Assessment of γ-GC bioavailability in liquid medium and heat-treated *E. coli*

Treatment in liquid medium was first investigated to determine if γ-GC can be absorbed through the cuticle in wild-types using the same conditions (i.e. concentrations, age, and treatment time) as were used for NAC concentrations in Chapter 2 (Figure 2-9). In M9 liquid medium, the γ-GC treatments tested (0.5, 5 and 10 mM) showed no change in GSH levels in worms after 2 h incubation (Figure 4-4A). Though alimentary ingestion would be the most relevant delivery method to model oral bioavailability, treatment in liquid medium may potentially provide useful data on γ-GC bioavailability. The 2 h treatment period was selected based on previous rodent studies that had showed that maximum increases in GSH occur between 1.5-2 h post γ-GC treatment (98). GSH levels were measured in wild-types due to the *gcs-1*(*ok436)* VC337 population being genetically heterogenous for the *gcs-1*(*ok436*) mutation (Figure 4-2B). Use of the viable heterozygotes for the *gcs-1*(*ok436*) mutation would have required manual sorting of the population, which was not necessary for the wild-type population.

Reproduction and lifespan of wild-type worms treated with γ-GC were measured using heat-treated *E. coli* as the food source (Figure 4-4B-D). No difference in brood size was observed in any of the γ-GC concentrations tested (0-10 mM). The single dose tested, 5 mM γ-GC did not show any difference in lifespan in wild-types. This dose was selected according to a previous study that showed optimal increases in lifespan when treated with 5 mM NAC (298).

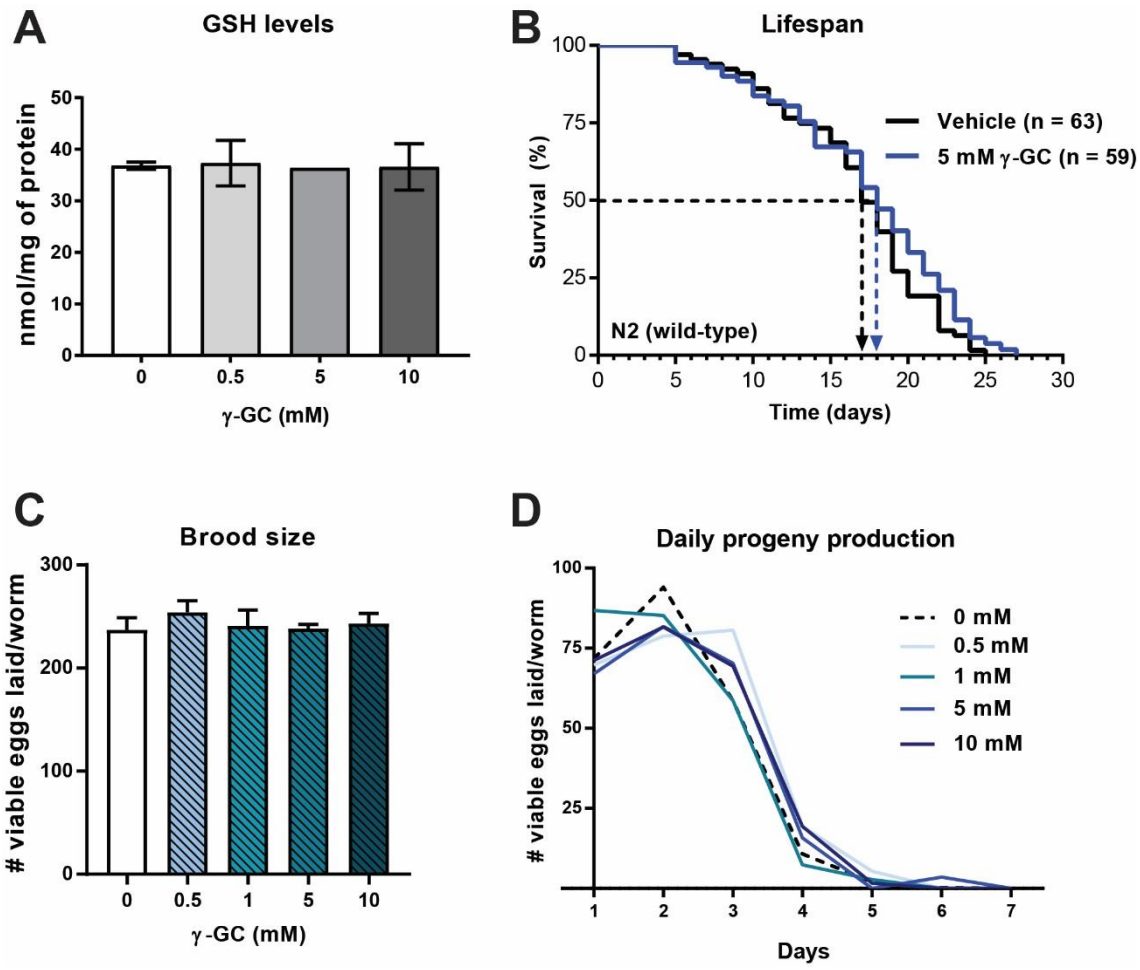

Figure 4-4. Effects of γ-GC supplementation on GSH levels, lifespan and reproduction in wild-type worms in liquid medium or heat-treated *E. coli*

(A) Day 1 old adult wild-type worms were treated with γ-GC (0-10 mM) for 2 h in liquid medium (n=1-2). (B) Survival curves of wild-type worms fed with heat-treated E. coli *supplemented with 5 mM γ-GC or vehicle (PBS). (C & D) Brood size and daily progeny production of worms treated with γ-GC (0-10 mM) in heat-treated* E. coli. *No significant effects on lifespan, GSH levels, or brood size were observed for any of the γ-GC concentrations tested.*

4.3.2 Cryo-electron microscopy to confirm the formation and structural properties of liposomes

Examination of liposome suspensions using light microscopy could only resolve the larger liposomes and did not provide comprehensive information on the heterogeneity of sizes and morphologies. Cryo-electron microscopy (Cryo-EM) was used to validate the presence of liposomes loaded with the PBS vehicle. Cryo-EM was considered the most suitable method for liposome structure characterisation due to the fixation process requiring no chemical, and hence structural modifications (368) and thereby should maintain the structural integrity of the liposomes in their native state. The method proved suitable for visualising small (SUV, <100 nm) and large (LUV, 0.1-1 μm) unilamellar liposomes as well as multilamellar vesicles (MLV) and multivesicular vesicles (MVV) (Figure 4-5B). When preparing liposomes, extrusion rather than sonication was used to achieve structural integrity. Sonication could potentially result in thiol autooxidation due to overheating and increased sample aeration.

Liposome suspensions were extruded through a 1.0 μm track-etched polycarbonate filter and displayed considerable heterogeneous structures and sizing patterns (Figure 4-5B). This variability may be challenging for maintaining consistency of compound treatments between groups. The reproducibility of liposome sizing patterns, including calculating the size distribution was tested for the vehicle-loaded liposomes by nanoparticle tracking analysis (Figure 4-5C).

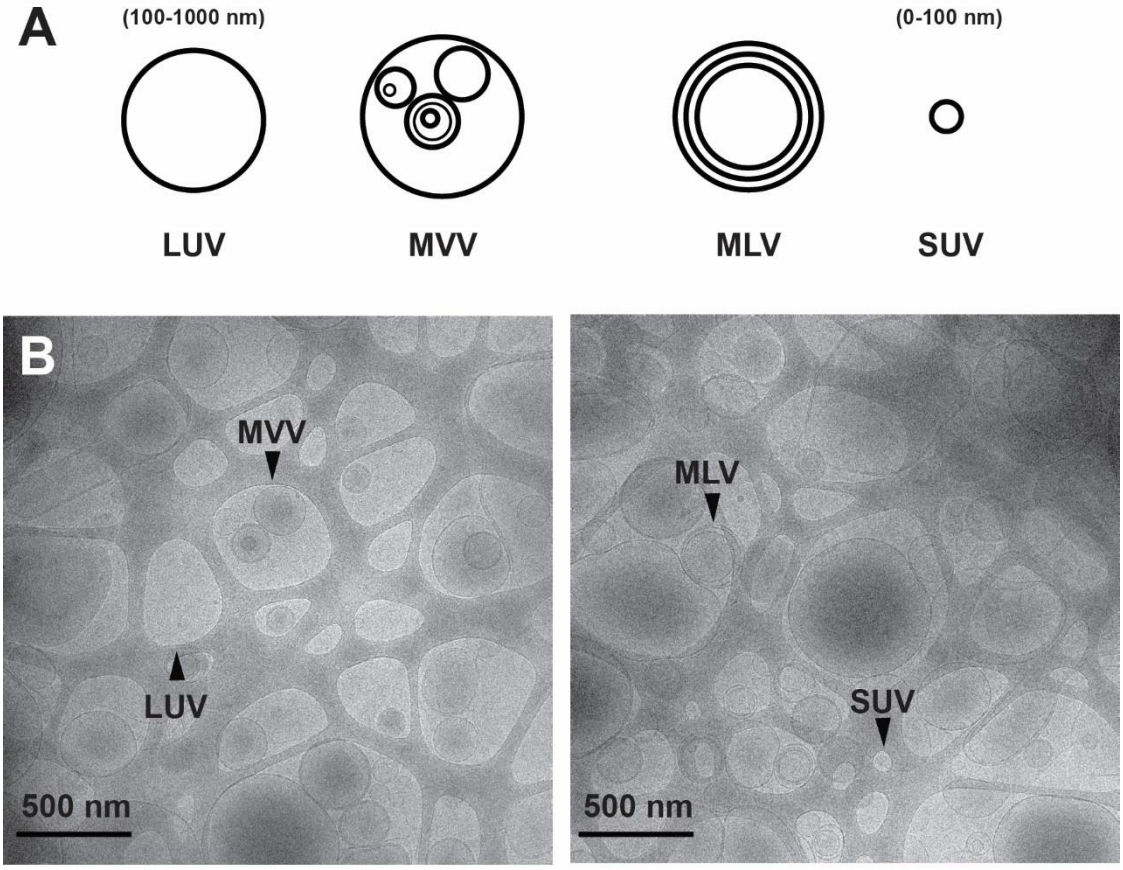

C) Table of size distribution (%) of PBS-loaded liposome suspensions

Sample	0-100nm	100-200nm	200-350nm	350-500nm	500-650nm	650-800nm	800-1000nm	liposomes/ml
Rep. 1	0.0 ± 0.0	1.1 ± 0.6	22.4 ± 2.2	13.5 ± 4.2	25.6 ± 6.2	18.6 ± 5.9	18.5 ± 5.0	4.60×10^{8}
Rep. 2	0.0 ± 0.0	0.1 ± 0.0	16.9 ± 3.9	17.6 ± 4.6	14.7 ± 2.4	26.0 ± 3.0	24.6 ± 5.7	4.69×10^{8}
Rep. 3	0.1 ± 0.1	12.0 ± 6.0	10.1 ± 4.5	14.8 ± 1.1	23.0 ± 6.9	21.7 ± 5.2	18.3 ± 6.9	4.66×10^{8}

Figure 4-5. Characterisation of liposome structures and heterogeneity

Liposomes formed using the PBS vehicle-loaded control were imaged by Cryo-EM. (A) Schematics show the structure-based classification groups of liposomes, which can be categorised based on number of bilayers: multilaminar vesicles (MLV) or multivesicular vesicles (MVV) and by size, such as large (LUV) or small (SUV) unilamellar vesicles. B) Shows the Cryo-EM images of liposomes containing heterogenous structures. C) The comparison of repeated measurements of the relative size (nm) distribution ranges and total number of liposomes (liposomes/ml). Results are calculated as the mean percentage ±SEM for size distribution and mean only for the total number of liposomes.

4.3.3 Maximum tolerated liposome dose-response over the lifespan of *C. elegans*

To determine whether liposomes were toxic to the worms or affected lifespan, an initial liposome toxicity evaluation study was conducted at a range of concentrations added to the *E. coli* feed. One vial of the lyophilised liposome kits was hydrated with 1 ml sterile 1× PBS buffer. An *E. coli* OP50 suspension (100 µl) was diluted with liposome concentrations ranging between 0.5% - 10% and added to 35 mm NGM plates. A significant decrease in lifespan ($p<0.001$) was observed for the three highest liposome-containing *E. coli* lawns (10%, 5% and 2%) (Figure 4-6). The maximum lifespan for each group showed a near-dose dependent response, with the higher the concentration the lower the median lifespan. Accordingly, for the liposome encapsulation of γ-GC, concentrations that were later used ranged between 0.1-1%.

4.3.4 Compound screening to test the effect of γ-GC on lifespan

The effect of liposomal γ-GC on wild-type lifespan was tested over the concentration range of 1.36 mM-13.6 mM liposomal γ-GC. FUdR (100 µM) was included in the NGM to inhibit larval hatching and enable a more comprehensive test range of γ-GC concentrations. Worms treated with 1.36 mM γ-GC encapsulated in 0.1% liposome concentrations showed a significant increase in lifespan ($p<0.01$), compared to the 0.1% liposome vehicle only control (4-7A). The higher concentrations showed no significant differences in lifespan in these worms (4-7B-D), indicating that the lower liposomal γ-GC concentration (1.36 mM) may be optimal dose for lifespan increase.

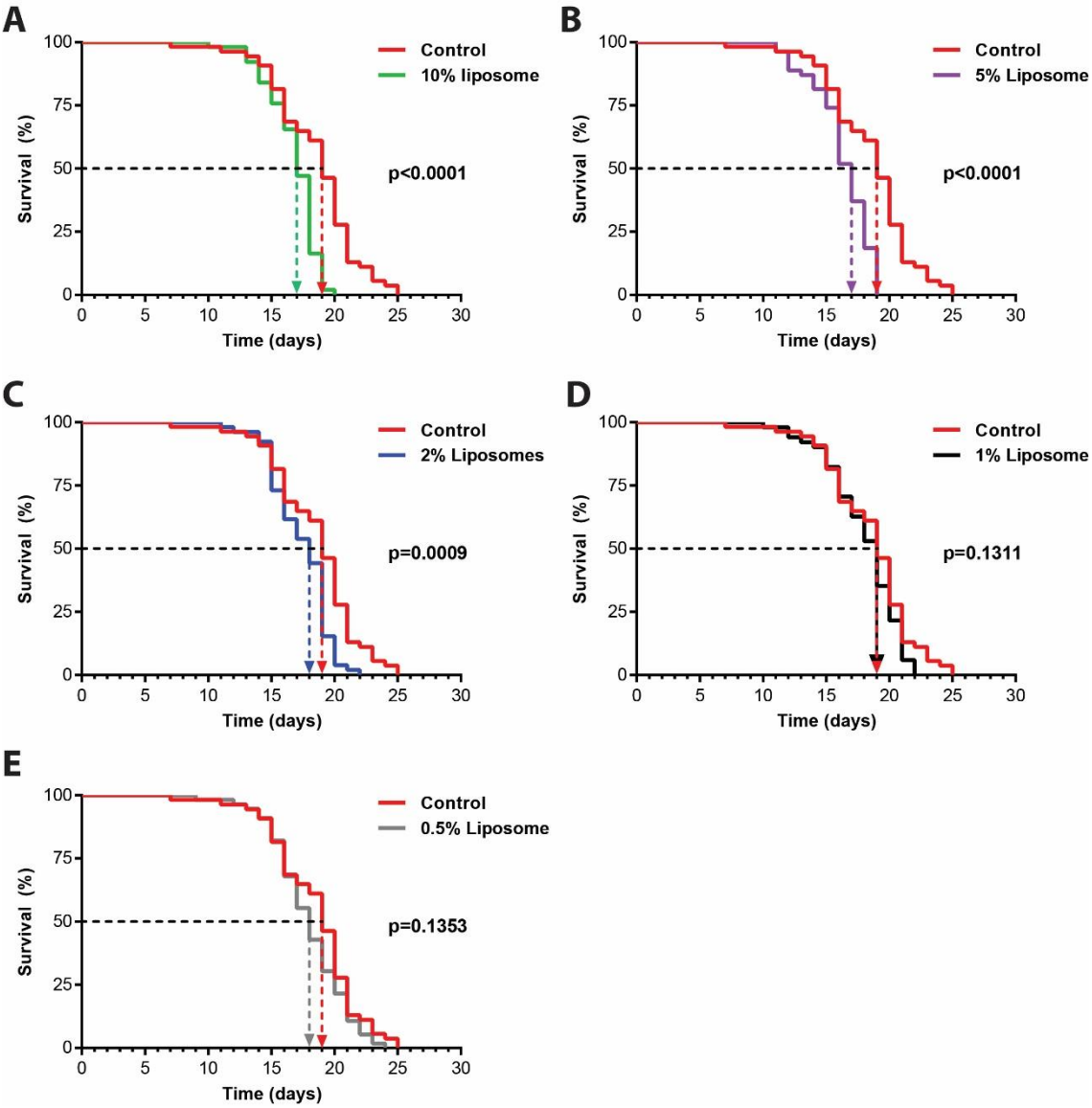

Figure 4-6. Effect of liposome concentration on wild-type *C. elegans* lifespan

Lifespan assay (log-rank test) comparing the survival of wild-type C. elegans *fed with a range of liposome concentrations (v/v) added to* E. coli. *A significant ($p<0.001$) decline in lifespan was observed at (A) 10%, (B) 5%, and C) 2% liposome concentrations when compared to the control that was fed with* E. coli *OP50 only. No significant differences in lifespan were observed at the lower liposome concentrations (D) 1% and (E) 0.5%. Survival curves represent a single experiment where each liposome treatments are compared to the control (shown in red). Log-rank tests were used to compare each liposome treatment to the control.*

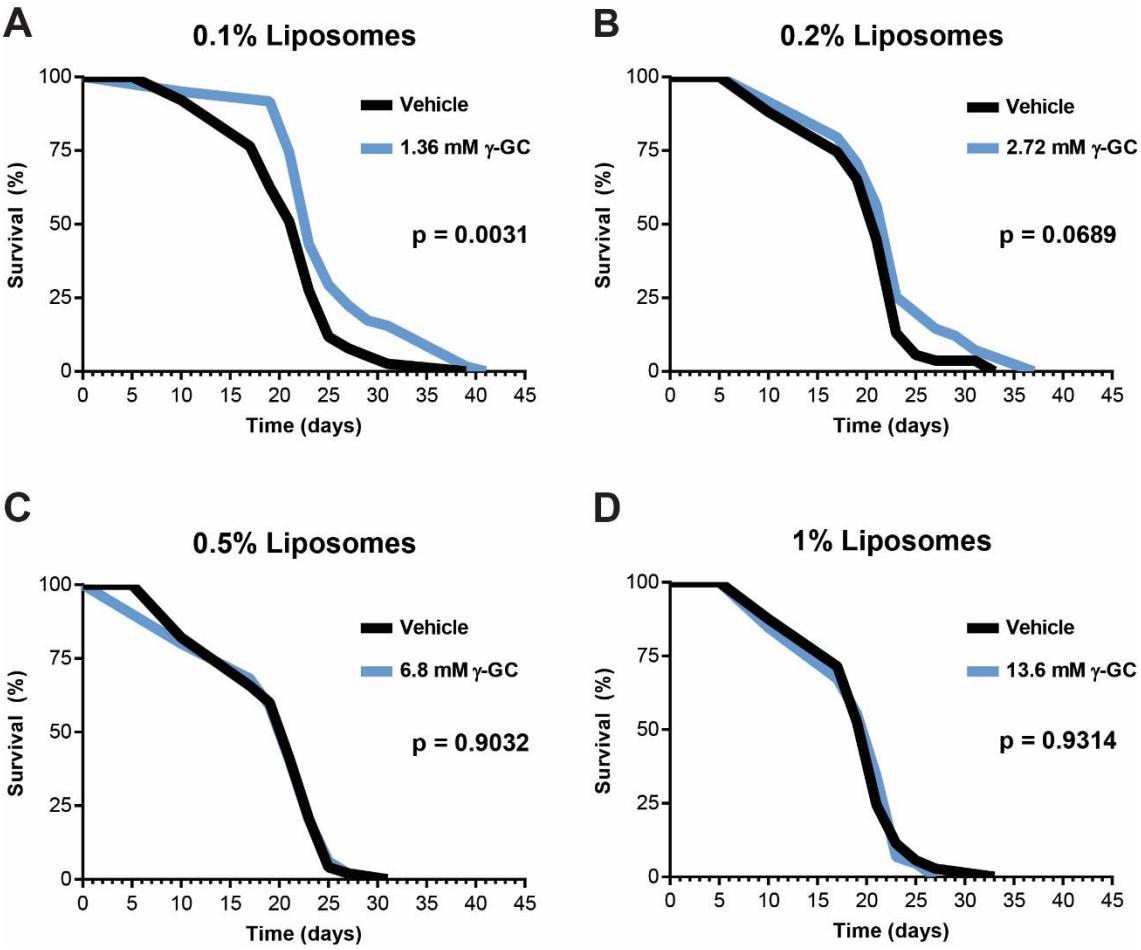

Figure 4-7. Lifespan screening of wild-type worms treated with liposomal γ-GC

*Worms treated with a range of diluted liposomal γ-GC (1.36 mM to 13.6 mM) concentrations were compared to the vehicle only control. 100 μM FUdR was included in the NGM. Survival was scored at day 5, 10, 17 and every second day thereafter until death. A significant increase in lifespan was observed only for (D) 0.1% liposome encapsulated 1.36 mM γ-GC (*p*=0.0031) when compared to the vehicle control. No significant differences in lifespan were observed in any of the higher concentrations of liposomes tested. Log-rank tests were used to compare each γ-GC treatment group with the vehicle control.*

4.3.5 Determining optimal treatment time for liposomal γ-GC bioavailability

An initial assessment of the bioavailability of liposomal γ-GC was carried out by synchronising eggs on plates seeded with *E. coli* and liposome suspensions and allowed to develop through the larval cycles until the harvesting of young adults (day 0) after 3 days (Figure 4-8A). No significant difference between the γ-GC (1.7 mM) and vehicle only groups was observed for any of the measured thiol levels in wild-type worms (Figure 4-8B). Subsequent experimentation explored whether γ-GC treatment, using several administration methods, could provide any benefit to the GSH-compromised *gcs-1*(*ok436*) strain by monitoring the physiological responses (movement, pharyngeal pumping, egg-laying) that are considered predictive measures of *C. elegans* lifespan (113).

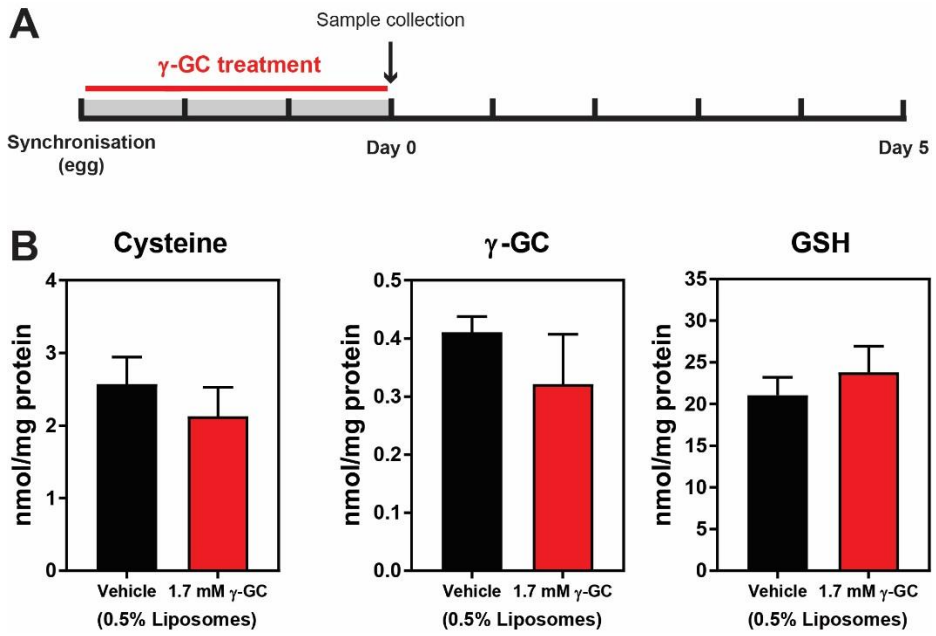

Figure 4-8. Thiol levels in worms treated with liposomal γ-GC

Thiols were measured in worms treated with liposome-encapsulated thiols for the duration of larval development and were harvested at day 0. Unpaired t-tests indicated no significant difference between the liposomal γ-GC (n=5) and the vehicle control (n=2). Data presented as mean ±SEM.

4.3.6 Pre-treatment with γ-GC may offer protection to *gcs-1*(*ok436*) mutants against acute hydrogen peroxide exposure

Initial experiments to investigate the therapeutic potential of γ-GC in GSH compromised *gcs-1*(*ok436*) worms involved a γ-GC pre-treatment prior to an acute oxidative insult (H_2O_2). Both the pre-treatment with γ-GC (2 h) and the insult with H_2O_2 (1 h) were conducted in liquid medium to allow for short experimental treatment times. A previous report has shown that 3 h pre-treatment with 50 μM GSH in *gcs-1*(*ok436*) worms increased the 24 h survival rates of subsequent arsenic-induced oxidative stress (369). If γ-GC is taken up and directly used in GSH synthesis, it could provide an advantageous substrate-based approach to increase GSH levels above homeostasis and enhance the oxidative stress resistance of *gcs-1*(*ok436*) worms. The LC_{50} dose for H_2O_2 in *gcs-1*(*ok436*) worms was determined to be 2.19 mM after 6 h recovery (Figure 4-9A), which was selected for subsequent stress-tests using pre-treated γ-GC *gcs-1*(*ok436*) worms. Survival rates were increased by 20% for pre-treatment with 2 mM γ-GC and by 10% for 5 mM γ-GC (Figure 4-9B). The degree of this apparent modest protective effect of γ-GC pre-treatment against the H_2O_2 insult is limited due to the data from this experiment being conducted as a single independent measurement. Accordingly, this data is to be treated as preliminary findings before significance can be assessed through repeated measurements.

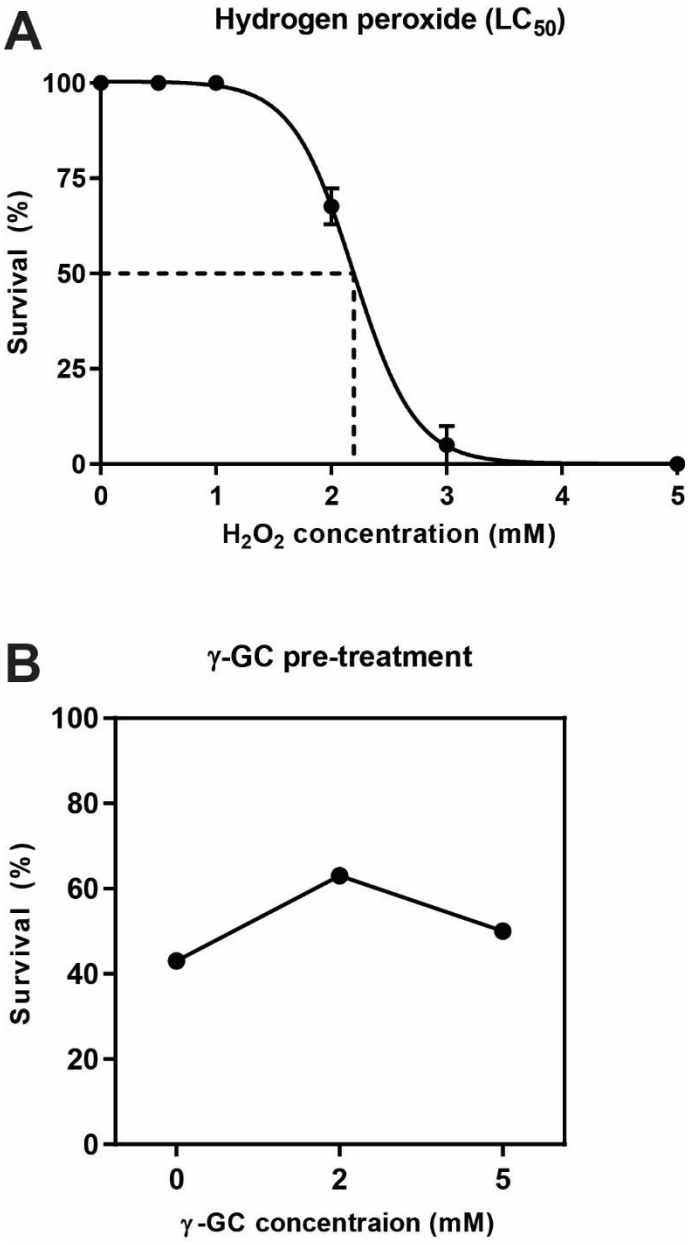

Figure 4-9. Hydrogen peroxide LC_{50} pre-treated with γ-GC

gcs-1*(*ok436*) worms were scored for survival after 1 h exposure to increasing concentrations of hydrogen peroxide (H_2O_2). Survival was scored 6 h after H_2O_2 treatment. (A) The LC_{50} for* gcs-1*(*ok436*) worms (2.19 mM) was determined from three independent experiments, with 19-70 worms scored per treatment. Data are presented as mean ±SEM. (B) Pre-treatment with 2 and 5 mM γ-GC for 2 h appeared to increase the mean survival of* gcs-1*(*ok436*) mutant worms (n=1). Between 8-14 worms were scored per treatment.*

4.3.7 Liposomal γ-GC only increases brood size in *gcs-1*(*ok436*) worms

Initial brood size experiments were conducted by adding a range of concentrations of γ-GC (0-10 mM) to the worm's heat-treated *E. coli* feed (Figure 4-10). The *gcs-1*(*ok436*) worms did not show any significant increases in brood size when treated with any of the concentrations tested (Figure 4-10).

Egg-laying rates were measured in the presence of liposomal γ-GC to determine if encapsulation of γ-GC could increase its availability (Figure 4-11). At 6.6 mM liposomal γ-GC concentration, a significant (p<0.05) increase in brood size (15%) was observed, which coincided with a marked increase (27%) in the daily progeny production at day 2 (Figure 4-13C). Interestingly, when comparing the progeny production over the 0.1-1% range of tested liposomal vehicle concentrations there appeared to be a slight dose-dependent increase in brood size with the higher concentrations of liposomes. This may have been due to the cholesterol content of the liposomes, which is a key nutrient in the NGM media used for worm propagation (370).

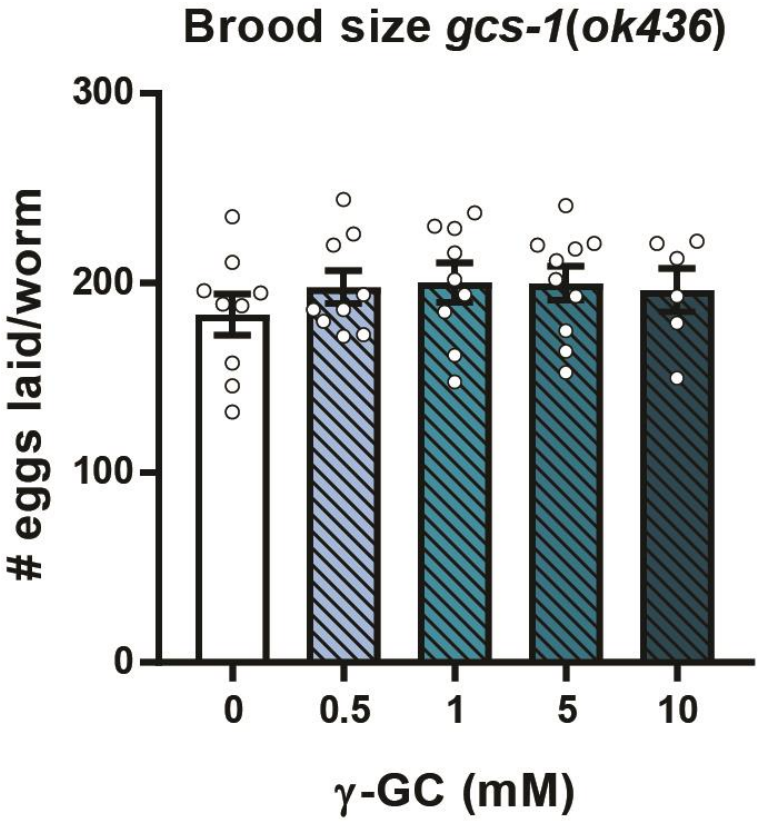

Figure 4-10. Effect on brood size of *gcs-1*(*ok436*) worms fed γ-GC at a range of concentrations in heat-treated *E. coli*

An egg-laying assay compared the brood sizes of C. elegans *fed with equimolar concentrations of γ-GC added to heat-treated* E. coli. *Progeny production was monitored until the self-fertile reproduction cycle ceased. A one-way ANOVA was performed followed by Dunnett's multiple comparison analysis to compare the mean of each thiol concentration with the control. Data presented as mean ±SEM (n=6-10). Treatments were performed in two individual experimental repeats.*

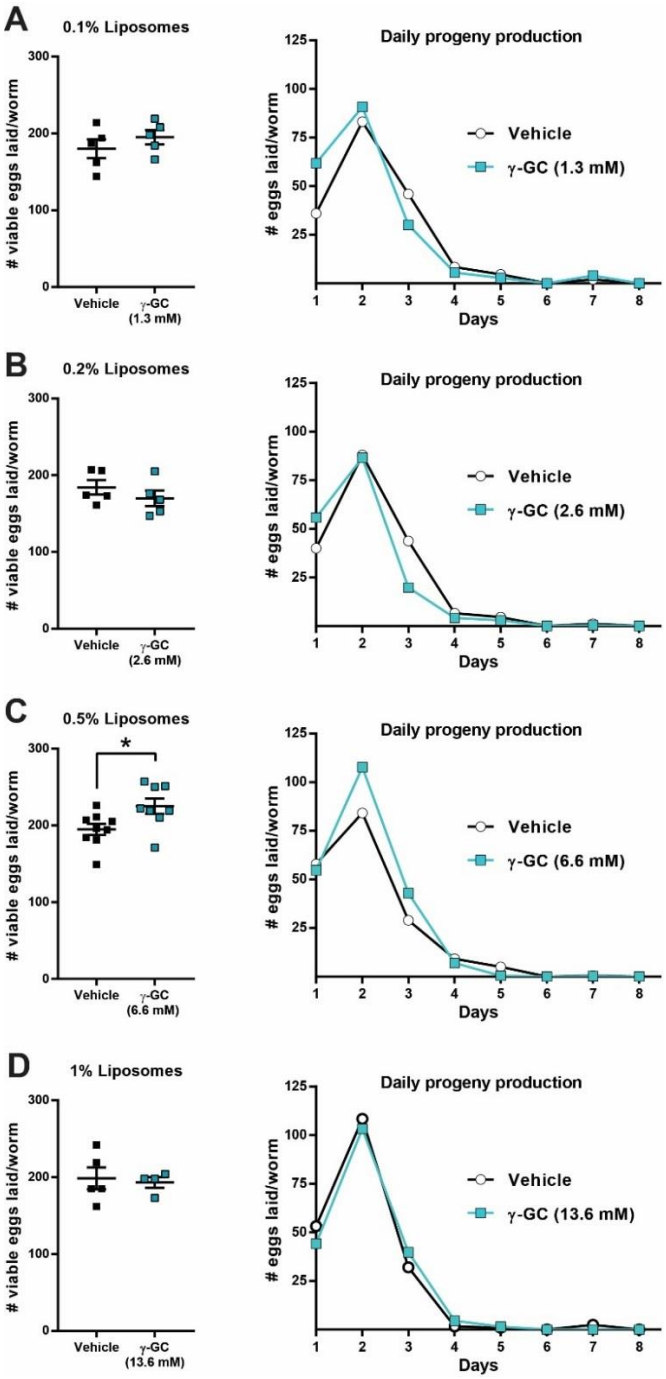

Figure 4-11. Brood sizes of *gcs-1(ok436)* worms treated with liposomal γ-GC

Total brood size (left) and daily progeny production (right) were measured in gcs-1(ok436) *mutants treated with liposomal γ-GC (1.3 mM-13.6 mM). Prior to reaching reproductive maturity, worms were transferred to plates containing liposome concentrations diluted in OP50 (0.1-1%). Analysis of the brood size comparisons were performed using unpaired t-tests (±SEM. *p<0.05). Daily progeny production is presented as the mean only (n=4-8 worms per treatment).*

4.3.8 Liposomal γ-GC had no effect on thrashing in *gcs-1(ok436)* worms but appeared to cause declines in pharyngeal pumping

Thrashing (Figure 4-12) and pharyngeal pumping rates (Figure 4-13) in *gcs-1*(*ok436*) worms maintained an age-dependent decline for each of the liposomal γ-GC concentrations up to day 9 of adulthood. No differences were observed in the thrashing rates of liposomal γ-GC-treated *gcs-1*(*ok436*) worms when compared to respective aged-matched controls (Figure 4-12). One notable observation was the degree of variance in the thrashing rates of worms treated with the higher liposomal concentrations. For the highest liposomal concentration tested (1%), large variances in the oldest treatment group (day 9) made it difficult to conclude if liposomal γ-GC had any effect on the motility in these GSH-compromised worms (Figure 4-12D).

Pharyngeal pumping rates of the worms were typically lower in the older γ-GC-treated worms (Figure 4-13). Statistical analysis indicated that the lowest liposomal γ-GC treatment (1.36 mM) resulted in a decline in the pumping rate at day 9 when compared to the vehicle control ($p<0.01$). The significance of this finding only being observed in the lowest liposome concentrations tested is possibly due to the level of variance of the higher liposomal concentrations in day 9 worms (Figure 4-13).

This thiol-associated effect could be interpreted to indicate that any extension in lifespan in these worms could be due to dietary restriction. It should also be noted that when antioxidants decrease pharyngeal pumping rate, yet increase lifespan, the increase in longevity may be due to mechanisms linked with dietary restriction rather than the antioxidant *per se*.

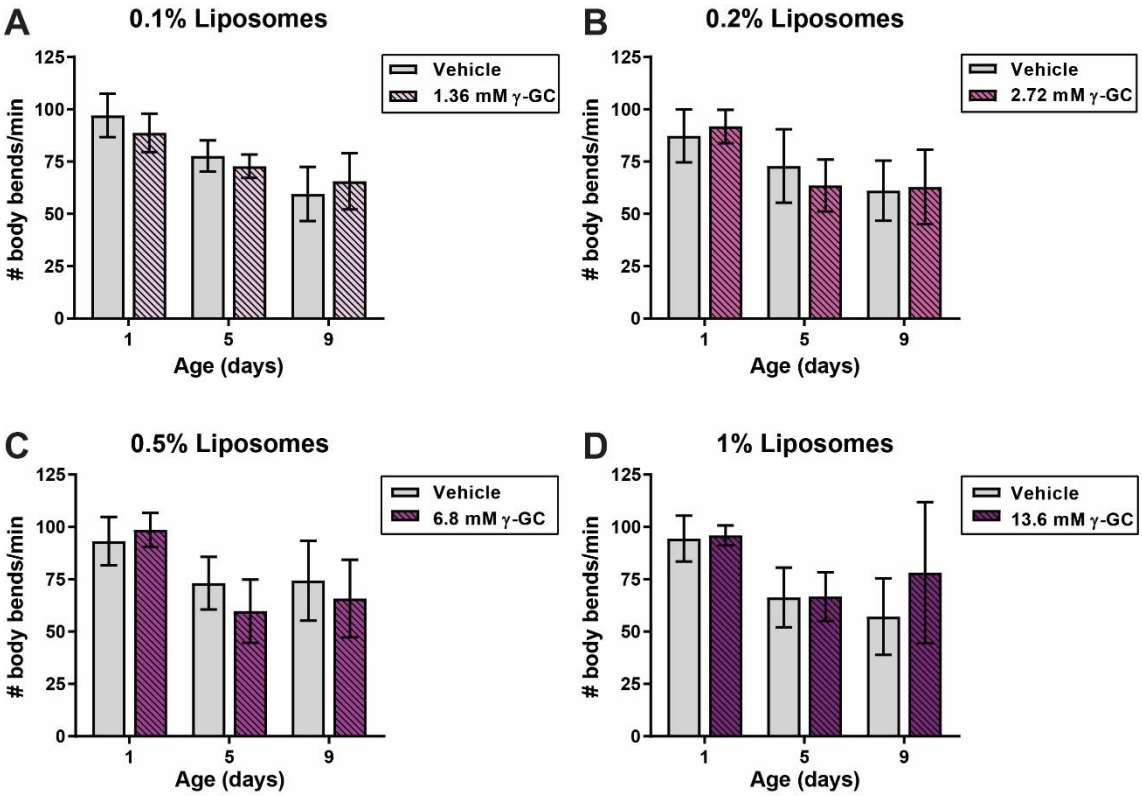

Figure 4-12. Thrashing in aged *gcs-1*(*ok436*) worms treated with liposomal γ-GC

Aged worms were transferred daily to fresh NGM plates seeded with E. coli *OP50 diluted with liposome suspensions (%) containing either PBS (vehicle) or γ-GC. A two-way ANOVA was used with a Bonferroni multiple comparison test to compare treatments between days. Data represents the mean 95% CI of two independent experimental repeats. Thrashing rates of n=6 worms per data point are presented. No significant difference was observed between groups.*

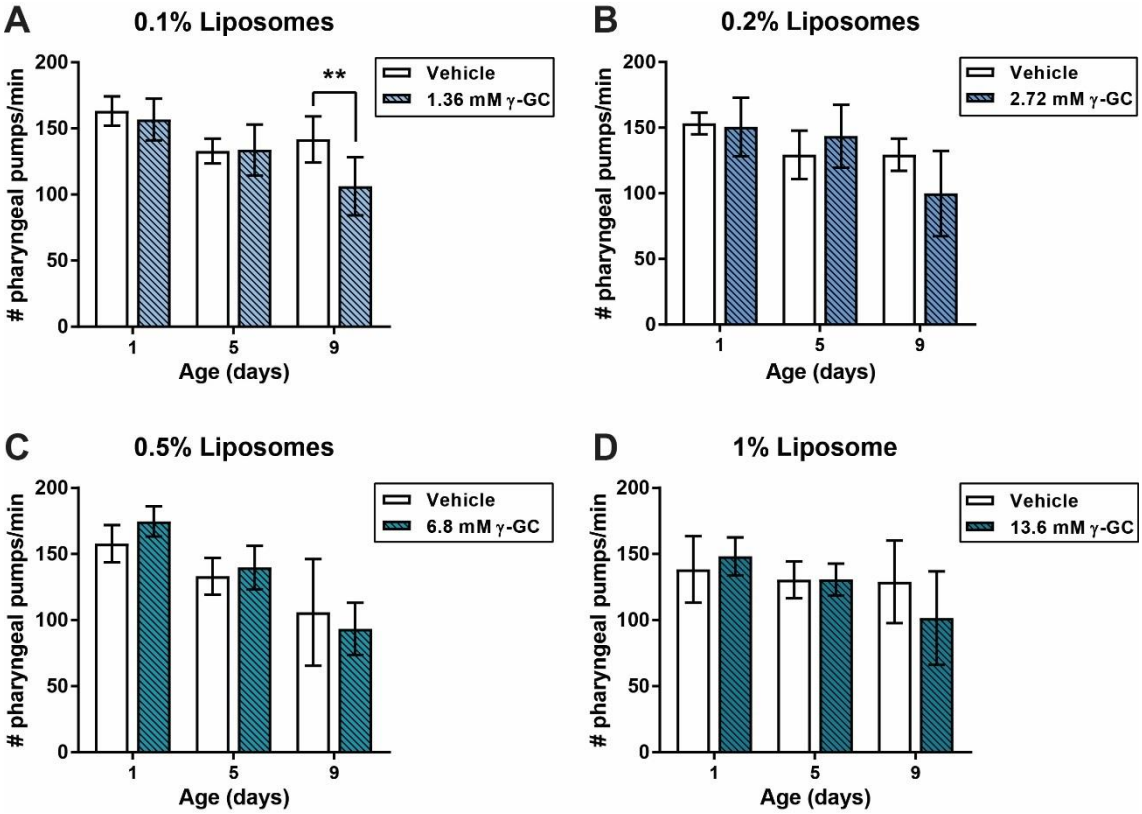

Figure 4-13. Pharyngeal pumping in aged *gcs-1*(*ok436*) worms treated with liposomal γ-GC

Aged worms were transferred daily to fresh NGM plates seeded with E. coli *OP50 diluted with liposome suspensions (%) containing either PBS (vehicle) or γ-GC. A two-way ANOVA was performed for each data set with a Bonferroni multiple comparison test to compare treatments between days. Data represents the mean 95% CI of three independent experimental repeats. Pumping rates of n=9 worms per data point are presented, **p<0.01.*

4.3.9 Liposomal γ-GC does not increase lifespan in *gcs-1*(*ok436*) worms

The unexpected decline in pharyngeal pumping of γ-GC-treated *gcs-1*(*ok436*) worms was further investigated by assessing the effect of 1.36 mM liposomal γ-GC on longevity (Figure 4-14). No difference was observed in the lifespan of the *gcs-1*(*ok436*) worms, which ruled out any possible effect that the decline in pharyngeal pumping may have led to differences in longevity.

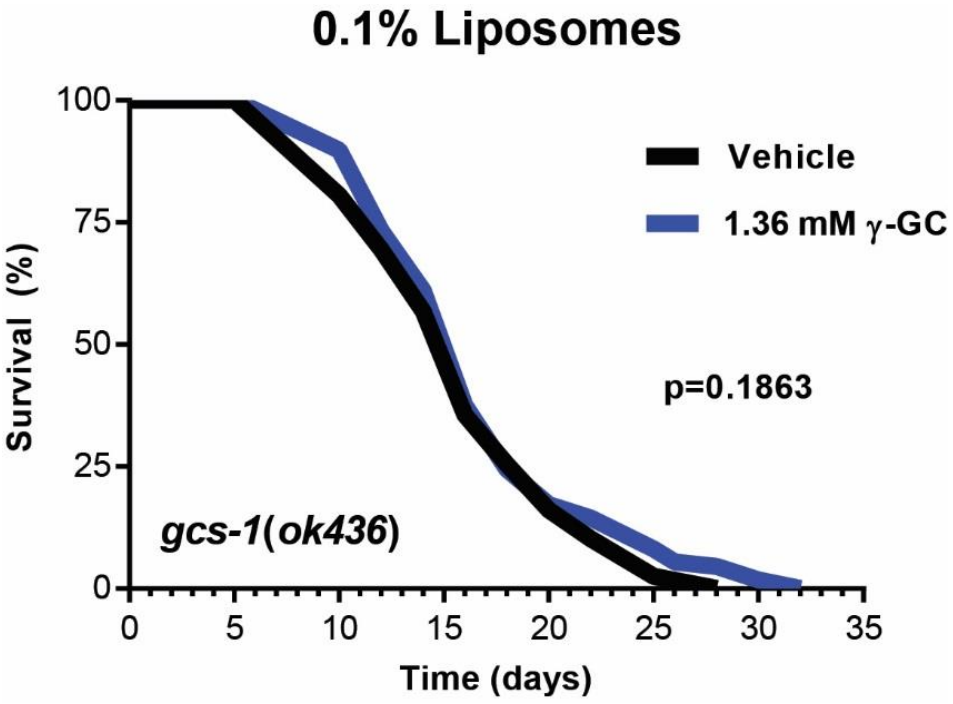

Figure 4-14. Survival of liposomal γ-GC treated gcs-1(ok436) worms

gcs-1(ok436) worms treated with 1.36 mM γ-GC (n=114) and vehicle only control, liposomes (n=118). Survival was scored at day 5, 10 and every second day thereafter until death. A log-rank tests was used to compare treatment groups. No significant difference in lifespan was observed.

4.4 Discussion

4.4.1 Testing substrate-based therapies to increase GSH *in vivo* using *C. elegans*

A recently established curated database (DrugAge) detailing lifespan-extending compounds in 27 different model organisms, including *C. elegans*, yeast, flies, and mice has reported that the most relevant categories relate to glutathione (GSH) and antioxidant activity (371). Accordingly, in this work the focus was to explore the therapeutic potential of the immediate GSH precursor, γ-glutamylcysteine (γ-GC), to increase cellular GSH levels and potentially lifespan in the worm.

Strategies for increasing GSH levels have focused mainly on cysteine delivery. *N*-acetylcysteine (NAC) is the used as a low-toxicity source of cysteine, as cysteine is prone to autooxidation in the presence of the transition metals, copper and iron (372). The acetyl group increases the resistance of cysteine to autooxidation (373). NAC has been suggested to only be an effective antioxidant if supplying cysteine for GSH synthesis, rather than as an antioxidant in its own right (374). Before being fed into the *de novo* GSH synthesis pathway, deacetylation of NAC must occur. However, the specific mechanism for entry of NAC and subsequent cellular deacetylation in various mammalian cells is not completely understood (374). Reported benefits of NAC administration in *C. elegans* using various treatment methods often assume increases in GSH levels without actually measuring any changes (Table 4-1).

Table 4-1. Summary of NAC and GSH treatments in *C. elegans* studies

Thiol	Administration method (concentration)	GSH increase?	Differences attributed to thiol treatment	Ref.
NAC	NGM (2.5 mM)	Not assessed	Increased lifespan in *gas-1*(*fc21*) mutants.	(375)
	NGM (5 or 10 mM)	Not assessed	Increased lifespan in worms subjected to visible light.	(376)
	NGM (100 or 500 μM)	Not assessed	Attenuated mtDNA copy number declines and ATP decreases caused by oxidative stressors at 100 μM but not 500 μM NAC.	(377)
	NGM (10 mM)	Not assessed	Attenuates food avoidance behaviour in *prmt-1* mutants.	(378)
	NGM (0 -100 mM)	Not assessed	Increase lifespan (5 mM) and brood size (5 mM) in WT. Increase fluorescence in *hsp-16.2* and *sod-3* following 5 mM NAC treatment. Protection from ultraviolet (UV) radiation (5 mM).	(298)
	Not detailed (5 mM)	Not assessed	Attenuation of TiO_2-NPs-induced ROS and motility.	(379)
	Liquid (61.3 & 123 μM)	Not assessed	Protection from silver nanoparticle toxicity.	(380)
	NGM (10 mM)	Not assessed	No difference in lifespan.	(381)
	NGM (5 mM)	Not assessed	Increased survival for *sdhb-1* mutant worms under hyperoxia, but no difference for WT.	(382)
	NGM (5 mM)	Not assessed	Decreased ROS formation, but no difference in lifespan in WT.	(299)
GSH	NGM (3 mM) GSH pre-treatment	Not assessed	WT worms pre-treated with GSH, partially restored brood size from selenite (Na_2SeO_3) exposure; GSH pre-treatment in *glrx-21* mutants had no effect.	(212)
	NGM (3 mM) GSH	Not assessed	Partially restored motility in selenite-exposed (Na_2SeO_3) WT worms. GSH required *daf-18* and *pink-1* to restore selenium-induced movement deficits.	(383)
	Not specified (3 & 10 mM)	Not assessed	Administered GSH promoted the reduction of disulfide groups in the cuticle.	(224)
	Liquid & NGM (0-10 mM)	Not assessed	Partial protection from selenite-exposed (Na_2SeO_3) lethality and motility in WT.	(211)
	NGM (5 mM)	↔	No change in GSH levels or lifespan; Decreased $A\beta_{42}$-induced paralysis/protein carbonyl content; Increase in pumping/motility in $A\beta_{42}$ oligomer fed worms.	(384)
	Liposome (90, 180, 360 μg)	Not assessed	Increased lifespan.	(363)
	Liquid K medium (50 μM)	Not assessed	GSH pre-treatment increased survival of arsenite stress in *gcs-1*(*ok436*) VC337 strain.	(137)

$A\beta_{42}$, Amyloid beta-42; ATP, adenosine triphosphate; *gas-1*(*fc21*), mitochondrial complex I mutant; *gcs-1*, glutamylcysteine synthetase-1; *glrx-21*, glutaredoxins-21; *hsp-16.2*, heat shock protein-16.2; mtDNA, mitochondrial DNA; Na_2SeO_3, sodium selenite; *prmt-1*, protein arginine methyltransferase; *pink-1*, PTEN-induced kinase-1; *sdhb-1*, succinate dehydrogenase complex subunit B; *sod-3*, superoxide dismutase-3; TiO_2-NPs, Titanium oxide nanoparticles; WT, Wild-types.

Oral bioavailability must be demonstrated for γ-GC if it is to be an effective and practical approach to treat chronic depletion of GSH in humans. This has remained problematic for substrate-based treatments aimed at increasing GSH that suffer from poor oral bioavailability, such as GSH itself (385). Increases in cellular GSH, have been demonstrated in rodent models using intraperitoneal (97), intravenous (98) or intracereboventricular (102) delivery of γ-GC. These direct injection approaches avoid any oral administration issues due to first-pass metabolism. In a human pilot study (n=14), oral administration of 2 g γ-GC resulted in an average 53% ±47% increase in lymphocytic cellular GSH levels, indicating that γ-GC is orally bioavailable (112). Others have suggested that this increase of GSH post-supplementation of γ-GC in humans was likely due to the extracellular degradation of γ-GC by the γ-glutamyl transpeptidase (γ-GT) enzyme thus providing a source of cysteine, rather than membrane transport intact γ-GC (386). While this is a valid alternative hypothesis, degradation of γ-GC by the enzymatic action of γ-GT may not provide a comprehensive mechanistic explanation of how exogenous γ-GC leads to increases in GSH. The presence of putative dipeptide transporters for certain γ-glutamyl amino acids provides the basis for the possible direct uptake of γ-GC (387). Passive transport of intact GSH from the plasma into the cell is not thermodynamically favourable as plasma levels range between 2 and 20 μM and cellular levels are between 1 and 10 mM in humans (388). Conversely, intracellular γ-GC concentrations are exceedingly low in the presence of glutathione synthetase (GS) which make it favourable for passive cellular transport. While the therapeutic potential of γ-GC remains relatively unexplored, rapid models such as *C. elegans,* that can provide evidence of how γ-GC leads to increases in cellular GSH are necessary to understand its broad therapeutic application for human disease.

4.4.2 Demonstrating compound bioavailability in worms

Evaluation of bioavailability (systemic uptake) and bioactivity (activity following absorption) of exogenous compounds are important considerations when testing antioxidant compounds (389). The inconsistency between the effects of antioxidants in *C. elegans* lifespan studies has recently been reviewed by the Halliwell group (287). They focused on experimental design to avoid common methodology pitfalls (287). For example, artefacts such as delaying development and fecundity or causing dietary restriction leading to lifespan extension, independent of the mechanism of antioxidant action (287), was considered in the design of our experimentation investigating the therapeutic potential of γ-GC.

The three distinct routes for compound delivery to *C. elegans* include, ingestion, uptake through the hypodermis, or uptake via exposed sensory neuronal endings (390). Absorption of compounds through the hypodermis can be obstructed due to the complex outer cuticle of the worm. The relatively simple alimentary system in *C. elegans* make the worm a suitable model for the rapid assessment of bioavailability of compounds via oral administration (391). In this chapter, several experiments were conducted to investigate the hypothesis that oral administration is the most effective delivery route for the immediate GSH precursor, γ-GC with the uptake through the hypodermis, or via exposed sensory neuronal endings being negligible.

Common methods of investigating the effect of compound treatment on the lifespan of *C. elegans* include the addition of the compound in the solid nematode growth medium (NGM). This strategy, however, may lead to poor oral bioavailability (392). Moreover, addition of compounds in the NGM without attenuation of the bacteria may lead to the compound becoming metabolised by the *E. coli* itself before it can be absorbed

by the worm. Methods such as these, often assume the mechanism of action is occurring without measuring the bioavailability.

Liposomes are effective drug delivery systems that have been shown to markedly increase the oral administration of hydrophilic (363) and hydrophobic (393) compounds in *C. elegans*. The potential benefits of liposome-encapsulation of therapeutic compounds added to the *E. coli* feed include increased compound stability, simulating a diet-ingested delivery mode, and potentially avoiding compound metabolism by the *E. coli*. Indirect effects that occur by the *E. coli* providing an intermediary metabolic pathway are problematic for investigating the potential efficacy of compounds that may extend lifespan.

The likelihood that the thiol compounds are strictly taken up by the worm via pharyngeal ingestion and not through the hypodermis, can serve as the basis to investigate the possible similarities of systemic bioavailability of orally-administered γ-GC between humans and *C. elegans*. There was no indication that the γ-GC is effectively absorbed through the cuticle of wild-type worms within 2 h, based on treatments in M9 buffer (Figure 4-4A). This may be due to either the exposure time (2 h) in liquid medium being insufficient for uptake or that γ-GC is not able to permeate the worm's cuticle. While the use of liposome delivery systems for encapsulation of pharmacological agents has been of interest to increase bioavailability, factors that limit their use for therapeutic applications include, poor stability, batch-to-batch irreproducibility, low entrapment coefficients, difficulties in controlling liposome size, toxicity, and short circulation half-life of vesicles (394, 395).

4.4.3 Future developments for the use of liposomes in *C. elegans*

To further develop liposomes as a delivery method for compound treatment in the *C. elegans* model, several considerations still need to be addressed to ensure reproducibility. Liposome stability will depend on the composition of liposome mixtures and the need to maintain consistent storage conditions, notably atmosphere and temperature. Lipids from biological sources (e.g., egg yolk) contain significant levels of polyunsaturated fatty acids and are inherently more prone to oxidation compared to their synthetic counterparts (396).

The commercial liposome kit (Sigma Aldrich, L4395) resulted in considerable structural variability in the generated liposomes, including vesicle size and particle concentration, which has been an ongoing concern regarding the use of liposomes as drug delivery systems (394). Nanoparticle tracking analysis was used to quantitatively measure liposome size which offered an improved method to determine the differences in size distribution of liposome suspensions. The use of flow cytometry to sort particles by size provides the potential to prepare homogenous liposome suspensions.

It has been noted that ingestion of liposomes may affect lipid metabolism in *C. elegans* (27). The initial liposome study reported that worms treated with liposome-encapsulated MilliQ showed no significant difference in lifespan when compared to worms fed *E. coli* OP50 alone (363). In this current work, no significant differences in lifespan was observed when liposome content added to the *E. coli* was <1%.

4.4.4 Screening for optimal dosing of γ-GC concentrations to increase lifespan

C. elegans is an effective *in vivo* model for investigating the potential of compounds to extend lifespan (397). However, drug delivery methods vary greatly which makes it

difficult to compare results between studies (392). There has been debate in regard to the differences in environmental conditions that can affect metabolism and longevity, in particular maintaining worms in liquid or on solid medium (398-401). In this work, initial lifespan screening efforts using liquid methods (402) encountered turbidity problems with the bacterial feed obscuring the ability to view worm viability. Another limitation of using liquid protocols over extended periods, is the potential for thiol compounds to readily oxidise in aqueous solutions (403).

To alleviate the limitations of screening compounds in liquid medium, a simple screening method was employed to allow lifespan analysis to be conducted on solid NGM with liposome-encapsulated γ-GC (363). It has previously been advised to minimise the FUdR concentration in antioxidant screening methods to avoid the introduction of artefacts that affect longevity (287). The inclusion of 100 μM FUdR in the NGM was determined to be the lowest concentration that inhibited larval development in this work. As liposomes have also been demonstrated to increase the chemical stability of compounds (404), the screening method was designed so that worms were scored and transferred to new plates containing freshly seeded liposomes at days 5, 10 and 15 with scoring continued every subsequent second day.

Screening methods that involve a large number of test compounds may encounter workload limitations when exploring dose dependency (405). This approach may not detect the true therapeutic potential of certain compounds if the incorrect concentration is selected. Recent data suggests that several antioxidant compounds including, NAC, resveratrol and vitamin C, display an inverted "U-shaped' dose-dependent effect on lifespan (406), that is postulated to be due to a concentration dependent pro-oxidant/antioxidant balance. Time-to-treatment must also be considered in the dosing

regimen. This is illustrated by a study showing that treatment with epigallocatechin-3-gallate (EGCG) in early-to-mid adult worms had an increase in lifespan which was absent when the worms were treated after 12 days of adulthood (407). This may be indicative of the compound being orally bioavailable only in young worms as pharyngeal pumping tends to decline considerably after 12 days.

4.4.5 What is the bioavailability profile of exogenous γ-GC in wild-type worms?

The previous experimental work in this thesis demonstrated that the endogenous changes in GSH levels can be quantified with LC-MS/MS. However, it remains to be determined if treatment with exogenous γ-GC results in changes of the cellular GSH levels of wild-types. To test this hypothesis, γ-GC treatments in liquid medium and with liposomes were used to test if acute (2 h) or prolonged (3 days) exposure had any effect on increasing cellular GSH. No significant difference was observed in any of the concentrations tested in liquid medium over the 2 h treatment, suggesting that absorption does not occur through the hypodermis over this time course. Prolonged treatment of 1.7 mM liposomal γ-GC was carried out over the entire worm's larval lifecycle (3 days) to determine if an extended period of treatment would lead to increased GSH levels. At the single concentration tested there was no evidence that liposomal γ-GC increased the concentrations of GSH or any of the thiols measured (Figure 4-8). This may be due to liposome degradation when exposed to atmospheric conditions over the 3-day period.

The transparent body of the nematode has recently been exploited in the development of redox biosensors that allow for *in vivo* visualisation of glutathione redox status (408). The use of the genetically encoded Grx1-roGFP2 fluorescent biosensor enables real-time, *in vivo* measurement of the GSH/GSSG ratio of *C. elegans* (300). Applications of these worms with fluorescent plated-based screens could provide a rapid method to test a range

of γ-GC concentrations by measuring the fluorescent ratios corresponding to the reduced to oxidised state of the glutathione redox couple (GSH:GSSG). Kinetic screens in liquid medium could be an interesting approach to provide critical information about optimal time and concentration-dependent dosing variables to inform later analytical experiments.

4.4.6 Treating GSH-compromised worms with liposomal γ-GC

The *gcs-1*(*ok436*) mutant (VC337 strain) was employed as a model for compromised GSH synthesis, which has been used previously in several studies (42, 137, 224, 409). In this work, *gcs-1*(*ok436*) worms were used to model GSH deficiency caused by glutamate cysteine ligase dysfunction and test the hypothesis that γ-GC could bypass the rate-limiting step and provide a more effective substrate-based treatment than NAC and GSH. Several treatment methods of absorption were tested, including thiols added to heat-treated *E. coli*, and γ-GC treatment using liquid medium and liposomes.

Pre-treatment with γ-GC for 2 h in liquid medium prior to the 1 h exposure to an LC_{50} dose of H_2O_2 increased the worm's survival rates after 6 h recovery. Testing the protective effect of γ-GC from a bolus H_2O_2 insult using a pre-treatment approach may offer valuable information regarding the possibility that γ-GC bypasses the dysfunctional GCS-1 enzyme. Pre-treatment with 2 mM γ-GC showed an apparent 20% increase in the survival rates compared to the vehicle only control group, though is yet to be considered significant without independent repeat measurements (Figure 4-9B). This preliminary finding is in agreement with a previous study that demonstrated that a 3 h pre-treatment with 50 μM GSH in liquid medium affords protection against subsequent exposure to arsenite in *gcs-1*(*ok436*) worms (137). Treatment with equimolar concentrations of NAC or GSH should simply provide a source of cysteine based on their cellular uptake. A pre-

treatment model comparing equimolar concentrations of NAC and GSH using *gcs-1*(*ok436*) worms should be suitable for exploring the hypothesis that γ-GC could perhaps transiently increase the GSH concentrations above homeostasis.

Fertility of nematodes was monitored for both the wild-type and *gcs-1*(*ok436*) mutants. Delays in reproduction may affect the lifespan of the animal according to the disposable soma theory (410). This theory stipulates that an organism must carefully allocate resources between reproduction and somatic maintenance, depending on the animal's environment (411). Accordingly, brood sizes were monitored in *gcs-1*(*ok436*) worms treated with concentrations of non-liposomal γ-GC (0-10 mM) added to heat-treated *E. coli* (Figure 4-10). No differences were observed in any of the treatment groups compared to the control. Treatment of *gcs-1*(*ok436*) worms with 6.6 mM liposomal γ-GC increased the brood size and the daily egg-laying rate (Figure 4-11C). No differences in brood size were observed in the lower (1.3 mM and 2.6 mM) or higher (13.6 mM) tested doses.

While liposomal γ-GC treatment increased brood size, it did not affect motility or lifespan in *gcs-1*(*ok436*) worms. Pharyngeal pumping was monitored as a precaution in case any mechanisms were induced by the treatments that could potentially lead to dietary restriction-dependent increases in lifespan. Dietary restriction has been shown to extend lifespan in many model organisms including, yeast, *C. elegans* and mammals (412). Measuring the pharyngeal pumping rate is one index used to monitor nutrient intake in *C. elegans* (413). Mutations in *eat* genes lead to a decrease in caloric uptake caused by a decline in pharyngeal muscle contraction rate (414). The majority of *eat* mutants exhibit an increased longevity phenotype due to the restriction that the pharyngeal pumping rates places on caloric intake (415). In this study, there was evidence of γ-GC contributing to

the decline in the pharyngeal pumping rates of aged *gcs-1*(*ok436*) worms but was only observed in the day 9 old adults which may have been too late to significantly affect caloric intake.

Motility was monitored by measuring the thrashing rate as another potential predictor of longevity to investigate if liposomal γ-GC showed any benefit in *gcs-1*(*ok436*) worms. Thrashing behaviours varied considerably between treatment groups in day 9 adult *gcs-1*(*ok436*) worms, which appeared to correlate with the amount of liposome concentrations added to the *E. coli* (Figure 4-12). This may be explained by the variations in the heterogeneity of vesicle sizes in the liposome suspensions (Figure 4-5). The results presented herein indicate that while the higher liposomal concentrations (>0.1%) used in this work did not significantly affect lifespan, they may however affect other behaviours of the worm. It was concluded that liposomal γ-GC does not increase the thrashing behaviour of *gcs-1*(*ok436*) mutant worms up to 9-day old adults. Because the spread between the physiological responses of worms likely increases due to ageing, larger numbers would be required to have sufficient power to conclude any true effects on the role of γ-GC on motility. Since increases in brood size and stress resistance were observed in *gcs-1*(*ok436*) worms treated with γ-GC, future work should look at measuring thiol levels in isogenic populations of the heterozygotes *gcs-1(ok436)* (+/-) worms.

4.5 Conclusions and chapter Summary

In this chapter, the overall aim was to use *C. elegans* to explore the therapeutic potential of γ-GC. Several reports have previously shown that both NAC and GSH supplementation are beneficial against markers of oxidative stress in worms (Table 4-1). However, no reports directly demonstrate that these substrate-based treatments increase GSH levels in worms. The focus was to apply a delivery method that would make exogenous γ-GC orally bioavailable. Options for delivery included, attenuation of growth of *E. coli* by heat-treatment, liposome encapsulation and treatment in liquid medium. The proposition that γ-GC would be a more effective substrate-based therapy for age-related treatments is based on the hypothesis that γ-GC can be taken up intact and effectively bypass any GCL rate-limitation in *de novo* synthesis, which cannot be achieved using cysteine prodrugs or intact GSH itself. It remains unclear what the optimal treatment time and concentration for γ-GC in wild-type worms is to determine therapeutically efficacious dose levels. Rigorous kinetic analysis may provide evidence to answer this outstanding question. Once the bioavailability profile of γ-GC is fully understood using *C. elegans*, further utilisation of the model can be applied to measure several antioxidant biomarkers that provide evidence of γ-GC's protective value (287, 416).

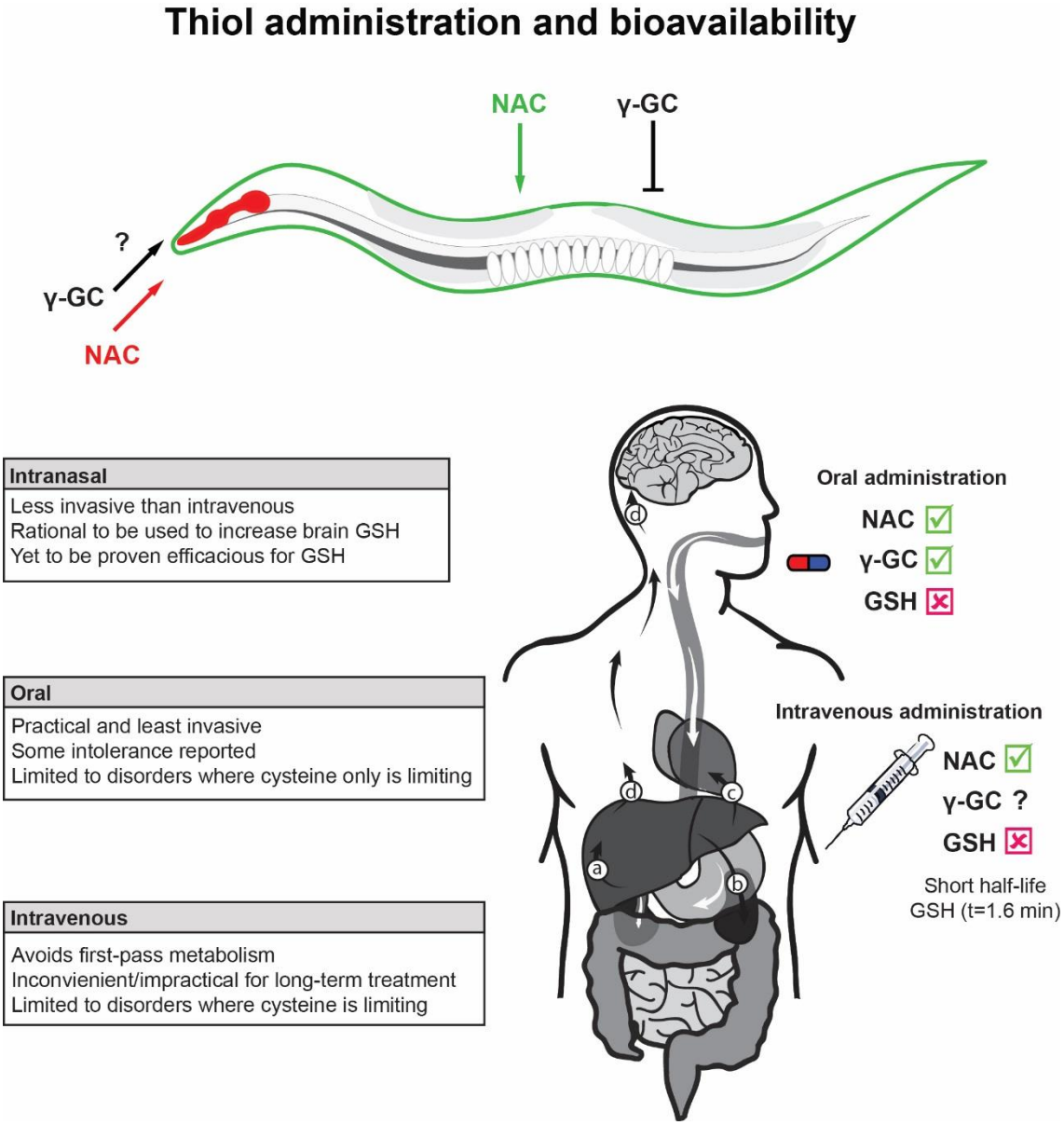

Figure 4-15. Proposed model comparing the mode of bioavailability in *C. elegans* and humans

In C. elegans, it is proposed that NAC may be taken up in the worm via the hypodermis whereas γ-GC has not been shown to increase GSH levels after 2 h treatment. In humans, oral administration of γ-GC may perhaps offer an advantage over other substrate-based approaches, such as NAC and GSH. After γ-GC is absorbed by the small intestine (white arrows) it is proposed to be effectively taken up by the (a) liver where it is converted to GSH above homeostatic levels and transported to other organs, such as (b) kidneys (c), the heart and (d) brain. Alternatively, it may be absorbed into the bloodstream directly to be made available for systemic distribution.

CHAPTER FIVE

General conclusions and future directions

5 Chapter Five

5.1 General conclusions and future directions

Ageing leads to the elderly becoming more vulnerable to numerous oxidative stress-related diseases. The free radical theory of ageing was postulated over 60 years ago in an attempt to explain how the partial reduction of oxygen can lead to damaging effects that accumulate and contribute to tissue degeneration during ageing. Since then, efforts to mitigate ageing in humans and other eukaryote models using antioxidant therapies have generally been inconclusive and have occasionally even been shown to decrease lifespan (For review see (21)). The observations in evolutionary divergent organisms that show pro-oxidant treatments can lead to the hormesis effect and an increase in lifespan is evidence of the how interactions between pro-oxidant and antioxidant networks can affect the ageing process (417). Understanding how oxidative stress is intrinsically linked with redox balance and how this affects cellular signalling in ageing can potentially provide an explanation for the inconsistencies between the free radical theory and the hormesis hypothesis. When investigating the effect of ROS and free radicals in ageing, it is imperative to define the molecular mechanisms that affect the changes in the redox balance rather than simply assuming a dichotomous nature exists between the beneficial role of antioxidants and the damaging effects of ROS (418).

GSH's highly reactive sulfhydryl group allows it to act as a direct scavenger (419) or as a cofactor in enzymatic reactions to neutralise ROS and free radicals (76). Given the extensive number of cysteine residues present in the mammalian proteome (~214,000), understanding the role of GSH in maintaining the structure/function relationship of proteins as a post-translational modifier (i.e. by protein *S*-glutathionylation) is an interesting prospect for future investigations. Considering the level of conservation

between worms and mammals, work to further understand which cysteine residues are prone to potential modification with human ageing may benefit from the application of the *C. elegans* model.

Over the past two decades, a paradigm shift has started to emerge that views the role of ROS and free radicals as signalling molecules. The free radical theory of ageing has been instrumental in gaining momentum to understand the biology of ageing and has remained relevant within the field. Since its inception, many studies have offered alternative theories which collectively reiterate the complexity of the ageing process. Elucidating the primary cause of how this balance is initially disrupted with ageing is a difficult problem to solve. To this end, a unifying theory for ageing is perhaps impossible to elucidate at the biological level.

5.1.1 Project scope, key findings and contributions to further understand redox biology, ageing and *C. elegans* physiology

During this research, a novel LC-MS/MS method was developed that enabled the metabolomic profiling of the glutathione cycle in ageing worms. Quantifiable analytes include the thiol precursors, cysteine and γ-GC, which allowed an investigation to determine if cysteine becomes limiting or if the rate of enzymatic production of γ-GC declines during ageing. Results that show a decline in the levels of cysteine with a concomitant decline in both γ-GC and GSH would suggest that cysteine limitation is a major cause of GSH decline. However, the levels of cysteine did not significantly decline over the first 10 days of adulthood. Corresponding declines of γ-GC and GSH, without any changes in GSSG levels, suggested lowered GCL activity significantly contributes to the changes in glutathione homeostasis. This metabolomic approach provided evidence to support the hypothesis that the majority of the net loss of GSH levels in ageing worms

is likely due to a decline in the *de novo* synthesis pathway. Several studies have shown a beneficial health effect in wild-type worms treated with NAC (Table 4.1). However, no study to date has confirmed that the benefits afforded by NAC are due to increased GSH levels. In this study, we demonstrated that cysteine levels are limiting from as early as day 1 of adulthood. The bioavailability profile of the dose-dependent increase was observed for each thiol after 2 h NAC treatment in liquid M9 medium only (Chapter 2, Figure 2-9). Though this work was informative about cysteine availability in worms, the data from the aged worms indicated that the rate of decline in γ-GC production was perhaps due to, at least in part, the decline in enzymatic activity of the GCL enzyme homologue in worms.

Our interest in investigating the enzyme activity of the rate-limiting GCL enzyme step was to first confer the functional role of the uncharacterised GCLM subunit in the worm. Using reverse genetics (RNA*i*), we showed that knocking down the *gclm* gene in worms corresponded with a decline in GSH and an increase in cysteine levels. We also report the first phenotypic assessment of several behavioural and physiological changes associated with the function of the *gclm* gene in aged worms. These included the observation of increased incidence of vulval rupture phenotypes and effects on reproduction, stress resistance, pharyngeal pumping, thrashing movement and lifespan.

In mammals, the complex nature of GCL regulation occurs at the transcriptional, post-transcriptional and post-translational levels. Each of GCL's two heterodimeric subunits are encoded at two separate loci under independent transcriptional and post-transcriptional regulation. Considering the complexity of the regulatory control of the GCL enzyme, there no reports as yet of investigations into the post-translational controls affecting the rate-limiting step of GSH synthesis in any aged models. A recent study that

conducted deep proteome sequencing in aged worms at 1, 5 and 10 day old adults, showed that the abundance of each of the proteins involved in the cellular metabolism of GSH (including GCS-1, GCLM, GSS-1 and GSR-1) did not change significantly (420). The observed declines in GCL holoenzyme activity during this period may be a result of post-translational perturbations in the interactions of GCS-1 and GCLM. In support of this hypothesis, others have shown that long-lived *daf-2*(*e1370*) worms which have approximately 14-fold higher GSH levels than wild-types have no differences in the transcript levels of the genes involved in GSH metabolism (148). The authors concluded that the *de novo* synthesis pathway appears to be essential for the extreme long-lived *daf-2*(*e1370*) mutants and suggested that this is due to the regulation of GCS-1 and GCLM subunits at the post-transcriptional level (148). These reports taken together suggest that the decline in GSH synthesis in aged wild-type worms observed in this work may be explained by complex regulatory dysfunction occurring at the post-translational level.

The age-related changes in GCL holoenzyme formation should be further investigated using *C. elegans*. It should be noted that if measuring these levels in whole worm lysates, resolution of tissue-specific levels will not be possible. Moreover, the relative abundance of each subunit is rarely present in the cell at a 1:1 ratio, with the GCLM subunit for the holoenzyme formation almost always limiting in higher eukaryotes. The addition of a reducing agent in order to dissociate the two subunits would be required to assay the levels of holoenzyme and the respective levels of each subunit. However, no antibodies are commercially-available for either of the *C. elegans* subunits and it is unknown if any mouse GCLC or GCLM antibodies would present any cross-reactivity for the worm homologs.

Another technical challenge would be an investigation of age-related changes in GCL activity in aged-matched cohorts. Large sample numbers would be required to provide sufficient GCL quantities and would unavoidably involve the addition of FUdR. Enzyme activity studies performed using recombinant proteins rather than worm homogenates, would not be able to simulate the age-related dysregulation of the enzyme. Moreover, methods that use fluorescent probes to measure the enzyme activity of GCL are unable to distinguish derivatisation of the fluorescent probe with either γ-GC or GSH (421), and thus measurements are made based on the production of GSH which is also dependent on the glutathione synthetase activity. To address this in the current study, the measurement of γ-GC was used as a proxy for the GCL enzyme function.

Finally, the work described in Chapter 4 looked to apply *C. elegans* as an ageing model to explore γ-GC's therapeutic potential against chronic GSH depletion. Protection afforded by GSH levels against the age-induced perturbations of the thiol signalling pathways can potentially be sustained by treating with γ-GC. Future work using the nematode to investigate the therapeutic potential of γ-GC should look at determining the protective profile against markers of oxidative stress including, lipid peroxidation, DNA oxidation, and oxidative modifications of proteins.

5.1.2 The future for γ-GC: Safety, efficacy and therapeutic applications

Though the decline in GSH levels are associated with many age-related diseases linked to oxidative stress, causation is yet to be determined for the majority of conditions. Disease states associated with low GSH levels may benefit from treatment with γ-GC. Oral supplementation with γ-GC offers a unique substrate-based approach to elevate GSH levels above dysfunctional GCL related lowered homeostasis. Administration of esterified forms of substrates may also be effective to increase GSH levels, however the

de-esterification reaction once inside the cells may prove to be harmful with prolonged usage, particularly for low-molecular weight thiol compounds that can pass the blood-brain barrier.

One potential fate of excess γ-GC could be an increase in 5-oxoproline possibly causing 5-oxoprolinuria (266). The build-up of 5-oxoproline is a characteristic of a rare autosomal recessive disorder of glutathione synthetase (GS) deficiency (GSSD) (422). With as few as 70 cases reported world-wide, patients with GSSD suffer from low levels (~20%) of GSH compared to healthy controls (108) and typically present in the neonatal period with haemolytic anaemia, metabolic acidosis and neurological impairment (423). GSSD leads to excess γ-GC being subsequently hydrolysed to 5-oxoproline and cysteine by γ-glutamyl cyclotransferase (423). The accumulation of 5-oxoproline is reported to be the major cause of the metabolic acidosis (108). Safety assessments of γ-GC in Wistar rats have shown no differences in single acute (2000 mg/kg body weight) or daily repeated doses (1000 mg/kg body weight) in the haematological and clinical chemistry profiles, including urine analysis, between treatment and control groups (364). This suggests that metabolic acidosis does not occur as a result of γ-GC treatments in rats, which is perhaps due to the γ-GC being rapidly converted to GSH by GS and thus preventing the synthesis of 5-oxoproline. Understanding how treatment with γ-GC leads to increases in GSH is a mechanism that remains poorly defined. Demonstrating if γ-GC is transported directly into the cell, could likely become synonymous with the discovery and identification of the putative dipeptide membrane transporters.

5.1.3 Future work to understand thiol biology with *C. elegans*

It has recently been suggested that *C. elegans* could potentially be the subject of the first complete animal model of redox signal transduction (424). The understanding of the

influence of GSH and other low-molecular weight thiols on the redox environment during ageing would contribute to our understanding of redox-related regulatory mechanisms. The detection range and sensitivity of the LC-MS/MS method for thiol analysis enabled the accurate monitoring of the key metabolites involved in the *de novo* GSH synthesis pathway in ageing worms. Further applications of this LC-MS/MS method in our nematode studies are focusing on expanding the detection capacity to the measurement of the other biologically relevant thiols that include cysteinylglycine (CysGly), homocysteine (HCys) and coenzyme A (CoA). The inclusion of homocysteine and cysteinylglycine data will provide more comprehensive views of the extracellular degradation of glutathione to cysteinylglycine due to the gamma-glutamyl transpeptidase activity, and how the transsulfuration pathway provides sulfur via homocysteine for cysteine biosynthesis (Figure 5-1). Previous work has shown that the levels of homocysteine increase by over 2-fold in the livers of aged mice (425). This increase in homocysteine was shown to directly affect the catalytic activity of the mouse GCL enzyme. The authors report that the accumulation of homocysteine adversely leads to the inhibition of the GCL activity, which was likely due to competitive inhibition of the cysteine-binding site. This illustrates the multifaceted levels of regulation of the GCL enzyme which remains to be completely understood.

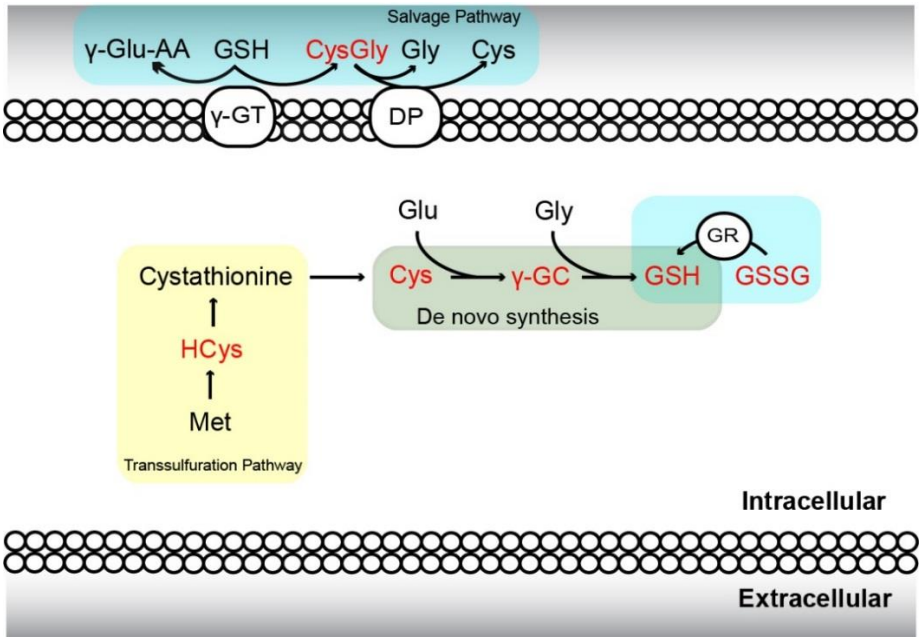

Figure 5-1. Further applications of LC-MS/MS to understand thiol biology

Cysteinylglycine (CysGly) levels could be used as an indicator of the extracellular degradation of GSH by gamma-glutamyl transpeptidase (γ-GT) providing further insight into GSH homeostasis via the extracellular salvage synthesis pathway. Profiling of homocysteine (HCys) can explore the potential role of transsulfuration pathway in the regulation or dysfunction of glutamate cysteine ligase (GCL) activity.

Advances in redox proteomics techniques hold promise to further our understanding of how post-translational modifications influence signalling events of the redox proteome (426, 427). The ability to use proteomic approaches to delineate how GSH functions as a post-translational modifier will be vital to further understanding how GSH's decline influences ageing. Building on established proteomic methods used in *C. elegans*, such as OxiCat (124), which measures the reversible oxidation of cysteine residues, will allow a global view of the changes in post-translational modifications over the *C. elegans* lifespan. Systematic investigations of the distinct signalling effects of the various cysteine modifications that contribute to the global redox-network are required to elucidate the susceptible signalling pathways of disease and ageing and to identify appropriate therapeutic targets (428-430).

Profiling of the global *S*-glutathionylated proteins of *Drosophila* and *E. coli* lysates has been conducted using clickable chemistry with GSH-analogue probes (431). Bioinformatic analysis of *S*-glutathionylated proteins demonstrated that the cysteine residues positioned adjacent to more negatively charged amino acids have a higher frequency of *S*-glutathionylation (431), indicating a possible selective structure-based pattern. Recent reports have demonstrated that worms exhibit changes in protein *S*-thiolation patterns (i.e. *S*-glutathionylation and *S*-cysteinylation) of targeted cysteine residues (432). This evidence of the occurrence of *S*-glutathionylation and the short life span of *C. elegans* offers the opportunity to explore age-dependent changes in a rapid ageing model.

5.1.4 Concluding remarks

In conclusion, the key finding of this thesis is that glutathione homeostasis declines with age in *C. elegans* in a manner that is an amenable for modelling glutathione changes in human ageing. Should this work encourage future research to model the human decline of GSH using *C. elegans*, it will undoubtedly enable a greater understanding of the multifaceted levels of GSH decline and thus can be used to form appropriate therapeutic strategies for many age-related diseases and disorders.

6 References

1. Partridge L. 2014. Intervening in ageing to prevent the diseases of ageing. *Trends Endocrinol Metab* 25: 555-7
2. United Nations DoEaSA, Population Division. 2017. World Population Prospects: The 2017 Revision, Key Findings and Advance Tables. Working Paper No. ESA/P/WP/248
3. Fries JF, Bruce B, Chakravarty E. 2011. Compression of morbidity 1980-2011: a focused review of paradigms and progress. *J Aging Res* 2011: 261702
4. Lopez-Otin C, Blasco MA, Partridge L, Serrano M, Kroemer G. 2013. The hallmarks of aging. *Cell* 153: 1194-217
5. Tosato M, Zamboni V, Ferrini A, Cesari M. 2007. The aging process and potential interventions to extend life expectancy. *Clin Interv Aging* 2: 401-12
6. Weinert BT, Timiras PS. 2003. Invited review: Theories of aging. *J Appl Physiol* 95: 1706-16
7. Harman D. 1956. Aging: a theory based on free radical and radiation chemistry. *J Gerontol* 11: 298-300
8. Gladyshev VN. 2014. The Free Radical Theory of Aging Is Dead. Long Live the Damage Theory! *Antioxid Redox Signal* 20: 727-31
9. Sies H. 1986. Biochemistry of Oxidative Stress. *Angew Chem Int Ed Engl* 25: 1058-71
10. de la Asuncion JG, Millan A, Pla R, Bruseghini L, Esteras A, Pallardo FV, Sastre J, Vina J. 1996. Mitochondrial glutathione oxidation correlates with age-associated oxidative damage to mitochondrial DNA. *FASEB J* 10: 333-8
11. Lee J, Koo N, Min DB. 2004. Reactive oxygen species, aging, and antioxidative nutraceuticals. *Compr Rev Food Sci Food Saf* 3: 21-33
12. Jones DP. 2008. Radical-free biology of oxidative stress. *Am J Physiol Cell Physiol* 295: C849-68
13. Sohal RS, Orr WC. 2012. The redox stress hypothesis of aging. *Free Radic Biol Med* 52: 539-55
14. Yu BP, Yang R. 1996. Critical evaluation of the free radical theory of aging - A proposal for the oxidative stress hypothesis. *Ann NY Acad Sci* 786: 1-11
15. Circu ML, Aw TY. 2010. Reactive oxygen species, cellular redox systems, and apoptosis. *Free Radic Biol Med* 48: 749-62
16. Droge W. 2002. Free radicals in the physiological control of cell function. *Physiol Rev* 82: 47-95
17. Mailloux RJ, Harper ME. 2011. Uncoupling proteins and the control of mitochondrial reactive oxygen species production. *Free Radic Biol Med* 51: 1106-15
18. Zhang YQ, Ikeno Y, Qi WB, Chaudhuri A, Li Y, Bokov A, Thorpe SR, Baynes JW, Epstein C, Richardson A, Van Remmen H. 2009. Mice Deficient in Both Mn Superoxide Dismutase and Glutathione Peroxidase-1 Have Increased Oxidative Damage and a Greater Incidence of Pathology but No Reduction in Longevity. *J Gerontol A Biol Sci Med Sci* 64: 1212-20
19. Van Raamsdonk JM, Hekimi S. 2010. Reactive Oxygen Species and Aging in *Caenorhabditis elegans*: Causal or Casual Relationship? *Antioxid Redox Signal* 13: 1911-53
20. Ristow M, Schmeisser S. 2011. Extending life span by increasing oxidative stress. *Free Radic Biol Med* 51: 327-36

21. Sadowska-Bartosz I, Bartosz G. 2014. Effect of antioxidants supplementation on aging and longevity. *Biomed Res Int* 2014: 404680
22. Carr AC, Frei B. 1999. Toward a new recommended dietary allowance for vitamin C based on antioxidant and health effects in humans. *Am J Clin Nutr* 69: 1086-107
23. Poljsak B, Milisav I. 2012. The neglected significance of "antioxidative stress". *Oxid Med Cell Longev* 2012: 480895
24. Ristow M, Zarse K, Oberbach A, Kloting N, Birringer M, Kiehntopf M, Stumvoll M, Kahn CR, Bluher M. 2009. Antioxidants prevent health-promoting effects of physical exercise in humans. *Proc Natl Acad Sci U.S.A* 106: 8665-70
25. Rattan SI. 2008. Hormesis in aging. *Ageing Res Rev* 7: 63-78
26. Johnston AD, Ebert PR. 2012. The Redox System in *C. elegans*, a Phylogenetic Approach. *J Toxicol* 2012: 546915
27. Back P, Braeckman BP, Matthijssens F. 2012. ROS in aging *Caenorhabditis elegans*: damage or signaling? *Oxid Med Cell Longev* 2012: 608478
28. Sies H, Berndt C, Jones DP. 2017. Oxidative Stress. *Annu Rev Biochem*
29. Jones DP. 2015. Redox theory of aging. *Redox Biol* 5: 71-9
30. Jones DP, Sies H. 2015. The Redox Code. *Antioxid Redox Signal* 23: 734-46
31. Schafer FQ, Buettner GR. 2001. Redox environment of the cell as viewed through the redox state of the glutathione disulfide/glutathione couple. *Free Radic Biol Med* 30: 1191-212
32. Rebrin I, Sohal RS. 2008. Pro-oxidant shift in glutathione redox state during aging. *Adv Drug Deliv Rev* 60: 1545-52
33. Go YM, Jones DP. 2013. Thiol/disulfide redox states in signaling and sensing. *Crit Rev Biochem Mol Biol* 48: 173-81
34. Herrmann JM, Dick TP. 2012. Redox Biology on the rise. *Biol Chem* 393: 999-1004
35. Winterbourn CC, Hampton MB. 2015. Redox biology: Signaling via a peroxiredoxin sensor. *Nat Chem Biol* 11: 5-6
36. Molavian H, Tonekaboni AM, Kohandel M, Sivaloganathan S. 2015. The Synergetic Coupling among the Cellular Antioxidants Glutathione Peroxidase/Peroxiredoxin and Other Antioxidants and its Effect on the Concentration of H_2O_2. *Sci Rep* 5: 13620
37. Pollak N, Dolle C, Ziegler M. 2007. The power to reduce: pyridine nucleotides--small molecules with a multitude of functions. *Biochem J* 402: 205-18
38. Lu SC. 2009. Regulation of glutathione synthesis. *Mol Aspects Med* 30: 42-59
39. Forman HJ, Zhang H, Rinna A. 2009. Glutathione: overview of its protective roles, measurement, and biosynthesis. *Mol Aspects Med* 30: 1-12
40. Zhang H, Forman HJ. 2012. Glutathione synthesis and its role in redox signaling. *Semin Cell Dev Biol* 23: 722-8
41. Berndt C, Lillig CH, Flohe L. 2014. Redox regulation by glutathione needs enzymes. *Front Pharmacol* 5: 168
42. Romero-Aristizabal C, Marks DS, Fontana W, Apfeld J. 2014. Regulated spatial organization and sensitivity of cytosolic protein oxidation in *Caenorhabditis elegans*. *Nat Commun* 5: 5020
43. Winterbourn CC. 2015. Are free radicals involved in thiol-based redox signaling? *Free Radic Biol Med* 80: 164-70
44. Schieber M, Chandel NS. 2014. ROS function in redox signaling and oxidative stress. *Curr Biol* 24: R453-62

45. Winterbourn CC, Hampton MB. 2008. Thiol chemistry and specificity in redox signaling. *Free Radic Biol Med* 45: 549-61
46. Jacob C, Giles GI, Giles NM, Sies H. 2003. Sulfur and selenium: the role of oxidation state in protein structure and function. *Angew Chem Int Ed Engl* 42: 4742-58
47. Gallogly MM, Mieyal JJ. 2007. Mechanisms of reversible protein glutathionylation in redox signaling and oxidative stress. *Curr Opin Pharmacol* 7: 381-91
48. Miseta A, Csutora P. 2000. Relationship between the occurrence of cysteine in proteins and the complexity of organisms. *Mol Biol Evol* 17: 1232-9
49. Deponte M, Lillig CH. 2015. Enzymatic control of cysteinyl thiol switches in proteins. *Biol Chem* 396: 401-13
50. Mohanasundaram KA, Haworth NL, Grover MP, Crowley TM, Goscinski A, Wouters MA. 2015. Potential role of glutathione in evolution of thiol-based redox signaling sites in proteins. *Front Pharmacol* 6: 1
51. Jones DP. 2010. Redox sensing: orthogonal control in cell cycle and apoptosis signalling. *J Intern Med* 268: 432-48
52. Jones DP, Go YM. 2011. Mapping the cysteine proteome: analysis of redox-sensing thiols. *Curr Opin Chem Biol* 15: 103-12
53. Hohn A, Konig J, Grune T. 2013. Protein oxidation in aging and the removal of oxidized proteins. *J Proteomics* 92: 132-59
54. Sies H. 2014. Role of metabolic H_2O_2 generation: redox signaling and oxidative stress. *J Biol Chem* 289: 8735-41
55. Kemp M, Go YM, Jones DP. 2008. Nonequilibrium thermodynamics of thiol/disulfide redox systems: a perspective on redox systems biology. *Free Radic Biol Med* 44: 921-37
56. Schmidt B, Ho L, Hogg PJ. 2006. Allosteric disulfide bonds. *Biochemistry* 45: 7429-33
57. Klatt P, Lamas S. 2000. Regulation of protein function by S-glutathiolation in response to oxidative and nitrosative stress. *Eur J Biochem* 267: 4928-44
58. Brigelius-Flohe R. 2016. Mixed results with mixed disulfides. *Arch Biochem Biophys* 595: 81-7
59. Ghezzi P, Bonetto V, Fratelli M. 2005. Thiol-disulfide balance: From the concept of oxidative stress to that of redox regulation. *Antioxid Redox Signal* 7: 964-72
60. Dalle-Donne I, Rossi R, Giustarini D, Colombo R, Milzani A. 2007. S-glutathionylation in protein redox regulation. *Free Radic Biol Med* 43: 883-98
61. Shelton MD, Chock PB, Mieyal JJ. 2005. Glutaredoxin: role in reversible protein s-glutathionylation and regulation of redox signal transduction and protein translocation. *Antioxid Redox Signal* 7: 348-66
62. Kamata H, Hirata H. 1999. Redox regulation of cellular signalling. *Cell Signal* 11: 1-14
63. Ghezzi P. 2013. Protein glutathionylation in health and disease. *Biochim Biophys Acta* 1830: 3165-72
64. Forman HJ. 2016. Glutathione - From antioxidant to post-translational modifier. *Arch Biochem Biophys* 595: 64-7
65. Mieyal JJ, Gallogly MM, Qanungo S, Sabens EA, Shelton MD. 2008. Molecular mechanisms and clinical implications of reversible protein S-glutathionylation. *Antioxid Redox Signal* 10: 1941-88

66. Mailloux RJ, Xuan JY, McBride S, Maharsy W, Thorn S, Holterman CE, Kennedy CR, Rippstein P, deKemp R, da Silva J, Nemer M, Lou M, Harper ME. 2014. Glutaredoxin-2 is required to control oxidative phosphorylation in cardiac muscle by mediating deglutathionylation reactions. *J Biol Chem* 289: 14812-28
67. Gallogly MM, Shelton MD, Qanungo S, Pai HV, Starke DW, Hoppel CL, Lesnefsky EJ, Mieyal JJ. 2010. Glutaredoxin regulates apoptosis in cardiomyocytes via NFkappaB targets Bcl-2 and Bcl-xL: implications for cardiac aging. *Antioxid Redox Signal* 12: 1339-53
68. Xiong Y, Uys JD, Tew KD, Townsend DM. 2011. S-glutathionylation: from molecular mechanisms to health outcomes. *Antioxid Redox Signal* 15: 233-70
69. Sabens Liedhegner EA, Gao XH, Mieyal JJ. 2012. Mechanisms of altered redox regulation in neurodegenerative diseases--focus on S--glutathionylation. *Antioxid Redox Signal* 16: 543-66
70. Rossi R, Giustarini D, Milzani A, Dalle-Donne I. 2009. Cysteinylation and homocysteinylation of plasma protein thiols during ageing of healthy human beings. *J Cell Mol Med* 13: 3131-40
71. Giustarini D, Dalle-Donne I, Lorenzini S, Milzani A, Rossi R. 2006. Age-related influence on thiol, disulfide, and protein-mixed disulfide levels in human plasma. *J Gerontol A Biol Sci Med Sci* 61: 1030-8
72. Townsend DM, Tew KD, Tapiero H. 2003. The importance of glutathione in human disease. *Biomed Pharmacother* 57: 145-55
73. Meister A, Anderson ME. 1983. Glutathione. *Annu Rev Biochem* 52: 711-60
74. Richman PG, Meister A. 1975. Regulation of gamma-glutamyl-cysteine synthetase by nonallosteric feedback inhibition by glutathione. *J Biol Chem* 250: 1422-6
75. Ballatori N, Krance SM, Notenboom S, Shi S, Tieu K, Hammond CL. 2009. Glutathione dysregulation and the etiology and progression of human diseases. *Biol Chem* 390: 191-214
76. Deponte M. 2013. Glutathione catalysis and the reaction mechanisms of glutathione-dependent enzymes. *Biochim Biophys Acta* 1830: 3217-66
77. Aquilano K, Baldelli S, Ciriolo MR. 2014. Glutathione: new roles in redox signaling for an old antioxidant. *Front Pharmacol* 5: 196
78. Tsuchiya K, Mulcahy RT, Reid LL, Disteche CM, Kavanagh TJ. 1995. Mapping of the glutamate-cysteine ligase catalytic subunit gene (GLCLC) to human chromosome 6p12 and mouse chromosome 9D-E and of the regulatory subunit gene (GLCLR) to human chromosome 1p21-p22 and mouse chromosome 3H1-3. *Genomics* 30: 630-2
79. Fraser JA, Saunders RDC, McLellan LI. 2002. *Drosophila melanogaster* glutamate-cysteine ligase activity is regulated by a modifier subunit with a mechanism of action similar to that of the mammalian form. *J Biol Chem* 277: 1158-65
80. Dahl EL, Mulcahy RT. 2001. Cell-type specific differences in glutamate cysteine ligase transcriptional regulation demonstrate independent subunit control. *Toxicol Sci* 61: 265-72
81. Franklin CC, Backos DS, Mohar I, White CC, Forman HJ, Kavanagh TJ. 2009. Structure, function, and post-translational regulation of the catalytic and modifier subunits of glutamate cysteine ligase. *Mol Aspects Med* 30: 86-98

82. Yang Y, Chen Y, Johansson E, Schneider SN, Shertzer HG, Nebert DW, Dalton TP. 2007. Interaction between the catalytic and modifier subunits of glutamate-cysteine ligase. *Biochem Pharmacol* 74: 372-81
83. Yan N, Meister A. 1990. Amino acid sequence of rat kidney gamma-glutamylcysteine synthetase. *J Biol Chem* 265: 1588-93
84. Huang CS, Chang LS, Anderson ME, Meister A. 1993. Catalytic and regulatory properties of the heavy subunit of rat kidney gamma-glutamylcysteine synthetase. *J Biol Chem* 268: 19675-80
85. Chen Y, Shertzer HG, Schneider SN, Nebert DW, Dalton TP. 2005. Glutamate cysteine ligase catalysis: dependence on ATP and modifier subunit for regulation of tissue glutathione levels. *J Biol Chem* 280: 33766-74
86. Yang Y, Dieter MZ, Chen Y, Shertzer HG, Nebert DW, Dalton TP. 2002. Initial characterization of the glutamate-cysteine ligase modifier subunit Gclm(-/-) knockout mouse. Novel model system for a severely compromised oxidative stress response. *J Biol Chem* 277: 49446-52
87. Fraser JA, Kansagra P, Kotecki C, Saunders RD, McLellan LI. 2003. The modifier subunit of *Drosophila* glutamate-cysteine ligase regulates catalytic activity by covalent and noncovalent interactions and influences glutathione homeostasis *in vivo*. *J Biol Chem* 278: 46369-77
88. Toroser D, Sohal RS. 2005. Kinetic characteristics of native gamma-glutamylcysteine ligase in the aging housefly, Musca domestica L. *Biochem Biophys Res Commun* 326: 586-93
89. Luchak JM, Prabhudesai L, Sohal RS, Radyuk SN, Orr WC. 2007. Modulating longevity in *Drosophila* by over- and underexpression of glutamate-cysteine ligase. *Ann N Y Acad Sci* 1119: 260-73
90. Orr WC, Radyuk SN, Prabhudesai L, Toroser D, Benes JJ, Luchak JM, Mockett RJ, Rebrin I, Hubbard JG, Sohal RS. 2005. Overexpression of glutamate-cysteine ligase extends life span in *Drosophila melanogaster*. *J Biol Chem* 280: 37331-8
91. Radyuk SN, Gambini J, Borras C, Serna E, Klichko VI, Vina J, Orr WC. 2012. Age-dependent changes in the transcription profile of long-lived *Drosophila* over-expressing glutamate cysteine ligase. *Mech Ageing Dev* 133: 401-13
92. Liu R, Choi J. 2000. Age-associated decline in gamma-glutamylcysteine synthetase gene expression in rats. *Free Radic Biol Med* 28: 566-74
93. Suh JH, Shenvi SV, Dixon BM, Liu H, Jaiswal AK, Liu RM, Hagen TM. 2004. Decline in transcriptional activity of Nrf2 causes age-related loss of glutathione synthesis, which is reversible with lipoic acid. *Proc Natl Acad Sci U.S.A* 101: 3381-6
94. Krzywanski DM, Dickinson DA, Iles KE, Wigley AF, Franklin CC, Liu RM, Kavanagh TJ, Forman HJ. 2004. Variable regulation of glutamate cysteine ligase subunit proteins affects glutathione biosynthesis in response to oxidative stress. *Arch Biochem Biophys* 423: 116-25
95. Liu RM. 2002. Down-regulation of gamma-glutamylcysteine synthetase regulatory subunit gene expression in rat brain tissue during aging. *J Neurosci Res* 68: 344-51
96. Ferguson G, Bridge W. 2016. Glutamate cysteine ligase and the age-related decline in cellular glutathione: The therapeutic potential of gamma-glutamylcysteine. *Arch Biochem Biophys* 593: 12-23

97. Anderson ME, Meister A. 1983. Transport and direct utilization of gamma-glutamylcyst(e)ine for glutathione synthesis. *Proc Natl Acad Sci U.S.A* 80: 707-11
98. Le TM, Jiang H, Cunningham GR, Magarik JA, Barge WS, Cato MC, Farina M, Rocha JB, Milatovic D, Lee E, Aschner M, Summar ML. 2011. gamma-Glutamylcysteine ameliorates oxidative injury in neurons and astrocytes in vitro and increases brain glutathione in vivo. *Neurotoxicology* 32: 518-25
99. Nakamura YK, Dubick MA, Omaye ST. 2012. gamma-Glutamylcysteine inhibits oxidative stress in human endothelial cells. *Life Sci* 90: 116-21
100. Nakamura YK, Dubick MA, Omaye ST. 2012. Modulation of oxidative stress by gamma-glutamylcysteine (GGC) and conjugated linoleic acid (CLA) isomer mixture in human umbilical vein endothelial cells. *Food Chem Toxicol* 50: 1854-9
101. Dringen R, Kranich O, Loschmann PA, Hamprecht B. 1997. Use of dipeptides for the synthesis of glutathione by astroglia-rich primary cultures. *J Neurochem* 69: 868-74
102. Pileblad E, Magnusson T. 1992. Increase in rat brain glutathione following intracerebroventricular administration of gamma-glutamylcysteine. *Biochem Pharmacol* 44: 895-903
103. Hayashi H, Iimuro M, Matsumoto Y, Kaneko M. 1998. Effects of gamma-glutamylcysteine ethyl ester on heart mitochondrial creatine kinase activity: involvement of sulfhydryl groups. *Eur J Pharmacol* 349: 133-6
104. Drake J, Kanski J, Varadarajan S, Tsoras M, Butterfield DA. 2002. Elevation of brain glutathione by gamma-glutamylcysteine ethyl ester protects against peroxynitrite-induced oxidative stress. *J Neurosci Res* 68: 776-84
105. Drake J, Sultana R, Aksenova M, Calabrese V, Butterfield DA. 2003. Elevation of mitochondrial glutathione by gamma-glutamylcysteine ethyl ester protects mitochondria against peroxynitrite-induced oxidative stress. *J Neurosci Res* 74: 917-27
106. Sugimoto M, Kuhlenkamp J, Ookhtens M, Aw TY, Reeve J, Jr., Kaplowitz N. 1985. Gamma-glutamylcysteine: a substrate for glutathione S-transferases. *Biochem Pharmacol* 34: 3643-7
107. Grant CM, MacIver FH, Dawes IW. 1997. Glutathione synthetase is dispensable for growth under both normal and oxidative stress conditions in the yeast Saccharomyces cerevisiae due to an accumulation of the dipeptide gamma-glutamylcysteine. *Mol Biol Cell* 8: 1699-707
108. Ristoff E, Hebert C, Njalsson R, Norgren S, Rooyackers O, Larsson A. 2002. Glutathione synthetase deficiency: Is gamma-glutamylcysteine accumulation a way to cope with oxidative stress in cells with insufficient levels of glutathione? *J Inherit Metab Dis* 25: 577-84
109. Quintana-Cabrera R, Fernandez-Fernandez S, Bobo-Jimenez V, Escobar J, Sastre J, Almeida A, Bolanos JP. 2012. gamma-Glutamylcysteine detoxifies reactive oxygen species by acting as glutathione peroxidase-1 cofactor. *Nat Commun* 3:718
110. Dalton TP, Chen Y, Schneider SN, Nebert DW, Shertzer HG. 2004. Genetically altered mice to evaluate glutathione homeostasis in health and disease. *Free Radic Biol Med* 37: 1511-26

111. Stark AA, Porat N, Volohonsky G, Komlosh A, Bluvshtein E, Tubi C, Steinberg P. 2003. The role of gamma-glutamyl transpeptidase in the biosynthesis of glutathione. *Biofactors* 17: 139-49
112. Zarka MH, Bridge WJ. 2017. Oral administration of gamma-glutamylcysteine increases intracellular glutathione levels above homeostasis in a randomised human trial pilot study. *Redox Biol* 11: 631-6
113. Huang C, Xiong CJ, Kornfeld K. 2004. Measurements of age-related changes of physiological processes that predict lifespan of *Caenorhabditis elegans*. *Proc Natl Acad Sci U.S.A* 101: 8084-9
114. Friedman DB, Johnson TE. 1988. A mutation in the *age-1* gene in *Caenorhabditis elegans* lengthens life and reduces hermaphrodite fertility. *Genetics* 118: 75-86
115. Kenyon C, Chang J, Gensch E, Rudner A, Tabtiang R. 1993. A *C. elegans* mutant that lives twice as long as wild type. *Nature* 366: 461-4
116. Lapierre LR, Hansen M. 2012. Lessons from *C. elegans*: signaling pathways for longevity. *Trends Endocrinol Metab* 23: 637-44
117. Murphy CT. 2006. The search for DAF-16/FOXO transcriptional targets: Approaches and discoveries. *Exp Gerontol* 41: 910-21
118. Kenyon CJ. 2010. The genetics of ageing. *Nature* 464: 504-12
119. Murphy CT, McCarroll SA, Bargmann CI, Fraser A, Kamath RS, Ahringer J, Li H, Kenyon C. 2003. Genes that act downstream of DAF-16 to influence the lifespan of *Caenorhabditis elegans*. *Nature* 424: 277-83
120. Kenyon C. 2005. The plasticity of aging: insights from long-lived mutants. *Cell* 120: 449-60
121. Yanase S, Yasuda K, Ishii N. 2002. Adaptive responses to oxidative damage in three mutants of *Caenorhabditis elegans* (*age-1*, *mev-1* and *daf-16*) that affect life span. *Mech Ageing Dev* 123: 1579-87
122. Lin K, Hsin H, Libina N, Kenyon C. 2001. Regulation of the *Caenorhabditis elegans* longevity protein DAF-16 by insulin/IGF-1 and germline signaling. *Nat Genet* 28: 139-45
123. Moreno-Arriola E, Cardenas-Rodriguez N, Coballase-Urrutia E, Pedraza-Chaverri J, Carmona-Aparicio L, Ortega-Cuellar D. 2014. *Caenorhabditis elegans*: A Useful Model for Studying Metabolic Disorders in Which Oxidative Stress Is a Contributing Factor. *Oxid Med and Cell Longev*: 705253
124. Kumsta C, Thamsen M, Jakob U. 2011. Effects of oxidative stress on behavior, physiology, and the redox thiol proteome of *Caenorhabditis elegans*. *Antioxid Redox Signal* 14: 1023-37
125. Sakamoto T, Maebayashi K, Nakagawa Y, Imai H. 2014. Deletion of the four phospholipid hydroperoxide glutathione peroxidase genes accelerates aging in *Caenorhabditis elegans*. *Genes Cells* 19: 778-92
126. Jee C, Vanoaica L, Lee J, Park BJ, Ahnn J. 2005. Thioredoxin is related to life span regulation and oxidative stress response in *Caenorhabditis elegans*. *Genes Cells* 10: 1203-10
127. Brys K, Vanfleteren JR, Braeckman BP. 2007. Testing the rate-of-living/oxidative damage theory of aging in the nematode model *Caenorhabditis elegans*. *Exp Gerontol* 42: 845-51
128. Gruber J, Chen CB, Fong S, Ng LF, Teo E, Halliwell B. 2015. *Caenorhabditis elegans*: What We Can and Cannot Learn from Aging Worms. *Antioxid Redox Signal* 23: 256-79

129. Gusarov I, Pani B, Gautier L, Smolentseva O, Eremina S, Shamovsky I, Katkova-Zhukotskaya O, Mironov A, Nudler E. 2017. Glycogen controls *Caenorhabditis elegans* lifespan and resistance to oxidative stress. *Nat Commun* 8: 15868
130. Hertweck M, Gobel C, Baumeister R. 2004. *C. elegans* SGK-1 is the critical component in the Akt/PKB kinase complex to control stress response and life span. *Dev Cell* 6: 577-88
131. Asamoto H, Ichibangase T, Saimaru H, Uchikura K, Imai K. 2007. Existence of low-molecular-weight thiols in *Caenorhabditis elegans* demonstrated by HPLC-fluorescene detection utilizing 7-chloro-N-[2-(dimethylamino)ethyl]-2,1,3-benzoxadiazole-4-sulfonamide. *Biomed Chromatogr* 21: 999-1004
132. Luersen K, Stegehake D, Daniel J, Drescher M, Ajonina I, Ajonina C, Hertel P, Woltersdorf C, Liebau E. 2013. The glutathione reductase GSR-1 determines stress tolerance and longevity in *Caenorhabditis elegans*. *Plos One* 8: e60731
133. Urban N, Tsitsipatis D, Hausig F, Kreuzer K, Erler K, Stein V, Ristow M, Steinbrenner H, Klotz LO. 2016. Non-linear impact of glutathione depletion on *C. elegans* life span and stress resistance. *Redox Biol* 11: 502-15
134. Bito T, Misaki T, Yabuta Y, Ishikawa T, Kawano T, Watanabe F. 2017. Vitamin B12 deficiency results in severe oxidative stress, leading to memory retention impairment in *Caenorhabditis elegans*. *Redox Biol* 11: 21-9
135. Salgueiro WG, Goldani BS, Peres TV, Miranda-Vizuete A, Aschner M, da Rocha JBT, Alves D, Avila DS. 2017. Insights into the differential toxicological and antioxidant effects of 4-phenylchalcogenil-7-chloroquinolines in *Caenorhabditis elegans*. *Free Radic Biol Med* 110: 133-41
136. An JH, Blackwell TK. 2003. SKN-1 links *C. elegans* mesendodermal specification to a conserved oxidative stress response. *Genes Dev* 17: 1882-93
137. Liao VHC, Yu CW. 2005. *Caenorhabditis elegans gcs-1* confers resistance to arsenic-induced oxidative stress. *Biometals* 18: 519-28
138. Blackwell TK, Steinbaugh MJ, Hourihan JM, Ewald CY, Isik M. 2015. SKN-1/Nrf, stress responses, and aging in *Caenorhabditis elegans*. *Free Radic Biol Med* 88: 290-301
139. Oliveira RP, Porter Abate J, Dilks K, Landis J, Ashraf J, Murphy CT, Blackwell TK. 2009. Condition-adapted stress and longevity gene regulation by *Caenorhabditis elegans* SKN-1/Nrf. *Aging Cell* 8: 524-41
140. Inoue H, Hisamoto N, An JH, Oliveira RP, Nishida E, Blackwell TK, Matsumoto K. 2005. The *C. elegans* p38 MAPK pathway regulates nuclear localization of the transcription factor SKN-1 in oxidative stress response. *Genes Dev* 19: 2278-83
141. Wang J, Robida-Stubbs S, Tullet JM, Rual JF, Vidal M, Blackwell TK. 2010. RNAi screening implicates a SKN-1-dependent transcriptional response in stress resistance and longevity deriving from translation inhibition. *PLoS Genet* 6: e1001048
142. An JH, Vranas K, Lucke M, Inoue H, Hisamoto N, Matsumoto K, Blackwell TK. 2005. Regulation of the *Caenorhabditis elegans* oxidative stress defense protein SKN-1 by glycogen synthase kinase-3. *Proc Natl Acad Sci U.S.A* 102: 16275-80
143. Choe KP, Przybysz AJ, Strange K. 2009. The WD40 repeat protein WDR-23 functions with the CUL4/DDB1 ubiquitin ligase to regulate nuclear abundance and activity of SKN-1 in *Caenorhabditis elegans*. *Mol Cell Biol* 29: 2704-15
144. Migliori V, Mapelli M, Guccione E. 2012. On WD40 proteins Propelling our knowledge of transcriptional control? *Epigenetics* 7: 815-22

145. Tang L, Choe KP. 2015. Characterization of *skn-1*/*wdr-23* phenotypes in *Caenorhabditis elegans*; pleiotrophy, aging, glutathione, and interactions with other longevity pathways. *Mech Ageing Dev* 149: 88-98
146. Li S, Armstrong CM, Bertin N, Ge H, Milstein S, Boxem M, Vidalain PO, Han JD, Chesneau A, Hao T, Goldberg DS, Li N, Martinez M, Rual JF, Lamesch P, Xu L, Tewari M, Wong SL, Zhang LV, Berriz GF, Jacotot L, Vaglio P, Reboul J, Hirozane-Kishikawa T, Li Q, Gabel HW, Elewa A, Baumgartner B, Rose DJ, Yu H, Bosak S, Sequerra R, Fraser A, Mango SE, Saxton WM, Strome S, Van Den Heuvel S, Piano F, Vandenhaute J, Sardet C, Gerstein M, Doucette-Stamm L, Gunsalus KC, Harper JW, Cusick ME, Roth FP, Hill DE, Vidal M. 2004. A map of the interactome network of the metazoan *C. elegans*. *Science* 303: 540-3
147. Przybysz AJ, Choe KP, Roberts LJ, Strange K. 2009. Increased age reduces DAF-16 and SKN-1 signaling and the hormetic response of *Caenorhabditis elegans* to the xenobiotic juglone. *Mech Ageing Dev* 130: 357-69
148. Spanier B, Rubio-Aliaga I, Hu H, Daniel H. 2010. Altered signalling from germline to intestine pushes *daf-2*;*pept-1 Caenorhabditis elegans* into extreme longevity. *Aging Cell* 9: 636-46
149. Choe KP, Leung CK, Miyamoto MM. 2012. Unique structure and regulation of the nematode detoxification gene regulator, SKN-1: implications to understanding and controlling drug resistance. *Drug Metab Rev* 44: 209-23
150. Crook-McMahon HM, Olahova M, Button EL, Winter JJ, Veal EA. 2014. Genome-wide screening identifies new genes required for stress-induced phase 2 detoxification gene expression in animals. *BMC Biol* 12: 64
151. Wu H, Huang C, Taki FA, Zhang Y, Dobbins DL, Li L, Yan H, Pan X. 2015. Benzo-alpha-pyrene induced oxidative stress in *Caenorhabditis elegans* and the potential involvements of microRNA. *Chemosphere* 139: 496-503
152. Mora-Lorca JA, Saenz-Narciso B, Gaffney CJ, Naranjo-Galindo FJ, Pedrajas JR, Guerrero-Gomez D, Dobrzynska A, Askjaer P, Szewczyk NJ, Cabello J, Miranda-Vizuete A. 2016. Glutathione reductase *gsr-1* is an essential gene required for *Caenorhabditis elegans* early embryonic development. *Free Radic Biol Med* 96: 446-61
153. Homolya L, Varadi A, Sarkadi B. 2003. Multidrug resistance-associated proteins: Export pumps for conjugates with glutathione, glucuronate or sulfate. *Biofactors* 17: 103-14
154. James CE, Davey MW. 2009. Increased expression of ABC transport proteins is associated with ivermectin resistance in the model nematode *Caenorhabditis elegans*. *Int J Parasitol* 39: 213-20
155. Margis R, Dunand C, Teixeira FK, Margis-Pinheiro M. 2008. Glutathione peroxidase family - an evolutionary overview. *FEBS J* 275: 3959-70
156. Herbette S, Roeckel-Drevet P, Drevet JR. 2007. Seleno-independent glutathione peroxidases. More than simple antioxidant scavengers. *FEBS J* 274: 2163-80
157. Flohe L, Brigelius-Flohe R. 2012. Selenoproteins of the Glutathione Peroxidase Family. *Selenium: Its Molecular Biology and Role in Human Health, Third Edition*: 167-80
158. Flohe L, Toppo S, Cozza G, Ursini F. 2011. A comparison of thiol peroxidase mechanisms. *Antioxid Redox Signal* 15: 763-80
159. Yan F, Chen X, Zheng X. 2017. Protective effect of mulberry fruit anthocyanin on human hepatocyte cells (LO2) and *Caenorhabditis elegans* under hyperglycemic conditions. *Food Res Int* 102: 213-24

160. Xu Z, Feng SL, Shen SA, Wang HD, Yuan M, Liu J, Huang Y, Ding CB. 2016. The antioxidant activities effect of neutral and acidic polysaccharides from Epimedium acuminatum Franch. on *Caenorhabditis elegans*. *Carbohydr Polym* 144: 122-30
161. Song S, Zhang X, Wu H, Han Y, Zhang J, Ma E, Guo Y. 2014. Molecular basis for antioxidant enzymes in mediating copper detoxification in the nematode *Caenorhabditis elegans*. *PLoS One* 9: e107685
162. Li H, Shi R, Ding F, Wang H, Han W, Ma F, Hu M, Ma CW, Huang Z. 2016. Astragalus Polysaccharide Suppresses 6-Hydroxydopamine-Induced Neurotoxicity in *Caenorhabditis elegans*. *Oxid Med Cell Longev* 2016: 4856761
163. Simonetta SH, Romanowski A, Minniti AN, Inestrosa NC, Golombek DA. 2008. Circadian stress tolerance in adult *Caenorhabditis elegans*. *J Comp Physiol A Neuroethol Sens Neural Behav Physiol* 194: 821-8
164. Benner J, Daniel H, Spanier B. 2011. A glutathione peroxidase, intracellular peptidases and the TOR complexes regulate peptide transporter PEPT-1 in *C. elegans*. *PLoS One* 6: e25624
165. Spanier B. 2014. Transcriptional and functional regulation of the intestinal peptide transporter PEPT1. *J Physiol* 592: 871-9
166. Sheehan D, Meade G, Foley VM, Dowd CA. 2001. Structure, function and evolution of glutathione transferases: implications for classification of non-mammalian members of an ancient enzyme superfamily. *Biochem J* 360: 1-16
167. Kim Y, Cha SJ, Choi HJ, Kim K. 2017. Omega Class Glutathione S-Transferase: Antioxidant Enzyme in Pathogenesis of Neurodegenerative Diseases. *Oxid Med Cell Longev*: 5049532
168. Lindblom TH, Dodd AK. 2006. Xenobiotic detoxification in the nematode *Caenorhabditis elegans*. *J Exp Zool A Comp Exp Biol* 305: 720-30
169. Dancy BM, Brockway N, Ramadasan-Nair R, Yang Y, Sedensky MM, Morgan PG. 2016. Glutathione S-transferase mediates an ageing response to mitochondrial dysfunction. *Mech Ageing Dev* 153: 14-21
170. Campbell AM, Teesdale-Spittle PH, Barrett J, Liebau E, Jefferies JR, Brophy PM. 2001. A common class of nematode glutathione S-transferase (GST) revealed by the theoretical proteome of the model organism *Caenorhabditis elegans*. *Comp Biochem Physiol B Biochem Mol Biol* 128: 701-8
171. van Rossum AJ, Brophy PM, Tait A, Barrett J, Jefferies JR. 2001. Proteomic identification of glutathione S-transferases from the model nematode *Caenorhabditis elegans*. *Proteomics* 1: 1463-8
172. Lee JH, Kim YG, Kim M, Kim E, Choi H, Kim Y, Lee J. 2017. Indole-associated predator-prey interactions between the nematode *Caenorhabditis elegans* and bacteria. *Environ Microbiol* 19: 1776-90
173. Negi H, Saikia SK, Kanaujia R, Jaiswal S, Pandey R. 2017. 3beta-Hydroxy-urs-12-en-28-oic acid confers protection against ZnONPs induced adversity in *Caenorhabditis elegans*. *Environ Toxicol Pharmacol* 53: 105-10
174. Ayyadevara S, Bharill P, Dandapat A, Hu C, Khaidakov M, Mitra S, Shmookler Reis RJ, Mehta JL. 2013. Aspirin inhibits oxidant stress, reduces age-associated functional declines, and extends lifespan of *Caenorhabditis elegans*. *Antioxid Redox Signal* 18: 481-90
175. McElwee JJ, Schuster E, Blanc E, Piper MD, Thomas JH, Patel DS, Selman C, Withers DJ, Thornton JM, Partridge L, Gems D. 2007. Evolutionary conservation of regulated longevity assurance mechanisms. *Genome Biol* 8: R132

176. McElwee JJ, Schuster E, Blanc E, Thomas JH, Gems D. 2004. Shared transcriptional signature in *Caenorhabditis elegans* dauer larvae and long-lived *daf-2* mutants implicates detoxification system in longevity assurance. *J Biol Chem* 279: 44533-43
177. LaCourse EJ, Perally S, Hernandez-Viadel M, Wright HA, Brophy PM. 2008. A proteomics approach to quantify protein levels following RNA interference: Case study with glutathione transferase superfamily from the model metazoan *Caenorhabditis elegans*. *J Proteome Res* 7: 3314-8
178. Jones LM, Staffa K, Perally S, LaCourse EJ, Brophy PM, Hamilton JV. 2010. Proteomic analyses of *Caenorhabditis elegans* dauer larvae and long-lived *daf-2* mutants implicates a shared detoxification system in longevity assurance. *J Proteome Res* 9: 2871-81
179. Perally S, Lacourse EJ, Campbell AM, Brophy PM. 2008. Heme transport and detoxification in nematodes: subproteomics evidence of differential role of glutathione transferases. *J Proteome Res* 7: 4557-65
180. Greetham D, Morgan C, Campbell AM, van Rossum AJ, Barrett J, Brophy PM. 2004. Evidence of glutathione transferase complexing and signaling in the model nematode *Caenorhabditis elegans* using a pull-down proteomic assay. *Proteomics* 4: 1989-95
181. Tawe WN, Eschbach ML, Walter RD, Henkle-Duhrsen K. 1998. Identification of stress-responsive genes in *Caenorhabditis elegans* using RT-PCR differential display. *Nucleic Acids Res* 26: 1621-7
182. Kahn NW, Rea SL, Moyle S, Kell A, Johnson TE. 2008. Proteasomal dysfunction activates the transcription factor SKN-1 and produces a selective oxidative-stress response in *Caenorhabditis elegans*. *Biochem J* 409: 205-13
183. Park SK, Tedesco PM, Johnson TE. 2009. Oxidative stress and longevity in *Caenorhabditis elegans* as mediated by SKN-1. *Aging Cell* 8: 258-69
184. Detienne G, Van de Walle P, De Haes W, Schoofs L, Temmerman L. 2016. SKN-1-independent transcriptional activation of glutathione S-transferase 4 (GST-4) by EGF signaling. *Worm* 5: e1230585
185. Leung CK, Empinado H, Choe KP. 2012. Depletion of a nucleolar protein activates xenobiotic detoxification genes in *Caenorhabditis elegans* via Nrf /SKN-1 and p53/CEP-1. *Free Radic Biol Med* 52: 937-50
186. Hasegawa K, Miwa S, Isomura K, Tsutsumiuchi K, Taniguchi H, Miwa J. 2008. Acrylamide-responsive genes in the nematode *Caenorhabditis elegans*. *Toxicol Sci* 101: 215-25
187. Hasegawa K, Miwa S, Tajima T, Tsutsumiuchi K, Taniguchi H, Miwa J. 2007. A rapid and inexpensive method to screen for common foods that reduce the action of acrylamide, a harmful substance in food. *Toxicol Lett* 175: 82-8
188. Rangaraju S, Solis GM, Andersson SI, Gomez-Amaro RL, Kardakaris R, Broaddus CD, Niculescu AB, 3rd, Petrascheck M. 2015. Atypical antidepressants extend lifespan of *Caenorhabditis elegans* by activation of a non-cell-autonomous stress response. *Aging Cell* 14: 971-81
189. Rathor L, Akhoon BA, Pandey S, Srivastava S, Pandey R. 2015. Folic acid supplementation at lower doses increases oxidative stress resistance and longevity in *Caenorhabditis elegans*. *Age* 37: 113
190. Stefanello ST, Gubert P, Puntel B, Mizdal CR, de Campos MM, Salman SM, Dornelles L, Avila DS, Aschner M, Soares FA. 2015. Protective effects of novel

organic selenium compounds against oxidative stress in the nematode *Caenorhabditis elegans*. *Toxicol Rep* 2: 961-7

191. Buchter C, Zhao L, Havermann S, Honnen S, Fritz G, Proksch P, Watjen W. 2015. TSG (2,3,5,4'-Tetrahydroxystilbene-2-O- beta -D-glucoside) from the Chinese Herb Polygonum multiflorum Increases Life Span and Stress Resistance of *Caenorhabditis elegans*. *Oxid Med Cell Longev* 2015: 124357
192. Kampkotter A, Pielarski T, Rohrig R, Timpel C, Chovolou Y, Watjen W, Kahl R. 2007. The Ginkgo biloba extract EGb761 reduces stress sensitivity, ROS accumulation and expression of catalase and glutathione S-transferase 4 in *Caenorhabditis elegans*. *Pharmacol Res* 55: 139-47
193. Rocheleau S, Arbour M, Elias M, Sunahara GI, Masson L. 2015. Toxicogenomic effects of nano- and bulk-TiO2 particles in the soil nematode *Caenorhabditis elegans*. *Nanotoxicology* 9: 502-12
194. Inokuchi A, Yamamoto R, Morita F, Takumi S, Matsusaki H, Ishibashi H, Tominaga N, Arizono K. 2015. Effects of lithium on growth, maturation, reproduction and gene expression in the nematode *Caenorhabditis elegans*. *J Appl Toxicol* 35: 999-1006
195. Lei L, Wu S, Lu S, Liu M, Song Y, Fu Z, Shi H, Raley-Susman KM, He D. 2017. Microplastic particles cause intestinal damage and other adverse effects in zebrafish Danio rerio and nematode *Caenorhabditis elegans*. *Sci Total Environ* 619-620: 1-8
196. Kotlar I, Colonnello A, Aguilera-Gonzalez MF, Avila DS, de Lima ME, Garcia-Contreras R, Ortiz-Plata A, Soares FAA, Aschner M, Santamaria A. 2017. Comparison of the Toxic Effects of Quinolinic Acid and 3-Nitropropionic Acid in *C. elegans*: Involvement of the SKN-1 Pathway. *Neurotox Res* 33: 259-67
197. Wang Y, Jian FL, Wu JY, Wang SC. 2012. Stress-Response Protein Expression and DAF-16 Translocation were Induced in Tributyltin-Exposed *Caenorhabditis elegans*. *Bull Environ Contam Toxicol* 89: 704-11
198. Settivari R, VanDuyn N, LeVora J, Nass R. 2013. The Nrf2/SKN-1-dependent glutathione S-transferase pi homologue GST-1 inhibits dopamine neuron degeneration in a *Caenorhabditis elegans* model of manganism. *Neurotoxicology* 38: 51-60
199. Ayyadevara S, Engle MR, Singh SP, Dandapat A, Lichti CF, Benes H, Shmookler Reis RJ, Liebau E, Zimniak P. 2005. Lifespan and stress resistance of *Caenorhabditis elegans* are increased by expression of glutathione transferases capable of metabolizing the lipid peroxidation product 4-hydroxynonenal. *Aging Cell* 4: 257-71
200. Ayyadevara S, Dandapat A, Singh SP, Siegel ER, Shmookler Reis RJ, Zimniak L, Zimniak P. 2007. Life span and stress resistance of *Caenorhabditis elegans* are differentially affected by glutathione transferases metabolizing 4-hydroxynon-2-enal. *Mech Ageing Dev* 128: 196-205
201. Singh SP, Niemczyk M, Zimniak L, Zimniak P. 2009. Fat accumulation in *Caenorhabditis elegans* triggered by the electrophilic lipid peroxidation product 4-Hydroxynonenal (4-HNE). *Aging (Albany NY)* 1: 68-80
202. Petit E, Michelet X, Rauch C, Bertrand-Michel J, Terce F, Legouis R, Morel F. 2009. Glutathione transferases kappa 1 and kappa 2 localize in peroxisomes and mitochondria, respectively, and are involved in lipid metabolism and respiration in *Caenorhabditis elegans*. *FEBS J* 276: 5030-40

203. Morel F, Aninat C. 2011. The glutathione transferase kappa family. *Drug Metab Rev* 43: 281-91
204. Burmeister C, Luersen K, Heinick A, Hussein A, Domagalski M, Walter RD, Liebau E. 2008. Oxidative stress in *Caenorhabditis elegans*: protective effects of the Omega class glutathione transferase (GSTO-1). *FASEB J* 22: 343-54
205. Schieber M, Chandel NS. 2014. TOR signaling couples oxygen sensing to lifespan in *C. elegans*. *Cell Rep* 9: 9-15
206. Berndt C, Lillig CH, Holmgren A. 2008. Thioredoxins and glutaredoxins as facilitators of protein folding. *Biochim Biophys Acta* 1783: 641-50
207. Lillig CH, Berndt C, Holmgren A. 2008. Glutaredoxin systems. *Biochim Biophys Acta* 1780: 1304-17
208. Johnson WM, Yao C, Siedlak SL, Wang WZ, Zhu XW, Caldwell GA, Wilson-Delfosse AL, Mieyal JJ, Chen SG. 2015. Glutaredoxin deficiency exacerbates neurodegeneration in *C. elegans* models of Parkinson's disease. *Hum Mol Genet* 24: 1322-35
209. Johnson WM, Golczak M, Choe K, Curran PL, Miller OG, Yao C, Wang W, Lin J, Milkovic NM, Ray A, Ravindranath V, Zhu X, Wilson MA, Wilson-Delfosse AL, Chen SG, Mieyal JJ. 2016. Regulation of DJ-1 by glutaredoxin 1 *in vivo*: Implications for Parkinson's Disease. *Biochemistry* 55: 4519-32
210. Johnson WM, Wilson-Delfosse AL, Chen SG, Mieyal JJ. 2015. The roles of redox enzymes in Parkinson's disease: Focus on glutaredoxin. *Ther Targets Neurol Dis* 2: e790
211. Morgan KL, Estevez AO, Mueller CL, Cacho-Valadez B, Miranda-Vizuete A, Szewczyk NJ, Estevez M. 2010. The glutaredoxin GLRX-21 functions to prevent selenium-induced oxidative stress in *Caenorhabditis elegans*. *Toxicol Sci* 118: 530-43
212. Estevez AO, Mueller CL, Morgan KL, Szewczyk NJ, Teece L, Miranda-Vizuete A, Estevez M. 2012. Selenium induces cholinergic motor neuron degeneration in *Caenorhabditis elegans*. *Neurotoxicology* 33: 1021-32
213. Arner ES, Holmgren A. 2000. Physiological functions of thioredoxin and thioredoxin reductase. *Eur J Biochem* 267: 6102-9
214. Lu J, Holmgren A. 2014. The thioredoxin antioxidant system. *Free Radic Biol Med* 66: 75-87
215. Arodin L, Miranda-Vizuete A, Swoboda P, Fernandes AP. 2014. Protective effects of the thioredoxin and glutaredoxin systems in dopamine-induced cell death. *Free Radic Biol Med* 73: 328-36
216. Miranda-Vizuete A, Fierro Gonzalez JC, Gahmon G, Burghoorn J, Navas P, Swoboda P. 2006. Lifespan decrease in a *Caenorhabditis elegans* mutant lacking TRX-1, a thioredoxin expressed in ASJ sensory neurons. *FEBS Lett* 580: 484-90
217. Fierro-Gonzalez JC, Cornils A, Alcedo J, Miranda-Vizuete A, Swoboda P. 2011. The thioredoxin TRX-1 modulates the function of the insulin-like neuropeptide DAF-28 during dauer formation in *Caenorhabditis elegans*. *PLoS One* 6: e16561
218. Gonzalez-Barrios M, Fierro-Gonzalez JC, Krpelanova E, Mora-Lorca JA, Pedrajas JR, Penate X, Chavez S, Swoboda P, Jansen G, Miranda-Vizuete A. 2015. *Cis*- and *trans*-regulatory mechanisms of gene expression in the ASJ sensory neuron of *Caenorhabditis elegans*. *Genetics* 200: 123-34
219. Fierro-Gonzalez JC, Gonzalez-Barrios M, Miranda-Vizuete A, Swoboda P. 2011. The thioredoxin TRX-1 regulates adult lifespan extension induced by dietary

restriction in *Caenorhabditis elegans*. *Biochem Biophys Res Commun* 406: 478-82

220. McCallum KC, Liu B, Fierro-Gonzalez JC, Swoboda P, Arur S, Miranda-Vizuete A, Garsin DA. 2016. TRX-1 Regulates SKN-1 Nuclear Localization Cell Non-autonomously in *Caenorhabditis elegans*. *Genetics* 203: 387-402
221. Cacho-Valadez B, Munoz-Lobato F, Pedrajas JR, Cabello J, Fierro-Gonzalez JC, Navas P, Swoboda P, Link CD, Miranda-Vizuete A. 2012. The characterization of the *Caenorhabditis elegans* mitochondrial thioredoxin system uncovers an unexpected protective role of thioredoxin reductase 2 in beta-amyloid peptide toxicity. *Antioxid Redox Signal* 16: 1384-400
222. Lacey BM, Hondal RJ. 2006. Characterization of mitochondrial thioredoxin reductase from *C. elegans*. *Biochem Biophys Res Commun* 346: 629-36
223. Jimenez-Hidalgo M, Kurz CL, Pedrajas JR, Naranjo-Galindo FJ, Gonzalez-Barrios M, Cabello J, Saez AG, Lozano E, Button EL, Veal EA, Fierro-Gonzalez JC, Swoboda P, Miranda-Vizuete A. 2014. Functional characterization of thioredoxin 3 (TRX-3), a *Caenorhabditis elegans* intestine-specific thioredoxin. *Free Radic Biol Med* 68: 205-19
224. Stenvall J, Fierro-Gonzalez JC, Swoboda P, Saamarthy K, Cheng Q, Cacho-Valadez B, Arner ES, Persson OP, Miranda-Vizuete A, Tuck S. 2011. Selenoprotein TRXR-1 and GSR-1 are essential for removal of old cuticle during molting in *Caenorhabditis elegans*. *Proc Natl Acad Sci U.S.A* 108: 1064-9
225. Gladyshev VN, Krause M, Xu XM, Korotkov KV, Kryukov GV, Sun QA, Lee BJ, Wootton JC, Hatfield DL. 1999. Selenocysteine-containing thioredoxin reductase in *C. elegans*. *Biochem Biophys Res Commun* 259: 244-9
226. Li W, Bandyopadhyay J, Hwaang HS, Park BJ, Cho JH, Il Lee J, Ahnn J, Lee SK. 2012. Two thioredoxin reductases, *trxr-1* and *trxr-2*, have differential physiological roles in *Caenorhabditis elegans*. *Mol Cells* 34: 209-18
227. Taskov K, Chapple C, Kryukov GV, Castellano S, Lobanov AV, Korotkov KV, Guigo R, Gladyshev VN. 2005. Nematode selenoproteome: the use of the selenocysteine insertion system to decode one codon in an animal genome? *Nucleic Acids Res* 33: 2227-38
228. Li WH, Shi YC, Chang CH, Huang CW, Liao VHC. 2014. Selenite protects *Caenorhabditis elegans* from oxidative stress via DAF-16 and TRXR-1. *Mol Nutr Food Res* 58: 863-74
229. Boehler CJ, Raines AM, Sunde RA. 2014. Toxic-selenium and low-selenium transcriptomes in *Caenorhabditis elegans*: toxic selenium up-regulates oxidoreductase and down-regulates cuticle-associated genes. *PLoS One* 9: e101408
230. Boehler CJ, Raines AM, Sunde RA. 2013. Deletion of Thioredoxin Reductase and Effects of Selenite and Selenate Toxicity in *Caenorhabditis elegans*. *Plos One* 8: e71525
231. Winterbourn CC. 2017. Biological Production, Detection, and Fate of Hydrogen Peroxide. *Antioxid Redox Signal*
232. Wood ZA, Schroder E, Robin Harris J, Poole LB. 2003. Structure, mechanism and regulation of peroxiredoxins. *Trends Biochem Sci* 28: 32-40
233. Isermann K, Liebau E, Roeder T, Bruchhaus I. 2004. A peroxiredoxin specifically expressed in two types of pharyngeal neurons is required for normal growth and egg production in *Caenorhabditis elegans*. *J Mol Biol* 338: 745-55

234. Bhatla N, Horvitz HR. 2015. Light and Hydrogen Peroxide Inhibit *C. elegans* Feeding through Gustatory Receptor Orthologs and Pharyngeal Neurons. *Neuron* 85: 804-18
235. Olahova M, Taylor SR, Khazaipoul S, Wang JL, Morgan BA, Matsumoto K, Blackwell TK, Veal EA. 2008. A redox-sensitive peroxiredoxin that is important for longevity has tissue- and stress-specific roles in stress resistance. *Proc Natl Acad Sci U.S.A* 105: 19839-44
236. Henderson D, Huebner C, Markowitz M, Taube N, Harvanek ZM, Jakob U, Knoefler D. 2018. Do developmental temperatures affect redox level and lifespan in *C. elegans* through upregulation of peroxiredoxin? *Redox Biol* 14: 386-90
237. Spiro Z, Arslan MA, Somogyvari M, Nguyen MT, Smolders A, Dancso B, Nemeth N, Elek Z, Braeckman BP, Csermely P, Soti C. 2012. RNA interference links oxidative stress to the inhibition of heat stress adaptation. *Antioxid Redox Signal* 17: 890-901
238. Olahova M, Veal EA. 2015. A peroxiredoxin, PRDX-2, is required for insulin secretion and insulin/IIS-dependent regulation of stress resistance and longevity. *Aging Cell* 14: 558-68
239. Thamsen M, Kumsta C, Li F, Jakob U. 2011. Is Overoxidation of Peroxiredoxin Physiologically Significant? *Antioxid Redox Signal* 14: 725-30
240. Olmedo M, O'Neill JS, Edgar RS, Valekunja UK, Reddy AB, Merrow M. 2012. Circadian regulation of olfaction and an evolutionarily conserved, nontranscriptional marker in *Caenorhabditis elegans*. *Proc Natl Acad Sci U.S.A* 109: 20479-84
241. Edgar RS, Green EW, Zhao Y, van Ooijen G, Olmedo M, Qin X, Xu Y, Pan M, Valekunja UK, Feeney KA, Maywood ES, Hastings MH, Baliga NS, Merrow M, Millar AJ, Johnson CH, Kyriacou CP, O'Neill JS, Reddy AB. 2012. Peroxiredoxins are conserved markers of circadian rhythms. *Nature* 485: 459-64
242. De Haes W, Frooninckx L, Van Assche R, Smolders A, Depuydt G, Billen J, Braeckman BP, Schoofs L, Temmerman L. 2014. Metformin promotes lifespan through mitohormesis via the peroxiredoxin PRDX-2. *Proc Natl Acad Sci U.S.A* 111: E2501-E9
243. Li G, Gong J, Lei H, Liu J, Xu XZ. 2016. Promotion of behavior and neuronal function by reactive oxygen species in *C. elegans*. *Nat Commun* 7: 13234
244. Ranjan M, Gruber J, Ng LF, Halliwell B. 2013. Repression of the mitochondrial peroxiredoxin antioxidant system does not shorten life span but causes reduced fitness in *Caenorhabditis elegans*. *Free Radic Biol Med* 63: 381-9
245. Hanschmann EM, Godoy JR, Berndt C, Hudemann C, Lillig CH. 2013. Thioredoxins, glutaredoxins, and peroxiredoxins--molecular mechanisms and health significance: from cofactors to antioxidants to redox signaling. *Antioxid Redox Signal* 19: 1539-605
246. Flohe L. 2016. The impact of thiol peroxidases on redox regulation. *Free Radic Res* 50: 126-42
247. Consortium T*Ce*S. 1998. Genome sequence of the nematode *C. elegans*: a platform for investigating biology. *Science* 282: 2012-8
248. Tissenbaum HA. 2015. Using *C. elegans* for aging research. *Invertebr Reprod Dev* 59: 59-63
249. Giustarini D, Tsikas D, Colombo G, Milzani A, Dalle-Donne I, Fanti P, Rossi R. 2016. Pitfalls in the analysis of the physiological antioxidant glutathione (GSH)

and its disulfide (GSSG) in biological samples: An elephant in the room. *J Chromatogr B Analyt Technol Biomed Life Sci* 1019: 21-8

250. Monostori P, Wittmann G, Karg E, Turi S. 2009. Determination of glutathione and glutathione disulfide in biological samples: An in-depth review. *J Chromatogr B Analyt Technol Biomed Life Sci* 877: 3331-46
251. Tietze F. 1969. Enzymic Method for Quantitative Determination of Nanogram Amounts of Total and Oxidized Glutathione: Applications to Mammalian Blood and Other Tissues. *Anal Biochem* 27: 502-22
252. Rahman I, Kode A, Biswas SK. 2006. Assay for quantitative determination of glutathione and glutathione disulfide levels using enzymatic recycling method. *Nat Protoc* 1: 3159-65
253. Fenn JB, Mann M, Meng CK, Wong SF, Whitehouse CM. 1989. Electrospray ionization for mass spectrometry of large biomolecules. *Science* 246: 64-71
254. Wilm M. 2011. Principles of electrospray ionization. *Mol Cell Proteomics* 10: M111.009407
255. Kebarle P, Tang L. 1993. From Ions in Solution to Ions in the Gas-Phase - the Mechanism of Electrospray Mass-Spectrometry. *Anal Chem* 65: A972-A86
256. Ho CS, Lam CW, Chan MH, Cheung RC, Law LK, Lit LC, Ng KF, Suen MW, Tai HL. 2003. Electrospray ionisation mass spectrometry: principles and clinical applications. *Clin Biochem Rev* 24: 3-12
257. Picotti P, Aebersold R. 2012. Selected reaction monitoring-based proteomics: workflows, potential, pitfalls and future directions. *Nat Methods* 9: 555-66
258. Carroll D, Howard D, Zhu H, Paumi CM, Vore M, Bondada S, Liang Y, Wang C, St Clair DK. 2016. Simultaneous quantitation of oxidized and reduced glutathione via LC-MS/MS: An insight into the redox state of hematopoietic stem cells. *Free Radic Biol Med* 97: 85-94
259. Moore T, Le A, Niemi AK, Kwan T, Cusmano-Ozog K, Enns GM, Cowan TM. 2013. A new LC-MS/MS method for the clinical determination of reduced and oxidized glutathione from whole blood. *J Chromatogr B Analyt Technol Biomed Life Sci* 929: 51-5
260. Lee SG, Yim J, Lim Y, Kim JH. 2016. Validation of a liquid chromatography tandem mass spectrometry method to measure oxidized and reduced forms of glutathione in whole blood and verification in a mouse model as an indicator of oxidative stress. *J Chromatogr B Analyt Technol Biomed Life Sci* 1019: 45-50
261. Anderson EN, Corkins ME, Li JC, Singh K, Parsons S, Tucey TM, Sorkac A, Huang H, Dimitriadi M, Sinclair DA, Hart AC. 2016. *C. elegans* lifespan extension by osmotic stress requires FUdR, base excision repair, FOXO, and sirtuins. *Mech Ageing Dev* 154: 30-42
262. Aitlhadj L, Sturzenbaum SR. 2010. The use of FUdR can cause prolonged longevity in mutant nematodes. *Mech Ageing Dev* 131: 364-5
263. Davies SK, Leroi AM, Bundy JG. 2012. Fluorodeoxyuridine affects the identification of metabolic responses to *daf-2* status in *Caenorhabditis elegans*. *Mech Ageing Dev* 133: 46-9
264. Masuda M, Toriumi C, Santa T, Imai K. 2004. Fluorogenic derivatization reagents suitable for isolation and identification of cysteine-containing proteins utilizing high-performance liquid chromatography-tandem mass spectrometry. *Anal Chem* 76: 728-35
265. Caito SW, Aschner M. 2015. Quantification of Glutathione in *Caenorhabditis elegans*. *Curr Protoc Toxicol* 64: 6 18 1-6

266. Liu Y, Hyde AS, Simpson MA, Barycki JJ. 2014. Emerging regulatory paradigms in glutathione metabolism. *Adv Cancer Res* 122: 69-101
267. Zhu P, Oe T, Blair IA. 2008. Determination of cellular redox status by stable isotope dilution liquid chromatography/mass spectrometry analysis of glutathione and glutathione disulfide. *Rapid Commun Mass Spectrom* 22: 432-40
268. Quintana-Cabrera R, Bolanos JP. 2013. Glutathione and gamma-glutamylcysteine in hydrogen peroxide detoxification. *Methods Enzymol* 527: 129-44
269. Sulston JE, Brenner S. 1974. DNA of *Caenorhabditis elegans*. *Genetics* 77: 95-104
270. Harwood DT, Kettle AJ, Brennan S, Winterbourn CC. 2009. Simultaneous determination of reduced glutathione, glutathione disulphide and glutathione sulphonamide in cells and physiological fluids by isotope dilution liquid chromatography-tandem mass spectrometry. *J Chromatogr B Analyt Technol Biomed Life Sci* 877: 3393-9
271. Ey J, Schomig E, Taubert D. 2007. Dietary sources and antioxidant effects of ergothioneine. *J Agric Food Chem* 55: 6466-74
272. Hsieh CL, Yeh KW, De Kok LJ, Pan RN, Kuo YH, Tseng MH. 2012. Simultaneous determination of sulphur metabolites in Arabidopsis thaliana via LC-ESI-MS/MS and (3)(4)S-metabolic labelling. *Phytochem Anal* 23: 324-31
273. Enns GM, Moore T, Le A, Atkuri K, Shah MK, Cusmano-Ozog K, Niemi AK, Cowan TM. 2014. Degree of glutathione deficiency and redox imbalance depend on subtype of mitochondrial disease and clinical status. *PLoS One* 9: e100001
274. Haberhauer-Troyer C, Delic M, Gasser B, Mattanovich D, Hann S, Koellensperger G. 2013. Accurate quantification of the redox-sensitive GSH/GSSG ratios in the yeast Pichia pastoris by HILIC-MS/MS. *Anal Bioanal Chem* 405: 2031-9
275. Rossi R, Milzani A, Dalle-Donne I, Giustarini D, Lusini L, Colombo R, Di Simplicio P. 2002. Blood glutathione disulfide: *In vivo* factor or *in vitro* artifact? *Clin Chem* 48: 742-53
276. Flohe L. 2013. The fairytale of the GSSG/GSH redox potential. *Biochim Biophys Acta* 1830: 3139-42
277. Julius M, Lang CA, Gleiberman L, Harburg E, DiFranceisco W, Schork A. 1994. Glutathione and morbidity in a community-based sample of elderly. *J Clin Epidemiol* 47: 1021-6
278. Fletcher RH, Fletcher SW. 1994. Glutathione and ageing: ideas and evidence. *Lancet* 344: 1379-80
279. Tong JC, Fitzmaurice PS, Moszczynska A, Mattina K, Ang LC, Boileau I, Furukawa Y, Sailasuta N, Kish SJ. 2016. Do glutathione levels decline in aging human brain? *Free Radic Biol Med* 93: 110-7
280. Perry TL, Hansen S, Gandham SS. 1981. Postmortem changes of amino compounds in human and rat brain. *J Neurochem* 36: 406-10
281. Rae CD, Williams SR. 2017. Glutathione in the human brain: Review of its roles and measurement by magnetic resonance spectroscopy. *Anal Biochem* 529: 127-43
282. van Lieshout EM, Peters WH. 1998. Age and gender dependent levels of glutathione and glutathione S-transferases in human lymphocytes. *Carcinogenesis* 19: 1873-5
283. Winther JR, Thorpe C. 2014. Quantification of thiols and disulfides. *Biochim Biophys Acta* 1840: 838-46

284. Smyth DG, Konigsberg W, Blumenfeld OO. 1964. Reactions of N-Ethylmaleimide with Peptides and Amino Acids. *Biochem J* 91: 589-&
285. Kuninori T, Nishiyama J. 1985. Some Properties of Diastereomers Formed in the Reactions of N-Ethylmaleimide with Biological Thiols. *Agric Biol Chem* 49: 2453-4
286. Giustarini D, Dalle-Donne I, Milzani A, Fanti P, Rossi R. 2013. Analysis of GSH and GSSG after derivatization with N-ethylmaleimide. *Nat Protoc* 8: 1660-9
287. Gruber J, Ng LF, Poovathingal SK, Halliwell B. 2009. Deceptively simple but simply deceptive--*Caenorhabditis elegans* lifespan studies: considerations for aging and antioxidant effects. *FEBS Lett* 583: 3377-87
288. Roos G, Foloppe N, Messens J. 2013. Understanding the pK_a of redox cysteines: the key role of hydrogen bonding. *Antioxid Redox Signal* 18: 94-127
289. Van Laer K, Hamilton CJ, Messens J. 2013. Low-molecular-weight thiols in thiol-disulfide exchange. *Antioxid Redox Signal* 18: 1642-53
290. Jones DP, Carlson JL, Samiec PS, Sternberg P, Jr., Mody VC, Jr., Reed RL, Brown LA. 1998. Glutathione measurement in human plasma. Evaluation of sample collection, storage and derivatization conditions for analysis of dansyl derivatives by HPLC. *Clin Chim Acta* 275: 175-84
291. Jones DP, Liang Y. 2009. Measuring the poise of thiol/disulfide couples *in vivo*. *Free Radic Biol Med* 47: 1329-38
292. Camera E, Picardo M. 2002. Analytical methods to investigate glutathione and related compounds in biological and pathological processes. *J Chromatogr B Analyt Technol Biomed Life Sci* 781: 181-206
293. Nakashima F, Shibata T, Kamiya K, Yoshitake J, Kikuchi R, Matsushita T, Ishii I, Gimenez-Bastida JA, Schneider C, Uchida K. 2018. Structural and functional insights into S-thiolation of human serum albumins. *Sci Rep* 8: 932
294. Jiang X, Chen J, Bajic A, Zhang C, Song X, Carroll SL, Cai ZL, Tang M, Xue M, Cheng N, Schaaf CP, Li F, MacKenzie KR, Ferreon ACM, Xia F, Wang MC, Maletic-Savatic M, Wang J. 2017. Quantitative real-time imaging of glutathione. *Nat Commun* 8: 16087
295. Cossetti C, Di Giovamberardino G, Rota R, Pastore A. 2018. Pitfalls in the quantitative imaging of glutathione in living cells. *Nat Commun* 9: 1588
296. Jiang X, Chen J, Wang J. 2018. Reply to 'Pitfalls in the quantitative imaging of glutathione in living cells'. *Nat Commun* 9: 1589
297. Godel H, Graser T, Foldi P, Pfaender P, Furst P. 1984. Measurement of free amino acids in human biological fluids by high-performance liquid chromatography. *J Chromatogr* 297: 49-61
298. Oh SI, Park JK, Park SK. 2015. Lifespan extension and increased resistance to environmental stressors by N-acetyl-L-cysteine in *Caenorhabditis elegans*. *Clinics (Sao Paulo)* 70: 380-6
299. Schulz TJ, Zarse K, Voigt A, Urban N, Birringer M, Ristow M. 2007. Glucose restriction extends *Caenorhabditis elegans* life span by inducing mitochondrial respiration and increasing oxidative stress. *Cell Metab* 6: 280-93
300. Back P, De Vos WH, Depuydt GG, Matthijssens F, Vanfleteren JR, Braeckman BP. 2012. Exploring real-time in vivo redox biology of developing and aging *Caenorhabditis elegans*. *Free Radic Biol Med* 52: 850-9
301. Braeckman BP, Smolders A, Back P, De Henau S. 2016. In Vivo Detection of Reactive Oxygen Species and Redox Status in *Caenorhabditis elegans*. *Antioxid Redox Signal* 25: 577-92

302. Morgan B, Ezerina D, Amoako TN, Riemer J, Seedorf M, Dick TP. 2013. Multiple glutathione disulfide removal pathways mediate cytosolic redox homeostasis. *Nat Chem Biol* 9: 119-25
303. Montero D, Tachibana C, Rahr Winther J, Appenzeller-Herzog C. 2013. Intracellular glutathione pools are heterogeneously concentrated. *Redox Biol* 1: 508-13
304. Winther JR, Jakob U. 2013. Redox control: A black hole for oxidized glutathione. *Nat Chem Biol* 9: 69-70
305. Croll NA, Smith JM, Zuckerman BM. 1977. The aging process of the nematode *Caenorhabditis elegans* in bacterial and axenic culture. *Exp Aging Res* 3: 175-89
306. Giustarini D, Galvagni F, Tesei A, Farolfi A, Zanoni M, Pignatta S, Milzani A, Marone IM, Dalle-Donne I, Nassini R, Rossi R. 2015. Glutathione, glutathione disulfide, and S-glutathionylated proteins in cell cultures. *Free Radic Biol Med* 89: 972-81
307. Bukowski MR, Bucklin C, Picklo MJ. 2015. Quantitation of protein S-glutathionylation by liquid chromatography-tandem mass spectrometry: correction for contaminating glutathione and glutathione disulfide. *Anal Biochem* 469: 54-64
308. Forman HJ, Dickinson DA. 2003. Oxidative signaling and glutathione synthesis. *Biofactors* 17: 1-12
309. Backos DS, Fritz KS, McArthur DG, Kepa JK, Donson AM, Petersen DR, Foreman NK, Franklin CC, Reigan P. 2013. Glycation of glutamate cysteine ligase by 2-deoxy-d-ribose and its potential impact on chemoresistance in glioblastoma. *Neurochem Res* 38: 1838-49
310. Lim J, Nakamura BN, Mohar I, Kavanagh TJ, Luderer U. 2015. Glutamate Cysteine Ligase Modifier Subunit (Gclm) Null Mice Have Increased Ovarian Oxidative Stress and Accelerated Age-Related Ovarian Failure. *Endocrinology* 156: 3329-43
311. McConnachie LA, Mohar I, Hudson FN, Ware CB, Ladiges WC, Fernandez C, Chatterton-Kirchmeier S, White CC, Pierce RH, Kavanagh TJ. 2007. Glutamate cysteine ligase modifier subunit deficiency and gender as determinants of acetaminophen-induced hepatotoxicity in mice. *Toxicol Sci* 99: 628-36
312. Dalton TP, Dieter MZ, Yang Y, Shertzer HG, Nebert DW. 2000. Knockout of the mouse glutamate cysteine ligase catalytic subunit (Gclc) gene: embryonic lethal when homozygous, and proposed model for moderate glutathione deficiency when heterozygous. *Biochem Biophys Res Commun* 279: 324-9
313. Di Tommaso P, Moretti S, Xenarios I, Orobitg M, Montanyola A, Chang JM, Taly JF, Notredame C. 2011. T-Coffee: a web server for the multiple sequence alignment of protein and RNA sequences using structural information and homology extension. *Nucleic Acids Res* 39: W13-7
314. Nava GM, Lee DY, Ospina JH, Cai SY, Gaskins HR. 2009. Genomic analyses reveal a conserved glutathione homeostasis pathway in the invertebrate chordate Ciona intestinalis. *Physiol Genomics* 39: 183-94
315. Kamath RS, Fraser AG, Dong Y, Poulin G, Durbin R, Gotta M, Kanapin A, Le Bot N, Moreno S, Sohrmann M, Welchman DP, Zipperlen P, Ahringer J. 2003. Systematic functional analysis of the *Caenorhabditis elegans* genome using RNAi. *Nature* 421: 231-7

316. Timmons L, Court DL, Fire A. 2001. Ingestion of bacterially expressed dsRNAs can produce specific and potent genetic interference in *Caenorhabditis elegans*. *Gene* 263: 103-12
317. Timmons L, Fire A. 1998. Specific interference by ingested dsRNA. *Nature* 395: 854
318. Grishok A. 2005. RNAi mechanisms in *Caenorhabditis elegans*. *FEBS Lett* 579: 5932-9
319. Brenner S. 1974. Genetics of *Caenorhabditis elegans*. *Genetics* 77: 71-94
320. Kamath RS, Ahringer J. 2003. Genome-wide RNAi screening in *Caenorhabditis elegans*. *Methods* 30: 313-21
321. Kamath RS, Martinez-Campos M, Zipperlen P, Fraser AG, Ahringer J. 2001. Effectiveness of specific RNA-mediated interference through ingested double-stranded RNA in *Caenorhabditis elegans*. *Genome Biol* 2: RESEARCH0002
322. Lionaki E, Tavernarakis N. 2013. Assessing aging and senescent decline in *Caenorhabditis elegans*: cohort survival analysis. *Methods Mol Biol* 965: 473-84
323. Ullrich M, Liang V, Chew YL, Banister S, Song XM, Zaw T, Lam H, Berber S, Kassiou M, Nicholas HR, Gotz J. 2014. Bio-orthogonal labeling as a tool to visualize and identify newly synthesized proteins in *Caenorhabditis elegans*. *Nat Protoc* 9: 2237
324. Chew YL, Fan XC, Gotz J, Nicholas HR. 2013. PTL-1 regulates neuronal integrity and lifespan in *C. elegans*. *J Cell Sci* 126: 2079-91
325. Gruber J, Ng LF, Fong S, Wong YT, Koh SA, Chen CB, Shui GH, Cheong WF, Schaffer S, Wenk MR, Halliwell B. 2011. Mitochondrial Changes in Ageing *Caenorhabditis elegans* - What Do We Learn from Superoxide Dismutase Knockouts? *Plos One* 6: e19444
326. Ryu D, Mouchiroud L, Andreux PA, Katsyuba E, Moullan N, Nicolet-Dit-Felix AA, Williams EG, Jha P, Lo Sasso G, Huzard D, Aebischer P, Sandi C, Rinsch C, Auwerx J. 2016. Urolithin A induces mitophagy and prolongs lifespan in *C. elegans* and increases muscle function in rodents. *Nat Med* 22: 879-88
327. Hobert O. 2002. PCR fusion-based approach to create reporter gene constructs for expression analysis in transgenic *C. elegans*. *Biotechniques* 32: 728-30
328. Mello CC, Kramer JM, Stinchcomb D, Ambros V. 1991. Efficient gene transfer in *C. elegans*: extrachromosomal maintenance and integration of transforming sequences. *EMBO J* 10: 3959-70
329. Yu C, Zhang Y, Yao S, Wei Y. 2014. A PCR based protocol for detecting indel mutations induced by TALENs and CRISPR/Cas9 in zebrafish. *PLoS One* 9: e98282
330. Norris AD, Kim HM, Colaiacovo MP, Calarco JA. 2015. Efficient Genome Editing in *Caenorhabditis elegans* with a Toolkit of Dual-Marker Selection Cassettes. *Genetics* 201: 449-58
331. Hsu PD, Scott DA, Weinstein JA, Ran FA, Konermann S, Agarwala V, Li Y, Fine EJ, Wu X, Shalem O, Cradick TJ, Marraffini LA, Bao G, Zhang F. 2013. DNA targeting specificity of RNA-guided Cas9 nucleases. *Nat Biotechnol* 31: 827-32
332. Berber S, Wood M, Llamosas E, Thaivalappil P, Lee K, Liao BM, Chew YL, Rhodes A, Yucel D, Crossley M, Nicholas HR. 2016. Homeodomain-Interacting Protein Kinase (HPK-1) regulates stress responses and ageing in *C. elegans*. *Sci Rep* 6: 19582
333. Sagasti A, Hisamoto N, Hyodo J, Tanaka-Hino M, Matsumoto K, Bargmann CI. 2001. The CaMKII UNC-43 activates the MAPKKK NSY-1 to execute a lateral

signaling decision required for asymmetric olfactory neuron fates. *Cell* 105: 221-32

334. Farboud B, Meyer BJ. 2015. Dramatic Enhancement of Genome Editing by CRISPR/Cas9 Through Improved Guide RNA Design. *Genetics* 199: 959-71
335. Kim HM, Colaiacovo MP. 2016. CRISPR-Cas9-Guided Genome Engineering in *C. elegans*. *Curr Protoc Mol Biol* 115: 31.7.1-.7.18
336. Griffith OW, Bridges RJ, Meister A. 1979. Transport of gamma-glutamyl amino acids: role of glutathione and gamma-glutamyl transpeptidase. *Proc Natl Acad Sci U.S.A* 76: 6319-22
337. Maulik M, Mitra S, Bult-Ito A, Taylor BE, Vayndorf EM. 2017. Behavioral Phenotyping and Pathological Indicators of Parkinson's Disease in *C. elegans* Models. *Front Genet* 8: 77
338. Knoefler D, Thamsen M, Koniczek M, Niemuth NJ, Diederich AK, Jakob U. 2012. Quantitative *in vivo* redox rensors uncover oxidative stress as an early event in life. *Mol Cell* 47: 767-76
339. Laranjeiro R, Harinath G, Burke D, Braeckman BP, Driscoll M. 2017. Single swim sessions in *C. elegans* induce key features of mammalian exercise. *BMC Biol* 15: 30
340. Sies H. 2017. Hydrogen peroxide as a central redox signaling molecule in physiological oxidative stress: Oxidative eustress. *Redox Biol* 11: 613-9
341. Van Raamsdonk JM, Hekimi S. 2012. Superoxide dismutase is dispensable for normal animal lifespan. *Proc Natl Acad Sci U.S.A* 109: 5785-90
342. Bansal A, Zhu LJ, Yen K, Tissenbaum HA. 2015. Uncoupling lifespan and healthspan in *Caenorhabditis elegans* longevity mutants. *Proc Natl Acad Sci U.S.A* 112: E277-86
343. Boulin T, Etchberger JF, Hobert O. 2006. Reporter gene fusions. *WormBook*: 1-23
344. Wenick AS, Hobert O. 2004. Genomic cis-regulatory architecture and trans-acting regulators of a single interneuron-specific gene battery in *C. elegans*. *Dev Cell* 6: 757-70
345. Wightman B, Ha I, Ruvkun G. 1993. Posttranscriptional regulation of the heterochronic gene lin-14 by lin-4 mediates temporal pattern formation in *C. elegans*. *Cell* 75: 855-62
346. Merritt C, Rasoloson D, Ko D, Seydoux G. 2008. 3' UTRs are the primary regulators of gene expression in the *C. elegans* germline. *Curr Biol* 18: 1476-82
347. Kaletsky R, Lakhina V, Arey R, Williams A, Landis J, Ashraf J, Murphy CT. 2016. The *C. elegans* adult neuronal IIS/FOXO transcriptome reveals adult phenotype regulators. *Nature* 529: 92-6
348. Consortium CeDM. 2012. Large-scale screening for targeted knockouts in the *Caenorhabditis elegans* genome. *G3 (Bethesda)* 2: 1415-25
349. Friedland AE, Tzur YB, Esvelt KM, Colaiacovo MP, Church GM, Calarco JA. 2013. Heritable genome editing in *C. elegans* via a CRISPR-Cas9 system. *Nat Methods* 10: 741-3
350. Dickinson DJ, Goldstein B. 2016. CRISPR-Based Methods for *Caenorhabditis elegans* Genome Engineering. *Genetics* 202: 885-901
351. Kim H, Ishidate T, Ghanta KS, Seth M, Conte D, Jr., Shirayama M, Mello CC. 2014. A co-CRISPR strategy for efficient genome editing in *Caenorhabditis elegans*. *Genetics* 197: 1069-80

352. Paix A, Wang YM, Smith HE, Lee CYS, Calidas D, Lu T, Smith J, Schmidt H, Krause MW, Seydoux G. 2014. Scalable and Versatile Genome Editing Using Linear DNAs with Microhomology to Cas9 Sites in *Caenorhabditis elegans*. *Genetics* 198: 1347-56
353. Chiu H, Schwartz HT, Antoshechkin I, Sternberg PW. 2013. Transgene-free genome editing in *Caenorhabditis elegans* using CRISPR-Cas. *Genetics* 195: 1167-71
354. Paix A, Folkmann A, Rasoloson D, Seydoux G. 2015. High Efficiency, Homology-Directed Genome Editing in *Caenorhabditis elegans* Using CRISPR-Cas9 Ribonucleoprotein Complexes. *Genetics* 201: 47-54
355. van Schendel R, Roerink SF, Portegijs V, van den Heuvel S, Tijsterman M. 2015. Polymerase Theta is a key driver of genome evolution and of CRISPR/Cas9-mediated mutagenesis. *Nat Commun* 6: 7394
356. Waaijers S, Boxem M. 2014. Engineering the *Caenorhabditis elegans* genome with CRISPR/Cas9. *Methods* 68: 381-8
357. Ashrafi K, Chang FY, Watts JL, Fraser AG, Kamath RS, Ahringer J, Ruvkun G. 2003. Genome-wide RNAi analysis of *Caenorhabditis elegans* fat regulatory genes. *Nature* 421: 268-72
358. Schmokel V, Memar N, Wiekenberg A, Trotzmuller M, Schnabel R, Doring F. 2016. Genetics of lipid-storage management in *Caenorhabditis elegans* embryos. *Genetics* 202: 1071-83
359. Harman D. 1957. Prolongation of the normal life span by radiation protection chemicals. *J Gerontol* 12: 257-63
360. Perez VI, Bokov A, Van Remmen H, Mele J, Ran QT, Ikeno Y, Richardson A. 2009. Is the oxidative stress theory of aging dead? *Biochim Biophys Acta Gen Subj* 1790: 1005-14
361. Pun PBL, Gruber J, Tang SY, Schaffer S, Ong RLS, Fong S, Ng LF, Cheah I, Halliwell B. 2010. Ageing in nematodes: do antioxidants extend lifespan in *Caenorhabditis elegans*? *Biogerontology* 11: 17-30
362. Halliwell B. 2012. Free radicals and antioxidants: updating a personal view. *Nutr Rev* 70: 257-65
363. Shibamura A, Ikeda T, Nishikawa Y. 2009. A method for oral administration of hydrophilic substances to *Caenorhabditis elegans*: Effects of oral supplementation with antioxidants on the nematode lifespan. *Mech Ageing Dev* 130: 652-5
364. Chandler SD, Zarka MH, Vinaya Babu SN, Suhas YS, Raghunatha Reddy KR, Bridge WJ. 2012. Safety assessment of gamma-glutamylcysteine sodium salt. *Regul Toxicol Pharmacol* 64: 17-25
365. Edgley ML, Baillie DL, Riddle DL, Rose AM. 2006. Genetic balancers. *WormBook*: 1-32
366. Bibi S, Kaur R, Henriksen-Lacey M, McNeil SE, Wilkhu J, Lattmann E, Christensen D, Mohammed AR, Perrie Y. 2011. Microscopy imaging of liposomes: from coverslips to environmental SEM. *Int J Pharm* 417: 138-50
367. Bello S, Krogsboll LT, Gruber J, Zhao ZJ, Fischer D, Hrobjartsson A. 2014. Lack of blinding of outcome assessors in animal model experiments implies risk of observer bias. *J Clin Epidemiol* 67: 973-83
368. Frederik PM, Hubert DH. 2005. Cryoelectron microscopy of liposomes. *Methods Enzymol* 391: 431-48

369. Liao VH, Yu CW. 2005. *Caenorhabditis elegans gcs-1* confers resistance to arsenic-induced oxidative stress. *Biometals* 18: 519-28
370. Stiernagle T. 2006. Maintenance of *C. elegans*. *WormBook*: 1-11
371. Barardo D, Thornton D, Thoppil H, Walsh M, Sharifi S, Ferreira S, Anzic A, Fernandes M, Monteiro P, Grum T, Cordeiro R, De-Souza EA, Budovsky A, Araujo N, Gruber J, Petrascheck M, Fraifeld VE, Zhavoronkov A, Moskalev A, de Magalhaes JP. 2017. The DrugAge database of aging-related drugs. *Aging Cell*
372. Munday R. 1989. Toxicity of thiols and disulphides: involvement of free-radical species. *Free Radic Biol Med* 7: 659-73
373. Atkuri KR, Mantovani JJ, Herzenberg LA, Herzenberg LA. 2007. N-Acetylcysteine--a safe antidote for cysteine/glutathione deficiency. *Curr Opin Pharmacol* 7: 355-9
374. Rushworth GF, Megson IL. 2014. Existing and potential therapeutic uses for N-acetylcysteine: the need for conversion to intracellular glutathione for antioxidant benefits. *Pharmacol Ther* 141: 150-9
375. Polyak E, Ostrovsky J, Peng M, Dingley SD, Tsukikawa M, Kwon YJ, McCormack SE, Bennett M, Xiao R, Seiler C, Zhang Z, Falk MJ. 2018. N-acetylcysteine and vitamin E rescue animal longevity and cellular oxidative stress in pre-clinical models of mitochondrial complex I disease. *Mol Genet Metab* 123: 449-62
376. De Magalhaes Filho CD, Henriquez B, Seah NE, Evans RM, Lapierre LR, Dillin A. 2018. Visible light reduces *C. elegans* longevity. *Nat Commun* 9: 927
377. Smith RL, Tan JME, Jonker MJ, Jongejan A, Buissink T, Veldhuijzen S, van Kampen AHC, Brul S, van der Spek H. 2017. Beyond the polymerase-gamma theory: Production of ROS as a mode of NRTI-induced mitochondrial toxicity. *Plos One* 12: e0187424
378. Sha L, Daitoku H, Araoi S, Kaneko Y, Takahashi Y, Kako K, Fukamizu A. 2017. Asymmetric Arginine Dimethylation Modulates Mitochondrial Energy Metabolism and Homeostasis in *Caenorhabditis elegans*. *Mol Cell Biol* 37
379. Wu QL, Wang W, Li YX, Li YP, Ye BP, Tang M, Wang DY. 2012. Small sizes of TiO2-NPs exhibit adverse effects at predicted environmental relevant concentrations on nematodes in a modified chronic toxicity assay system. *J Hazard Mater* 243: 161-8
380. Yang XY, Gondikas AP, Marinakos SM, Auffan M, Liu J, Hsu-Kim H, Meyer JN. 2012. Mechanism of Silver Nanoparticle Toxicity Is Dependent on Dissolved Silver and Surface Coating in *Caenorhabditis elegans*. *Environ Sci Technol* 46: 1119-27
381. Yang W, Hekimi S. 2010. A mitochondrial superoxide signal triggers increased longevity in *Caenorhabditis elegans*. *PLoS Biol* 8: e1000556
382. Huang J, Lemire BD. 2009. Mutations in the *C. elegans* succinate dehydrogenase iron-sulfur subunit promote superoxide generation and premature aging. *J Mol Biol* 387: 559-69
383. Estevez AO, Morgan KL, Szewczyk NJ, Gems D, Estevez M. 2014. The neurodegenerative effects of selenium are inhibited by FOXO and PINK1/PTEN regulation of insulin/insulin-like growth factor signaling in *Caenorhabditis elegans*. *Neurotoxicology* 41: 28-43
384. Cascella R, Evangelisti E, Zampagni M, Becatti M, D'Adamio G, Goti A, Liguri G, Fiorillo C, Cecchi C. 2014. S-linolenoyl glutathione intake extends life-span

and stress resistance via Sir-2.1 upregulation in *Caenorhabditis elegans*. *Free Radic Biol Med* 73: 127-35

385. Witschi A, Reddy S, Stofer B, Lauterburg BH. 1992. The systemic availability of oral glutathione. *Eur J Clin Pharmacol* 43: 667-9
386. Bachhawat AK, Yadav S. 2018. The glutathione cycle: Glutathione metabolism beyond the gamma-glutamyl cycle. *IUBMB Life* 70: 585-92
387. Lu SC. 1999. Regulation of hepatic glutathione synthesis: current concepts and controversies. *FASEB J* 13: 1169-83
388. Anderson ME, Meister A. 1980. Dynamic state of glutathione in blood plasma. *J Biol Chem* 255: 9530-3
389. Abourashed EA. 2013. Bioavailability of Plant-Derived Antioxidants. *Antioxidants (Basel)* 2: 309-25
390. Kaletta T, Hengartner MO. 2006. Finding function in novel targets: *C. elegans* as a model organism. *Nat Rev Drug Discov* 5: 387-98
391. Hunt PR. 2017. The *C. elegans* model in toxicity testing. *J Appl Toxicol* 37: 50-9
392. Zheng SQ, Ding AJ, Li GP, Wu GS, Luo HR. 2013. Drug absorption efficiency in *Caenorhbditis elegans* delivered by different methods. *PLoS One* 8: e56877
393. Kashima N, Fujikura Y, Komura T, Fujiwara S, Sakamoto M, Terao K, Nishikawa Y. 2012. Development of a method for oral administration of hydrophobic substances to *Caenorhabditis elegans*: pro-longevity effects of oral supplementation with lipid-soluble antioxidants. *Biogerontology* 13: 337-44
394. Gomez-Hens A, Fernandez-Romero JM. 2006. Analytical methods for the control of liposomal delivery systems. *TrAC-Trends Analyt Chem* 25: 167-78
395. Parnham MJ, Wetzig H. 1993. Toxicity screening of liposomes. *Chem Phys Lipids* 64: 263-74
396. Hernandez-Caselles T, Villalain J, Gomez-Fernandez JC. 1990. Stability of liposomes on long term storage. *J Pharm Pharmacol* 42: 397-400
397. Maglioni S, Arsalan N, Ventura N. 2016. *C. elegans* screening strategies to identify pro-longevity interventions. *Mech Ageing Dev* 157: 60-9
398. Braeckman BP, Houthoofd K, De Vreese A, Vanfleteren JR. 2002. Assaying metabolic activity in ageing *Caenorhabditis elegans*. *Mech Ageing Dev* 123: 105-19
399. Braeckman BP, Houthoofd K, Vanfleteren JR. 2002. Assessing metabolic activity in aging *Caenorhabditis elegans*: concepts and controversies. *Aging Cell* 1: 82-8
400. Van Voorhies WA. 2002. Rebuttal to Braeckman et al: 'Assessing metabolic activity in aging *Caenorhabditis elegans*: concepts and controversies'. *Aging Cell* 1: 102-3
401. Braeckman BP, Houthoofd K, Vanfleteren JR. 2002. Rebuttal to Van Voorhies: 'the influence of metabolic rate on longevity in the nematode *Caenorhabditis elegans*'. *Aging Cell* 1: 89-90
402. Solis GM, Petrascheck M. 2011. Measuring *Caenorhabditis elegans* life span in 96 well microtiter plates. *J Vis Exp* 49: e2496
403. Bagiyan GA, Koroleva IK, Soroka NV, Ufimtsev AV. 2003. Oxidation of thiol compounds by molecular oxygen in aqueous solutions. *Russ Chem Bull* 52: 1135-41
404. Coimbra M, Isacchi B, van Bloois L, Torano JS, Ket A, Wu XJ, Broere F, Metselaar JM, Rijcken CJF, Storm G, Bilia R, Schiffelers RM. 2011. Improving solubility and chemical stability of natural compounds for medicinal use by incorporation into liposomes. *Int J Pharm* 416: 433-42

405. Ye X, Linton JM, Schork NJ, Buck LB, Petrascheck M. 2014. A pharmacological network for lifespan extension in *Caenorhabditis elegans*. *Aging Cell* 13: 206-15
406. Desjardins D, Cacho-Valadez B, Liu JL, Wang Y, Yee C, Bernard K, Khaki A, Breton L, Hekimi S. 2017. Antioxidants reveal an inverted U-shaped dose-response relationship between reactive oxygen species levels and the rate of aging in *Caenorhabditis elegans*. *Aging Cell* 16: 104-12
407. Xiong LG, Chen YJ, Tong JW, Gong YS, Huang JA, Liu ZH. 2018. Epigallocatechin-3-gallate promotes healthy lifespan through mitohormesis during early-to-mid adulthood in *Caenorhabditis elegans*. *Redox Biol* 14: 305-15
408. Schwarzlander M, Dick TP, Meye AJ, Morgan B. 2015. Dissecting Redox Biology using Fluorescent Protein Sensors. *Antioxid Redox Signal*
409. Yoon DS, Choi Y, Cha DS, Zhang P, Choi SM, Alfhili MA, Polli JR, Pendergrass D, Taki FA, Kapalavavi B, Pan X, Zhang B, Blackwell TK, Lee JW, Lee MH. 2017. Triclosan Disrupts SKN-1/Nrf2-Mediated Oxidative Stress Response in *C. elegans* and Human Mesenchymal Stem Cells. *Sci Rep* 7: 12592
410. Zhou KI, Pincus Z, Slack FJ. 2011. Longevity and stress in *Caenorhabditis elegans*. *Aging (Albany NY)* 3: 733-53
411. Kirkwood TB, Holliday R. 1979. The evolution of ageing and longevity. *Proc R Soc Lond B Biol Sci* 205: 531-46
412. Taormina G, Mirisola MG. 2014. Calorie restriction in mammals and simple model organisms. *Biomed Res Int* 2014: 308690
413. Gomez-Amaro RL, Valentine ER, Carretero M, LeBoeuf SE, Rangaraju S, Broaddus CD, Solis GM, Williamson JR, Petrascheck M. 2015. Measuring Food Intake and Nutrient Absorption in *Caenorhabditis elegans*. *Genetics* 200: 443-54
414. Avery L. 1993. The genetics of feeding in *Caenorhabditis elegans*. *Genetics* 133: 897-917
415. Lakowski B, Hekimi S. 1998. The genetics of caloric restriction in *Caenorhabditis elegans*. *Proc Natl Acad Sci U.S.A* 95: 13091-6
416. Halliwell B. 1999. Establishing the significance and optimal intake of dietary antioxidants: the biomarker concept. *Nutr Rev* 57: 104-13
417. Ristow M, Schmeisser K. 2014. Mitohormesis: Promoting Health and Lifespan by Increased Levels of Reactive Oxygen Species (ROS). *Dose Response* 12: 288-341
418. Sies H. 2015. Oxidative stress: a concept in redox biology and medicine. *Redox Biol* 4: 180-3
419. Haenen GRMM, Bast A. 2014. Glutathione revisited: a better scavenger than previously thought. *Front Pharmacol* 5: 260
420. Narayan V, Ly T, Pourkarimi E, Murillo AB, Gartner A, Lamond AI, Kenyon C. 2016. Deep proteome analysis identifies age-related processes in *C. elegans*. *Cell Syst* 3: 144-59
421. White CC, Viernes H, Krejsa CM, Botta D, Kavanagh TJ. 2003. Fluorescence-based microtiter plate assay for glutamate-cysteine ligase activity. *Anal Biochem* 318: 175-80
422. Shi ZZ, Habib GM, Rhead WJ, Gahl WA, He X, Sazer S, Lieberman MW. 1996. Mutations in the glutathione synthetase gene cause 5-oxoprolinuria. *Nat Genet* 14: 361-5
423. Atwal PS, Medina CR, Burrage LC, Sutton VR. 2016. Nineteen-year follow-up of a patient with severe glutathione synthetase deficiency. *J Hum Genet* 61: 669-72

424. Miranda-Vizuete A, Veal EA. 2016. *Caenorhabditis elegans* as a model for understanding ROS function in physiology and disease. *Redox Biol* 11: 708-14
425. Toroser D, Sohal RS. 2007. Age-associated perturbations in glutathione synthesis in mouse liver. *Biochem J* 405: 583-9
426. Yang J, Carroll KS, Liebler DC. 2016. The Expanding Landscape of the Thiol Redox Proteome. *Mol Cell Proteomics* 15: 1-11
427. Gu L, Robinson RA. 2016. Proteomic approaches to quantify cysteine reversible modifications in aging and neurodegenerative diseases. *Proteomics Clin Appl* 10: 1159-77
428. Go YM, Chandler JD, Jones DP. 2015. The cysteine proteome. *Free Radic Biol Med* 84: 227-45
429. Go YM, Roede JR, Walker DI, Duong DM, Seyfried NT, Orr M, Liang Y, Pennell KD, Jones DP. 2013. Selective targeting of the cysteine proteome by thioredoxin and glutathione redox systems. *Mol Cell Proteomics* 12: 3285-96
430. Go YM, Jones DP. 2013. The redox proteome. *J Biol Chem* 288: 26512-20
431. Feng S, Chen Y, Yang F, Zhang L, Gong Y, Adilijiang G, Gao Y, Deng H. 2015. Development of a Clickable Probe for Profiling of Protein Glutathionylation in the Central Cellular Metabolism of *E. coli* and *Drosophila*. *Chem Biol* 22: 1461-9
432. Henze A, Homann T, Rohn I, Aschner M, Link CD, Kleuser B, Schweigert FJ, Schwerdtle T, Bornhorst J. 2016. *Caenorhabditis elegans* as a model system to study post-translational modifications of human transthyretin. *Sci Rep* 6: 37346

APPENDICES

Appendix A-1. Primers used in PCR fusion for GFP transcriptional *gclm* reporter

Name	Sequence
GF1	TGGATGCTCCAGATGATATTCCAT
GF2	TTCCATCCTACGTTGAATCCAATTC
GF3	CTCGTCGATAGAGAGGAAGTTGCATG
GF4	GTGAAAAGTTCTTCTCCTTTACTCAT**TTCAACGAAAATTCCGTTCGGAAAAG**
GF5	GTGAAAAGTTCTTCTCCTTTACTCAT**TTTTCGAATGTGCTGCACTGAAAG**
GF6	CTTTTCCGAACGGAATTTTCGTTG**AAATGAGTAAAGGAGAAGAACTTTTCAC**
GF7	CTTTCAGTGCAGCACATTCGAA**AAATGAGTAAAGGAGAAGAACTTTTCAC**
AA18	ATGAGTAAAGGAGAAGAACTTTTCACTGG

Appendix A-2. Primer sequences for constructing CRISPR/Cas9 sgRNA vectors

Table A-2. Single guide RNAs (sgRNAs) were designed to target exon 1 of the E01A2.1a for the strategy to produce mutants for the *gclm* gene.

Primer	Sequence
#1†	5′-GAGAGATTGCTCAGAAATTGGGTTTTAGAGCTAGAAATAGCAAG-3′
#2†	5′-GACCCGATTTCGTCTTCACACGTTTTAGAGCTAGAAATAGCAAG-3′
sgRNA uniR	5′-AAACATTTAGATTTGCAATTCAATTA-3′

†Forward primers used for constructing guide #1 and #2. The CRISPR-targeting RNA (crRNA) sequences are underlined.

sgRNA uniR = sgRNA universal reverse primer. Outlined in the method from Norris *et al.* (2015).